

**The 7TM-independent (*trans*) function of the Adhesion GPCR
Latrophilin-1 in *C. elegans* neuron morphogenesis and germ cell
proliferation**

Thesis submitted for the degree of
Dr. med.

Medical Faculty
Leipzig University

Submitted by: Daniel Matúš

Date and place of birth: 13.06.1996, Levoča (Slovakia)

Carried out at: Rudolf Schönheimer Institute of Biochemistry
Medical Faculty, Leipzig University

Supervisors: Prof. Dr. med. Torsten Schöneberg
Prof. Simone Prömel, D.Phil (Oxon)

Decision on the awarding of the doctoral degree: 26.04.2022

Table of Contents

Table of Contents.....	2
List of Figures	4
Abbreviations and Acronyms	5
1 Adhesion G protein-coupled receptors (aGPCRs).....	7
1.1 Roles of Adhesion GPCRs in physiology and pathology	7
1.2 Unique structural features of Adhesion GPCRs.....	8
1.3 Mechanisms of Adhesion GPCR function	9
1.3.1 <i>Cis</i> function	9
1.3.2 <i>Trans</i> function	11
1.4 Latrophilins as prototypical Adhesion GPCRs	11
2 The model organism <i>Caenorhabditis elegans</i> (<i>C. elegans</i>).....	12
2.1 Physiological functions of Latrophilin-1 (LAT-1) in <i>C. elegans</i>	13
2.2 <i>C. elegans</i> male copulatory behavior as a model for neurodevelopment and neuronal function.....	15
2.3 The reproductive system of <i>C. elegans</i> hermaphrodites as a model for stem cell biology and Notch signaling	17
3 Aim of this study	19
4 Publications and manuscripts	20
4.1 Latrophilin-1 drives neuron morphogenesis and shapes chemo- and mechanosensation-dependent behavior in <i>C. elegans</i> via a <i>trans</i> function.....	20
4.2 The N terminus-only (<i>trans</i>) function of the Adhesion GPCR Latrophilin-1 cross-talks with the Notch pathway to control cell proliferation in the stem cell niche (manuscript).....	42
4.3 G Proteins and GPCRs in <i>C. elegans</i> Development: A Story of Mutual Infidelity (Review)	104
5 Summary	123
6 References.....	128
7 Appendix.....	137
7.1 Supplemental material for “Latrophilin-1 drives neuron morphogenesis and shapes chemo- and mechanosensation-dependent behavior in <i>C. elegans</i> via a <i>trans</i> function”.....	137
Supplementary Figure 1	137
Supplementary Table 1	138
Supplementary Table 2	140
Supplementary Table 3	150
Supplementary Table 4	158

Supplementary Table 5	160
Supplementary Table 6	161
Supplementary Table 7	162
Supplementary Files	163
Supplementary References.....	164
7.2 Supplemental material for “The N terminus-only (<i>trans</i>) function of the Adhesion GPCR Latrophilin-1 cross-talks with the Notch pathway to control cell proliferation in the stem cell niche”	165
Supplementary Figure 1	165
Supplementary Figure 2	166
Supplementary Figure 3	167
Supplementary Figure 4	168
Supplementary Table 1	169
Supplementary Table 2	170
Supplementary Table 3	171
Supplementary Table 4	172
7.3 Depiction of contribution	173
7.4 Statement of authorship.....	175
7.5 Curriculum vitae.....	176
7.6 Publications and presentations	177
7.7 Acknowledgments.....	178

List of Figures

Figure 1: Adhesion GPCR structure..... 9
Figure 2: Adhesion GPCR modes of function 10
Figure 3: Latrophilin-1 functions in *C. elegans*..... 14
Figure 4: Anatomy of the *C. elegans* reproductive and nervous system..... 16
Figure 5: Notch signaling in the distal *C. elegans* germline. 17

Abbreviations and Acronyms

7TM	Seven transmembrane helices domain
aGPCR	Adhesion G protein-coupled receptor
cAMP	Cyclic adenosine monophosphate
<i>C. elegans</i>	Caenorhabditis elegans
Cas9	CRISPR-associated protein 9
CIRL	Calcium-independent receptor of α-Latrotoxin
CRISPR	Clustered Regularly Interspaced Short Palindromic Repeats
<i>D. melanogaster</i>	Drosophila melanogaster
DAG	Diacyl glycerol
DAPI	4',6-diamidino-2-phenylindole
dCIRL	Calcium-independent receptor of α-Latrotoxin in <i>D. melanogaster</i>
DNA	Deoxyribonucleic acid
DTC	Distal tip cell
EdU	5-ethynyl-2'-deoxyuridine
FBF-1	Fem-3 mRNA binding factor-1
FBF-2	Fem-3 mRNA binding factor-2
FLRT	Fibronectin leucine-rich repeat transmembrane protein
FMI-1	Flamingo homolog of ADGRC group in <i>C. elegans</i>-1
GAIN	GPCR autoproteolysis-inducing domain
GEF	Guanine nucleotide exchange factor
GFP	Green fluorescent protein
GLD-1	Defective in germline development-1
GLD-2	Defective in germline development-2
GLD-3	Defective in germline development-3
GLP-1	Abnormal germ line proliferation-1
GPCR	G protein-coupled receptor
GPR126	G protein-coupled receptor 126
GPS	GPCR proteolysis site
GSA-1	G protein subunit alpha-1
HIM-3	High incidence of males-3
HOA	Sensory neuron of the <i>C. elegans</i> hook sensillum
HOB	Sensory neuron of the <i>C. elegans</i> hook sensillum
HRM	Hormone-binding domain
IP ₃	Inositol triphosphate
LAG-2	Lin-12 and glp-1 phenotype-2
LAT-1	Latrophilin-like protein-1 (also Latrophilin-1)
LAT-2	Latrophilin-like protein-2 (also Latrophilin-2)
LPHN1-3	Mammalian Latrophilin-1/2/3
LST-1	Lateral signaling target-1
mRNA	Messenger RNA

PCA	Sensory neuron type A of the <i>C. elegans</i> post cloacal sensillia
PCB	Sensory neuron type B of the <i>C. elegans</i> post cloacal sensillia
PCC	Sensory neuron type C of the <i>C. elegans</i> post cloacal sensillia
PCR	P olymerase c hain reaction
PH3 antibody	Anti- p hospho- h istone 3 antibody
PKA	P rotein k inase A
PKC	P rotein k inase C
PLC- β	B eta-type p hospholipase C
RACE-PCR	R apid a mplification of c DNA- e nds with p olymerase c hain reaction
RBL	R hamnose- b inding l ectin domain
REC-8	R ecombination abnormal- 8
RNA	R ibonucleic a cid
RNA-Seq	RNA S equencing
SPC	Male-specific sensory neuron associated with copulatory spicules (type C)
SPD	Male-specific sensory neuron associated with copulatory spicules (type D)
SPV	Male-specific sensory neuron associated with copulatory spicules (type V)
SYGL-1	S ynthetic g ermline proliferation defective- 1

1 Adhesion G protein-coupled receptors (aGPCRs)

G protein-coupled receptors (GPCRs) are essential proteins on cell surfaces that are comprised of an extracellular N terminus, a seven transmembrane helices domain (7TM) and an intracellular C terminus. Their name originates from their interaction with intracellular heterotrimeric G proteins, which enables them to transduce extracellular cues into a cell, activating various downstream signaling pathways. Ligands of GPCRs encompass proteins, peptides, sugars, lipids, and even ions or photons.

The class of Adhesion G protein-coupled receptors is considered the second largest class of GPCRs with 33 genes found in the human genome^{1,2}. In 2015, the International Union of Basic and Clinical Pharmacology published a unified nomenclature³, which will be used for mammalian receptors throughout this thesis. Interestingly, despite their abundance and functional relevance in a multitude of physiological processes, such as development⁴⁻⁶, metabolism^{7,8}, immunity^{9,10}, and neurophysiology¹¹⁻¹⁴, aGPCRs remain enigmatic molecules. Most of them are still considered orphan receptors and data on their signaling mechanisms is sparse.

1.1 Roles of Adhesion GPCRs in physiology and pathology

The body of data on the relevance of Adhesion GPCRs is growing rapidly and makes it clear that they are essential in various physiological contexts. It is therefore not surprising that mutations or alterations in expression of these receptors are associated with different pathologies in humans or mammalian model organisms.

There is a striking amount of evidence that places aGPCRs as essential regulators of neurodevelopment, for example in axon tract formation¹¹, synaptogenesis^{12,13} and myelination^{14,15}. Therefore, mutations in aGPCR genes can result in severe neurological diseases, such as bilateral frontoparietal polymicrogyria¹⁶, microcephaly with rhombencephalosynapsis¹⁷ and Usher syndrome type II¹⁸, which are caused by mutated ADGRG1, ADGRL2 and ADGRV1, respectively. There is also evidence for the association of autism spectrum disorders with variants of the receptors ADGRL3 and ADGRB1¹⁹⁻²¹. In addition to functions in the developing nervous system, aGPCRs were shown to ensure correct branching of the embryonic lung and kidney^{4,5}, establishment of the skin^{22,23} as well as the formation of a functioning cardiovascular system^{6,24} and skeletal apparatus²⁵. Findings in *Drosophila melanogaster* (*D. melanogaster*) and *Caenorhabditis elegans* (*C. elegans*) further suggest the evolutionary conservation of developmental functions of these receptors^{26,27}.

However, Adhesion GPCRs have been found to be relevant in a plethora of different physiological contexts beyond their role in development. For example, Latrophilins, ADGRE2, ADGRG1, ADGRG5, and ADGRG6 have been proposed to act as metabotropic mechanosensors²⁸⁻³², ADGRG1 is involved in the regulation of muscle hypertrophy³⁰, ADGRG1 and ADGRL3 seem to be important in beta-cell function of

pancreatic islets^{7,8} and the entire group ADGRE1-5 is expressed in various hematopoietic cells (summarized in ³³) and can influence activation, adhesion and migration of neutrophils out of blood vessels¹⁰.

Many aGPCRs are further associated with different forms of cancer (summarized in ³⁴). To only name a few, ADGRB1 functions as a tumor suppressor and is therefore often mutated or down regulated in malignant tumors^{35,36}, such as glioblastoma^{37,38}, pulmonary adenocarcinoma³⁹ or colorectal cancer⁴⁰. Other connections of Adhesion GPCRs to neoplasia are ADGRG1 in melanoma⁴¹, ADGRG2 in parathyroid tumors⁴² and ADGRC1 to haematopoietic cancers^{43,44}.

This vast entanglement of aGPCRs in physiology and pathology makes them interesting candidates for pharmacological modulation. Unfortunately, the lack of a detailed understanding of Adhesion GPCR signaling greatly hinders progress in this direction. It is therefore inevitable to elucidate this remarkable class of receptors to enable new treatments of aGPCR-associated diseases in the future.

1.2 Unique structural features of Adhesion GPCRs

In order to tap into the pharmacological potential of Adhesion GPCRs, one first needs to understand their structure and mechanisms of function. There are some hallmark features that define Adhesion GPCRs as a unique class of receptors (summarized in ³, Figure 1). One very striking characteristic is the size of their extracellular N termini, which can reach up to 5800 amino acids⁴⁵, harboring a multitude of different domains. Since many of the described domains resemble features found in molecules that are involved in cell-cell and cell-matrix adhesion, the name Adhesion GPCR was coined shortly after the discovery and cloning of the first aGPCR genes^{46,47}. The early suggestion that these domains could bind adhesion molecules and extracellular matrix components and thereby integrate adhesion and cellular signaling was later confirmed by identifying interaction partners such as chondroitin sulfate glycosaminoglycans for the receptors ADGRE2/5^{48,49}, collagens III and IV for ADGRG1/6^{50,51}, laminin for ADGRG6²⁹, integrin receptors for ADGRB1⁵² and ADGRE5⁴⁹, and multiple synaptic adhesion molecules for ADGRL1-3⁵³⁻⁵⁵, respectively.

Despite the enormous complexity in the composition of the extracellular N terminus, some features can be found throughout all members of the aGPCR class. One such hallmark feature is the GPCR proteolysis site (GPS)^{56,57}, which forms the C-terminal portion of the GPCR autoproteolysis-inducing domain (GAIN)⁵⁸. The latter one can induce autoproteolytic cleavage in the GPS, rendering an N-terminal and a C-terminal fragment of the receptor⁵⁹. However, the N-terminal fragment is likely not shed from the rest of the molecule, but rather forms a heterodimeric complex with its C-terminal counterpart⁵⁹. While some aGPCRs need to be cleaved to be functional, some do not require this modification and others are not cleaved at all (summarized in ⁶⁰).

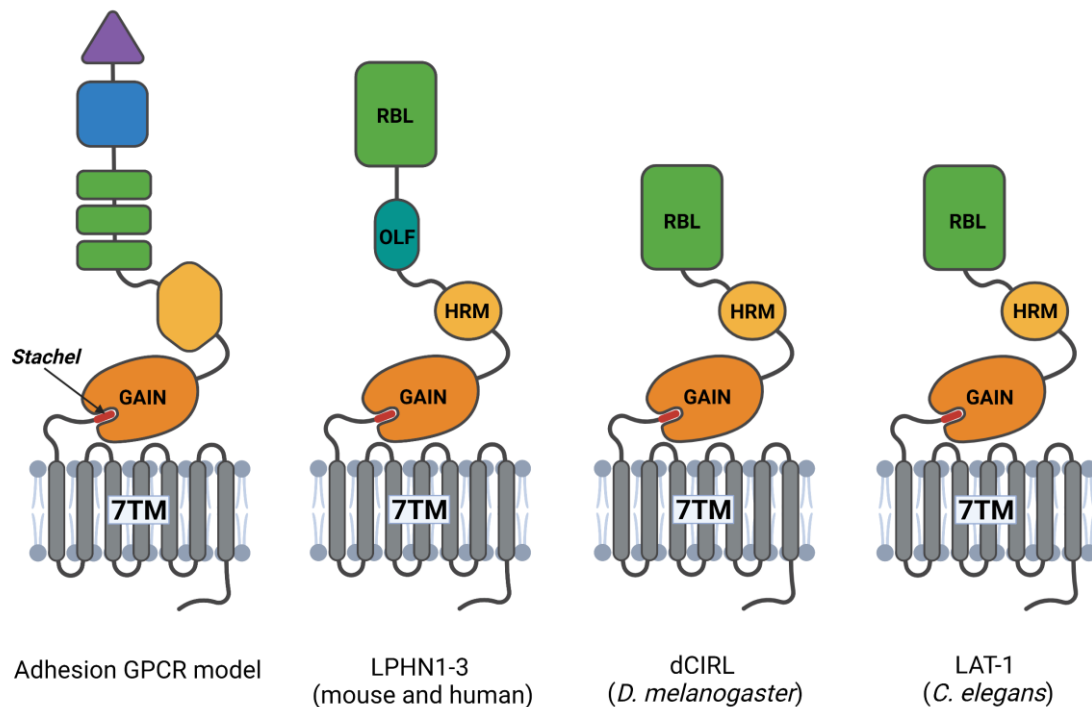


Figure 1: Adhesion GPCR structure. Depicted are a general model of an Adhesion GPCR with a multitude of different domains in its extracellular N terminus and models of Latrophilin homologs in different species. LPHN1-3: mammalian Latrophilin-1/2/3, dCIRL: calcium-independent receptor of α -Latrotoxin in *D. melanogaster*, LAT-1: Latrophilin-1 in *C. elegans*, RBL: rhamnose-binding lectin domain, HRM: hormone-binding domain, GAIN: GPCR autoproteolysis-inducing domain, 7TM: seven transmembrane helices domain. Image created with BioRender.com.

1.3 Mechanisms of Adhesion GPCR function

Being a special class of receptors, it was not surprising when it was found that Adhesion GPCRs also function via unique mechanisms. On the one hand side, they are able to mediate classical GPCR signaling by transducing extracellular cues through their 7TM into the cell (7TM-dependent (*cis*) function), which leads to the activation of G proteins or other downstream effectors (see section 1.3.1, Figure 2). Conversely, it was shown that aGPCRs are also able to function independently of the 7TM and C terminus, solely via their extracellular N termini (7TM-independent (*trans*) function), possibly acting themselves as a cue for other receptors or mediating adhesion (see section 1.3.2, Figure 2).

1.3.1 *Cis* function

The 7TM-dependent *cis* mode of Adhesion GPCRs seems analogous to canonical GPCR signaling in regard to the employed downstream effectors. These include different heterotrimeric G proteins, for example, G_s , $G_{i/o}$, $G_{q/11}$ or $G_{12/13}$ (summarized in ⁶¹). G_s and $G_{i/o}$ enhance or inhibit adenylyl cyclase activity, respectively, and therefore regulate cyclic adenosine monophosphate (cAMP) production and the activation of protein kinase A (PKA). $G_{q/11}$ promotes the generation of inositol triphosphate (IP₃) and diacyl glycerol (DAG) through beta-type phospholipase C

(PLC- β), which subsequently leads to protein kinase C (PKC) activation and calcium ion release from the endoplasmatic reticulum. $G_{12/13}$ mediates its function via guanine nucleotide exchange factors (GEFs) of small G proteins such as Rho. Interestingly, there is also some evidence on aGPCR *cis* signaling mediated by non-G proteins like beta-arrestins⁶².

Unlike downstream effector recruitment, the mechanism underlying aGPCR activation has recently been found to be considerably different from other GPCRs. In 2014, Liebscher *et al.* proposed a model, whereby Adhesion GPCRs harbor a peptide sequence (*Stachel*) C-terminally of the GPS cleavage site (Figure 1), which acts as a tethered agonist for the receptor⁶³. This phenomenon was subsequently found to be a common mechanism employed by multiple Adhesion GPCRs^{32,64–66}.

It is still debated how the *Stachel* peptide is able to activate the receptor, since crystallographic data suggests it to be concealed within the GAIN domain⁵⁸. Because many Adhesion GPCRs undergo autoproteolysis, one mechanism to expose the peptide could be via cleavage of the receptor at the GPS and subsequent detachment of the N-terminal fragment, for example by mechanical force, as has been suggested for ADGRG6²⁹. This model is especially intriguing for Adhesion GPCRs that have been proposed to act as mechanosensors^{28–32}. Conversely, there are some Adhesion GPCRs whose function does not depend on autoproteolytic cleavage (summarized in⁶⁰). An alternative model of how the *Stachel* peptide is revealed would therefore be by conformational changes, as it was proposed for ADGRG5³². Support for this hypothesis came from a recent study that revealed movements within the GAIN domain to regulate *Stachel* peptide exposure⁶⁷.

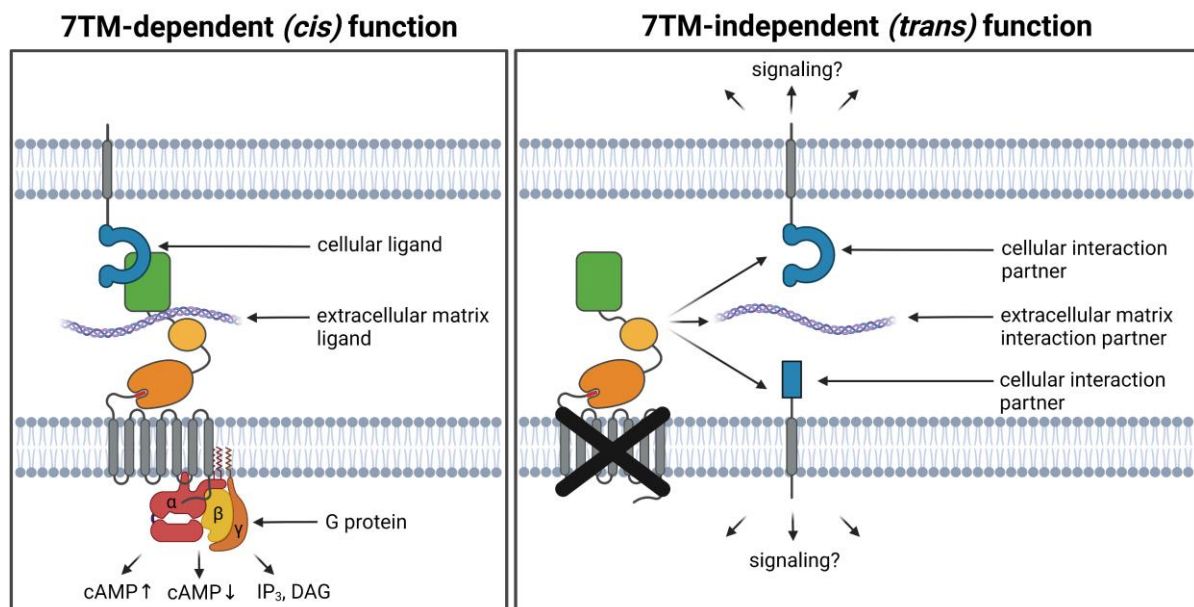


Figure 2: Adhesion GPCR modes of function. Left: *Cis* function is dependent on the interaction of the seven transmembrane helices domain (7TM) with intracellular effectors such as G proteins that activate various downstream pathways. Right: Receptors with deletions in the 7TM are able to fulfil *trans* functions, possibly mediating adhesion or triggering signaling pathways through interaction partners on the same or adjacent cells. cAMP: cyclic adenosine monophosphate, IP_3 : inositol triphosphate, DAG: diacyl glycerol. Image created with BioRender.com.

1.3.2 *Trans* function

One highly intriguing discovery about Adhesion GPCRs was their ability to fulfil some of their functions independently of the 7TM and intracellular C terminus, solely through their extracellular N termini. Since signals cannot be transduced into the cell via the receptor itself in this context, as is the case for *cis* functions, this feature was termed *trans* mode. However, the possible functions of the sole N terminus are not restricted to interactions with molecules on adjacent cells as is implied by “*trans*”, but can possibly also involve extracellular matrix components and molecules located on the same cell. The result of such interactions could be cell-cell/cell-matrix adhesion or the induction of signaling cascades through other receptors. *Trans* functions have been shown to apply to multiple aGPCRs in different species, such as Latrophilins in *C. elegans*⁶⁸, ADGRG6 in mice and its homolog GPR126 in zebrafish²⁴, ADGRE5 and ADGRB1/2 in mice⁶⁹⁻⁷¹, and ADGRG2 in humans⁷², suggesting this to be a common way of functioning for these receptors.

Understanding the mechanisms underlying *trans* functions via *in vitro* studies is difficult, since standard approaches for assessing GPCR function, such as second messenger assays, are not applicable. Therefore, *in vivo* studies must be performed, which can be cumbersome to establish. As a result, data on the effects triggered by *trans* functions on a molecular level are scarce. Furthermore, it can only be speculated whether the N terminus remains connected to the rest of the receptor or is detached when acting in *trans*. Since Adhesion GPCRs are cleaved at the GPS⁵⁹, one could hypothesize the N-terminal fragment to be liberated in order to function independently of its C-terminal counterpart. Another possible mechanism can be deduced from transcriptome and splice variant analyses. There are some Adhesion GPCR variants that would translate to a protein comprising only the N-terminal part of the receptor without a 7TM domain or C terminus^{45,73,74}. The resulting proteins could possibly mediate *trans* functions independently of full-length receptors. Intriguingly, some of these variants also showed tissue-specific expression patterns^{45,73}. Thereby, *trans* functions could also be regulated independently of canonical *cis* signaling by differential expression of certain messenger RNAs (mRNAs).

It is still unclear how sole Adhesion GPCR N termini generated by autoproteolysis or alternative splicing could be implemented into a physiological context. Furthermore, it remains to be answered if the *trans* mode can trigger signaling cascades or is limited to conveying cell-cell or cell-matrix adhesion. To elucidate these topics, further *in vivo* investigations are indispensable.

1.4 Latrophilins as prototypical Adhesion GPCRs

One of the first receptors that have been utilized as models to unravel mechanisms of Adhesion GPCR function are the Latrophilins. Humans and other mammals contain three receptor paralogs ADGRL1-3^{75,76} (Figure 1). ADGRL4 is considered Latrophilin-like due to homology in the 7TM region, but its extracellular domains

greatly resemble the ones of ADGRE1-5³, making functional similarities to Latrophilins unlikely.

The name Latrophilin originates from the observation of ADGRL1 – a Latrophilin homolog in rat – being the target of α -Latrotoxin, which is the main neurotoxin responsible for the effects of black widow spider venom⁷⁷. Hence it was also given the name of calcium-independent receptor of α -Latrotoxin (CIRL)^{75,77}. The neurotoxic effect of α -Latrotoxin results from the formation of a cation channel, which is facilitated by ADGRL1. This in turn leads to calcium influx and neurotransmitter vesicle secretion^{78–80}. However, α -Latrotoxin also leads to cAMP and inositol phosphate accumulation in ADGRL1-transfected cells^{75,77}, indicating a possible second effect via canonical G_s and G_q signaling pathways, the latter of which was later confirmed⁸¹. In the past decade, endogenous ligands of mammalian Latrophilins, namely Teneurins/Lasso⁵⁴, Neurexins⁵³ and Fibronectin leucine-rich repeat transmembrane proteins (FLRTs)⁵⁵ were found.

In the class of Adhesion GPCRs, Latrophilins are considered prototypical due to their high evolutionary conservation (Figure 1)⁸². Therefore, homologs of Latrophilins can be found in a multitude of species, including the nematode *C. elegans* (LAT-1, LAT-2)^{83,84} and the common fruit fly *D. melanogaster* (dCIRL)⁸⁵. Interestingly, the identification of an ancient aGPCR-like molecule in choanoflagellates indicates that precursors of Adhesion GPCRs originated before multicellular life⁸⁶.

Their prototypic qualities make Latrophilins the perfect candidates to study general mechanisms underlying Adhesion GPCR signaling. It is therefore not surprising that important functional hallmarks, such as the GPS or the GAIN domain, have originally been described in members of this group^{57,58}. Latrophilins are also on the frontiers of translational Adhesion GPCR research, as can be seen by first clinical trials investigating the treatment of pediatric asthma using a recombinant human Latrophilin-3 antibody⁸⁷. It is plausible that future investigations of Latrophilins can further enhance our knowledge about the entire class of aGPCRs.

2 The model organism *Caenorhabditis elegans* (*C. elegans*)

The roundworm *Caenorhabditis elegans* (*C. elegans*) was first introduced by Sydney Brenner in 1973⁸⁸ as a model organism to study development and behavior. It was the first multicellular organism, whose genome was fully sequenced⁸⁹ and whose complete cell lineage from the fertilized oocyte to the adult animal could be described^{90,91}. The roundworm has also set a milestone in neurobiological research, since it is the only organism to date in which all neuronal connections – the so-called “connectome” – are known⁹², giving valuable insights into the formation of synapses and neuronal circuits. It is these kinds of major achievements that made *C. elegans* a popular invertebrate model system in the recent years, setting it at the

center of the discovery of a multitude of molecular mechanisms, such as apoptosis⁹³, RNA interference⁹⁴, and the Notch signaling pathway⁹⁵.

Next to its great scientific importance, *C. elegans* also displays some desirable perks when working with it in the laboratory. Most nematodes of a population are hermaphrodites, which are able to produce both sperm and oocytes and yield approximately 250 genetically identical progeny that grow to adulthood within four days, when kept at room temperature⁹⁶. Thereby, homozygous strains are easily maintained in large numbers, allowing for high throughput experiments. There is also a small percentage of worms (0.05%) that lost one of the two X chromosomes due to gonosomal non-disjunction and therefore develop a male phenotype⁹⁷. These can be crossed with hermaphrodites to combine their genetic backgrounds and generate new strains. The nematode is also transparent, which enables researchers to perform microscopy *in vivo*, for example, via the use of fluorescent markers to visualize protein expression and distribution. The thorough characterization of the invariant amount of somatic cells^{90,91} further enables physiological analyses in single cell resolution, which is especially useful when studying neuronal circuits.

In general, one can say that the simplicity of *C. elegans*, combined with its technical advantages and great potential for unravelling molecular details of various physiological processes, render the roundworm a perfect candidate to study basic mechanisms of Adhesion GPCR signaling.

2.1 Physiological functions of Latrophilin-1 (LAT-1) in *C. elegans*

Only three Adhesion GPCRs are known in *C. elegans*, with Latrophilin-like protein-1 (LAT-1) – or in short Latrophilin-1 – being the one that was most extensively studied in the past^{83,84}. The other two aGPCRs are Latrophilin-like protein-2 (LAT-2) and Flamingo (FMI-1), the latter representing a homolog to the ADGRC group in mammals^{83,98}. Adhering to the *C. elegans* nomenclature rules of genes and proteins, *lat-1* is used for the *Latrophilin-1* gene and LAT-1 for the corresponding protein in the following.

It was shown that LAT-1 is needed in the organization of the mitotic spindle along the anterior-posterior axis in the early *C. elegans* embryo (Figure 3)²⁶. In this context, the receptor acts in *cis*, coupling to the G α_s protein GSA-1 to ultimately increase cAMP levels in distinct blastomeres⁶⁵. However, it is yet unclear how this non-directional effect is translated into a cue for polarization. Still, the importance of this function of LAT-1 is stressed by data obtained from mutants homozygous for the null allele *lat-1(ok1465)* (from now on termed *lat-1* mutant). These worms display 70% embryonic or larval developmental arrest and consecutive lethality, likely due to cumulative aberrations in polarity and morphogenesis after the initial defects in spindle orientation²⁶. Additionally to this defect in development, surviving *lat-1* mutants display reduced brood size, suggesting another function of LAT-1 in fertility⁶⁸ (Figure 3). Unpublished data from the Prömel lab further hinted LAT-1 to be

involved in germ cell proliferation as well as apoptosis. These observations can be used as a starting point to understand how LAT-1 regulates fertility in *C. elegans*. Intriguingly, transgenic complementation assays that reintroduced either the whole *lat-1* locus or just the part encoding for the N terminus and the first transmembrane helix, respectively, into *lat-1* mutants showed that the LAT-1 functions in development and fertility are likely realized via different mechanisms (Figure 3). Both, embryonic lethality and brood size defect were ameliorated (also termed “rescued”) by expression of full-length *lat-1*. However, only fertility was rescued in a strain solely expressing the membrane-bound N terminus of the receptor⁶⁸. This suggests a *trans* function of LAT-1 in the reproductive system of *C. elegans* next to the canonical *cis* function in embryonic development. Interestingly, cleavage of the receptor was dispensable for its function in fertility, indicating that liberation of the N terminus through autoproteolysis is not essential in this context⁶⁸. On the other hand, transcriptome analyses using pooled RNA-Sequencing (RNA-Seq) data from multiple sources predicted physiological variants of *lat-1* comprised only of the N terminus⁷⁴, which could mediate *trans* functions. The co-existence of *cis* and *trans* modes of LAT-1 in *C. elegans* renders the nematode the ideal model to study mechanisms of Adhesion GPCRs signaling *in vivo*.

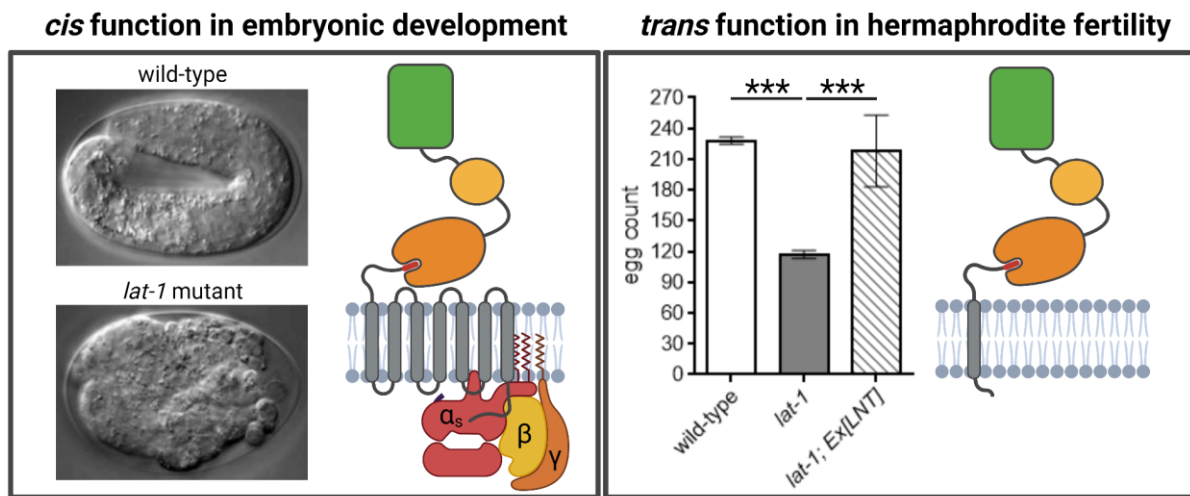


Figure 3: Latrophilin-1 functions in *C. elegans*. Left: *lat-1* mutants display severe embryonic defects²⁶ that can only be ameliorated by expression of a full-length receptor (images adapted from ²⁶). In this context, LAT-1 acts in *cis* by binding the G_s protein GSA-1⁶⁵. Right: Adult *lat-1* mutants (here abbreviated *lat-1*) have a reduced brood size, which can be ameliorated by a construct translating to the N terminus and the first transmembrane domain of the receptor (LNT)⁶⁸, suggesting a *trans* function. n > 90, ***: p < 0.001. Image created with BioRender.com.

While the established phenotypes in lethality and fertility enabled researchers to easily study LAT-1 function in *C. elegans* hermaphrodites, data on physiological relevance of the receptor in male worms is scarce. However, mating experiments using *lat-1* mutant males and wild-type hermaphrodites yield a significantly reduced number of progeny and concomitantly an increased amount of unfertilized oocytes compared to crossings with wild-type males⁶⁸. This suggests a function of LAT-1 in either copulation behavior or sperm function.

A role in sperm generation or maturation could be explained by a function in the gonad, which has been shown to express *lat-1* in the hermaphrodite²⁶. Copulation on the other hand is realized by an intricate system of neuronal circuits and their muscular effector cells. A neuronal function of LAT-1 in copulation would be intriguing, since Latrophilins and their homologs have been shown to have important roles in synaptic function in mammals^{13,99,100} as well as in mechanosensory neurons of *D. melanogaster*^{28,101,102}. Interestingly, there is evidence for neuronal expression of LAT-1 in the hermaphrodite^{26,103,104}, which could also be the case for the male. It would be especially interesting, whether LAT-1 employs *trans* functions, as is the case in the reproductive system of the hermaphrodite, since until now, neuronal functions of Latrophilins were always associated with *cis* signaling^{101,102,105}. Studying neuronal functions of Latrophilins in *C. elegans* could therefore greatly complement the studies performed in other organisms.

2.2 *C. elegans* male copulatory behavior as a model for neurodevelopment and neuronal function

Since this study aims to analyze neuronal functions of LAT-1 in the *C. elegans* male, the following section gives an overview of its nervous system (Figure 4). The establishment of the first connectome – a map that includes all neuron positions and their synaptic connections – was one of the greatest breakthroughs achieved using the roundworm *C. elegans*⁹². Soon after its discovery, the nematode was used in a multitude of studies unravelling general mechanisms of neurotransmission, synaptogenesis, as well as axon and dendrite development (summarized in^{106–108}). The male-specific nervous system in particular caught the eye of many scientists, since the stereotypical male mating behavior was an easy-to-handle physiological readout to study the functions of the required neuronal circuits. There are a distinct number of processes that need to take place for a successful mating between a *C. elegans* male and hermaphrodite. First, the roaming male has to find its partner. This is likely realized via a diffusible cue emitted by the hermaphrodite that can be detected by sensory neurons of the male¹⁰⁹, which are located in the anterior portion of the body, next to the pharynx. Once a male has found a mate and the ray-shaped processes of its tail have made contact to the hermaphrodite's cuticle, a stereotypic response is initiated, regulated by ray sensory neurons¹¹⁰. Thereby, the male starts backward locomotion along the side of the hermaphrodite's body, turning to the other side, when reaching its head or tail. This movement is halted, when the male identifies the vulva via sensory neurons such as HOA and HOB¹¹⁰. To ensure proper sperm transfer, the last step of mating requires the insertion of the male spicules – bilateral sex organs comprised of six cells enclosed within a hardened cuticle – into the hermaphrodite's vulvar opening. The muscles that enable this are innervated by SPC neurons^{110,111}. However, more neurons are needed for maintaining vulvar contact, coordinated spicule positioning and subsequent sperm transfer, such as PCA, PCB, PCC, SPV and SPD^{110–112}.

The thorough understanding of the neuronal circuits underlying copulation and simplicity of the animal makes the *C. elegans* male a suitable candidate for investigating general mechanisms of neuronal function *in vivo* at a rapid speed. Additionally, knowledge about the complete cell lineage and morphogenesis of the nematode enables detailed analyses concerning neuron migration and axon and dendrite formation¹¹³. New insights concerning the organization and function of the nervous system can then be followed up in other organisms, such as mammals, to find evolutionary conserved mechanisms that could complement neuronal functions known to date.

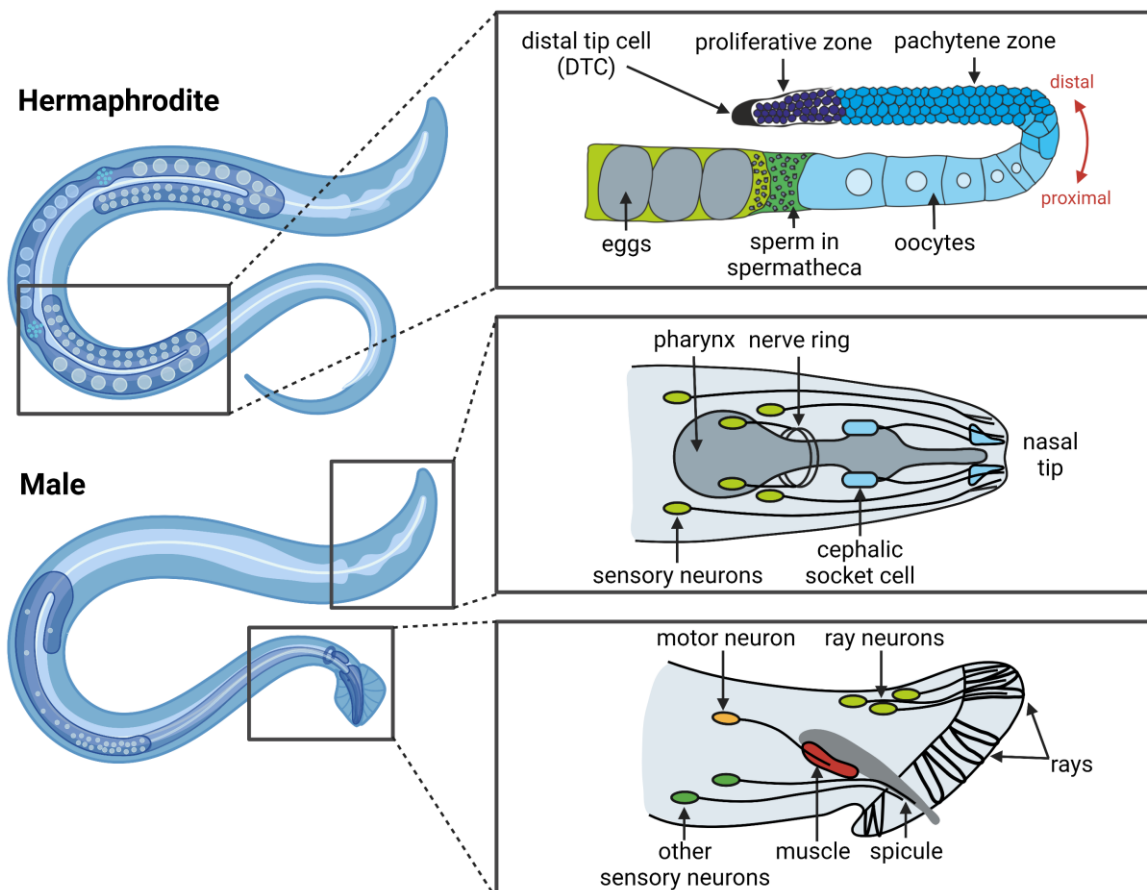


Figure 4: Anatomy of the *C. elegans* reproductive and nervous system. Top: Hermaphrodites contain two identical tubular gonads in which germ cells are organized in a linear fashion. In the most distal part of the gonad, germ cells proliferate (dark blue) and only enter meiosis when losing contact to the distal tip cell (DTC). After being temporarily arrested in the pachytene, germ cells differentiate to oocytes and undergo the remaining meiotic phases. In this region, germ cells are surrounded by gonadal sheath cells (not shown). Meiosis is completed only after fertilization of the oocytes by sperm that are generated during larval development and stored in the somatic spermatheca. Bottom: The nervous system of *C. elegans* males is similar to the hermaphrodite in the head region, harboring a multitude of neurons that extend their dendrites along the pharynx towards the nasal tip. Some of these dendrites are enclosed by processes of neuronal support cells such as the cephalic socket cell. The nerve ring is a complex network located around the pharynx composed of axons and dendrites of various neurons. The male tail contains the copulatory organ (spicule) as well as multiple neurons necessary for mating. Ray-like structures at the tail tip contain dendrites of sensory ray neurons for hermaphrodite recognition. Other sensory neurons, such as HOA or HOB, are essential for finding the vulva. Motor neurons, such as SPC, innervate the muscles relevant for spicule positioning and sperm transfer. Image created with BioRender.com.

2.3 The reproductive system of *C. elegans* hermaphrodites as a model for stem cell biology and Notch signaling

LAT-1 function in *C. elegans* hermaphrodite fertility could originate in the gonad, which was shown to highly express *lat-1*²⁶. The *C. elegans* reproductive system was intensely studied in the past decades and this section shortly sums up the most important anatomical and functional features of both the somatic gonad and the germ cells (Figure 4). General anatomy and physiology is summarized in ^{114–117}. Hermaphroditic nematodes contain two tubular U-shaped gonads. During larval stages of *C. elegans* the gonads are programmed to produce a fixed number of sperm, which are then stored in an organ called the spermatheca. In adults, gamete production is then switched to oocytes and seizes only, when all sperm from the spermatheca have been used for fertilization. Concerning the gonadal structure, germ cells are located in the center of the tube, surrounded by somatic cells that form plexus-like protrusions to enclose single germ cells and on the other hand limit the gonad to the body cavity. The somatic cell capping the end of the gonad is aptly called distal tip cell (DTC) and the others gonadal sheath cells. The germ cells within the tube undergo the stages of mitosis and meiosis as they wander from the distal towards the proximal end of the gonad. The specific stages of mitosis/meiosis can be easily defined via morphology of germ cell nuclei or certain stage markers, such as REC-8 and HIM-3, which show the transition from mitosis to meiosis^{118,119}. The proliferative zone lies at the distal end of the gonad, where germ cells cycle through mitotic divisions. This zone is in part considered to be a stem cell pool and is controlled by Notch signaling (Figure 5). In particular, the Notch ligand LAG-2 on the DTC activates the Notch receptor GLP-1 on the germ cells^{120,121}, which leads to expression and translation of LST-1 and SYGL-1 in distal germ cells¹²². These direct targets of Notch signaling cooperate with the RNA-binding proteins FBF-1 and FBF-2 to suppress various other pathways^{123–125}. The most intensively studied targets of the resulting regulatory effects are GLD-1, which is an inhibitor of proliferation^{126,127}, and GLD-2/3, which function as initiators of meiotic fate^{128,129}.

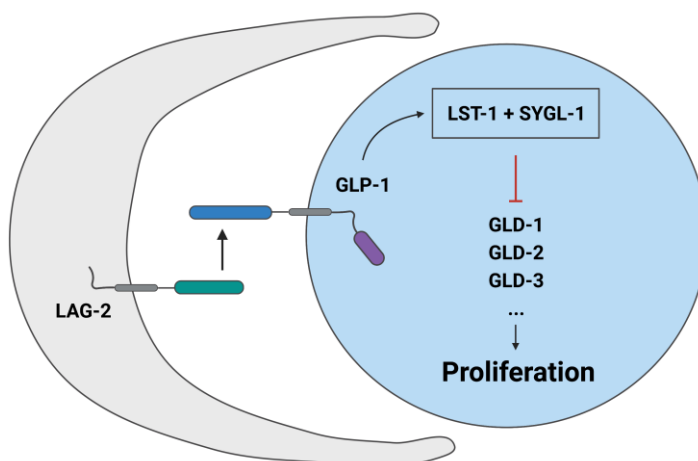


Figure 5: Notch signaling in the distal *C. elegans* germline. The Notch ligand LAG-2 on the distal tip cell (DTC) activates the Notch receptor GLP-1 on germ cells^{120,121}, which leads to expression and translation of the direct Notch targets LST-1 and SYGL-1¹²². These in turn repress various anti-proliferative (e.g. GLD-1)^{126,127} and meiosis-promoting (e.g. GLD2/3)^{128,129} effectors, ultimately upholding the proliferative fate of germ cells in the distal germline. Image created with BioRender.com.

With increasing distance from the DTC – i.e. in more proximal parts of the gonad – Notch signaling decreases and germ cells are able to enter meiotic prophase I, temporarily arrest in pachytene, differentiate to oocytes and complete meiotic divisions. During ovulation, oocytes are being pushed through the spermatheca by rhythmic contractions of the gonadal sheath cells and can then be fertilized by sperm. The fertilized oocytes are flushed into the uterus, where they form an egg shell, undergo first embryonic divisions and are then laid as eggs through the vulva. Containing all stages from stem cell to differentiated gamete in a linear organization makes the *C. elegans* gonad an excellent model to study the physiology of stem cells, the cell cycle and cues that affect the decision between proliferation and meiotic entry such as the Notch pathway. Since the latter is an evolutionary conserved mechanism for stem cell maintenance (summarized in ^{130,131}) and mutations of Notch pathway components are found in a multitude of human cancers (summarized in ¹³²), identifying new regulators will be essential for future medical and pharmacological research. Interestingly, there is evidence that Adhesion GPCRs can crosstalk with Notch¹³³, which renders them promising targets in drug development. However, data on the mechanisms underlying the interaction of aGPCRs and components of the Notch pathway is scarce, which hinders progress in this direction. *C. elegans* has already been a linchpin in stem cell and Notch research in the past and would therefore also be an ideal system to elucidate the relationship of Notch and aGPCR signaling.

3 Aim of this study

The class of Adhesion GPCRs has been found to have a multitude of important roles in mammalian physiology and is associated with severe human pathologies, many of which affect the nervous system. Despite their obvious relevance, knowledge about aGPCR signaling is rare. While there is a growing body of data concerning 7TM-dependent (*cis*) functions, molecular mechanisms of 7TM-independent (*trans*) functions remain elusive. Since the latter possibly involve interactions with adjacent cells or extracellular matrix, *in vivo* analyses are indispensable to gain new insights. The Latrophilin homolog LAT-1 in the roundworm *C. elegans* presents a prototypic Adhesion GPCR with a known *trans* function in hermaphrodite fertility and, therefore, an ideal model to study this enigmatic mechanism *in vivo*.

There is preliminary evidence for a function of LAT-1 in the *C. elegans* male, which could originate from neurons. Since previously published neuronal functions of Latrophilins have always been associated with *cis* signaling, it would be intriguing to see whether LAT-1 acts in *cis* or *trans* in the *C. elegans* nervous system. Hence, the following goals will be addressed in the first part of this study:

1. Generate a detailed expression map of *Latrophilin-1* in the *C. elegans* male.
2. Elucidate whether the physiological role of Latrophilin-1 in the *C. elegans* male indeed involves neuronal functions.
3. Discover whether LAT-1 acts in *cis* or *trans* in this context.

Trans functions have been shown to be exerted by multiple Adhesion GPCRs in different contexts. However, it is still unknown if this mechanism indeed affects adjacent cells, if the receptor N terminus can act independently of full-length proteins and if signaling cascades can be activated in this way. The known *trans* function in *C. elegans* hermaphrodite fertility poses an ideal model to elucidate these questions *in vivo*. Therefore, the second part of this study will address the following goals:

1. Generate a detailed physiological model of the LAT-1 *trans* function in the hermaphrodite's gonad.
2. Define whether the receptor influences the same cells it is expressed on or acts non-cell autonomously.
3. Elucidate whether the splice variant repertoire of *lat-1* contains N-terminal variants capable of fulfilling *trans* functions.
4. Unravel whether LAT-1 *trans* function induces the activation of signaling cascades and define possible downstream effectors.

In summary, the experiments presented in the following are to lay the groundwork for elucidating *trans* functions of Adhesion GPCRs and will hopefully facilitate further research in this intriguing field, possibly even leading to first approaches to tap into the pharmacological potential of these receptors.

4 Publications and manuscripts

4.1 Latrophilin-1 drives neuron morphogenesis and shapes chemo- and mechanosensation-dependent behavior in *C. elegans* via a *trans* function

Authors: Daniel Matúš, Willem Berend Post, Susanne Horn, Torsten Schöneberg, Simone Prömel

Journal: Biochemical and Biophysical Research Communications

Impact Factor: 3.575

Submitted: 9 Oct 2021

Accepted: 2 Dec 2021

Published: available online: 5 Dec 2021, print article available: 22 Jan 2022

References: 39

Language: English

Publisher: Elsevier

PubMed ID: 34922196

DOI: <https://doi.org/10.1016/j.bbrc.2021.12.006>

TITLE

Latrophilin-1 drives neuron morphogenesis and shapes chemo- and mechanosensation-dependent behavior in *C. elegans* via a *trans* function

AUTHORS

Daniel Matúš¹, Willem Berend Post^{1,3}, Susanne Horn¹, Torsten Schöneberg¹, Simone Prömel^{3*}

AFFILIATIONS

¹Rudolf Schönheimer Institute of Biochemistry, Medical Faculty, Leipzig University, 04103
Leipzig, Germany

³Institute of Cell Biology, Department of Biology, Heinrich Heine University Düsseldorf,
40225 Düsseldorf, Germany

CONTACT INFORMATION

*Correspondence: proemel@uni-duesseldorf.de

ABSTRACT

Latrophilins are highly conserved Adhesion GPCRs playing essential roles in the mammalian nervous system and are associated with severe neurological disorders. Recently, it has been shown that murine Latrophilins mediate classical G-protein signals to drive synaptogenesis. However, there is evidence that Latrophilins in *Caenorhabditis elegans* can also function independently of their seven-transmembrane domain and C terminus (*trans* function). Here, we show that Latrophilin-1 acts in *trans* to mediate morphogenesis of sensory structures in the *C. elegans* nervous system. This *trans* function is physiologically relevant in copulation behavior. Detailed expression and RNA-Seq analyses revealed specific LAT-1-positive neurons and first insights into the genetic network that is modulated by the receptor function. We conclude that 7TM-independent functions of Latrophilins are essential for neuronal physiology, possibly complementing canonical functions via G protein-mediated signaling.

INTRODUCTION

Adhesion G protein-coupled receptors (aGPCRs) have essential functions in the nervous system, such as in myelination [1, 2], axon tract formation [3], and synaptogenesis [4, 5]. Mutations in aGPCRs can result in severe neurological pathologies like bilateral frontoparietal polymicrogyria [6], Usher syndrome type II [7], and microcephaly with rhombencephalosynapsis [8]. Furthermore, certain variations of LPHN3/ADGRL3 lead to a pre-disposition to autism spectrum disorders [9]. Despite their relevance, data on aGPCR signaling are rare. One group of aGPCRs with essential functions in the nervous system of various species, which can be considered prototypic representatives of the aGPCR class due to their evolutionary age, are Latrophilins. In mice, LPHN2/ADGRL2 and LPHN3/ADGRL3

induce synaptogenesis in the cerebellum [4] and the hippocampus [5], in the latter by activating canonical G protein signals [10]. Furthermore, the Latrophilin homolog dCIRL in *Drosophila melanogaster* mediates neuronal mechanosensation via G proteins [11]. While there is evidence for neuronal expression of the Latrophilin homolog LAT-1 in the nematode *Caenorhabditis elegans* [12, 13], physiological functions of the receptor in neurons are still unknown.

Here, we explored the conservation of neuronal Latrophilin functions in *C. elegans* males. Previous data suggested a function of LAT-1 in this sex [14], but the underlying processes remain elusive. We show that LAT-1 is expressed in a multitude of neurons, indicating a plethora of possible neuronal functions. Transcriptome analyses of *lat-1* mutants suggest that the receptor is involved in neurodevelopment, mechanosensation, and copulation behavior. More detailed analyses found LAT-1 to modulate the morphogenesis of male sensory rays and head sensillia. Intriguingly, these functions are mediated by the sole LAT-1 N terminus, suggesting a non-canonical *trans* function. This *trans* function, which has also been shown previously to play a role in fertility [14], influences copulation behavior. We present *C. elegans* as a valuable model to understand the complex involvement of Latrophilins in the nervous system and how *trans* functions could complement established G protein-dependent signaling of aGPCRs in vertebrates.

RESULTS

LAT-1 is expressed in multiple neurons and neuronal support cells of male *C. elegans*

To obtain a detailed expression map of *lat-1* in neurons of the *C. elegans* male we used a *lat-1p::GFP* transcriptional reporter co-expressing the NeuroPAL marker (Supplementary Table 1, Fig. 1A) and identified individual neurons [15]. In the head, we found LAT-1-

positive motor neurons, interneurons and various sensory neurons (Fig. 1B-C, Supplementary Table 1). Among these were ADL, ASI, ASK, AWA, AWC, and URY neurons, which mediate sexual attraction during copulation [16]. We also identified the non-neuronal cephalic socket (Fig. 1D) and sheath cells (Supplementary Fig. 1A).

In the midbody, *lat-1* was present in ventral nerve cord neurons, and in the mechanosensory ALM and AVM neurons (Supplementary Fig. 1B, C, Supplementary Table 1). In the tail, we found LAT-1-positive neuronal cells relevant for copulation behavior [16]: ray neurons (Fig. 1E-G), the sensory neurons HOB (Fig. 1H, I), PQR, PHA, and PHD (Supplementary Fig. 1D, E, Supplementary Table 1), which are essential for hermaphrodite sensing via mechano-/chemosensory cues. LAT-1 was also in PCA, PCB, PDC, PVY, SPC, SPD, and SPV, which coordinate sensory perception and motor function during mating (Supplementary Fig. 1F, G; Supplementary Table 1). The mechanosensory PLM and DVA neurons also strongly expressed *lat-1* (Fig. 1E, G, Supplementary Fig. 1H, I), but have no reported function in mating. *lat-1* was not detected in neuronal support cells of the tail. However, the anal depressor muscle was LAT-1-positive (Fig. 1H), which regulates spicule protraction together with the SPC neuron [17].

In summary, the *lat-1* expression profile suggests different functions in *C. elegans* males and hints towards a role of the receptor in copulation.

Transcriptome analyses suggest LAT-1 involvement in neurodevelopment, mechanosensation and copulation behavior

We performed transcriptome analyses by RNA-Seq on *lat-1(ok1465)* null-mutant adult males to identify significantly regulated genes (Supplementary Table 2). Subsequent enrichment analyses determined cells, phenotypes and Gene Ontology (GO) terms overrepresented among these genes (Supplementary Table 3). In an effort to separate general

and male-specific functions, additional analyses were performed, only using regulated genes enriched in males/expressed in male cells.

While upregulated genes gave no significant results, we identified neuronal/muscular cells among downregulated genes (Fig. 2A). In the subset of male-associated genes, neurons were more prominent (Fig. 2B). Most overrepresented phenotypes were associated with body morphology, locomotion and copulation (Fig. 2A). When analyzing male-associated genes, more phenotypes concerning copulation, locomotion, and neurodevelopment emerged (Fig. 2B). Significantly overrepresented GO terms featured ion homeostasis, extracellular/cytoskeletal filaments, metabolism, and neurodevelopment, the latter being represented more prominently in male-associated genes (Supplementary Table 3).

As expression analyses did not reveal many muscular cells expressing *lat-1*, we investigated whether genes supporting muscle cell overrepresentation were also expressed in neurons. Over 50 % of male-associated genes seemed neuron-specific and most of the remaining genes were expressed in both investigated cell types (Fig. 2C, Supplementary Table 4). A mainly neuronal LAT-1 function is therefore possible.

We further evaluated known functions of overrepresented neuronal cells. These comprised mainly neurodevelopment, locomotion, sensory functions (mostly mechanosensation), mating, and neuromodulation (Fig. 2D, Supplementary Table 5).

These findings suggest a role of LAT-1 in the *C. elegans* male nervous system, likely influencing neurodevelopment, locomotion, mechanosensation, and copulation.

LAT-1 exerts a 7TM-independent (*trans*) function in head sensillum and ray morphogenesis

As transcriptome analyses suggested a role for LAT-1 in neurodevelopment, we screened *lat-1*-mutant adult males for neuronal defects and identified severe morphological aberrations in sensory head sensillia and tail rays (Fig. 3A-D).

lat-1-mutant males showed dysmorphic, crude/shortened head dendrites. Socket cell processes did not exhibit a triangular shape as in wild-types (Fig. 3A, C). In the tail, *lat-1* mutants displayed dysmorphic ray structures (Fig. 3B, D). These defects were ameliorated in a *lat-1*-mutant strain expressing solely the membrane-tethered LAT-1 N terminus (LNT) (Fig. 3A-D), indicating a 7TM-independent (*trans*) function. Furthermore, the nerve ring of *lat-1* mutants was shifted anteriorly (Fig. 3E, F), which was not rescued by LNT expression. We did not observe axon migration defects along the ventral nerve cord (Fig. 3G), as was previously shown for mutants of the *C. elegans* aGPCR *fmi-1* [18].

These data suggest 7TM-dependent and 7TM-independent neuronal functions of LAT-1. The identified defects in *lat-1* mutants may be relevant for male copulation behavior.

The 7TM-independent (*trans*) function of LAT-1 is essential for male copulation behavior

To study a potential role of LAT-1 in mating, we determined copulation success by assessing sperm transfer to hermaphrodites. *lat-1* males showed a significant decrease in successful copulations with wild-type hermaphrodites compared to wild-type controls (Fig. 4A).

Male copulation behavior and the involved neurons are well studied [19]. The male is attracted to the hermaphrodite by pheromones. Once physical contact is established, chemo-/mechanosensory stimuli lead to hermaphrodite recognition by the male rays. Subsequently, the male initiates backward locomotion. Upon vulval contact, a complex neuronal network leads to halting, spicule insertion and sperm transfer.

Detailed behavioral analyses showed that *lat-1*-mutant males took longer to locate mates and spent less time copulating (Fig. 4B, C). They required significantly more hermaphrodite contacts to initiate copulatory behavior (Fig. 4D, E) and after backwards locomotion was initiated, *lat-1*-mutant males were defective in identifying the vulva, as seen by more vulva passes before attempting spicule insertion (Fig. 4F) and reduced vulval contact time (Fig.

4G). These defects were ameliorated by transgenic complementation of LNT (Fig. 4B-G), confirming a *trans* function. We also measured spicule protraction. While Oxotremorine M, a synthetic agonist of muscarinic acetylcholine receptors, induced spicule protraction in the majority of wild-type worms, *lat-1* males responded at significantly lower levels (Fig. 4H). This phenomenon was also rescued by the LNT.

Taken together, these data suggest that the *trans* function of LAT-1 is involved in multiple steps during copulation, which resonates with its vast neuronal expression profile (Fig. 1).

DISCUSSION

The involvement of Adhesion GPCRs and especially Latrophilins in the nervous system is highly interesting from a medical point of view since mutations in several receptors are associated with severe neurological and psychiatric pathologies [6-9]. Latrophilins mediate synaptogenesis in mammals [4, 5] via canonical G protein (*cis*) signaling [10]. Here, we show that the *C. elegans* homolog LAT-1 exerts 7TM-independent (*trans*) functions in the nervous system.

The broad neuronal expression of *lat-1* in the *C. elegans* male suggests that LAT-1 is relevant in the general organization of the nematode's nervous system, not only in certain specific circuits. Many of the identified neurons also show *lat-1* expression in the hermaphrodite [12], indicating possible sex-shared functions. However, although NeuroPAL [15] enabled precise neuron identification, cells harboring very low *lat-1* levels might not be identified. We also observed *lat-1* expression in cephalic sheath and socket cells forming the cephalic sensillum with CEM and CEP dendrites. Surprisingly, these neurons were LAT-1-negative. However, CEM was overrepresented in enrichment analyses, indicating transcriptional changes specific to this neuron. Additionally, we observed the *trans* function

of LAT-1 to influence socket cell morphogenesis. These data suggest a function of the aGPCR in the cephalic sensillum, possibly influencing CEM neurons by determining socket cell morphology and/or function. Interestingly, the anal depressor muscle expresses *lat-1*, leaving the possibility of a muscular LAT-1 function. However, the muscle is not essential for copulation [20]. A mainly neuronal function of LAT-1 is further supported as almost 100 % of male-associated genes dysregulated in *lat-1* mutants were expressed in the nervous system, while only half showed expression in muscle cells.

Enrichment analyses gave some indication for LAT-1 to be involved in neurodevelopment and copulation behavior, both of which were supported by physiological data. Dendrite morphogenesis depends on the interaction of neurons and extracellular matrix components [21]. It is conceivable that the LNT engages in such interactions, e.g. as a scaffold arranging cell-matrix adhesion. Defects in ray morphogenesis are mostly caused by alterations in ray structural cells or the adjacent hypodermis [22, 23]. However, correct positioning and morphogenesis of ray neurons also impacts ray morphology [24]. In *lat-1* mutants, ray morphology is altered, but expression of *lat-1* is only present in sensory ray neurons and not in surrounding tissues. This could indicate a non-cell autonomous function of LAT-1, influencing ray structural cells from adjacent neurons. Our transcriptome analyses revealed many genes as possible targets of LAT-1 function in neuron morphogenesis. Of these, PLX-2 and UNC-27 have been associated with ray morphogenesis [25, 26] and UNC-7 as well as UNC-55 were proposed to influence mating behavior [27, 28].

Guided by expression and RNA-Seq analyses we chose mating behavior as a physiological readout for LAT-1 function. We showed that LAT-1 acts in *trans* in multiple steps of copulation, which is in line with its vast neuronal expression profile. Defective sensing of the hermaphrodite and its vulva in *lat-1* mutants is especially intriguing, since it plausibly correlates with morphological defects we observed. LAT-1 seems to act *in trans* in several

contexts studied here. Although a LAT-1 *trans* function has been shown in fertility [14], this finding is intriguing, as previous neuronal functions of Latrophilins have consistently been associated with G protein-dependent signaling cascades and thus, with *cis* function [10, 11, 29]. As LAT-1 function in early embryonic development of *C. elegans* also entails *cis* signaling [30], it is unlikely that neuron morphology alterations in *lat-1* mutants result from defects in the embryo. However, the receptor could exert other canonical G protein-dependent functions, e.g. in nerve ring development. It would be intriguing to know whether Latrophilin *cis* functions in synaptogenesis or modulation of mechanosensory stimuli [10, 11] are evolutionary conserved and also present in *C. elegans*. A role of LAT-1 in mechanosensation surpassing the *trans* function in neurodevelopment is plausible considering the amount of LAT-1-positive mechanosensory neurons. The nature of the *trans* function and whether it involves signaling and/or adhesion remains to be determined.

Our work shows that Latrophilins have functions in *C. elegans* neurons. It presents insights into physiologically relevant *trans* functions of these receptors, which could complement canonical *cis* signaling.

MATERIALS AND METHODS

C. elegans maintenance and strains

C. elegans strains were maintained according to standard protocols [31] on *E. coli* OP50 at 22°C unless stated otherwise. For male generation, mixed populations were shifted to 34°C for 2 hours [31]. Strains used in the study are listed in Supplementary Table 6.

Generation of transgenic C. elegans lines

Transgenic strains were generated by DNA microinjection performed by NemaMetrix Inc. (Eugene, Oregon, USA). Injection mixes contained 1 ng/μl of a cosmid carrying the genomic locus of *lat-1* with a GFP after amino acid 581 and a subsequent stop codon (pTL20 [14]), 30 ng/μl *myo-2p::mCherry*-containing pPD118.33 (kind gift of Ralf Schnabel), and 89 ng/μl pBluescript II SK+ (Stratagene). Multiple independent transgenic lines were established.

Transcriptome (RNA-Seq) and enrichment analyses

Total RNA was extracted from 250 wild-type/*lat-1*-mutant *C. elegans* males in 5 samples (50 worms each) in TRIzol (ThermoFisher) following the manufacturer's protocol. Indexed cDNA libraries with an average insert size of 300 bp were constructed using the SMARTer Stranded Total RNA-Seq Kit v2 – Pico Input Mammalian (Takara) following the manufacturer's protocol with rRNA depletion. Paired-end sequencing of the samples was performed by Macrogen Europe using the NovaSeq6000 platform.

Mapping of raw data to the *C. elegans* genome wbps14 was performed using hisat2 2.1.0 [32] (Supplementary Table 7). Wild-type aliquot #5 was excluded based on low mapping percentage. Gene expression in fragments per kilobase per million mapped reads (FPKM) was obtained using stringtie v2.1.3b [33] based on transcript annotations in caenorhabditis_elegans.PRJNA13758.WBPS14.annotations.gff3 files. For shell scripts for

mapping (go.sh) and quality control (collect_stats.sh) see Supplementary files. Raw data can be accessed at the NCBI database (accession: PRJNA768843).

Enrichment analyses of significantly regulated genes ($p < 0.05$) were done using the WormBase Enrichment Tool ($q \leq 0.1$) [34, 35]. Male-associated genes were defined by being listed under the term “male” (WBbt:0007850) in WormBase. Characterization/categorizing of overrepresented terms was performed using information provided on Wormbase (WS280) and WormAtlas (<http://www.wormatlas.org>).

Neuron/ray morphology analyses

Z-stacks of 24 hours post-L4 males expressing *lat-1(ok1465);qaIs7524[lat-1p::GFP::lat-1+rol 6(su1006)]* were analyzed for neuronal defects: (1) severe (ectopic dendrite position, grossly dysmorphic dendrites, missing terminal differentiation of the cephalic socket cell), (2) moderate (slight dendrite/socket cell dysmorphia), (3) wild-type morphology. Ray morphology was analyzed on DIC images. Defects were defined as follows: (1) severe (abnormally thick/very short/dysmorphic/crooked or missing rays), (2) moderate (slightly shortened/crooked rays) and (3) wild-type morphology.

Analyses of copulation efficiency

L4 males were isolated for 24 hours, stained with 10 μ M MitoTracker Red CM-H2XRos (ThermoFisher) in M9 for 2 hours (dark) and left overnight to recover on *E. coli* OP50. 15 stained males and 15 anesthetized hermaphrodites (300 μ M levamisole, 30 minutes) were mated on a 5 μ l spot of *E. coli* OP50. Every hour, hermaphrodites containing MitoTracker-labelled sperm were counted.

Detailed analyses of copulation behavior

Male copulation behavior was assessed as previously described [36]. 15 *unc-64(e246)* 24 h-post-L4 hermaphrodites were incubated for 1 hour on plates with 5 μ l *E. coli* OP50. Single age-matched males were added and recorded for 10 minutes or until insemination. Characteristic stages of male mating behavior were analyzed [19]: (1) time until first copulation (time until initiation of male backwards locomotion), (2) copulation time (time the male displays copulation behavior/entire observation period), (3) contacts until copulation (physical male-hermaphrodite contacts until initiation of backwards locomotion), (4) successful male-hermaphrodite contacts (contacts leading to copulation behavior/all observed contacts), (5) mean vulva passes (times males passed the vulva midline/times they stopped and attempted spicule insertion during the entire observation period) and (6) time at vulva (time attempting spicule insertion/ copulation time).

Spicule protraction assay

For a standardized readout of spicule protraction, we adapted previously established protocols [37]. 20-40 24 h post-L4 males were placed in 31.5 μ L of water on a 2% agarose pad. 3.5 μ l 100 μ M Oxotremorine M or water (negative control) was added to induce spicule protraction. A coverslip was gently lowered onto the drop and protracted spicules were immediately assessed.

Microscopy

The following microscopes and settings were used. Confocal fluorescence imaging: LASX software on a Leica SP8 microscope (Z-stack spacing 0.3-0.5 μ m). Previously described settings were applied for NeuroPAL imaging [15]. DIC imaging of ray morphology: Leica SP8, LASX software. Spicule protraction/copulation behavior: Leica M165FC. Video

recordings: Leica EC3 camera and LAS EZ software. Images/videos were evaluated using Fiji [38] or VLC media player. Neuron mapping was performed on multiple worms according to existing guidelines [15, 39].

Statistical analyses

Numerical assay data were analyzed using GraphPad Prism version 7.0. For normally distributed data, a two-tailed Student's t-test or two-way ANOVA/Bonferroni post-hoc test were employed for comparing two/multiple groups, respectively. Categorical data was examined by Fisher's exact test. Significantly regulated gene products in RNA-Seq analyses were defined by a two-sided Wilcoxon rank test. Statistical levels were: * $p < 0.05$, ** $p < 0.01$, *** $p < 0.001$, n.s. = not significant.

ACKNOWLEDGEMENTS

The authors thank Ralf Schnabel for kindly providing plasmids and Rene Garcia and Oliver Hobert for generously sharing *C. elegans* strains.

This work was supported by grants from the Deutsche Forschungsgemeinschaft (DFG, German Research Foundation) through CRC 1423 (project number 421152132, C04 (S.P., T.S.)) and FOR 2149 (project number 246212759, P02 (S.P.) and P04 (T.S.)).

AUTHOR CONTRIBUTIONS

D.M., S.P. conceived/designed the study and experimental approaches. D.M., W.P. carried out experiments. D.M., S.H., T.S. analyzed the RNA-Seq data, D.M., S.P. wrote the manuscript.

COMPETING INTERESTS

The authors declare no competing interests.

FIGURES AND FIGURE LEGENDS

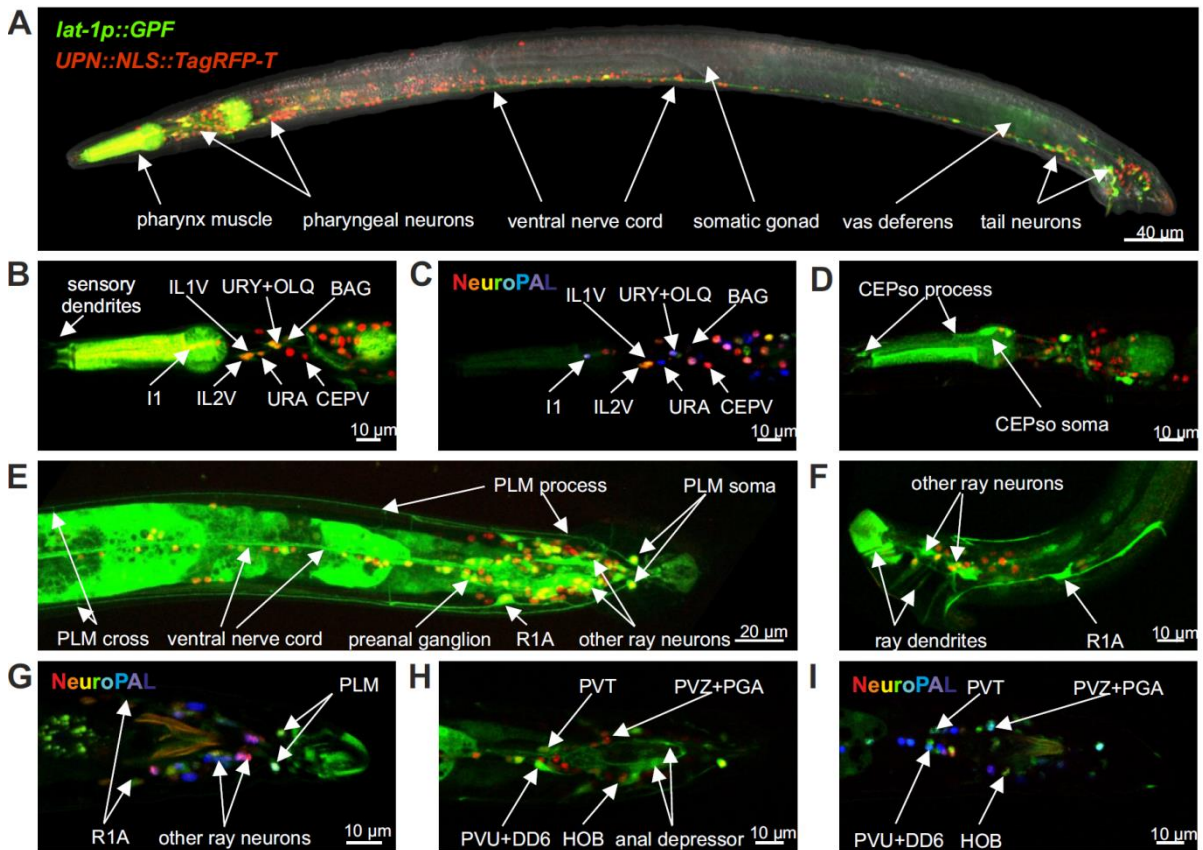


Figure 1: *C. elegans* male neurons expressing *lat-1*. Neurons (positive for pan-neuronal TagRFP-T) were assessed for *lat-1p::GFP* expression (A, B, E, F, H). Neuron types were identified using the NeuroPAL color code (C, G, I) [15, 39]. (A) overview; (B-D) lateral head; (E, G): dorsal tail; (F): lateral tail; (H, I): ventral tail. For additional images see Supplementary Figure 1, for all identified neurons see Supplementary Table 1. Non-neuronal cells expressing *lat-1*: pharynx muscle, reproductive system (A), cephalic socket cells (D).

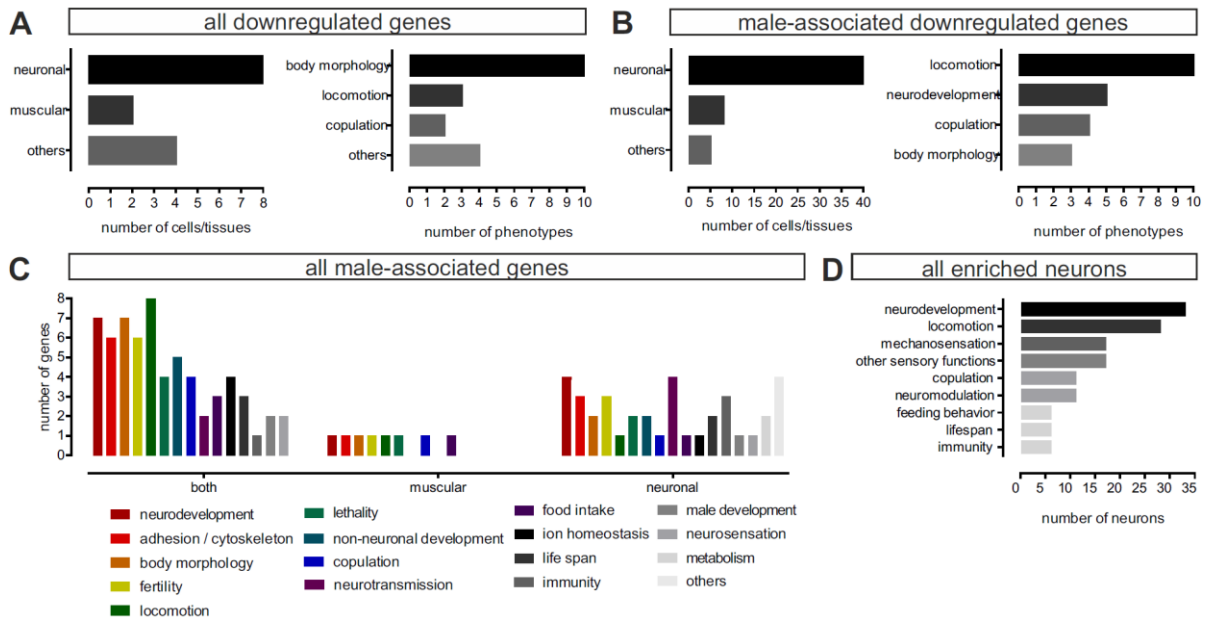


Figure 2: Enrichment analyses of *lat-1* mutants. (A, B) Summary of overrepresented terms among significantly downregulated transcripts of *lat-1* mutants compared to wild-type worms ($n = 250$, 5 aliquots). For details see Supplementary Tables 2 and 3. (C) Functions/expression profiles of male-associated genes. For details see Supplementary Table 4. (D) Functions of neurons identified during enrichment analyses according to WormBase (WS280). For details see Supplementary Table 5.

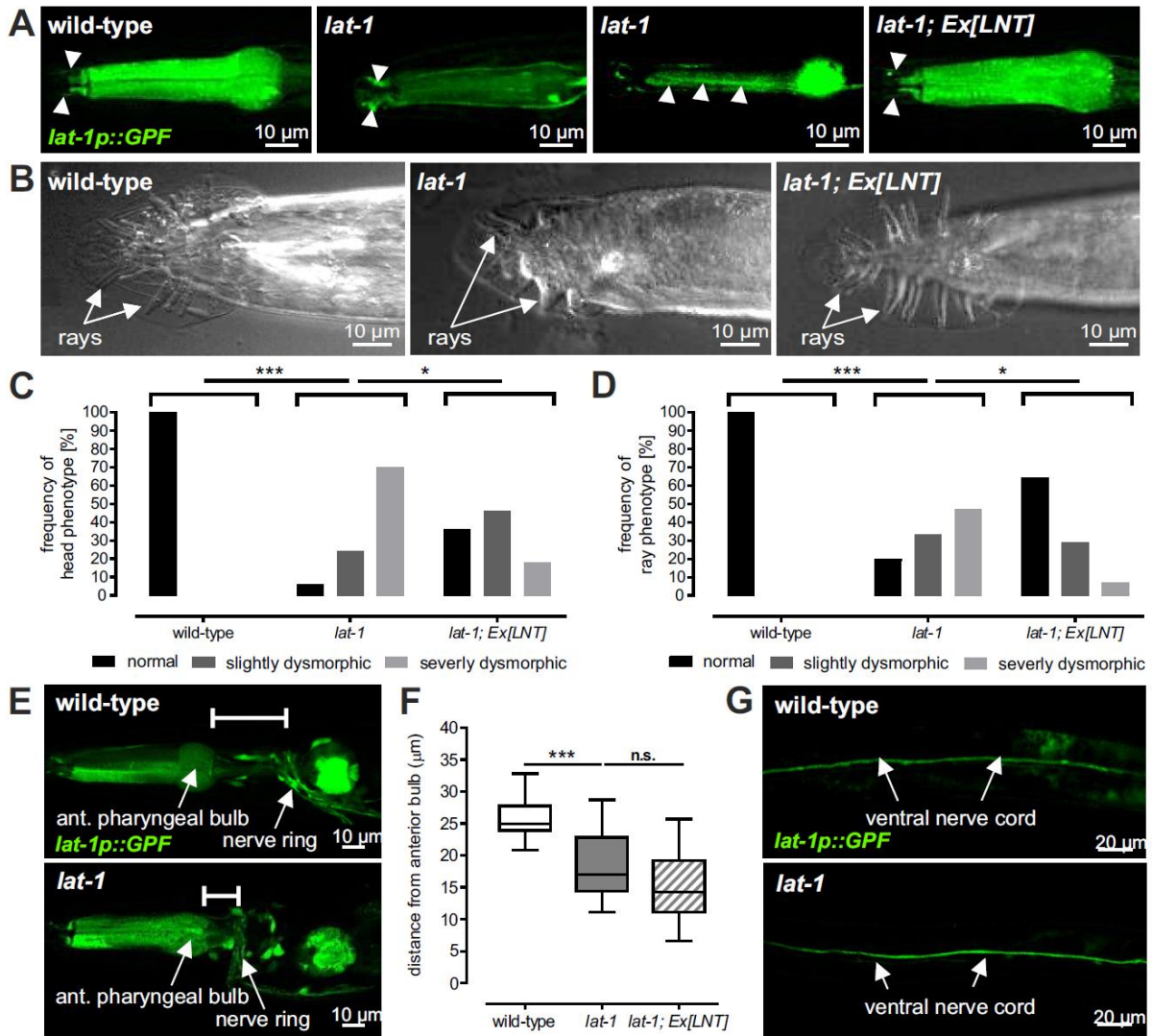


Figure 3: Defects in *lat-1*-mutant male neuron morphogenesis. (A) Abnormal dendritic (white triangles) and socket cell morphology in *lat-1* mutants expressing *lat-1p::GFP* is ameliorated by the sole LAT-1 N terminus (LNT). (B) *lat-1* mutants exhibit defective ray morphology, which is rescued by expressing the LNT. (C, D) Quantification of (A) and (B). $n > 11$. (E, F) The nerve ring in *lat-1* mutants is shifted to the anterior. This phenotype cannot be ameliorated by LNT expression. $n > 12$. (G) *lat-1* mutants show no defects of the ventral nerve cord.

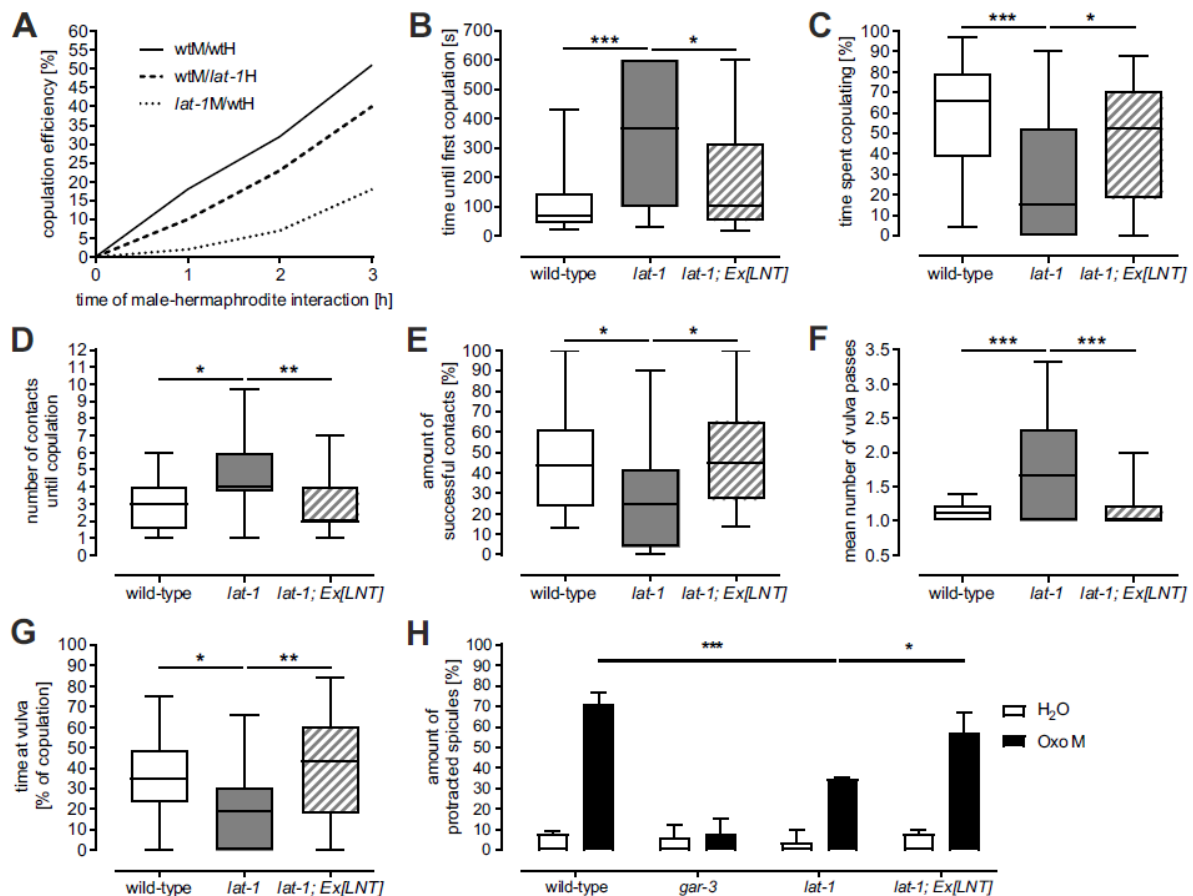


Figure 4: Defective copulation behavior in *lat-1*-mutant males. (A) Copulation efficiency measured by successful transfer of MitoTracker-labelled sperm is significantly reduced when *lat-1*-deficient males are mated to wild-type hermaphrodites. The reciprocal experiment yields only slight reductions in copulation efficiency. n = 60. (B-G) Mating behavior of *lat-1*-mutant males reveals a complex behavioral defect (Supplementary files). All defects were ameliorated in *lat-1* males expressing the LAT-1 N terminus (LNT). n > 15. (H) Oxotremorine M induces spicule protraction in wild-type males, but not that greatly in *lat-1* mutants. This phenotype was rescued by expression of the LNT. n > 35.

REFERENCES

- [1] K.R. Monk, S.G. Naylor, T.D. Glenn, S. Mercurio, J.R. Perlin, C. Dominguez, C.B. Moens, W.S. Talbot, A G protein-coupled receptor is essential for Schwann cells to initiate myelination, *Science*, 325 (2009) 1402-1405.
- [2] S. Giera, Y. Deng, R. Luo, S.D. Ackerman, A. Mogha, K.R. Monk, Y. Ying, S.J. Jeong, M. Makinodan, A.R. Bialas, B.S. Chang, B. Stevens, G. Corfas, X. Piao, The adhesion G protein-coupled receptor GPR56 is a cell-autonomous regulator of oligodendrocyte development, *Nat Commun*, 6 (2015) 6121.
- [3] L.B. Lindenmaier, N. Parmentier, C. Guo, F. Tissir, K.M. Wright, Dystroglycan is a scaffold for extracellular axon guidance decisions, *eLife*, 8 (2019).
- [4] R.S. Zhang, K. Liakath-Ali, T.C. Sudhof, Latrophilin-2 and latrophilin-3 are redundantly essential for parallel-fiber synapse function in cerebellum, *eLife*, 9 (2020).
- [5] G.R. Anderson, S. Maxeiner, R. Sando, T. Tsetsenis, R.C. Malenka, T.C. Sudhof, Postsynaptic adhesion GPCR latrophilin-2 mediates target recognition in entorhinal-hippocampal synapse assembly, *J Cell Biol*, 216 (2017) 3831-3846.
- [6] X. Piao, R.S. Hill, A. Bodell, B.S. Chang, L. Basel-Vanagaite, R. Straussberg, W.B. Dobyns, B. Qasrawi, R.M. Winter, A.M. Innes, T. Voit, M.E. Ross, J.L. Michaud, J.C. Descarie, A.J. Barkovich, C.A. Walsh, G protein-coupled receptor-dependent development of human frontal cortex, *Science*, 303 (2004) 2033-2036.
- [7] M.D. Weston, M.W. Luijendijk, K.D. Humphrey, C. Moller, W.J. Kimberling, Mutations in the VLGR1 gene implicate G-protein signaling in the pathogenesis of Usher syndrome type II, *Am J Hum Genet*, 74 (2004) 357-366.
- [8] M. Vezain, M. Lecuyer, M. Rubio, V. Dupe, L. Ratie, V. David, L. Pasquier, S. Odent, S. Coutant, I. Tournier, L. Trestard, H. Adle-Biassette, D. Vivien, T. Frebourg, B.J. Gonzalez, A. Laquerriere, P. Saugier-veber, A de novo variant in ADGRL2 suggests a novel mechanism underlying the previously undescribed association of extreme microcephaly with severely reduced sulcation and rhombencephalosynapsis, *Acta Neuropathol Commun*, 6 (2018) 109.
- [9] M. Arcos-Burgos, M. Muenke, Toward a better understanding of ADHD: LPHN3 gene variants and the susceptibility to develop ADHD, *Atten Defic Hyperact Disord*, 2 (2010) 139-147.
- [10] R. Sando, T.C. Sudhof, Latrophilin GPCR signaling mediates synapse formation, *eLife*, 10 (2021).
- [11] N. Scholz, C. Guan, M. Nieberler, A. Grotemeyer, I. Maiellaro, S. Gao, S. Beck, M. Pawlak, M. Sauer, E. Asan, S. Rothemund, J. Winkler, S. Promel, G. Nagel, T. Langenhan, R.J. Kittel, Mechano-dependent signaling by Latrophilin/CIRL quenches cAMP in proprioceptive neurons, *eLife*, 6 (2017).
- [12] M. Hammarlund, O. Hobert, D.M. Miller, 3rd, N. Sestan, The CeNGEN Project: The Complete Gene Expression Map of an Entire Nervous System, *Neuron*, 99 (2018) 430-433.
- [13] T. Langenhan, S. Prömel, L. Mestek, B. Esmaeili, H. Waller-Evans, C. Hennig, Y. Kohara, L. Avery, I. Vakonakis, R. Schnabel, A.P. Russ, Latrophilin signaling links anterior-posterior tissue polarity and oriented cell divisions in the *C. elegans* embryo, *Dev Cell*, 17 (2009) 494-504.
- [14] S. Prömel, M. Frickenhaus, S. Hughes, L. Mestek, D. Staunton, A. Woollard, I. Vakonakis, T. Schöneberg, R. Schnabel, A.P. Russ, T. Langenhan, The GPS motif is a molecular switch for bimodal activities of adhesion class G protein-coupled receptors, *Cell Rep*, 2 (2012) 321-331.

- [15] E. Yemini, A. Lin, A. Nejatbakhsh, E. Varol, R. Sun, G.E. Mena, A.D.T. Samuel, L. Paninski, V. Venkatachalam, O. Hobert, NeuroPAL: A Multicolor Atlas for Whole-Brain Neuronal Identification in *C. elegans*, *Cell*, 184 (2021) 272-288 e211.
- [16] S.W. Emmons, Neural Circuits of Sexual Behavior in *Caenorhabditis elegans*, *Annu Rev Neurosci*, 41 (2018) 349-369.
- [17] L.R. Garcia, P.W. Sternberg, *Caenorhabditis elegans* UNC-103 ERG-like potassium channel regulates contractile behaviors of sex muscles in males before and during mating, *J Neurosci*, 23 (2003) 2696-2705.
- [18] A. Steimel, L. Wong, E.H. Najarro, B.D. Ackley, G. Garriga, H. Hutter, The Flamingo ortholog FMI-1 controls pioneer-dependent navigation of follower axons in *C. elegans*, *Development*, 137 (2010) 3663-3673.
- [19] M.M. Barr, L.R. Garcia, Male mating behavior, *WormBook*, (2006) 1-11.
- [20] L.R. Garcia, P. Mehta, P.W. Sternberg, Regulation of distinct muscle behaviors controls the *C. elegans* male's copulatory spicules during mating, *Cell*, 107 (2001) 777-788.
- [21] M.G. Heiman, S. Shaham, DEX-1 and DYF-7 establish sensory dendrite length by anchoring dendritic tips during cell migration, *Cell*, 137 (2009) 344-355.
- [22] J.E. Sulston, H.R. Horvitz, Post-embryonic cell lineages of the nematode, *Caenorhabditis elegans*, *Dev Biol*, 56 (1977) 110-156.
- [23] R.Y. Yu, C.Q. Nguyen, D.H. Hall, K.L. Chow, Expression of *ram-5* in the structural cell is required for sensory ray morphogenesis in *Caenorhabditis elegans* male tail, *EMBO J*, 19 (2000) 3542-3555.
- [24] S.E. Baird, D.H. Fitch, I.A. Kassem, S.W. Emmons, Pattern formation in the nematode epidermis: determination of the arrangement of peripheral sense organs in the *C. elegans* male tail, *Development*, 113 (1991) 515-526.
- [25] F. Nakao, M.L. Hudson, M. Suzuki, Z. Peckler, R. Kurokawa, Z. Liu, K. Gengyo-Ando, A. Nukazuka, T. Fujii, F. Suto, Y. Shibata, G. Shioi, H. Fujisawa, S. Mitani, A.D. Chisholm, S. Takagi, The PLEXIN PLX-2 and the ephrin EFN-4 have distinct roles in MAB-20/Semaphorin 2A signaling in *Caenorhabditis elegans* morphogenesis, *Genetics*, 176 (2007) 1591-1607.
- [26] L. Jia, S.W. Emmons, Genes that control ray sensory neuron axon development in the *Caenorhabditis elegans* male, *Genetics*, 173 (2006) 1241-1258.
- [27] P.A. Correa, T. Gruninger, L.R. Garcia, DOP-2 D2-Like Receptor Regulates UNC-7 Innexins to Attenuate Recurrent Sensory Motor Neurons during *C. elegans* Copulation, *J Neurosci*, 35 (2015) 9990-10004.
- [28] G. Shan, W.W. Walthall, Copulation in *C. elegans* males requires a nuclear hormone receptor, *Dev Biol*, 322 (2008) 11-20.
- [29] M.A. Rahman, A.C. Ashton, F.A. Meunier, B.A. Davletov, J.O. Dolly, Y.A. Ushkaryov, Norepinephrine exocytosis stimulated by alpha-latrotoxin requires both external and stored Ca²⁺ and is mediated by latrophilin, G proteins and phospholipase C, *Philos Trans R Soc Lond B Biol Sci*, 354 (1999) 379-386.
- [30] A. Müller, J. Winkler, F. Fiedler, T. Sastradihardja, C. Binder, R. Schnabel, J. Kungel, S. Rothmund, C. Hennig, T. Schöneberg, S. Prömel, Oriented Cell Division in the *C. elegans* Embryo Is Coordinated by G-Protein Signaling Dependent on the Adhesion GPCR LAT-1, *PLoS Genet*, 11 (2015) e1005624.
- [31] S. Brenner, The genetics of *Caenorhabditis elegans*, *Genetics*, 77 (1974) 71-94.
- [32] D. Kim, J.M. Paggi, C. Park, C. Bennett, S.L. Salzberg, Graph-based genome alignment and genotyping with HISAT2 and HISAT-genotype, *Nat Biotechnol*, 37 (2019) 907-915.
- [33] M. Pertea, G.M. Pertea, C.M. Antonescu, T.C. Chang, J.T. Mendell, S.L. Salzberg, StringTie enables improved reconstruction of a transcriptome from RNA-seq reads, *Nat Biotechnol*, 33 (2015) 290-295.

- [34] D. Angeles-Albores, N.L. RY, J. Chan, P.W. Sternberg, Tissue enrichment analysis for *C. elegans* genomics, *BMC Bioinformatics*, 17 (2016) 366.
- [35] D. Angeles-Albores, R. Lee, J. Chan, P. Sternberg, Two new functions in the WormBase Enrichment Suite, *MicroPubl Biol*, 2018 (2018).
- [36] B. LeBoeuf, L.R. Garcia, *Caenorhabditis elegans* Male Copulation Circuitry Incorporates Sex-Shared Defecation Components To Promote Intromission and Sperm Transfer, *G3 (Bethesda)*, 7 (2017) 647-662.
- [37] S. Prömel, F. Fiedler, C. Binder, J. Winkler, T. Schöneberg, D. Thor, Deciphering and modulating G protein signalling in *C. elegans* using the DREADD technology, *Scientific reports*, 6 (2016) 28901.
- [38] J. Schindelin, I. Arganda-Carreras, E. Frise, V. Kaynig, M. Longair, T. Pietzsch, S. Preibisch, C. Rueden, S. Saalfeld, B. Schmid, J.Y. Tinevez, D.J. White, V. Hartenstein, K. Eliceiri, P. Tomancak, A. Cardona, Fiji: an open-source platform for biological-image analysis, *Nat Methods*, 9 (2012) 676-682.
- [39] T. Tekieli, E. Yemini, A. Nejatbakhsh, C. Wang, E. Varol, R.W. Fernandez, N. Masoudi, L. Paninski, O. Hobert, Visualizing the organization and differentiation of the male-specific nervous system of *C. elegans*, *Development*, 148 (2021).

4.2 The N terminus-only (*trans*) function of the Adhesion GPCR Latrophilin-1 cross-talks with the Notch pathway to control cell proliferation in the stem cell niche (manuscript)

Authors: Daniel Matúš, Franziska Fiedler, Victoria Elisabeth Groß, Claudia Binder, Johanna Lena Schön, Julia Luterán, Alexander Bernd Knierim, Torsten Schöneberg, Simone Prömel

Journal: Journal of Cell Biology

Impact Factor: 10.539

Submitted: 23 Apr 2021

Accepted: n. A.

Published: n. A.

References: 83

Language: English

Publisher: Rockefeller University Press

PubMed ID: n. A.

DOI: n. A.

TITLE

The N terminus-only (*trans*) function of the Adhesion GPCR Latrophilin-1 cross-talks with the Notch pathway to control cell proliferation in the stem cell niche

SHORT RUNNING TITLE

The *trans* function of Latrophilin-1 in cell proliferation

AUTHORS

Daniel Matúš¹, Franziska Fiedler¹, Victoria Elisabeth Groß^{1,3}, Claudia Binder¹, Johanna Lena Schön¹, Julia Luterán¹, Alexander Bernd Knierim^{1,2}, Torsten Schöneberg¹, Simone Prömel^{1,3*}

AFFILIATIONS

¹Rudolf Schönheimer Institute of Biochemistry, Medical Faculty, Leipzig University, 04103

Leipzig, Germany

²Leipzig University Medical Center, IFB Adiposity Diseases, 04103 Leipzig, Germany

³Institute of Cell Biology, Department of Biology, Heinrich Heine University Düsseldorf,

40225 Düsseldorf, Germany

CONTACT INFORMATION

*Correspondence: proemel@uni-duesseldorf.de

SUMMARY

Adhesion G protein-coupled receptors (aGPCRs) have versatile roles in numerous processes and show unique ways of signaling. Here, we show that the sole N terminus of the aGPCR Latrophilin-1 in the nematode *C. elegans* cross-talks with the Notch pathway to regulate cell proliferation rate and cell cycle progression in the gonadal stem cell niche.

ABSTRACT

Adhesion G protein-coupled receptors (aGPCRs) are unique molecules. They are able to transmit classical signals via G-protein activation as well as to mediate functions solely through their extracellular N termini, completely independent of the seven transmembrane helices domain (7TM) and the C terminus. This dual mode of action is highly unusual for GPCRs and allows for a plethora of possible cellular consequences. However, the physiological implications and molecular details of this N terminus-mediated signaling are not well understood. Here, we establish the N terminus-only (7TM-independent/*trans*) mode of the *Caenorhabditis elegans* aGPCR Latrophilin-1 (LAT-1) as a regulator of cell proliferation rate and cell cycle progression in the gonadal stem cell niche, which cross-talks with the Notch pathway. Mechanistic insights linking molecular details with *in vivo* effects show that LAT-1 functions *in trans* to negatively affect the Notch pathway by acting through distinct downstream effectors of the Notch receptor. These results further give insights into inhibitory Notch cues that solely affect germ cell proliferation, but not differentiation into meiotic cells. Finally, we provide evidence that this LAT-1 *trans* function does not engage simultaneous bidirectional signaling of the receptor and is probably realized by alternative splicing that specifically generates N terminus-only variants.

KEYWORDS

Adhesion G protein-coupled receptors, *trans* signaling, cell proliferation, stem cell niche, Notch pathway

INTRODUCTION

Cellular communication mediated by G protein-coupled receptors (GPCRs) typically relies on the transduction of an extracellular cue into a cell, which is mostly realized through the intracellular activation of G proteins via the seven transmembrane helices domain (7TM) of the receptor. This concept has recently also been confirmed for the class of Adhesion GPCRs (aGPCRs) (Bohnekamp and Schöneberg, 2011; Gupte et al., 2012). Like many other GPCRs, these receptors play essential roles in various physiological processes, but harbor structural features that distinguish them as a separate class within the GPCR superfamily (summarized in (Hamann et al., 2015)). One of these features is their extraordinarily long extracellular N terminus, comprising various domains and enabling the receptors to mediate signals and engage in cell-cell or cell-matrix adhesion (summarized in (Hamann et al., 2015)).

Remarkably and in contrast to other GPCRs, members of the class of aGPCRs are capable of transmitting functions only via these complex N termini, indicating non-canonical signaling mechanisms completely independent of their 7TM. Thereby, these receptors cannot only transduce extracellular cues into the cell they are expressed on by classic G protein-mediated cascades, but are also able to affect adjacent cells. This dual mode of action is highly uncommon for receptors, especially GPCRs. Thus far, one of the few well-characterized examples of this so-called bidirectional signaling are Eph receptors and their ligands Ephrins, which transmit a dual function in opposing cells in several physiological contexts,

particularly during development. Upon ligand-binding, the receptor tyrosine kinase Eph mediates a signal into the cell it is expressed on via its receptor tyrosine kinase activity. Additionally, it triggers a signal transduced by the Ephrin upon the binding of the two (summarized in (Pasquale, 2008)).

Our work and others' suggest that several aGPCRs, such as Latrophilins (Prömel et al., 2012), BAI1/ADGRB1 (Tu et al., 2018), GPR126/ADGRG6 (Patra et al., 2013), and CD97/ADGRE5 (Ward et al., 2018), harbor the ability to act bidirectionally, and there is further evidence for more (Okajima et al., 2010; Patat et al., 2016; Steimel et al., 2010). These cases imply that the dual mode of function is a common feature of this receptor class and data from several studies indicates that the sole N terminus independent of the 7TM is always sufficient to mediate effects (Patra et al., 2013; Prömel et al., 2012; Tu et al., 2018; Ward et al., 2018). However, while the understanding of the basic characteristics of the N terminus-only (7TM-independent) function and its cellular consequences is beginning to take shape, essential questions regarding the molecular models of this concept and its implications remain unanswered. For instance, it is unclear whether the whole receptor molecule is required at all times to fulfill both, classical G protein-mediated (*cis*) and N terminus-only/7TM-independent functions (*trans*), and whether the N terminus is attached to the entire receptor molecule, released or produced independently of the C-terminal parts to mediate its function. Autocatalytic cleavage at the G protein-coupled receptor proteolysis site (GPS) yielding an N-terminal fragment (NTF) and a C-terminal fragment (CTF) (Lin et al., 2004) is a hallmark feature of aGPCRs and might offer a possible mechanism for realizing the N terminus-only/7TM-independent function. However, our previous work showed that this cleavage is not vital for the 7TM-independent receptor mode of Latrophilin-1 (LAT-1) in *Caenorhabditis elegans* (Prömel et al., 2012), thus indicating that other mechanisms exist.

Addressing these questions on the details of the N terminus-only/7TM-independent aGPCR functions is particularly difficult as their physiological implications and the receiving cells remain unknown. Most insights have consequently been gained from *in vitro* and *ex vivo* studies, and information in a multicellular setting on the connection and integration of the classical G protein-mediated and the 7TM-independent function is sparse.

Here, we provide evidence that the N terminus-only/7TM-independent function of the aGPCR Latrophilin-1 (LAT-1) in *C. elegans* is vitally involved in a wide spectrum of physiological processes within the nematode. We identify it as a regulator of proliferative activity of germ cells in the gonadal stem cell niche by modulating cell cycle rate. In this context, LAT-1 negatively controls germ cell proliferation and cell cycle progression without altering differentiation into meiotic cells in a non-cell autonomous manner from the adjacent somatic cell. Mechanistic analyses revealed that this function is realized *in trans* by the receptor modulating the Notch signaling pathway in germ cells, thereby highlighting LAT-1's role in a cross-talk with Notch signals affecting proliferation without changing differentiation into meiotic cells. The absence of G protein-mediated LAT-1 function in this process indicates no simultaneous bidirectional signaling of LAT-1. Thus, we discuss the possibility of realizing the isolated *trans* signaling through alternative splicing of the receptor specifically generating N terminus-only variants and its impact on fine-tuning the Notch cascade.

RESULTS

The 7TM-independent function of LAT-1 mediates multiple processes in fertility

Previously, we showed that the membrane-tethered LAT-1 N terminus (aa 1-581, termed LNT) is sufficient to ameliorate fertility defects in *C. elegans* homozygous for the null allele *lat-1(ok1465)* (hereafter referred to as *lat-1*) (Langenhan et al., 2009; Prömel et al., 2012), indicating that the unusual 7TM-independent function of the receptor is involved in controlling aspects of reproduction. To gain insights into the mechanisms underlying this function, we first delineated its physiological impact by dissecting the *lat-1* mutant defects. These are generally characterized by a reduced brood size (wild-type: 228.2 ± 3.6 ; *lat-1*: 117.4 ± 4.0) (Langenhan et al., 2009; Prömel et al., 2012). At least three distinct processes involving the 7TM-independent LAT-1 function were identified in the self-fertilizing *C. elegans* hermaphrodite gonad, which produces a fixed number of sperm during larval development and variable amounts of oocytes in adulthood (Fig. 1A). Generation of both oocytes and sperm, are controlled by a complex network of mechanisms including Notch signaling (Fig. 1B).

First, we analyzed *lat-1* mutant sperm as previously obtained data led to the hypothesis that LAT-1 plays some role in sperm function (Prömel et al., 2012). Mutant hermaphrodites produce approximately the same amount of sperm as wild-type individuals (Figs. 1C, S1A) and the number of anucleate residual bodies, which form during spermatogenesis as remainders of budding spermatids (summarized in (L'Hernault, 2006)), appears to be constant (Fig. S1B, C). These data indicate largely intact sperm development and the correct timing of the sperm-oocyte switch during the transition of the last larval stage into adulthood. To assess a possible decline in sperm amount during the fertilization period leading to the reduced number of offspring, we examined sperm in the spermatheca 48 hours after the first ovulation (Fig. 1D) and the course of egg-laying (Fig. S1D). As *lat-1*

nematodes lay fewer fertilized eggs (Prömel et al., 2012) and thus, use less sperm than wild-type worms in a given time period, this should result in an accumulation of residual sperm over time. However, the sperm amount 48 hours after the first ovulation is not different from the amount in wild-types, indicating a significant loss of sperm during adulthood. This loss was evaluated by subtracting the number of laid eggs and residual sperm within the spermatheca from the initial sperm count (Fig. 1D). As sperm loss can be caused by impaired motility or defective directed locomotion and flushing out with egg-laying (summarized in (Han et al., 2010)), our data suggest that LAT-1 could play a role in sperm movement. Consistent with this hypothesis, the ovulation rate in *lat-1* mutants, which is initially similar to the one of wild-type worms, declines more rapidly over time (Fig. S1E). This is plausible as in *C. elegans*, ovulation is stimulated by signals produced in spermatozoa (reviewed in (Han et al., 2010)). Both phenotypes are rescued by transgenic LNT (Figs. 1D, S1E), showing that its role in sperm movement is mediated by the 7TM-independent function of LAT-1.

Besides this effect on sperm movement, we found that secondly, the 7TM-independent mode of LAT-1 also affects oocytes. We observed an increase in germ cell apoptosis using SYTO-12-staining in *lat-1* mutant hermaphrodites (Fig. 1E, F), which is rescued by the transgenic expression of *LNT* (Fig. 1F). Germ cells normally form oocytes in *C. elegans* adults and some undergo apoptosis as a physiological process during oogenesis (Fig. 1A) (summarized in (Gartner et al., 2008)).

When investigating the germline of *lat-1* mutants further, we observed an increase in mitotic events indicated by a greater number of nuclei stained with an anti-phospho-histone H3 (Ser10) (PH3) antibody, which marks the mitotic (M) phase (Figs. 1G, 3A). This phenotype was rescued by transgenic complementation with *LNT* (Fig. 1G), finally highlighting a third role of the LAT-1 7TM-independent mode. As proliferation is a vital and highly conserved

process for generating germ cells in many species, we sought to uncover the specifics of LAT-1 function as a so-far unidentified molecule in this context in more detail.

The loss of the 7TM-independent LAT-1 function increases proliferation without impairing the point of meiotic entry

The generation of germ cells during the adult life of *C. elegans* hermaphrodites is a tightly regulated process that entails a balance between cell proliferation (self-renewal) in the gonadal stem cell niche and differentiation into germ cell progenitors (entry into meiosis) (Fig. 1A, B). To delineate the 7TM-independent LAT-1 function in these processes, we first quantified the characteristics of the proliferative (mitotic) zone and all other zones within the adult hermaphrodite gonad. DAPI staining was used to assess the spatial organization of the gonad based on nuclear morphology (Fig. 2A). As it is known that gonad properties differ from larval stage L4 into and throughout adulthood (Kocsisova et al., 2019; Roy et al., 2016), hermaphrodites used in these and all subsequent analyses were exactly 24 hours post mid-L4. The worms were precisely staged, also to account for the fact that the majority of *lat-1* mutants (70-80%) are developmentally slower than the wild-type controls (Langenhan et al., 2009) (Fig. S2). Although more nuclei of *lat-1* mutants were in the M phase compared to wild-type nematodes (Fig. 1G), the overall number of nuclei in the proliferative zone as well as the zone size remained unchanged (wild-type: 236.1 ± 2.5 germ cells in 21.1 ± 0.2 rows; *lat-1*: 239.9 ± 3.1 germ cells in 20.1 ± 0.3 rows) (Fig. 2A, B). The same was true for the transition zone. Interestingly, the pachytene appeared slightly enlarged (Fig. 2A, B).

Although the determination of the proliferative zone based on nuclear morphology is a well-established measure (Hirsh et al., 1976), it does not allow for a precise demarcation of the zone, since in its proximal part, pre-meiotic nuclei can be present, which are morphologically indistinguishable from mitotic ones. To circumvent this issue, we used

REC-8 as a proliferative zone nuclei marker and HIM-3 as a meiotic-specific marker (Hansen et al., 2004). Antibody staining against both proteins confirmed that the size of the proliferative zone in *lat-1* mutants is not different from the one in wild-type hermaphrodites (Fig. 2C-F) despite the increased number of M-phase nuclei (Fig. 1G). These data also showed that the point of meiotic entry within the gonad in *lat-1* mutant hermaphrodites is not impaired or altered. Using REC-8 and HIM-3 to validate the zone sizes defined by DAPI staining, we subsequently determined the mitotic index of *lat-1* mutants, which is the percentage of M-phase (PH3-positive) nuclei within the total number of nuclei in the proliferative zone. This index, which accounts for potential zone size differences, was higher in *lat-1* than in wild-type hermaphrodites (Fig. 2G), thus confirming the initially observed higher number of M-phase nuclei (Fig. 1G). These data indicate that the frequency of germ cell division is altered in *lat-1* mutants. However, together with the observation that the number of germ cells in the proliferative zone of *lat-1* mutants is similar to the one in wild-types, these data highlight that the point of meiotic entry within the gonad is unchanged. Thus, the balance between proliferation and the decision for meiotic entry is not disrupted.

LAT-1 modulates the rate of germ cell proliferation

To address the question of whether the elevated frequency of mitotic events in *lat-1* mutants is due to an altered cell cycle (shift in the duration of cell cycle phases) or an increased cell proliferation rate (faster cell cycle progression) we assessed the cell cycle structure. EdU staining revealed that *lat-1* mutants have also more synthesis (S-) phase nuclei (Fig. 3A, B) and thus, a higher S index (the percentage of S-phase [EdU-positive] nuclei of the total number of nuclei in the proliferative zone) (Fig. 3C). In contrast to the distribution of PH3-positive nuclei, excessive S-phase nuclei in *lat-1* mutants were mostly located in the proximal end of the zone (Fig. 3B). We next examined the relative length of the gap phases

(G1, G2) by evaluating the DNA content (2n or 4n) of cells in the proliferative zone using DAPI fluorescence intensities as previously described in (Fox et al., 2011). Nuclei positive for PH3 in the prophase/metaphase have 4n DNA content, whereas anaphase/telophase nuclei have 2n DNA content (but respective daughters were summed up as 4n in this analysis), which is reflected in different DAPI fluorescence intensities (Fig. 3D). These 2n and 4n cells formed the basis for estimating the DNA equivalents of all other nuclei based on their DAPI fluorescence intensities. Due to different stages of DNA synthesis S-phase nuclei (identified by EdU staining) have a range of DNA content between 2n and 4n (Fig. 3D). All PH3- and EdU-negative cells were either in gap phase G1 (2n) or gap phase G2 (4n). Our analyses revealed that the general distribution of DNA content over the entire proliferative zone is similar in *lat-1* mutant and wild-type hermaphrodites, but with fewer nuclei in each of the gap phases (Fig. 3D). The ratio of the gap phase frequencies G1:G2 remained constant at ~1:20, as previously described for wild-type gonads (Fox et al., 2011). Taken together, these analyses led to an overall cell cycle structure of *lat-1* mutant gonads in which the M and S phases were prolonged while the gap phases were equally shortened (Fig. 3E). These altered cell cycle phase lengths were shifted back towards the wild-type when reintroducing LNT. Additionally, we assessed cell cycle progression using pulse-chase experiments. Animals fed with EdU for a short time (< 30 minutes) were examined either directly after the incubation or after 4 hours (Fig. 3F, G). In *lat-1* mutant, wild-type and *lat-1;Ex[LNT]* gonads dissected immediately after staining, all EdU-labeled cells were REC-8-positive (i.e. proliferative) (Fig. 3F). Interestingly, after 4 hours, more of these EdU-positive cells had entered meiosis in *lat-1* mutants than in wild-type (Fig. 3F), yielding faster cell cycling, which is also rescued by the LNT (Fig. 3G).

In summary, these results suggest a role of the 7TM-independent LAT-1 function in the control of cell cycle speed and thus, germ cell proliferation rate rather than sole changes in

cell cycle phases. Consistent with the observation that the pachytene of *lat-1* mutants contained more nuclei than that of wild-types worms (Fig. 2A, B), more cells enter meiosis due to the faster cell cycle although the point of meiotic entry itself within the gonad is not changed.

The N terminus of LAT-1 elicits a function from the DTC in a non-cell autonomous manner

In order to control proliferation and maintain the balance between self-renewal and meiotic entry, germ cells receive different signals from neighboring cells in the somatic gonad. As the 7TM-independent mode of LAT-1 is itself not able to mediate classical G protein-dependent signals into a cell, questions arose regarding where the LAT-1 function originates from and whether it is cell autonomous. Utilizing an integrated transcriptional *lat-1p::gfp* as well as an integrated translational *lat-1::gfp*, we observed strong *lat-1* expression in the entire somatic gonad of adult hermaphrodites, including the distal tip cell (DTC), the gonadal sheath cells and the spermatheca, but not in germ cells (Figs. 4A-C, S3A). To verify that the lack of germline expression was not due to silencing effects of the transgenes, a single-copy integrated transcriptional *lat-1p::mCherry* was employed, which was generated using CRISPR/Cas9 genome editing. Like the two other two constructs, this single-copy integrated *lat-1p::mCherry* also showed the expression of *lat-1* in the DTC and the gonadal sheath cells, but not in germ cells (Fig. 4D, E). Thus, the expression profile of the receptor suggests that it elicits its effect on germ cell proliferation from the surrounding somatic tissues in a non-cell autonomous manner. Since the main source of the signal controlling cell proliferation in the proliferative region is known to be the DTC (Fig. 1B) (Kimble and Crittenden, 2005), we elucidated the morphology of this cell in precisely staged 24 hours post mid-L4 *lat-1* hermaphrodites. While the plexus length was indistinguishable from that of wild-type nematodes, the cap length was slightly but significantly reduced (Fig. 4F, G).

To test whether the DTC was the origin of LAT-1 function, we employed a tissue-specific expression of *LNT* in the DTC as well as the gonadal sheath cells and spermatheca of *lat-1* mutants, respectively. Since *LNT* expression in the spermatheca (driven by *plc-1p*) did not ameliorate the reduced brood size in *lat-1* mutants (Fig. S3B), we focused further analyses on the other two tissues. The sole presence of LNT in the DTC (driven by *lag-2p*) resulted in a reduction of the mitotic index to wild-type levels (Fig. 4H). Interestingly, the expression of *LNT* in the gonadal sheath cells (*lim-7p*-driven) also significantly ameliorated the elevated mitotic index, albeit only partially (Fig. 4H). Further, LNT was able to rescue the elevated number of apoptotic cells in *lat-1* mutants when specifically present in the gonadal sheath cells, while it was not able to ameliorate this defect when expressed in the DTC (Fig. 4I). These data support the finding that the 7TM-independent function of LAT-1 in cell proliferation is separate from its role in the regulation of germ cell apoptosis. Further, they show that the presence of the LAT-1 N terminus in the DTC is sufficient to control cell proliferation in the proliferative zone of the hermaphrodite gonad in a non-cell autonomous manner - and thus *in trans*.

The LAT-1 splice variant repertoire contains N terminus-only receptor versions

As the LAT-1 7TM-independent function acts in a completely different biological context than that of its 7TM-dependent signal in embryogenesis (Langenhan et al., 2009; Prömel et al., 2012), the question arose as to why such a large receptor molecule is produced only when the extracellular entity is mediating a function in distinct contexts. The release of the N terminus by cleavage of the aGPCR at the GPS, the motif in the GAIN domain capable of autoproteolysis, could be one mechanism. However, our previous findings indicate that cleavage is not essential for overall LAT-1 function (Prömel et al., 2012). Interestingly, a recent study suggests the presence of several premature poly-A sites within *lat-1* transcripts

that, among others, render LAT-1 molecules consisting only of the N terminus (Tourasse et al., 2017). To gain insights into the prevalence of such variants, we analyzed existing transcriptome data generated by RNA-Seq from day 1 adult wild-type hermaphrodites (Chen et al., 2015), in which the coverage was sufficient for splice variant analyses (Fig. 5A). Generally, with more than 20 transcript forms, the repertoire of *lat-1* variants can be considered extensive. Although the largest fraction consisted of the entire receptor molecule (exons 1-8), approximately 2.3% of the variants comprised only the N-terminal exons in different combinations and versions, which are potentially able to transmit the 7TM-independent function (Fig. 5B). A 3' rapid amplification of cDNA-ends with PCR (RACE-PCR) from the mRNA of wild-type hermaphrodites confirmed the general presence of N terminus-only variants (Fig. 5C), suggesting that these variants of *lat-1* exist *in vivo*. It has to be noted that, to ensure correct transcript composition, rescue analyses were always performed with constructs containing the genomic locus of *lat-1* or modifications of it.

LAT-1 regulates Notch downstream targets

One key signaling cascade promoting germ cell proliferation, repressing meiotic entry, and thus, controlling the balance between them, is the Notch pathway. In *C. elegans*, the initial signal in this highly conserved cascade originates from the DTC, among others expressing the DSL ligand *lag-2*. The interaction of this membrane molecule with the Notch receptor GLP-1 on adjacent germ cells triggers the activation of the direct transcriptional targets SYGL-1 and LST-1. There is evidence that both subsequently function together with the RNA-binding proteins FBF-1 and FBF-2 to act via a multitude of different genes, such as GLD-1 and GLD-2, to promote proliferation and repress meiotic entry (Fig. 1B) (summarized in (Kimble and Crittenden, 2005) and (Hubbard and Schedl, 2019)). Some of the defects in *lat-1* nematodes resemble phenotypes reported in mutants of these Notch

pathway components. For instance an increased amount of proliferating cells accompanied by a higher mitotic index have been observed in the *glp-1* gain-of-function mutant *glp-1(ar202)* (Maciejowski et al., 2006). However, in contrast to this *glp-1* mutant, *lat-1* hermaphrodites did not display an enlarged proliferative zone, which is generally a sign for a shifted balance of proliferation versus meiotic cell fate. Proliferation and meiotic entry are both controlled by GLP-1; the molecule promotes proliferation and represses meiotic entry by acting through its direct targets, LST-1 and SYGL-1, which in turn activate *gld-1* repressors and other meiotic proteins. Only downstream, their regulation becomes more separated and diverse (Fig. 1B). Thus, we asked whether *lat-1* affects downstream targets that control cell proliferation without directly influencing meiotic entry and therefore the proliferative zone size. For this purpose, we examined a potential interplay of *lat-1* with *gld-1*, which inhibits cell proliferation (Francis et al., 1995; Kimble and Crittenden, 2005). First, we analyzed *gld-1* expression in *lat-1* mutants. While in wild-type hermaphrodites, *gld-1* expression starts and intensifies when the repressing effect of the Notch signal ceases at some distance from the DTC (Schumacher et al., 2005), a significant downregulation of *gld-1* was observed in the absence of *lat-1* in the distal gonad (Fig. 6A, B). We also quantified *gld-1* expression in more detail at three benchmark points as they give insights into *gld-1* regulation (Brenner and Schedl, 2016): the base level in the most distal germ cells (yellow dot) as well as the levels at the start of meiotic entry (red dot) and at the end of meiotic entry (blue dot). As wild-type and *lat-1* mutant gonads display the same zone distribution (Fig. 2A-F), these points were identical in both strains: base at 1 germ cell row, point of meiotic entry at ~19 germ cell rows, and end of meiotic entry at ~25 germ cell rows (Fig. 6A, B). We found that the levels at all three points were significantly reduced in *lat-1* mutants compared to the wild-type controls (Fig. 6C-E). However, it has to be noted that the

gld-1 expression level in *lat-1* mutants eventually reached the same level as in wild-type gonads, but in more proximal rows (Fig. 6B).

Next, we analyzed a genetic interaction of *lat-1* and *gld-1* to test whether both molecules act in the same pathway. The hypomorph *gld-1(op236)* appeared to almost phenocopy *lat-1* in distinct aspects: It did not have an enlarged proliferative zone (wild-type: 236.1 ± 2.5 germ cells; *lat-1*: 239.9 ± 3.1 germ cells, *gld-1*: 180.3 ± 8.5 germ cells) (Fig. 6F, H), but it did have an increased number of M-phase nuclei (Fig. 6F, H, Table S1) and a consistently higher mitotic index than wild-type and *lat-1* individuals (Fig. 6G, H). Such an elevated proliferation had already been shown for other *gld-1* mutants (Pinkston et al., 2006), which also display defects in meiotic entry and proximal germline tumors. For a better comparability, all our mitotic index analyses focus on the proliferative zone in the distal gonad. M-phase nuclei as well as M indices in the proliferative zone of *gld-1;lat-1* double mutants were indistinguishable from those of *gld-1(op236)* single mutants (Fig. 6F, G, H, Table S1). These data suggest that *gld-1* might act downstream of *lat-1* function.

To further corroborate this notion, we elucidated FBF-1, the RNA-binding protein inhibiting GLD-1 (Crittenden et al., 2002). The *fbf-1(ok224)* null mutant had a slightly smaller proliferative zone (wild-type: 236.1 ± 2.5 germ cells; *fbf-1*: 206.6 ± 5.3 germ cells) (Fig. 6F, H) and also fewer M-phase nuclei (Table S1). This resulted in a decreased mitotic index (Fig. 6G, H) and thus, showed the opposite effect as a loss of *lat-1*.

Lastly, we tested a potential link between *lat-1* and *lst-1* and *sygl-1*, the only two known direct downstream targets of the Notch receptor GLP-1. The *lst-1(ok814); sygl-1(tm5040)* double mutant displayed a shortened proliferative zone (wild-type: 236.1 ± 2.5 germ cells; *lst-1(ok814); sygl-1(tm5040)*: 156.6 ± 4.8 germ cells) and a slightly elevated mitotic index compared to the wild-type (Fig. 6 G, H, Table S1). The *lst-1; sygl-1; lat-1* triple mutant had

a mitotic index much higher than those in either of the two mutants *lst-1; sygl-1* and *lat-1* (Fig. 6G, H, Table S1), pointing to a parallel function of *lat-1* and *lst-1/sygl-1*.

Taken together, these results potentially suggest that LAT-1 can act as a positive regulator of the Notch downstream effector GLD-1 controlling germ cell proliferation, potentially acting via FBF-1, but not the direct targets of the Notch receptor, LST-1 and SYGL-1.

The function of the LAT-1 N terminus is dependent on *glp-1*

Our results suggest that LAT-1 modulates cell proliferation rate, but not differentiation into meiotic cells as such.

The discrepancy observed in *lat-1* mutants of increased proliferation without a change in proliferative zone size and the finding that LAT-1 likely acts through Notch downstream targets raised the question of whether LAT-1 function also involves the molecules of the Notch core pathway. Expression analyses revealed that LAT-1 levels are increased in the *glp-1* gain-of-function mutant *glp-1(ar202)* (Figs. 7A, S4). Further, the absence of LAT-1 leads to a reduced expression of the Notch ligand *lag-2* (Figs. 4F, S4), suggesting regulatory effects of LAT-1 on Notch pathway components and *vice versa*.

We then investigated whether there is also functional cross-talk between LAT-1 and the Notch core pathway components GLP-1 and LAG-2. Hermaphrodites carrying single loss-of-function (*lf*) or gain-of-function (*gf*) mutations in these molecules combine defects in germ cell proliferation and meiotic entry, leading to altered proliferation rates as well as a changed proliferative zone length (Figs. 6H, 7B-D, Table S1). As in the loss-of-function single mutant *glp-1(e2141)(lf)* the fewer observed PH3-positive germ cells (Figs. 6H, 7B) were proportional to a shorter proliferative zone (Figs. 6H, 7C), and the mitotic index was the same as in the wild-type (Figs. 6H, 7D) (Fox and Schedl, 2015; Michaelson et al., 2010). Interestingly, when crossed into a *lat-1* mutant background, the increase in PH3-stained cells

typical for *lat-1* single mutants was not detected (Figs. 6H, 7B) and the mitotic index of *lat-1;glp-1(lf)* mutants was consequently indistinguishable from the *glp-1(lf)* single mutant (Figs. 6H, 7D). Conversely, *glp-1(ar202)(gf)* mutants displayed a larger proliferative zone (Figs. 6H, 7B, C) with an increased mitotic index (Figs. 6H, 7D), indicating high proliferative activity. The additional *lat-1* mutation in this background did not affect this phenotype (Fig. 7B-D). This indicates that the LAT-1 function is potentially dependent on GLP-1. Interestingly, a *lat-1;lag-2(lf)* double mutant using the allele *lag-2(q420)* displayed an additive effect on the mitotic index in comparison to *lat-1* single mutants (Figs. 6H, 7D), indicating no genetic interaction between the two.

These data suggest that *lat-1* function might involve *glp-1*, but acts in parallel to *lag-2* to implement its role in the control of germ cell proliferation.

DISCUSSION

Besides classical signal transduction via G proteins, Latrophilins are able to mediate functions solely through their extracellular N termini independent of 7TM and the C terminus (Prömel et al., 2012). Although it is becoming increasingly clear that this highly unusual dual function is inherent to several aGPCRs (Patra et al., 2013; Tu et al., 2018; Ward et al., 2018), the physiological impact and molecular details of such functions and especially how they are integrated *in vivo* are poorly understood. In the present study, we show that this 7TM-independent mode is a frequently employed concept involved in different physiological and cellular contexts and that, in contrast to other aGPCRs (Tu et al., 2018; Ward et al., 2018), does not engage in simultaneous bidirectional signaling of the receptor. While we identified three contexts of N-terminus activity, it is conceivable that

several more exist, and although we did not detect any germline expression with our constructs, a LAT-1 function with effects in the germline cannot be ruled out entirely.

We provide mechanistic evidence that the 7TM-independent LAT-1 mode modulates germ cell proliferation in the stem cell niche of the gonad by acting solely *in trans*. Although it cannot be excluded that the three identified functions of the LAT-1 N terminus involve the same cascades on a molecular level, they all contribute to ensuring the correct brood size via different, independent processes that require LAT-1 in distinct cells. Thereby, the LAT-1 7TM-independent/*trans* mode of action affects both gamete types and their function with seemingly diverse effects on sperm movement, germ cell apoptosis, and cell proliferation.

Although it does not appear to be involved in sperm development, the LAT-1 *trans* function seems to be essential to sperm locomotion (Figs. 1C, D, S1). The sperm loss occurring in the course of *lat-1* mutant adulthood might be a result of impaired sperm movement. One cause of this could be faulty sperm guidance, which is generally characterized by sperm being flushed out of the reproductive system with laid eggs (reviewed in (Han et al., 2010)), or defective sperm, as previously suggested (Prömel et al., 2012). The details of this function require further investigation, as does the effect of LAT-1 on the regulation of germline apoptosis (Fig. 1E, F). A compensatory role of increased apoptotic events as a result of increased germ cell proliferation is unlikely. This is especially the case, as the 7TM-independent LAT-1 function in germ cell proliferation is separable from its role in apoptosis, with the latter being exerted solely from the gonadal sheath cells.

Our data show that LAT-1 mostly functions from the DTC (and to a lesser extent from the neighboring gonadal sheath cells) to modulate cell proliferation in the gonadal stem cell niche by toning down cell cycle progression (Figs. 3, 4). It is conceivable that this reduction

in cell cycle speed is a mechanism to fine-tune the proliferation rate in the gonad to regulate overall germ cell numbers. The potential role of the slightly reduced DTC cap size of *lat-1* mutants in this context remains elusive and requires further investigation. It has to be noted that the increase of the cell proliferation rate in *lat-1* mutants likewise leads to more germ cells entering meiosis although the point of meiotic entry within the gonad remains unaltered. This effect can also explain the observed elevated number of cells in the pachytene (Fig. 2A, B).

Even though a small impact of LAT-1 on meiotic entry cannot be excluded, it is most striking that the size of the proliferative zone remains unchanged in this context. This is highly unusual, as the balance between germ cell proliferation and entry into meiosis is tightly controlled by the Notch pathway, which stimulates proliferation and suppresses meiotic entry (Austin and Kimble, 1987; Berry et al., 1997; Fitzgerald and Greenwald, 1995; Henderson et al., 1997; Kimble and Crittenden, 2005; Lambie and Kimble, 1991). Thus, changes in one of the processes are coercively accompanied by an alteration in the other. A possible separate regulation of cell proliferation and meiotic entry has not been unambiguously described despite some indication in its favor. For instance, *glp-1(ar202)* gain-of-function mutants exhibit an increase in mitotically dividing germ cells that exceeds the amount expected by their enlarged proliferative zones (Maciejowski et al., 2006). Mutations in the Notch downstream effector *fbf-1* do not result in a dramatic change in proliferative zone size compared to *glp-1* loss-of-function mutants (Austin and Kimble, 1987). Likewise, *gld-1* mutations lead to a zone size reduction despite high proliferative activity (Jeong et al., 2011; Lamont et al., 2004). Further, in *glp-4* mutants, germ cells fail to proliferate properly but do not enter meiosis, showing that a decrease in proliferation does not automatically lead to germ cells differentiating into meiotic cells (Beanan and Strome, 1992). Consistently, previous works have already speculated that proliferation and

differentiation into meiotic cell fate are separable (Hubbard, 2007), and these studies suggest that a sole modulation of proliferative activity in the respective zone could be possible through selective downstream effectors.

Indeed, our findings show that LAT-1 appears to affect the function of the regulator of germ cell proliferation GLD-1 by modulating its protein level. In combination with functional analyses these data suggest LAT-1 acts upstream of GLD-1 (Fig. 6). It has to be noted that it remains elusive as to why *gld-1* loss-of-function mutants exhibit a slightly reduced proliferative zone size, which is astonishing considering the increase in germ cell proliferation. Further support for the scenario in which LAT-1 feeds into this downstream leg of the Notch pathway (Fig. 1B) stems from our *gld-1* expression analyses in *lat-1* gonads, which among others showed reduced GLD-1 levels (Fig. 6A-E). Base levels of GLD-1 have been previously shown to depend on Notch pathway components such as GLP-1 and FBF-1 activity (Brenner and Schedl, 2016), so an involvement of LAT-1 in the function of these molecules is conceivable. The fact that the curve describing GLD-1 levels in *lat-1* mutants resembles the opposite of the respective curves for *glp-1* and *fbf-1* loss-of-function mutants (Brenner and Schedl, 2016), but reaches the peak of expression several cell rows after the end of meiotic entry, indicates that LAT-1 might be a general inhibitor of *gld-1*. It is interesting that the pattern of *gld-1* expression in *lat-1* mutants is shifted proximally and is thus not entirely concomitant with the expression of the meiotic protein *him-3* (Fig. 2D, F).

These data are in line with our *fbf-1* analyses. In accordance with the phenotype of previously reported *fbf-1(ok91)* mutants (Lamont et al., 2004), the *fbf-1(ok224)* hermaphrodites used in this study exhibited a slightly decreased zone size (Fig. 6F). Further investigation also revealed a reduction in the mitotic index. It is plausible that this phenotype is converse to the one in *lat-1* mutants when LAT-1 acts upstream of this transcription factor

influencing *gld-1*. Thus, the reduced mitotic index in *fbf-1* null mutants and the epistatic effect of the *lat-1* null mutation in the *gld-1* loss-of-function mutant background support the hypothesis that these two Notch downstream effectors are targets of LAT-1 functions.

It is puzzling that LAT-1 modulation in this part of the Notch downstream pathway appears to involve the Notch receptor GLP-1 to a certain extent, although it circumvents its direct downstream targets LST-1 and SYGL-1 as well as its ligand LAG-2. This conclusion is highlighted by our studies of the *lat-1* effect on germ cells in sensitized backgrounds. As such, the mitotic index in *lat-1* mutant gonads, which increases in a *lag-2(lf)* or a *lst-1;sygl-1* mutant background, vanishes in *glp-1(lf)* mutants (Figs. 6, 7), suggesting the dependency of LAT-1 function on the GLP-1 receptor. Further, the lack of increase in the mitotic index in *lat-1;glp-1(ar202)* double mutant proliferative zones compared to the respective single mutants also points towards the two cross-talking with each other. The observation that *lag-2* expression is reduced in the *lat-1* mutant (Figs. 4F, S4) could be explained by a compensatory effect. In the absence of LAT-1 and its potential negative modulatory influence on Notch signaling, the stimulatory effect of LAG-2 increases. To prevent a potential “overshoot of proliferation”, *lag-2* could be downregulated.

The details on how LAT-1 is able to fulfill its function without changing Notch-dependent cell fate decisions by acting through Notch downstream molecules remain to be determined. Parallel pathways of *lat-1* and *lag-2/sygl-1/lst-1* are possible, which feed into a joint pathway through *fbf-1* and *gld-1* further downstream. However, consistent with the observation that LAT-1 only modulates cell proliferation rate but not meiotic entry, our expression and genetic analyses could potentially also support a scenario in which GLP-1 is regulated by LAT-1, but in a spatially distinct manner compared to LAG-2. Activity of the Notch ligand LAG-2 is at its highest in the first few distal cell rows of the germline, then decreasing with distance from the DTC (Crittenden et al., 2006; Henderson et al., 1994) (Fig. 7E). This is the

same region to which direct GLP-1 function is restricted through its downstream effectors SYGL-1 and LST-1 (Kershner et al., 2014; Shin et al., 2017) (Fig. 7E). However, GLP-1 is present in the entire proliferative zone (summarized in (Hubbard and Schedl, 2019)), suggesting other potential ligands and immediate effector molecules. Our tissue-specific rescue experiments support the notion that LAT-1 function may be required relatively uniformly in the entire proliferative zone and parts of the transition zone (Fig. 7E), as the elevated mitotic index in *lat-1* mutants is rescued by the receptor in the DTC and in the gonadal sheath cells, which are in close vicinity to the DTC (Fig. 4B). Thus, it might be conceivable that LAT-1 function in cell cycle progression is dependent on GLP-1 throughout the proliferative zone engaging FBF-1 and GLD-1, while the classical LAG-2/GLP-1 function via LST-1 and SYGL-1 is confined to the more distal region.

There are several ways in which LAT-1 might cross-talk with the Notch pathway. One plausible explanation is that LAT-1 function employs mechanisms that feed into the *fbf-1* and *gld-1* cascade. For instance, it might well involve components of the cell cycle control machinery. A cross-talk between these components with Notch signaling has been shown in *C. elegans* (Fox et al., 2011; Furuta et al., 2018; Jeong et al., 2011). Generally, the regulation of cell cycle progression by Notch for instance via cyclins or cyclin-dependent kinases has been reported in several organisms, including humans (Joshi et al., 2009).

A more speculative scenario is that LAT-1 constitutes a non-canonical Notch ligand. Although the key players of the Notch pathway have been well characterized in many species, novel molecules involved in Notch receptor modulation – including non-canonical ligands – are constantly being identified (summarized in (D'Souza et al., 2010)). Forming a highly diverse group of proteins all lacking the classical DSL domain, such ligands are able to mediate distinct effects and/or trigger different downstream effectors of the Notch pathway (summarized in (D'Souza et al., 2010)). For instance, one of these ligands identified

in *C. elegans* is *osm-11*, which has an activating effect on signaling of the Notch receptor LIN-12 in vulva development and cooperates with the classical Notch ligand DSL-1 (Komatsu et al., 2008). Likewise, LAT-1 might modulate the GLP-1 pathway.

Our findings on LAT-1 are especially intriguing since only the N terminus of the aGPCR is required to modulate parts of the Notch pathway. This function clearly mediates a non-cell autonomous *trans* effect elicited from the DTC, as demonstrated by the tissue-specific expression analyses as well as the lack of LAT-1 on germ cells or differentiated gametes (Figs. 4, S3A). Despite the clear evidence that several aGPCRs are able to engage in similar 7TM-independent modes of action (Patat et al., 2016; Patra et al., 2013; Tu et al., 2018; Ward et al., 2018), it is still debated whether this function is purely signaling or if it mainly involves adhesion. While adhesive components in LAT-1 function cannot be excluded, its modulatory role in the Notch pathway as well as the almost unchanged morphology of *lat-1*-expressing cells and their surrounding tissues clearly suggest an involvement in signaling. In this context, LAT-1 does not act bimodally *in cis* and *in trans*. Intriguingly, the *trans* function also seems to be separable at a molecular level due to alternative splicing, giving rise to a multitude of transcript variants (Fig. 5). Thereby, isolated N-terminal variants can be expressed *in vivo*, and it is plausible that they are regulated separately from the full-length receptor. These data are also in concordance with recent studies on other aGPCRs, highlighting a huge tissue-specific transcriptional variability as a potential common principle in the regulation of aGPCR function (Boucard et al., 2013; Knierim et al., 2019; Röthe et al., 2019). It has to be noted that no information is available on the presence of N-terminal variants in *C. elegans* somatic gonad cells, only data on whole adult hermaphrodites are available. The small proportion of N-terminal variants (2.3%) might be due to this fact. Besides different splice variants it is also conceivable that the 7TM-independent function is

brought about by the liberation of the N terminus through autoproteolysis at the GPS. This mechanism, which is a hallmark feature of many aGPCRs, has been described for LAT-1, but in previous studies we found that cleavage does not have a major impact on receptor function (Prömel et al., 2012). However, we cannot exclude a small effect of LAT-1 cleavage. In addition to the aspect of cell specificity, it would be highly interesting to gain insights into the dynamics of the different transcripts. It is known that LAT-1 *cis* function is essential for early embryonic development (Langenhan et al., 2009). Thus, the question arises whether *lat-1* transcription is switched to synthesize N-terminal variants in the somatic gonad of adult hermaphrodites compared to embryos as well as which molecular mechanisms underlie such switches. While *cis* and *trans* function seem to be involved in different developmental stages, it has to be noted that future analyses can unravel LAT-1 *cis* effects in adult nematodes and *trans* functions in the embryo. The latter is especially interesting as it is conceivable that the role of LAT-1 in the Notch pathway could be an essential complementary effect to its function in spindle orientation (Langenhan et al., 2009; Müller et al., 2015).

In summary, our results show that the LAT-1 N terminus acts in *trans* as a negative regulator of germ cell proliferation by toning down cell cycle speed. This effect is likely realized via the Notch receptor GLP-1 downstream effectors GLD-1 and/or possibly FBF-1, but not its ligand LAG-2 or the downstream effectors SYGL-1 and LST-1. The modulatory effect of LAT-1 on germ cell proliferation without an effect on mitotic/meiotic cell fate decision possibly involves so-far unidentified molecules or even an atypical Notch function to warrant the separation of both processes. Nonetheless, our data represent yet another set of evidence that germ cell proliferation and mitotic/meiotic cell fate decision are not inseparable.

Our study gives first insights into the mechanisms that integrate the *trans* action of an aGPCR in an *in vivo* context. It would be highly interesting to see whether this unusual signaling mode is conserved among species and is moreover applicable to the *trans* functions of other aGPCRs. Transcript analyses of the aGPCR *Gpr126* in Notch-deficient mice (D'Amato et al., 2016) gives a preliminary indication that several aGPCRs might indeed be candidates for a cross-talk with the Notch pathway. This is especially interesting since the significance of Notch for development, tissue homeostasis and stem cell balance (Kimble and Seidel, 2008; Kopan and Ilagan, 2009; Siebel and Lendahl, 2017) makes new potential regulators of the Notch pathway highly relevant for pharmacological and medical research.

MATERIALS AND METHODS

Materials and Reagents

All standard chemicals were from Sigma Aldrich, ThermoFisher Scientific or Carl Roth GmbH unless stated otherwise. All enzymes were obtained from New England Biolabs. The following reagents and resources were used:

REAGENT or RESOURCE	SOURCE	IDENTIFIER
Bacterial and Virus Strains		
<i>E. coli</i> DH5 α	ThermoFisher Scientific	18258012
<i>E. coli</i> OP50	CGC	N/A
<i>E. coli</i> SW106	NCI Frederick	N/A
Antibodies		
Rabbit anti-HIM-3	Monique Zetka	Zetka <i>et al.</i> , 1999
Rabbit anti-REC-8	Novus Biologicals	49230002
Rabbit anti-phospho Histone H3 (Ser10)	Merck Millipore	06-570
Goat anti-rabbit IRDye 680RD-conjugated	LiCor	926-68071
Chemicals		
4,6 diamidine-2-phenylindole (DAPI)	Sigma	D9542
Fluoromount G	ThermoFisher Scientific	00-4958-02
Levamisole hydrochloride	Applichem	A4341.0010
SYTO12 Green fluorescent nucleic acid stain	ThermoFisher Scientific	S7574
Critical Commercial Assays		
Click-iT EdU Alexa Fluor 488 Imaging Kit	ThermoFisher Scientific	C10337
TOPO TA Cloning Kit	ThermoFisher Scientific	450641
2 nd generation 5'/3' RACE Kit	Roche	3353621001
Expand High Fidelity PCR System	Roche	11732650001

Experimental Models: Cell Lines		
N/A		
Experimental Models: Organisms/Strains		
<i>Caenorhabditis elegans</i> strains, see <i>C. elegans</i> maintenance and strains	This paper	N/A
Oligonucleotides		
Primers, see Table S3	SeqLab	N/A
Scientific instruments		
LSM7	Leica	
DMi8 confocal microscope	Leica	
Axiovert Observer Z1 microscope	Zeiss	

***C. elegans* maintenance and strains**

C. elegans strains were maintained according to standard protocols (Brenner, 1974) on *E. coli* OP50 at 22 °C unless stated otherwise. All temperature-sensitive strains were kept at 15 °C (permissive temperature) for general cultivation and were shifted to 22 °C for experiments as embryos (*glp-1(ar202)* and *lat-1(ok1465); glp-1(ar202)*) or as adults for 6 hours (*glp-1(e2141)*, *lag-2(q420)*, *lat-1(ok1465); glp-1(e2141)*, *lat-1(ok1465); lag-2(q420)*, *lst-1(ok814); sygl-1(tm5040)*, and *lst-1(ok814); sygl-1(tm5040); lat-1(ok1465)*).

Wild-type worms were *C. elegans* var. Bristol strain N2 (Brenner, 1974). The following alleles were obtained from the *Caenorhabditis* Genetics Center (CGC), which is funded by the NIH Office of Research Infrastructure Programs (P40 OD010440): *lat-1(ok1465)* and *fbf-1(ok224)* (both generated by the *C. elegans* gene knockout consortium), *glp-1(e2141)* (Kodoyianni et al., 1992), *glp-1(ar202)* (Pepper et al., 2003), *gld-1(op236)* (Schumacher et al., 2005), *lag-2(q420)* (Lambie and Kimble, 1991), *lst-1(ok814); sygl-1(tm5040)* (Kershner et al., 2014; Singh et al., 2011), *ozIs5[gld-1::GFP + unc-119(+)]* (Schumacher et al., 2005), *qIs153[lag-2p::MYR::GFP + ttx-3p::DsRed]* (Byrd et al., 2014), and *tnIs6 [lim-7p::gfp +*

rol-6(su1006)] (Hall et al., 1999). The alleles *qaIs7524[lat-1p::GFP::lat-1 rol-6(su1006)]* and *aprEX77[pSP5 rol-6(su1006) pBSK]* were previously generated (Langenhan et al., 2009; Prömel et al., 2012) and *ItIs37 [pAA64; pie-1::mCherry::his-58; unc-119 (+)]* was generously provided by Diana S. Chu (San Francisco State University, USA). The following strains containing extrachromosomal or integrated arrays were generated in this study: *lat-1(ok1465) aprEx192[pTL20; mCherry; pBSK]*, *lat-1(ok1465) aprEx193[pJL13 mCherry pBSK]*, *lat-1(ok1465) aprEx194[pJL14 mCherry pBSK]*, *lat-1(ok1465) aprEx216[pDM3 mCherry pBSK]*, and *lat-1(ok1465) aprIs1[pTL20 rol-6(su1006) pBSK]*. The strain *lat-1(knu846 [lat-1 KO/KI mCherry intronic loxP::hygR::loxP])* was generated by NemaMetrix Inc. (Eugene, Oregon) using CRISPR/Cas9 genome editing. The following combination of transgenes/alleles were obtained using standard genetic techniques (Brenner, 1974): *ItIs37[pAA64; pie-1::mCherry::his-58; unc-119(+)]*; *qaIs7524[lat-1p:gfp::lat-1 rol-6(su1006)]*, *lat-1(knu846 [lat-1 KO/KI mCherry intronic loxP::hygR::loxP]) II*; *tnIs6 [lim-7p::gfp + rol-6(su1006)]*, *lat-1(knu846 [lat-1 KO/KI mCherry intronic loxP::hygR::loxP]) II*; *qIs153[lag-2p::myr::gfp + ttx-3p::DsRed]*, *lat-1(ok1465) qIs153[lag-2p::myr::gfp + ttx-3p::DsRed]*, *lat-1(ok1465); glp-1(ar202), glp-1(ar202)*; *qaIs7524[lat-1p::gfp::lat-1 rol-6(su1006)]*, *lat-1(ok1465); glp-1(e2141)*, *lat-1(ok1465); ozIs5[gld-1::gfp + unc-119(+)]*, *lat-1(ok1465); lag-2(q420), gld-1(op236)*; *lat-1(ok1465), lst-1(ok814); sygl-1(tm5040); lat-1(ok1465)*.

Generation of transgenic *C. elegans* lines

All transgenic strains with stably transmitting extrachromosomal arrays were generated using DNA microinjection performed by NemaMetrix Inc. (Eugene, Oregon). Plasmids were injected at a concentration of 1 ng/μl together with the coinjection marker, a modified pPD118.33 containing *myo-2p::mCherry* (kind gift of Ralf Schnabel (Technical University

Braunschweig, Germany)) (30 ng/μl), and pBluescript II SK+ vector DNA (Stratagene) as stuffer DNA to achieve a final concentration of 120 ng/μl. DNA was injected into the syncytical gonad of hermaphrodites. Transgenic progeny were isolated and stable lines were selected. Multiple independent transgenic lines were established for each transgene tested. For array integration in strain *lat-1(ok1465) aprIs1[pTL20 rol-6(su1006)] pBSK*, gamma irradiation was employed (Evans, 2006) on the strain carrying the respective extrachromosomal array that had previously been generated (Prömel et al., 2012).

Brood size assay

Hermaphrodite L4 larvae were individually placed on NGM plates containing *E. coli* OP50 to lay eggs at 22 °C and transferred onto a fresh plate every 24 hours. Each day, progeny was counted until egg laying ceased. Sterile and semi-sterile (less than 25 eggs) mothers were excluded from the assay.

Larval development assay

To assess the time of development, at least 800 synchronized wild-type and *lat-1* L1 larvae were placed on OP50-seeded NGM plates and incubated at 22 °C. After 8, 16, 24, 36, and 48 hours, the number of larvae in different developmental stages (L1, L2, L3, L4, adult) was scored.

Ovulation rate assay

Ovulation rate was determined in hermaphrodites 24 hours and 96 hours post mid-L4, respectively. Hermaphrodites were separately placed on *E. coli* OP50-seeded NGM plates and eggs/oocytes inside the uterus were counted. After 4 hours at 22 °C, eggs/oocytes on the plate and inside the uterus of the mother were counted. Ovulation rate per gonad was

calculated as ([eggs in and out of uterus after 4 hours] – [initial eggs inside uterus]) / (2 * 4 hours).

Fixation and antibody/DAPI staining

Antibody and DAPI staining were performed on extruded germlines. For this purpose, germlines of precisely synchronized 24 hours post mid-L4 hermaphrodites were dissected, fixed and stained as previously described (Francis et al., 1995; Jones et al., 1996). Anti-REC-8 staining was adapted from (Mohammad et al., 2018) and anti-HIM-3 staining was modified from (Bukhari et al., 2012). Adult hermaphrodites (24 hours post mid-L4) were transferred into 300 μ M levamisole (Applichem) in 0.1% Tween in PBS (PBST) for immobilization and gonad arms were exposed by cutting off the heads/tails with a scalpel blade. Gonads were fixed in 4% formaldehyde/PBST solution for 15 minutes for anti-phospho Histone H3 (anti-PH3) staining and 5 minutes in 3% formaldehyde/PBST solution for anti-REC-8 staining. After washing with PBST, the specimens were incubated in 100% ice-cold methanol at -20 °C for 5 minutes (anti-PH3) or 1 hour (anti-REC-8), respectively.

For anti-HIM-3 staining gonads were directly dissected on a superfrost slide (ThermoFisher), fixed in 1% formaldehyde/PBST solution for 5 minutes, and freeze-cracked by submerging slides with coverslips into liquid nitrogen and quickly removing the coverslip (Miller and Shakes, 1995). Subsequently, the gonads were post-fixed in 100% ice-cold methanol at -20 °C for 1 minute and were washed three times with PBST.

Blocking was performed for 30 minutes in 30% goat serum in PBST (anti-REC-8) or 1 hour in 1% bovine serum albumine in PBST (anti-HIM-3). No blocking step was necessary in anti-PH3 staining. Thereafter, the gonads were incubated overnight at 4 °C with rabbit anti-phospho Histone H3 (Ser10) (Millipore) 1:200 in 0.1% bovine serum albumine (BSA)-containing PBST, rabbit anti-REC-8 (Novus Biologicals) 1:100 in 30% goat serum/PBST, or

rabbit anti-HIM-3 (kindly provided by Monique Zetka) (Zetka et al., 1999) 1:100 in 1% BSA/PBST, respectively. For anti-HIM-3 staining, a piece of parafilm was added to the slide to prevent it from drying out. After washing three times with PBST, the gonads were incubated overnight in the dark at 4 °C with secondary goat anti-rabbit IRDye 680RD-conjugated antibody (LiCor) 1:1000 in PBST/0.1% BSA (anti-PH3), 1% BSA (anti-HIM-3) or 30% goat serum (anti-REC-8) and 1 ng/μl 4,6-diamidino-2-phenylindole (DAPI, Sigma). The gonads were mounted on 2% agarose pads in Fluoromount-G (ThermoFisher) for microscopy. To stain gonads exclusively with DAPI, formaldehyde/methanol-fixed gonads (as for anti-PH3 staining) were incubated for 2 hours at 4 °C in the dark with 1 ng/μl DAPI. Gonads were washed three times with M9 and mounted as described above.

Since the single copy integrated *lat-1p::mCherry* reporter used in this study shows only very faint expression, which is further reduced by even short formaldehyde fixation, we employed native microscopy to image the respective worm strains. Thereby, worms were dissected directly on a coverslip in 15 μl of 0,1% PBST containing 300 μM levamisole, which was subsequently inverted onto a glass slide and imaged immediately.

EdU labelling and pulse chase experiments

5-ethynyl-2'-deoxyuridine (EdU) staining of worms was conducted as previously described (Fox et al., 2011; Kocsisova et al., 2018). For incorporation of EdU into bacteria, an overnight culture of MG1693 bacteria (*E. coli* genetic stock center) was diluted 1:50 in M9 containing 1% glucose, 1.25 μg/ml thiamine, 0.5 μM thymidine, 1 mM MgSO₄, and 20 μM EdU (Click-iT EdU Alexa Fluor 488 Imaging Kit, ThermoFisher) and was grown for 24 hours at 37 °C. Staged adult hermaphrodites (24 hours post mid-L4) were transferred to NGM plates seeded with these bacteria and incubated for 30 minutes in the dark at room temperature. Subsequently, worms were washed off the plates and gonads were extruded and

fixed as described above. EdU staining was completed using the Click-iT EdU Alexa Fluor 488 Imaging Kit (ThermoFisher) according to the manufacturer's protocol. When combining antibody stainings with EdU labelling, antibody staining was performed between fixation and the Click-iT reaction.

EdU pulse-chase experiments were adopted from (Fox et al., 2011). After incubation on EdU-containing MG1693, worms were washed with M9 and transferred to a fresh NGM plate seeded with *E. coli* OP50. To evaluate the progression of cells in the gonad over time, nematodes were washed off at 0 and 4 hours after the EdU pulse. Gonads were extruded, fixed and stained as described above. Co-staining with the anti-REC-8 antibody allowed for the determination of the amount of EdU-positive/REC-8-negative cells. Since EdU is only incorporated into S-phase cells, EdU-positive/REC-8-negative cells must be daughters of these cells having entered meiotic division, but are carrying on the EdU labelling of their progenitors. By comparing the amount of such daughter cells at different timepoints, the amount of cells produced in the proliferative zone within a given time period was calculated.

DNA content quantification

DNA content quantification was performed as previously described (Fox et al., 2011). Images of gonads from 24 hours post mid-L4 hermaphrodites triple-stained with EdU, anti-PH3 and DAPI as indicated above were acquired with a Z-stack spacing of 0.3 μm . Every nucleus was marked by a manually defined region of interest (ROI) in each stack using Fiji (Schindelin et al., 2012). The mean DAPI fluorescence intensity of all ROIs for one nucleus was measured, summed up, and the background fluorescence of an empty space within the rachis of the gonad was subtracted. This intensity correlates with the DNA content of a given nucleus. Fluorescence values of PH3-negative/EdU-positive cells (S phase) and PH3-/EdU-negative (G phase) cells were subsequently normalized to those of PH3-positive cells (4n for

pro- and metaphase nuclei, $2n$ for daughters in ana- and telophase) to obtain a relative measure of DNA content expressed as multiples of the haploid genome equivalent ($1n$). When plotting these values for G phase cells in a histogram, two maxima ($2n$ and $4n$) occur: Cells of the $2n$ maximum were defined as G1, cells of the $4n$ maximum were defined as G2.

SYTO staining

Adult hermaphrodites (24 hours post mid-L4) were washed off NGM plates with NGM lacking phosphate buffer. Worms were then incubated overnight in the dark at room temperature with $33\ \mu\text{M}$ SYTO12 Green fluorescent nucleic acid stain (ThermoFisher) in NGM and a small amount of *E. coli* OP50. To remove the stained bacteria, worms were washed three times with NGM and transferred to NGM plates with fresh *E. coli* OP50 for 1 hour. Subsequently, stained worms were anesthetized with $300\ \mu\text{M}$ levamisole (Applichem) in M9 and were mounted on 2% agarose pads for microscopy.

Microscopy

All specimen were imaged using confocal imaging techniques. Differential interference contrast (DIC) and fluorescence imaging were performed using LASX software on a Leica SP8 microscope and Olympus Fluoview FV1000 software on an Olympus microscope, respectively. Z-stacks were taken with a spacing of $0.3\text{-}2\ \mu\text{m}$, depending on the specimen ($2\ \mu\text{m}$ for whole worms, $0.5\text{-}1\ \mu\text{m}$ for germlines, $0.5\ \mu\text{m}$ for sperm, and $0.3\ \mu\text{m}$ for DNA content analyses). Microscopic images were evaluated using Fiji (Schindelin et al., 2012) and ImageJ (Schneider et al., 2012).

Plexus and cap measurements of the DTC

To analyze DTC morphology, adult nematodes (24 hours post mid-L4) expressing *qIs153[lag-2p::myr::gfp + ttx-3p::DsRed]* were anesthetized with 300 μ M levamisole (Applichem) in M9 and mounted on 2% agarose pads for microscopy. A Z-projection of the resulting stacks of images was used to assess cap length (spanning the solid body of the cell) and plexus length (spanning the cap and processes of the cell up to the last visible intercalating process). Measurements were based on DTC morphology described in (Byrd et al., 2014).

Quantification of GLD-1 levels

To assess GLD-1 protein expression gonads of worms 24 hours post mid-L4 containing *ozIs5[gld-1::gfp + unc-119(+)]* were extruded, fixed and stained with DAPI as described above and subsequently mounted on 2% agarose pads for microscopy. To compare expression in different strains images were acquired with same exposure and detection settings. Z-projections of the resulting stacks of images were analysed as previously described (Brenner and Schedl, 2016) by using the “Plot Profile”-function in ImageJ (Schneider et al., 2012) to generate expression profiles of the distal germ cell rows of the gonad (ROI: a 35 pixel-wide line spanning 35 germ cell rows [wild-type] or 45 germ cell rows [*lat-1* mutants]). Fluorescence intensities of each germ cell row were obtained by dividing the plot profile into 35 or 45 equal sections, respectively. For each germ cell row, a mean fluorescence value was calculated by pooling fluorescence intensities of multiple germlines. Three essential points of the resulting distribution of GLD-1::GFP-fluorescence were then defined as shown previously (Brenner and Schedl, 2016): Base level (first row), start of meiotic entry (row with the most distal HIM-positive nucleus on average, deduced

from anti-HIM-3 stainings), and end of meiotic entry (the most proximal row on average where the last REC-8-positive cell is located).

Generation of transgenes

To generate constructs, recombineering was conducted. Accordingly, existing protocols (Dolphin and Hope, 2006; Tursun et al., 2009) were modified as previously described (Langenhan et al., 2009; Prömel et al., 2012) to generate LAT-1 transgenes using cosmids, PCR-amplified targeting cassettes and positive antibiotic selection. All transgenes are based on a construct comprising the genomic locus of *lat-1* containing *lat-1p::lat-1(1-581)::gfp* (pTL20) (Prömel et al., 2012). To introduce the respective promoter upstream of *lat-1*, a recombineering targeting cassette consisting of two parts, a spectinomycin selection cassette and the promoter sequence, was generated. For primer sequences, see Table S3.

lag-2p::lat-1(1-581)::gfp (pJL13)

A 2 kb promoter region of *lag-2* was amplified with primers lat1_1088F/lat1_1089R from genomic DNA of a mixed population of N2 and ligated into vector pCR2.1 using the TOPO TA Cloning Kit (ThermoFisher). From this vector the promoter was again amplified with primers lat1_1090F/ lat1_1091R with the forward primer introducing a *Pst*I site and the reverse primer containing an overhang with a homology to the vector pTL20. In parallel, the spectinomycin resistance gene was amplified from the Gateway cloning vector backbone pDON223 (Invitrogen) with primers lat1_1080F (introducing an overhang with a homology to pTL20) and lat1_1081R (containing a *Pst*I site). Both fragments were digested by *Pst*I (NEB) and ligated together using a T4 DNA Ligase (NEB). The ligated cassette was subsequently recombineered into pTL20 (*lat-1p::lat-1(1-581)::gfp*) replacing the *lat-1*

promoter using electrocompetent SW105 cells with a heat-induced recombinase of the λ -Red recombinase system (Warming et al., 2005).

plc-1p::lat-1(1-581)::gfp (pJL14)

The promoter region of *plc-1* (2 kb) was obtained via amplification from genomic DNA of a mixed N2 population using primers lat1_1084F/lat1_1085R. Following ligation into vector pCR2.1 using the TOPO TA Cloning Kit (ThermoFisher), the promoter was amplified with primers lat1_1086F/ lat1_1087R. While the forward primer introduced a *Pst*I site, the reverse primer contained an overhang with a homology to the vector pTL20. In parallel, the sequence of the spectinomycin resistance gene was amplified from the Gateway cloning vector backbone pDON223 (Invitrogen) with primers lat-1_1080F (containing an overhang with a homology to pTL20) and lat-1_1081R (introducing a *Pst*I site). Both fragments were digested by *Pst*I (NEB), ligated with a T4 DNA Ligase (NEB) and the resulting fragment was recombineered into pTL20 (*lat-1p::lat-1(1-581)::gfp*) replacing the *lat-1* promoter using electrocompetent SW105 cells with heat-induced recombinase of the λ -Red recombinase system (Warming et al., 2005).

lim-7p::lat-1(1-581)::gfp (pDM3)

The promoter region of *lim-7* (2 kb) was retrieved by PCR with primers lat1_1082F (containing a *Pst*I site) and lat1_1083R (harboring a homology sequence to pTL20) from vector pOH323, which was a kind gift from Oliver Hobert (Columbia University, New York, USA) (Hall et al., 1999). In parallel, primers lat1_1080F (containing an overhang with homologies to pTL20) and lat1_1081R (introducing a *Pst*I site) were used to amplify the spectinomycin resistance gene from the Gateway cloning vector pDON223 (Invitrogen). Both PCR products were digested with *Pst*I (NEB) and ligated using a T4 DNA Ligase

(NEB). The resulting fragment was recombineered into pTL20 (*lat-1p::lat-1(1-581)::gfp*), replacing the *lat-1* promoter using electrocompetent SW105 cells with a heat-induced recombinase of the λ -Red recombinase system (Warming et al., 2005).

RNA extraction and rapid amplification of 3' cDNA ends with PCR (RACE-PCR)

Total RNA was extracted from a mixed population of wild-type hermaphrodites using TRI Reagent (Sigma) according to the manufacturer's protocol and were transcribed into cDNA with the 2nd generation 5'/3' RACE Kit (Roche) in combination with the Expand High Fidelity PCR System (Roche) as described in the supplier's instructions. To ensure cDNA synthesis from mainly mRNA, a specific oligo(dT)-anchor primer was used. The cDNA mix was directly utilized as a template for the RACE-PCR. Amplification was run with a PCR anchor primer corresponding to the sequence of parts of the oligo(dT)-anchor primer used for cDNA synthesis and the gene-specific primers *lat1_1365F* and *lat1_1394F*, respectively. PCR products were separated via gel electrophoresis, cut out, purified with the Wizard SV Gel and PCR Clean-Up System (Promega) and cloned into the vector pCR2.1 using the TOPO TA Cloning Kit (ThermoFisher) for further analysis. For primer sequences, see Table S3.

Splice variant analyses

Publicly available RNA-Seq datasets from adult wild-type hermaphrodite *C. elegans* var. Bristol N2 were downloaded via the Sequence Read Archive (Kodama et al., 2012; Leinonen et al., 2011), reads were aligned to the WBcel235 genome (Howe et al., 2017) using STAR (Dobin and Gingeras, 2015) and transcript assembly was performed using StringTie (Pertea et al., 2015). Full-length transcripts were inspected and further analyses including

visualization were conducted with the Integrated Genomics Viewer (Robinson et al., 2011). Accession numbers and mapping statistics are given in Table S4.

QUANTIFICATION AND STATISTICAL ANALYSIS

Statistical analysis

Numerical assay data were analyzed with GraphPad Prism version 7.0 (GraphPad Software). If not stated otherwise, the data are presented in box plots with 90% confidence interval. Statistical analyses were performed using a two-tailed Student's t-test for comparing two groups and a two-way ANOVA in combination with a Bonferroni post-hoc test for comparing multiple groups, respectively. P values of $p \leq 0.05$ were considered statistically significant. All details are given in the respective Figure legend.

DESCRIPTION OF SUPPLEMENTAL MATERIAL

The supplemental material contains four figures and four tables.

Fig. S1 shows that nematodes lacking *lat-1* display a normal sperm development and a reduced ovulation rate. Fig. S2 proves that *lat-1* nematodes display an impaired larval development. Fig. S3 is a representation of *lat-1::GFP* expression and tissue-specific rescue of *lat-1* mutant brood size. Fig. S4 is a quantification of fluorescence levels of images given in Fig. 7A and Fig. 4F.

Table S1 contains PH3- and EdU-positive cell counts and denominators for index calculation.

Table S2 is a list of exon positions of *lat-1* variants analyzed in this study. Table S3 shows the sequences of primers used in the study. Table S4 lists all accession numbers and mapping statistics for transcript analysis of *lat-1* variants.

ACKNOWLEDGEMENTS

The authors thank Jana Winkler for help with establishing fertility phenotyping assays, Sonja Kallendrusch for advice and support with microscopy, Samantha Hughes for helpful discussions and Niko Fleischer for critically reading the manuscript. We are very grateful to Oliver Hobert and Ralf Schnabel for kindly providing plasmids, Diana S. Chu for generously sharing *C. elegans* strains and Monique Zetka for gifting the anti-HIM-3 antibody.

This work was supported by grants from the Deutsche Forschungsgemeinschaft (DFG, German Research Foundation) through CRC 1423 (project number 421152132; C04 (S.P., T.S.)), FOR 2149 (project number 246212759; P02 (S.P.) and P04 (T.S.)), Pr1534/1-1 (project number 254080357 (S.P.)), the European Social Fund (S.P.) and the Federal Ministry of Education and Research (BMBF), Germany (A.B.K., FKZ: 01EO1501).

AUTHOR CONTRIBUTIONS

S.P. conceived and designed the study and the experimental approaches. D.M., F.F., V.E.G., C.B., J.L.S., J.L. and A.B.K. carried out the experiments. D.M., F.F., V.E.G., A.B.K., T.S., and S.P. analyzed the data. D.M., F.F. and S.P. wrote the manuscript.

COMPETING INTERESTS

The authors declare no competing interests.

FIGURES AND FIGURE LEGENDS

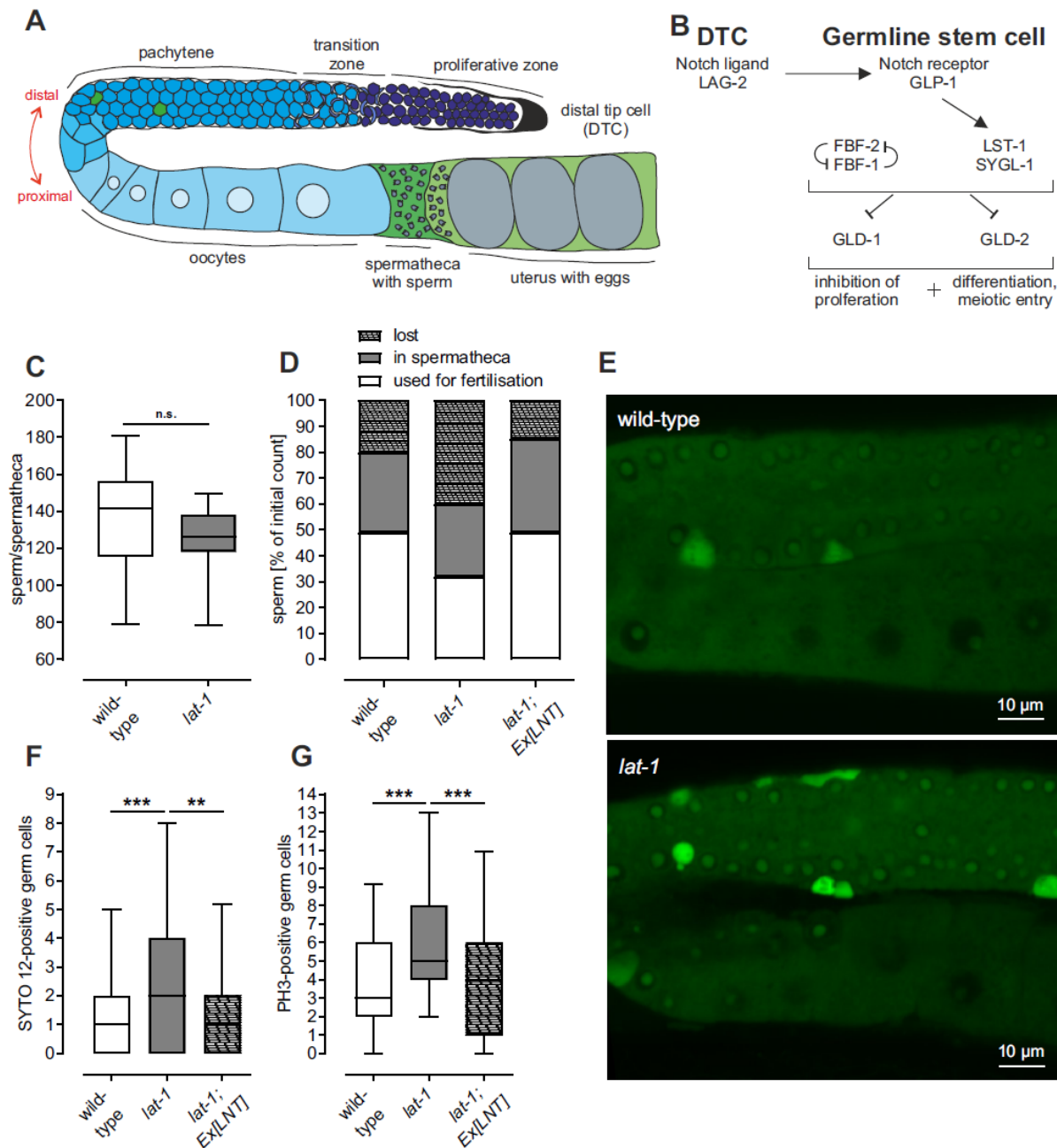


Fig. 1. Three distinct defects rescued by transgenic complementation with the LAT-1 N terminus (LNT) are the cause for reduced fertility in *lat-1* mutant hermaphrodites.

(A) Shown is one of the two symmetrical U-shaped gonad arms of a *C. elegans* adult hermaphrodite. In the fourth larval stage, a fixed number of sperm (approximately 150 per gonad) is produced and stored inside the spermatheca. Subsequently, the gonad switches to continuous oocyte production only. In the distal gonad, germ cell nuclei are not surrounded

by a complete membrane but reside in a common cytoplasm. They continually self-renew by mitotic division (dark blue) in the proliferative zone, which is distally enclosed by the distal tip cell (DTC) plexus and in part referred to as stem cell niche. Subsequently, germ cells enter meiotic divisions (crescent-shaped nuclei) in the transition zone and progress further through meiosis in the pachytene, where some germ cells undergo apoptosis (marked in green). Transition zone and pachytene are surrounded by the gonadal sheath cells (not shown). Near the loop, nuclei start to cellularize and to obtain plasma membranes. Due to coordinated contraction of the gonadal sheath cells, oocytes are pushed into the spermatheca, fertilized, and eggs are flushed into the uterus. After completing the first set of embryonic divisions, they are laid through the vulva (not shown). (B) Simplified model of the core Notch pathway components in the distal gonad (adapted from (Kimble and Crittenden, 2005) and (Hubbard and Schedl, 2019)). The Notch ligand LAG-2 (located on the DTC) binds the Notch receptor GLP-1 (located on germ cells). Proteolytic cleavage of the latter activates several transcriptional pathways. One thoroughly studied mechanism is the activation of the RNA-binding proteins FBF-1 and FBF-2, which are activated through the direct targets of GLP-1, LST-1 and SYGL-1. FBF-1 and FBF-2, which undergo mutual inhibition, further and together with LST-1 and SYGL-1 suppress transcription of various downstream effectors, such as GLD-2/GLD-3, which are responsible for initiation of meiosis, and GLD-1, which inhibits proliferation. By modulating these effectors, the Notch pathway ensures germ cell proliferation in the DTC niche of the *C. elegans* gonad. (C) DAPI staining reveals that the number of sperm residing inside the spermatheca of young adult *lat-1* mutants is not significantly different from the one in wild-type nematodes, albeit a little less. Nematodes of both strains were synchronized and selected for staining just after the first couple of ovulations to ensure that only a minimal amount of sperm was already used in fertilization or flushed out of the spermatheca. Data are shown as box plots with 90% confidence interval, n

≥ 20 . n.s. = not significant. (D) Sperm amount 48 hours post the first ovulation. Sperm was DAPI-stained and sperm loss was calculated as follows: $((\text{initial sperm in spermatheca}) - (\text{sperm in spermatheca after 48 hours}) - (\text{eggs laid in 48 hours})) / (\text{initial sperm in spermatheca})$. This loss is ameliorated in transgenic lines expressing *LNT*. $n \geq 15$. (E) Germlines of *lat-1* mutants exhibit more SYTO 12-stained germ cells compared to wild-type controls. Living adult nematodes 24 hours post mid-L4 were stained with SYTO 12 as a marker for apoptotic cells. (F) Quantification of SYTO 12 stainings from (E). Data are shown as box plots with 90% confidence interval, $n \geq 33$. ** $p < 0.01$; *** $p < 0.001$. (G) Elevated number of M-phase nuclei in the distal gonad of *lat-1* mutants stained with anti-PH3-antibody is rescued in a transgenic strain expressing *LNT*. Data are shown as box plots with 90% confidence interval, $n \geq 41$. *** $p < 0.001$.

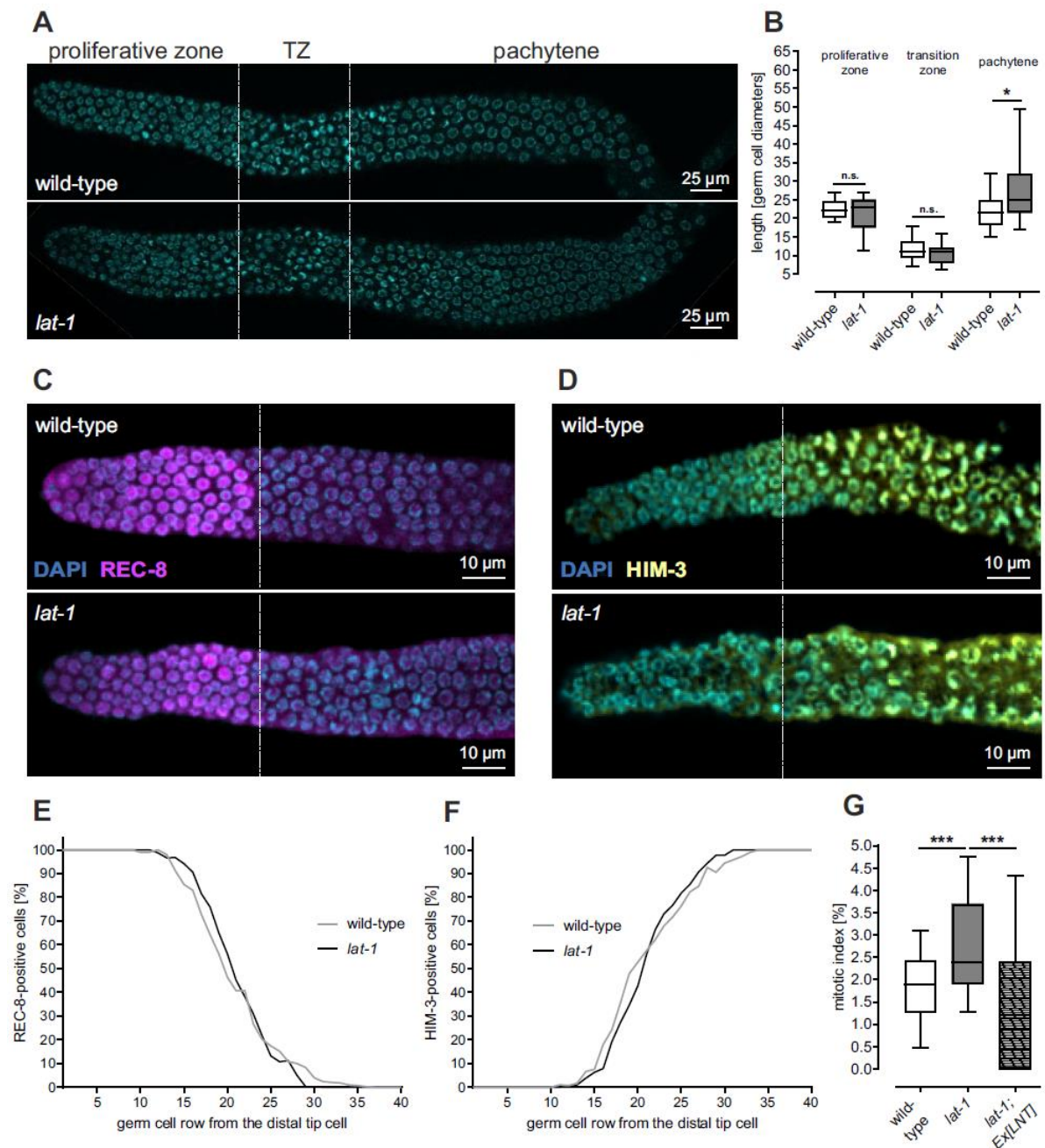


Fig. 2. Loss of the 7TM-independent LAT-1 function elevates the mitotic index but does not change the meiotic entry point. (A) Germ cells visualized by DAPI-staining in the gonads of wild-type and *lat-1* mutant nematodes 24 hours post mid-L4 (left: distal; right: proximal). While proliferative and transition zone (TZ) of the germline are unaltered in *lat-1* gonads, the pachytene seems to contain more germ cells. Zones were defined by nuclear morphology (Hirsh et al., 1976). The start of the TZ was defined as the first row containing more than one crescent-shaped nucleus, which mark leptotene/zygotene of meiotic

prophase I (Crittenden et al., 2019). Nuclei in rows distal to the TZ were counted as part of the proliferative zone. Equally, the most proximal row containing at least two crescent-shaped nuclei was defined as the end of the TZ and all nuclei proximal of this point were considered the pachytene. The pachytene reached till the loop of the gonad, where nuclear morphology changes due to chromatin remodeling. (B) Quantification of germline cell rows (given as germ cell diameters) in DAPI-stained gonads from (A) confirms unchanged proliferative and transition zones, but enlarged pachytene in *lat-1* mutants compared to wild-type. Data are shown as boxplots with 90% confidence interval, $n \geq 16$. n.s. = not significant; * $p < 0.05$. (C) REC-8 staining shows no difference in the size of the proliferative zone of *lat-1* mutants compared to wild-type. Extruded gonads of 24 hours post mid-L4 hermaphrodites were stained with an anti-REC-8 antibody (purple) and DAPI (blue) (left: distal; right: proximal). (D) HIM-3 staining showed no difference in the point of meiotic entry in *lat-1* mutants compared to wild-type. Extruded gonads of 24 hours post mid-L4 hermaphrodites were stained with an anti-HIM-3 antibody (yellow) and DAPI (blue) (left: distal; right: proximal). (E), (F) Quantification of the antibody stainings shown in (C) and (D) confirms no change in the transition from proliferative (REC-8-positive cells) to meiotic (HIM-3-positive cells) fate between *lat-1* mutant and wild-type germlines. Percentages were calculated as the amount of REC-8- or HIM-3-positive cells, respectively, from all nuclei in the corresponding germ cell row. $n \geq 26$ (REC-8), $n \geq 12$ (HIM-3). (G) Dividing the PH3-positive nuclei by the total number of nuclei in the proliferative zone (assessed by DAPI-staining) of *lat-1* mutants reveals an elevated mitotic index compared to the wild-type. This phenotype can be ameliorated by the sole expression of the LAT-1 N terminus. Raw data of PH3-positive cell counts and denominators for index calculation are shown in Table S1. $n \geq 20$, *** $p < 0.001$.

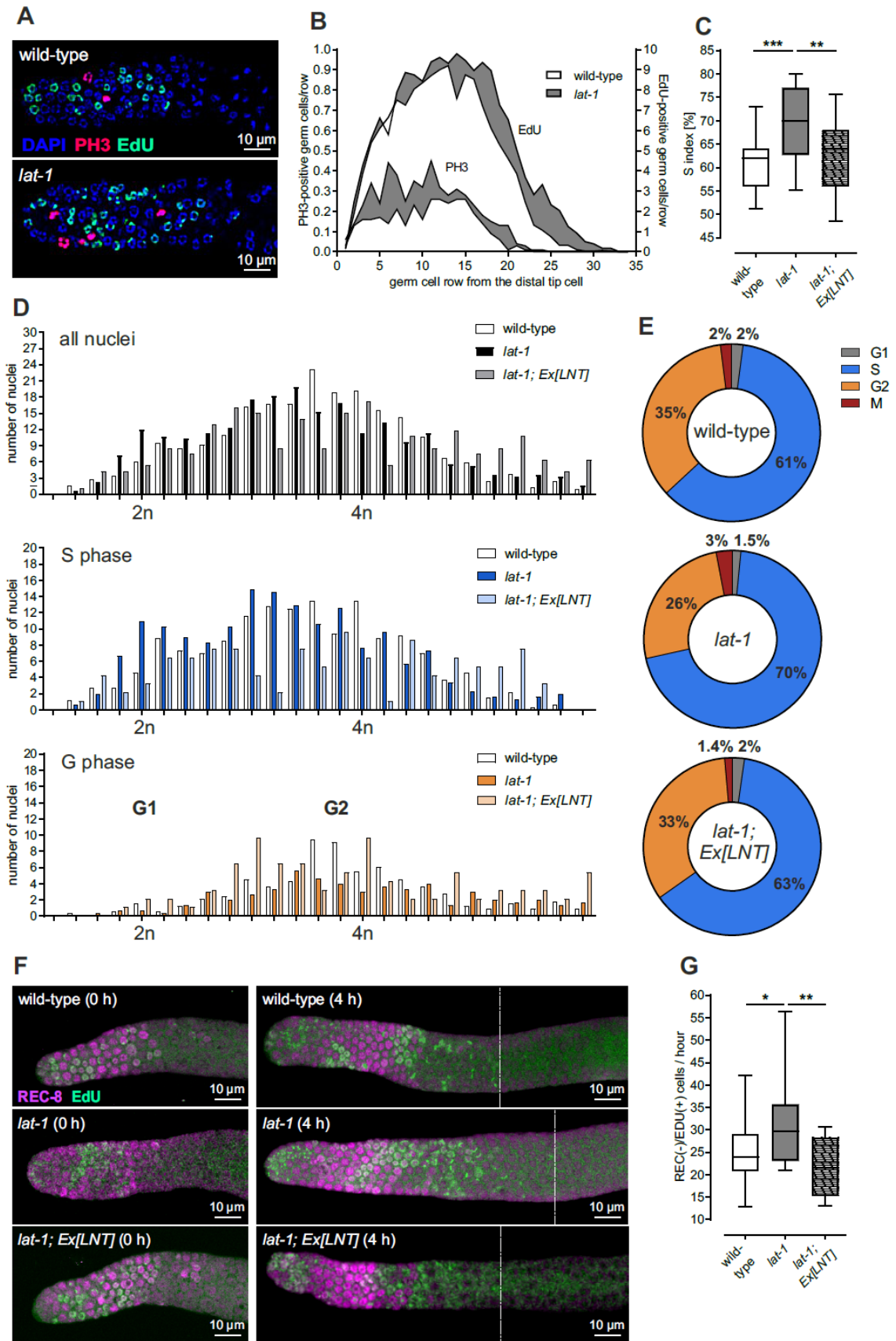


Fig. 3. LAT-1 regulates the cell cycle phase distribution and its speed of progression.

(A) The distal germline of *lat-1* mutant hermaphrodites displays more PH3-positive (M

phase) and EdU-positive (S phase) nuclei than wild-type controls. Hermaphrodites were stained 24 hours post mid-L4 with EdU by feeding of preincubated MG1693 bacteria, dissected and subsequently stained with DAPI (blue) and anti-PH3 antibody (magenta). Finally, EdU (green) was visualized by performing a Click-It reaction on the stained gonads.

(B) PH3- and EdU-stained germlines reveal a higher incidence of M- as well as S-phase nuclei in the proliferative zone of *lat-1* mutants compared to wild-type gonads. While the increase of PH3-positive M-phase nuclei in *lat-1* mutants appears to be spanning the entire proliferative zone, excessive S-phase (EdU-positive) nuclei are localized more proximally. Differences between *lat-1* mutant and wild-type are colored in grey. $n \geq 19$.

(C) The increased S index (calculated as the percentage of the number of EdU-positive nuclei from all nuclei in the proliferative zone) of *lat-1* mutant germlines is rescued by expression of the *lat-1* N terminus *LNT*. Raw data on EdU-positive cell counts and the denominators for index calculations are given in Table S1. Data are shown as boxplots with 90% confidence interval, $n \geq 20$. ** $p < 0.01$; *** $p < 0.001$.

(D) DNA content analysis of proliferative cells revealed more S-phase and less G-phase nuclei in *lat-1* mutants. Gonads of 24 hours post mid-L4 hermaphrodites were triple-stained with DAPI, EdU and anti-PH3 and nuclei were assessed for M phase, S phase and unlabeled Gap (G) phase. DAPI fluorescence intensity for each nucleus was measured and normalized to a fourth of the mean fluorescence intensity of PH3-positive M-phase nuclei (= 4n; anaphase and telophase daughters were summed up to one 4n nucleus) to obtain DNA content values as haploid genome equivalents (1 n). No significant changes in the distribution of DNA content were observed between wild-type and *lat-1* nuclei (M phase at 4n, S phase in the range between 2n and 4n and G phase as two maxima at 2n (G1) and 4n (G2)). However, the exceeding amount of M-phase and S-phase nuclei in *lat-1* mutants is accompanied by a general reduction in G1 and G2 nuclei. A rescue strain expressing the *LNT* resembled wild-type distributions.

(E) Relative cell cycle phase

durations based on (C), (D) and Fig. 2G. G1 and G2 indices were deduced from DNA content analysis in (D) (G1 index: $(1 - [\text{M index} + \text{S index}]) * G1 / [G1 + G2]$; G2-index: $(1 - [\text{M index} + \text{S index}]) * G2 / [G1 + G2]$). While *lat-1* mutants show extended M and S phases of proliferative cells, G1 and G2 phases are equally shortened. Expressing the *LNT* in *lat-1* mutants reverses the observed shift towards a wild-type cell cycle. (F) In *lat-1* mutant gonads, cell cycle progression is faster. EdU-pulse chase experiments were performed on 24 hours post mid-L4 hermaphrodites. Worms were stained with EdU by feeding of preincubated MG1693 bacteria, dissected directly after feeding or after 4 hours and subsequently stained with REC-8 antibody (purple). Finally, EdU (green) was visualized by performing a Click-It reaction on the stained gonads. While in gonads extruded directly after EdU incorporation (0 hours) all EdU-positive cells show a proliferative fate (REC-8-positive), after 4 hours several EdU-positive cells have entered meiosis (REC-8-negative). The number of these cells was significantly increased in *lat-1* mutants in comparison to the wild-type and was rescued by supplementing *LNT*. (G) Quantification of (F). Data are shown as boxplots with 90% confidence interval, $n \geq 15$. * $p < 0.05$; ** $p < 0.01$.

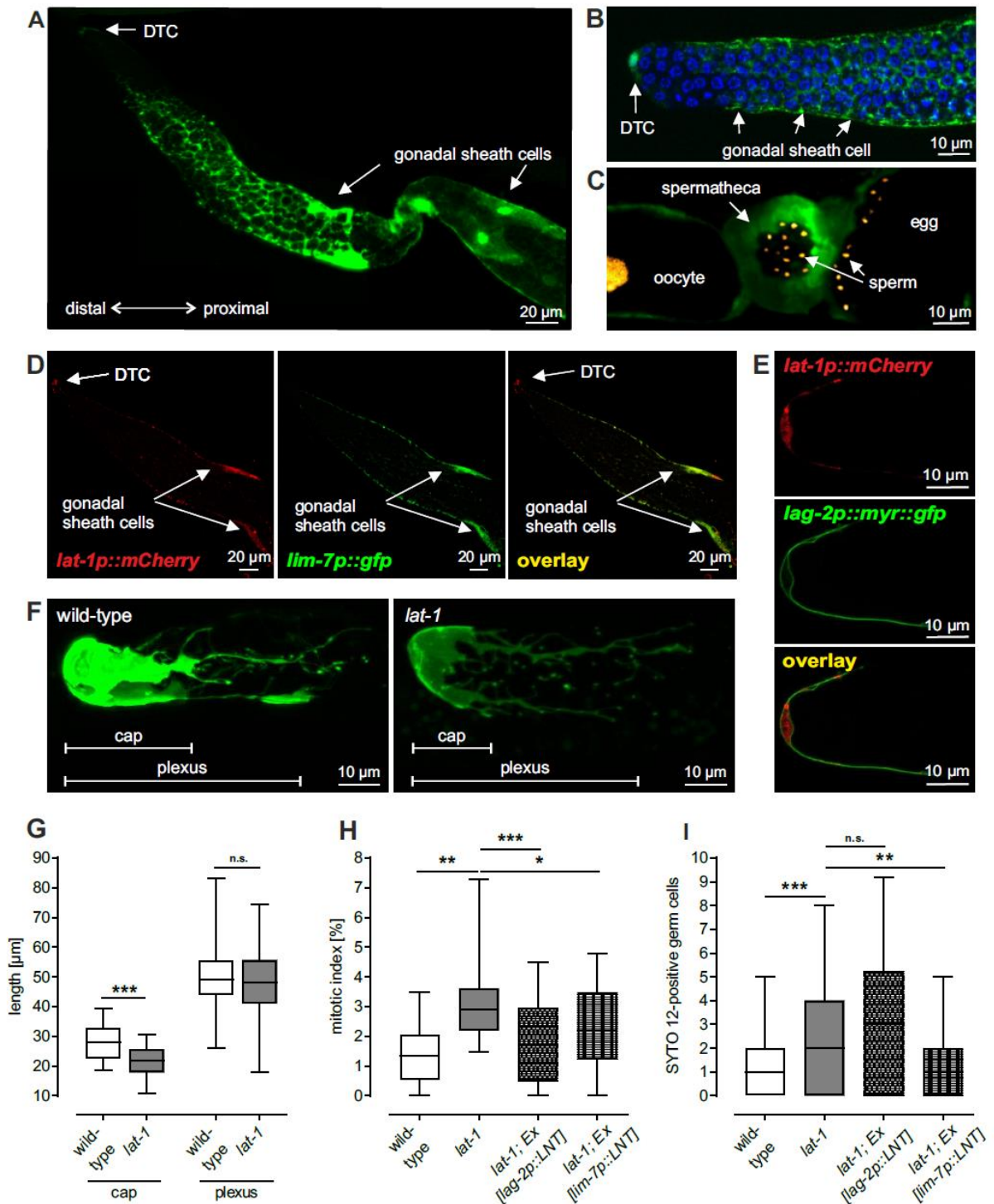


Fig. 4. The LAT-1 N terminus acts from somatic cells of the *C. elegans* gonad. (A)-(E) Expression of *lat-1* in the gonad. The receptor is present in all somatic cells of the gonad: distal tip cell (DTC), gonadal sheath cells and spermatheca (Spth). However, no expression is detectable inside germ cells, as well as in fully differentiated sperm or oocytes. For visualizing *lat-1* expression, either a multi-copy integrated *lat-1p::gfp* (A)-(C) or a

CRISPR/Cas9 genome-edited single-copy integrated *lat-1p::mCherry* (D), (E) was employed. Germ cell nuclei (C) were labeled by expressing *pie-1::mCherry::his-58*, gonadal sheath cells (D) by expressing *lim-7p::gfp* and DTC (E) by using *lag-2p::myr::gfp*. (F) Wild-type (left) and *lat-1* mutant (right) DTC visualized by *lag-2p::gfp* expression in 24 hours post mid-L4 animals. The morphology of the *lat-1* mutant DTC is largely intact compared to the wild-type DTC. Loss of *lat-1* only leads to a slightly reduced cap length, while the extension of the plexus over the proliferative zone is unchanged. Marker expression appears fainter in *lat-1* mutants. Quantification of expression levels are shown in Fig. S4. (G) Quantification of DTC parameters shown in (F) confirm the significantly reduced cap length of the DTC in *lat-1* mutants compared to wild-type controls. Data are shown as box plots with 90% confidence interval, $n \geq 42$. n.s. = not significant; *** $p < 0.001$. (H), (I) Tissue-specific expression of the LAT-1 N terminus (LNT) using promoters with activity restricted to distinct cell types in the somatic gonad reveals in which location LAT-1 is required to fulfil specific functions. While the increase of the mitotic index in *lat-1* mutants can be ameliorated by expression of *LNT* in the DTC driven by *lag-2p* and also, to a lesser extent, by its presence in the gonadal sheath cells (driven by *lim-7p*) (H), the elevated rate of apoptotic cells (indicated by SYTO 12-staining) is only rescued by *lim-7p*-driven expression of *lat-1*, restricting its presence to the gonadal sheath cells (I). Raw data on PH3-positive cell counts and denominators for index calculation can be found in Table S1. Data are shown as boxplots with 90% confidence interval. $n \geq 17$ (H), $n \geq 38$ (I). n.s. = not significant; * $p < 0.05$; ** $p < 0.01$; *** $p < 0.001$.

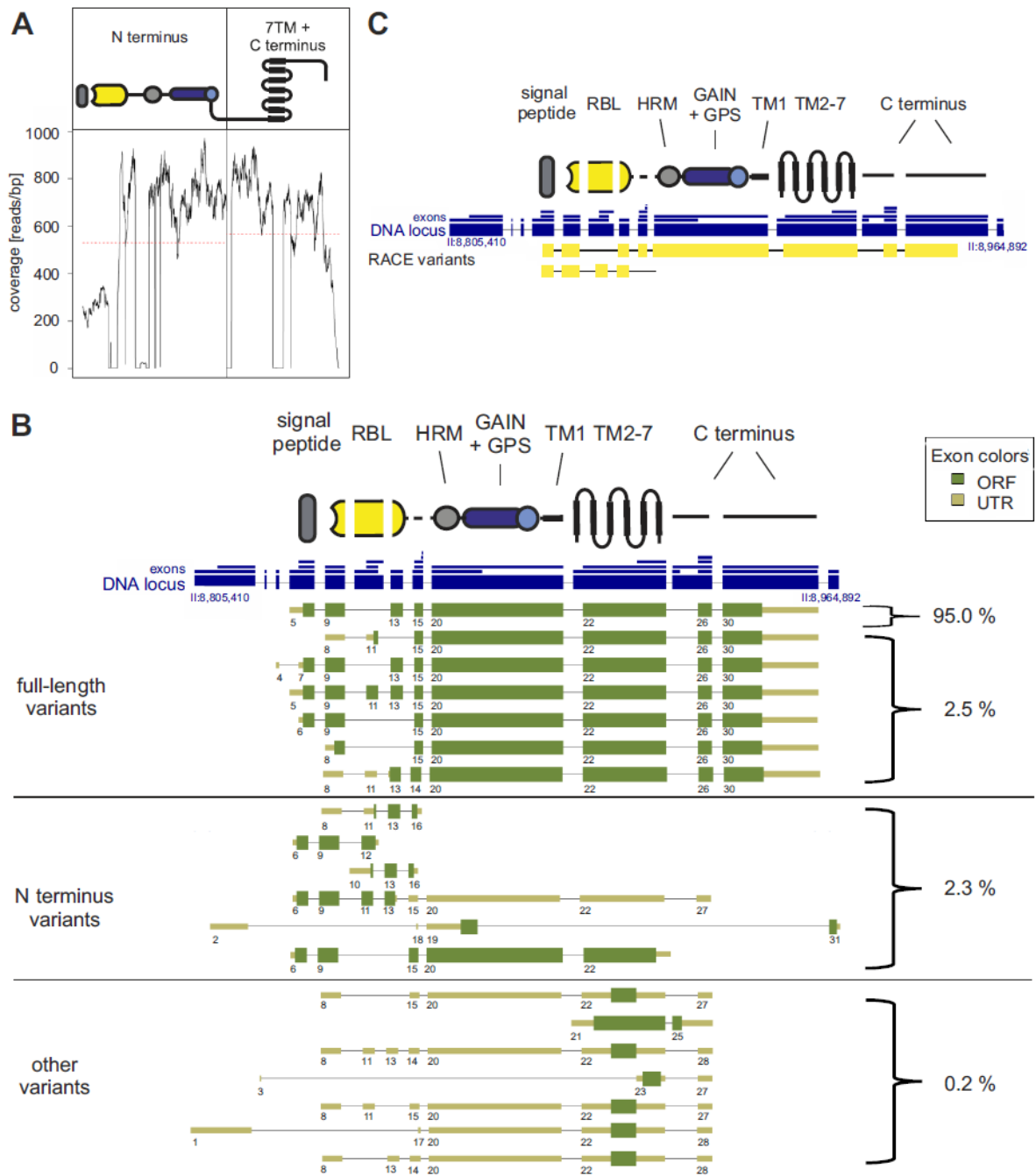


Fig. 5. Several transcripts containing only the N terminus of LAT-1 exist. (A) Read coverage of the *lat-1* locus extracted from available RNA-Seq data of day 1 adult wild-type hermaphrodites (Chen et al., 2015) shows an almost uniform distribution of reads over the entire locus. (B) Transcript variant repertoire of *lat-1* identified from RNA-Seq data (Chen et al., 2015). Several full-length variants exist which mostly differ in their N-terminus composition. N terminus only-containing variants make up 2.3% of the total *lat-1* variants in the hermaphrodite and seem mostly not to be membrane-anchored. Other variants, which

lack the N terminus, constitute less than 1%. Only full-length variants with an incidence of more than 0.01% are depicted. The genomic locus of LAT-1 is shown with its longest exons (large blue boxes) and size-condensed introns (faint blue lines). All exons found in the analysis are separately plotted above the locus (small blue boxes). The individual exon arrangements of transcripts are shown numbered. Transcripts were defined as a numeric sequence of exons. The longest bona fide open reading frame (ORF) is depicted in thick green boxes while the non-protein coding 5' and 3' untranslated regions (UTRs) are displayed thinner and in light green. 3' end exons with minor differences in length but identical 5' splice acceptor sites are considered as one 3' end exon. Different composition of the 5' start exon, 3' end exon and/or exons are considered as individual variants. The exact positions of the exons forming the variants are given in Table S2. (C) 3' RACE analyses of wild-type hermaphrodites rendered among others the full-length variant, which has been shown to be the most abundant one in RNA-Seq analyses. Further, a variant comprising the N terminus including RBL and HRM domain, but not the GAIN domain was amplified. RBL = rhamnose-binding lectin domain, HRM = hormone-binding domain, GPS = GPCR proteolytic site, GAIN = GPCR autoproteolysis-inducing domain.

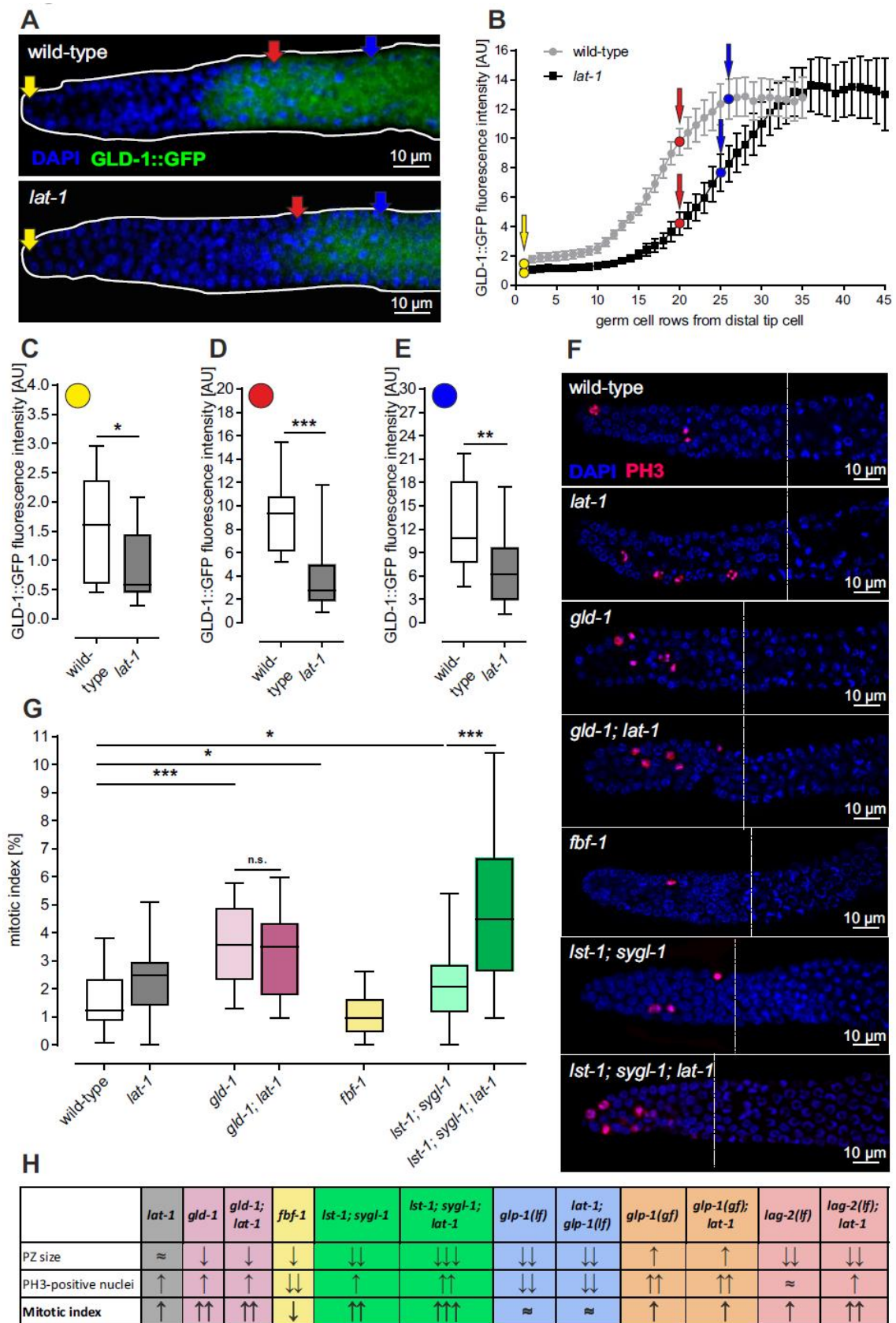


Fig. 6. LAT-1 exerts its effect on germ cell proliferation via distinct downstream effectors of the Notch pathway. (A) Expression of *gld-1* commences more proximal and is

fainter in *lat-1* mutant (bottom) than in wild-type (top) individuals. Gonads of *gld-1::gfp*-expressing (green) hermaphrodites of both genotypes 24 hours post mid-L4 were stained with DAPI (blue) and analyzed. (B)-(E) Quantification of *gld-1::gfp* expression and distribution in *lat-1* mutant and wild-type gonads by measuring fluorescence intensity (arbitrary units) with increasing distance from the distal tip cell based on images shown in (A). The absence of *lat-1* leads to a shift of *gld-1* expression to more proximal rows compared to wild-type. However, the same maximal expression level is reached eventually (B). Curves were calculated as described in the Methods section. Each point is shown as mean \pm SEM. Physiologically relevant points of expression were examined in more detail: base level (most distal row of the gonad, yellow, (C)), start of meiotic entry (mean most distal HIM-3-positive nucleus (based on Fig. 2D, F), red, (D)) and end of meiotic entry (most proximal REC-8-positive nucleus (based on Fig. 2C, E), blue, (E)). Expression at all these points in *lat-1* mutants is lower than in wild-type controls. Data are shown as boxplot with 90% confidence interval with $n \geq 16$. * $p < 0.05$; ** $p < 0.01$; *** $p < 0.001$. (F) Length of proliferative zones and amount of M-phase nuclei (magenta) in dissected and DAPI-stained (blue) gonads from wild-type, *lat-1*, *gld-1(op236)*, *gld-1(op236);lat-1*, *fbf-1(ok224)*, *lst-1(ok814);sygl-1(tm5040)*, and *lst-1(ok814);sygl-1(tm5040);lat-1(ok1465)* hermaphrodites. (G) Mitotic index quantification from DAPI- and PH3-stained gonads. *lat-1* and *gld-1* mutants exhibit increased mitotic indices. The *gld-1;lat-1* double mutant shows the same phenotype as the *gld-1* single mutant. *fbf-1* null mutants show a decreased mitotic index. While *lst-1;sygl-1* double mutants have a slightly increased mitotic index, the *lst-1;sygl-1;lat-1* triple mutant display a mitotic index higher than the *lst-1;sygl-1* and the *lat-1* mutant. The mitotic index was calculated by dividing all PH3-positive cells by the total amount of germ cells in the respective proliferative zone. Proximal tumors of *gld-1* mutants were excluded from this analysis. Raw data on PH3-positive cell counts and denominators

for index calculation can be found in Table S1. Data are shown as boxplot with 90% confidence interval, $n \geq 19$. (D) and $n \geq 27$ (E). n.s. = not significant; * $p < 0.05$; *** $p < 0.001$. (H) Schematic summary of all single and double mutant analyses conducted in this study. Changes in proliferative zone size, PH3-positive nuclei and mitotic index compared to wild-type nematodes are based on data from Figs. 6G and 7D.

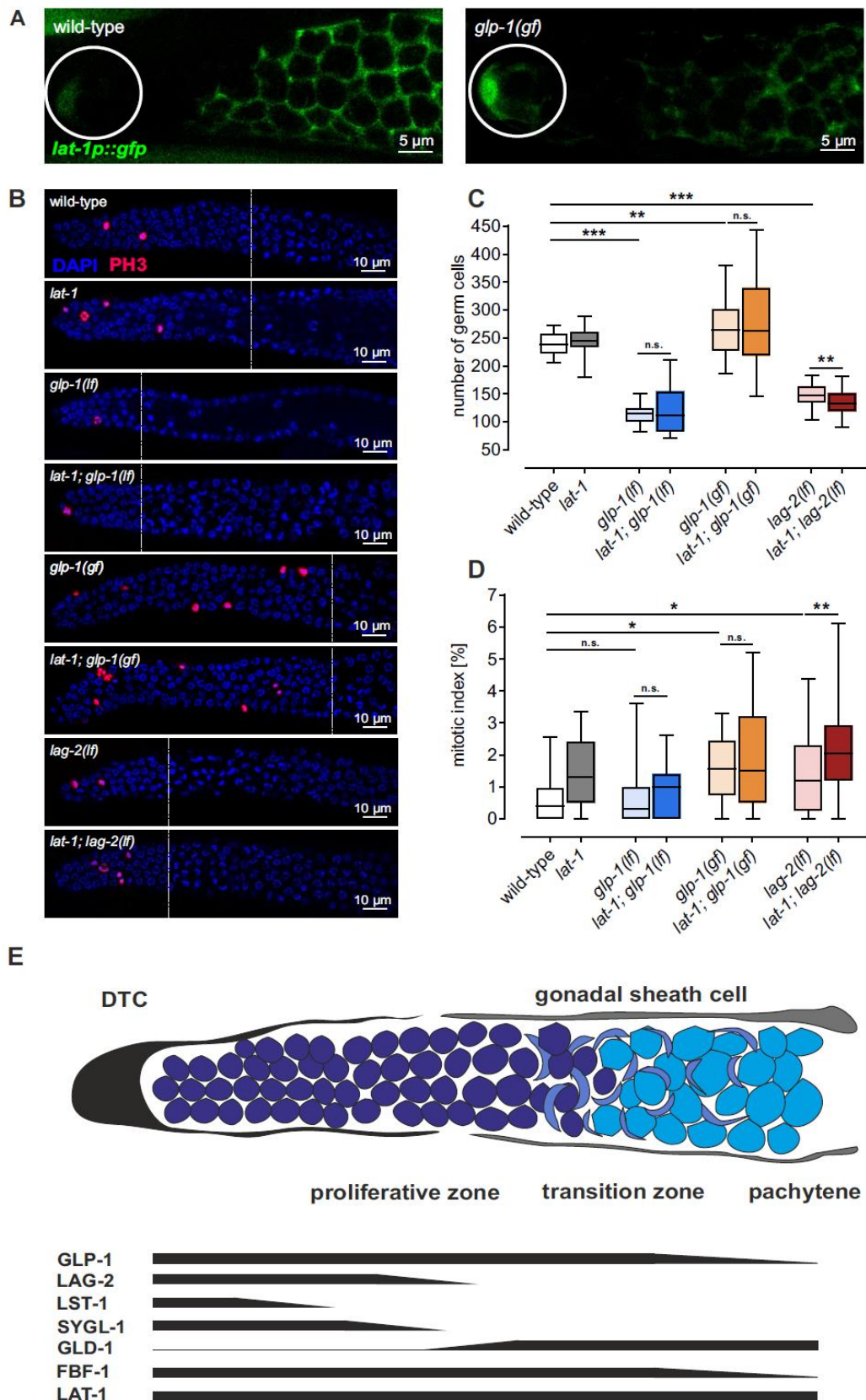


Fig. 7. LAT-1 function in proliferation depends on GLP-1, but not on LAG-2.

(A) Expression of *lat-1p::gfp* in the distal tip cell (circle) of wild-type (left) and *glp-*

l(ar202) (gain-of-function, gf) mutants (right). In *glp-1(gf)* distal tip cells, *lat-1* expression appears upregulated compared to the expression in the wild-type. Quantification of levels are shown in Fig. S4. (B) Comparison of proliferative zones of Notch pathway component single mutants and respective double mutants with *lat-1*. Gonads were dissected and DAPI- (blue) and PH3- (magenta) stained to visualize general and M-phase nuclei. (C) Quantification of proliferative zone sizes from dissected DAPI-stained gonads revealed that *lat-1;glp-1(gf)* and *lat-1;glp-1(lf)* double mutants have a similar zone size as the respective *glp-1* single mutants *glp-1(ar202)(gf)* and *glp-1(e2141)(lf)*. Data are shown as boxplot with 90% confidence interval, $n \geq 19$. n.s. = not significant; ** $p < 0.01$; *** $p < 0.001$. (D) Mitotic indices of different Notch single mutants and respective double mutants carrying *lat-1*. *glp-1(gf)* mutants (*glp-1(ar202)*) display an increase in the mitotic index, indicating high proliferative activity. The additional *lat-1* mutation does not affect this phenotype. Conversely, the *glp-1(lf)* mutant (*glp-1(e2141)*) as well as the respective double mutant with *lat-1* have a mitotic index similar to the one of the wild-type. The *lag-2(lf)* (*lag-2(q420)*) mutant shows an increase in the mitotic index. In *lat-1;lag-2(lf)* double mutants an additive effect of the single mutant indices is observed. The mitotic index was calculated by dividing all PH3-positive cells by the total amount of germ cells in the respective proliferative zone. Proximal tumors of *glp-1(gf)* mutants were excluded from this analysis. Raw data on PH3-positive cell counts and denominators for index calculation can be found in Table S1. Data are shown as boxplot with 90% confidence interval, $n \geq 19$. n.s. = not significant; * $p < 0.05$; ** $p < 0.01$. (E) Expression/Function of Notch pathway components throughout the proliferative zone and the transition zone of the gonad (adapted from (Hubbard and Schedl, 2019)). LAT-1 is present in the entire region in a pattern similar to the ones of GLP-1 and FBF-1.

ABBREVIATIONS

7TM	Seven transmembrane helices domain
ADGR	Consensual abbreviation for mammalian Adhesion GPCR genes, followed by a capital letter, indicating the receptor subfamily and a number corresponding to the individual subtype (e. g. ADGRL1)
aGPCR	Adhesion G protein-coupled receptor
<i>C. elegans</i>	<i>Caenorhabditis elegans</i>
CTF	C-terminal fragment
DIC	Differential interference contrast
DTC	Distal tip cell
<i>E. coli</i>	<i>Escherichia coli</i>
EdU	5-Ethynyl-2'-deoxyuridine
FBF-1	<i>Fem-3</i> mRNA binding factor 1
FBF-2	<i>Fem-3</i> mRNA binding factor 2
G1 phase	Gap phase 1
G2 phase	Gap phase 2
GAIN	G protein-coupled receptor autoproteolysis-inducing domain
GLD-1	Defective in germline development 1
GLD-2	Defective in germline development 2
GLP-1	Abnormal germline proliferation 1
GPCR	G protein-coupled receptor
GPS	G protein-coupled receptor proteolysis site
HIM-3	High Incidence of Males 3
HRM	Hormone-binding domain
LAG-2	Lin-12 and Glp-1 phenotype 2
LAT-1	Latrophilin-1
LIM-7	LIM domain family 7
LIN-12	Abnormal cell lineage 12
LNT	Membrane-tethered Latrophilin-1 N terminus
LST-1	Lateral signaling target 1
M index	Mitotic index
M phase	Mitotic phase
NGM	Nematode growth medium
NTF	N-terminal fragment
OSM-11	Osmotic avoidance abnormal 11
PBST	Phosphate Buffered Saline with Tween
PH3 antibody	Anti-phospho-histone H3 (Ser10) antibody
PIE-1	Pharynx and Intestine in Excess 1
PLC-1	Phospholipase C 1
RACE-PCR	rapid amplification of cDNA-ends with polymerase chain reaction
RBL	Rhamnose-binding lectin domain
REC-8	Recombination abnormal 8
ROI	Region of interest
ROL-6	Roller 6
S index	Synthesis index
S phase	Synthesis phase
Spth	Spermatheca

SYGL-1	Synthetic germline proliferation defective 1
TZ	Transition zone
UNC-119	Uncoordinated 119

REFERENCES

- Austin, J., and J. Kimble. 1987. *glp-1* is required in the germ line for regulation of the decision between mitosis and meiosis in *C. elegans*. *Cell*. 51:589-599.
- Beanan, M.J., and S. Strome. 1992. Characterization of a germ-line proliferation mutation in *C. elegans*. *Development*. 116:755-766.
- Berry, L.W., B. Westlund, and T. Schedl. 1997. Germ-line tumor formation caused by activation of *glp-1*, a *Caenorhabditis elegans* member of the Notch family of receptors. *Development*. 124:925-936.
- Bohnekamp, J., and T. Schöneberg. 2011. Cell adhesion receptor GPR133 couples to Gs protein. *J Biol Chem*. 286:41912-41916.
- Boucard, A.A., S. Maxeiner, and T.C. Sudhof. 2013. Latrophilins function as heterophilic cell-adhesion molecules by binding to teneurins: regulation by alternative splicing. *J Biol Chem*. 289:387-402.
- Brenner, J.L., and T. Schedl. 2016. Germline Stem Cell Differentiation Entails Regional Control of Cell Fate Regulator GLD-1 in *Caenorhabditis elegans*. *Genetics*. 202:1085-1103.
- Brenner, S. 1974. The genetics of *Caenorhabditis elegans*. *Genetics*. 77:71-94.
- Bukhari, S.I., A. Vasquez-Rifo, D. Gagne, E.R. Paquet, M. Zetka, C. Robert, J.Y. Masson, and M.J. Simard. 2012. The microRNA pathway controls germ cell proliferation and differentiation in *C. elegans*. *Cell Res*. 22:1034-1045.
- Byrd, D.T., K. Knobel, K. Affeldt, S.L. Crittenden, and J. Kimble. 2014. A DTC niche plexus surrounds the germline stem cell pool in *Caenorhabditis elegans*. *PLoS One*. 9:e88372.
- Chen, A.T., C. Guo, O.A. Itani, B.G. Budaitis, T.W. Williams, C.E. Hopkins, R.C. McEachin, M. Pande, A.R. Grant, S. Yoshina, S. Mitani, and P.J. Hu. 2015. Longevity Genes Revealed by Integrative Analysis of Isoform-Specific *daf-16/FoxO* Mutants of *Caenorhabditis elegans*. *Genetics*. 201:613-629.
- Crittenden, S.L., D.S. Bernstein, J.L. Bachorik, B.E. Thompson, M. Gallegos, A.G. Petcherski, G. Moulder, R. Barstead, M. Wickens, and J. Kimble. 2002. A conserved RNA-binding protein controls germline stem cells in *Caenorhabditis elegans*. *Nature*. 417:660-663.
- Crittenden, S.L., C. Lee, I. Mohanty, S. Battula, K. Knobel, and J. Kimble. 2019. Sexual dimorphism of niche architecture and regulation of the *Caenorhabditis elegans* germline stem cell pool. *Mol Biol Cell*. 30:1757-1769.
- Crittenden, S.L., K.A. Leonhard, D.T. Byrd, and J. Kimble. 2006. Cellular analyses of the mitotic region in the *Caenorhabditis elegans* adult germ line. *Mol Biol Cell*. 17:3051-3061.
- D'Amato, G., G. Luxan, G. del Monte-Nieto, B. Martinez-Poveda, C. Torroja, W. Walter, M.S. Bochter, R. Benedito, S. Cole, F. Martinez, A.K. Hadjantonakis, A. Uemura, L.J. Jimenez-Borreguero, and J.L. de la Pompa. 2016. Sequential Notch activation regulates ventricular chamber development. *Nat Cell Biol*. 18:7-20.
- D'Souza, B., L. Meloty-Kapella, and G. Weinmaster. 2010. Canonical and non-canonical Notch ligands. *Curr Top Dev Biol*. 92:73-129.
- Dobin, A., and T.R. Gingeras. 2015. Mapping RNA-seq Reads with STAR. *Curr Protoc Bioinformatics*. 51:1114-1119.
- Dolphin, C.T., and I.A. Hope. 2006. *Caenorhabditis elegans* reporter fusion genes generated by seamless modification of large genomic DNA clones. *Nucleic Acids Res*. 34:e72.
- Evans, T.C. 2006. Transformation and microinjection. In *WormBook*. The *C. elegans* Research Community, WormBook.
- Fitzgerald, K., and I. Greenwald. 1995. Interchangeability of *Caenorhabditis elegans* DSL proteins and intrinsic signalling activity of their extracellular domains in vivo. *Development*. 121:4275-4282.
- Fox, P.M., and T. Schedl. 2015. Analysis of Germline Stem Cell Differentiation Following Loss of GLP-1 Notch Activity in *Caenorhabditis elegans*. *Genetics*. 201:167-184.
- Fox, P.M., V.E. Vought, M. Hanazawa, M.H. Lee, E.M. Maine, and T. Schedl. 2011. Cyclin E and CDK-2 regulate proliferative cell fate and cell cycle progression in the *C. elegans* germline. *Development*. 138:2223-2234.
- Francis, R., M.K. Barton, J. Kimble, and T. Schedl. 1995. *gld-1*, a tumor suppressor gene required for oocyte development in *Caenorhabditis elegans*. *Genetics*. 139:579-606.

- Furuta, T., H.J. Joo, K.A. Trimmer, S.Y. Chen, and S. Arur. 2018. GSK-3 promotes S-phase entry and progression in *C. elegans* germline stem cells to maintain tissue output. *Development*. 145.
- Gartner, A., P.R. Boag, and T.K. Blackwell. 2008. Germline survival and apoptosis. *WormBook*:1-20.
- Gupte, J., G. Swaminath, J. Danao, H. Tian, Y. Li, and X. Wu. 2012. Signaling property study of adhesion G-protein-coupled receptors. *FEBS Lett*. 586:1214-1219.
- Hall, D.H., V.P. Winfrey, G. Blaeuer, L.H. Hoffman, T. Furuta, K.L. Rose, O. Hobert, and D. Greenstein. 1999. Ultrastructural features of the adult hermaphrodite gonad of *Caenorhabditis elegans*: relations between the germ line and soma. *Dev Biol*. 212:101-123.
- Hamann, J., G. Aust, D. Arac, F.B. Engel, C. Formstone, R. Fredriksson, R.A. Hall, B.L. Harty, C. Kirchhoff, B. Knapp, A. Krishnan, I. Liebscher, H.H. Lin, D.C. Martinelli, K.R. Monk, M.C. Peeters, X. Piao, S. Prömel, T. Schöneberg, T.W. Schwartz, K. Singer, M. Stacey, Y.A. Ushkaryov, M. Vallon, U. Wolfrum, M.W. Wright, L. Xu, T. Langenhan, and H.B. Schioth. 2015. International Union of Basic and Clinical Pharmacology. XCIV. Adhesion G protein-coupled receptors. *Pharmacological reviews*. 67:338-367.
- Han, S.M., P.A. Cottee, and M.A. Miller. 2010. Sperm and oocyte communication mechanisms controlling *C. elegans* fertility. *Developmental dynamics : an official publication of the American Association of Anatomists*. 239:1265-1281.
- Hansen, D., E.J. Hubbard, and T. Schedl. 2004. Multi-pathway control of the proliferation versus meiotic development decision in the *Caenorhabditis elegans* germline. *Dev Biol*. 268:342-357.
- Henderson, S.T., D. Gao, S. Christensen, and J. Kimble. 1997. Functional domains of LAG-2, a putative signaling ligand for LIN-12 and GLP-1 receptors in *Caenorhabditis elegans*. *Mol Biol Cell*. 8:1751-1762.
- Henderson, S.T., D. Gao, E.J. Lambie, and J. Kimble. 1994. lag-2 may encode a signaling ligand for the GLP-1 and LIN-12 receptors of *C. elegans*. *Development*. 120:2913-2924.
- Hirsh, D., D. Oppenheim, and M. Klass. 1976. Development of the reproductive system of *Caenorhabditis elegans*. *Dev Biol*. 49:200-219.
- Howe, K.L., B.J. Bolt, M. Shafie, P. Kersey, and M. Berriman. 2017. WormBase ParaSite - a comprehensive resource for helminth genomics. *Molecular and biochemical parasitology*. 215:2-10.
- Hubbard, E.J. 2007. *Caenorhabditis elegans* germ line: a model for stem cell biology. *Developmental dynamics : an official publication of the American Association of Anatomists*. 236:3343-3357.
- Hubbard, E.J.A., and T. Schedl. 2019. Biology of the *Caenorhabditis elegans* Germline Stem Cell System. *Genetics*. 213:1145-1188.
- Jeong, J., J.M. Verheyden, and J. Kimble. 2011. Cyclin E and Cdk2 control GLD-1, the mitosis/meiosis decision, and germline stem cells in *Caenorhabditis elegans*. *PLoS Genet*. 7:e1001348.
- Jones, A.R., R. Francis, and T. Schedl. 1996. GLD-1, a cytoplasmic protein essential for oocyte differentiation, shows stage- and sex-specific expression during *Caenorhabditis elegans* germline development. *Dev Biol*. 180:165-183.
- Joshi, I., L.M. Minter, J. Telfer, R.M. Demarest, A.J. Capobianco, J.C. Aster, P. Sicinski, A. Fauq, T.E. Golde, and B.A. Osborne. 2009. Notch signaling mediates G1/S cell-cycle progression in T cells via cyclin D3 and its dependent kinases. *Blood*. 113:1689-1698.
- Kershner, A.M., H. Shin, T.J. Hansen, and J. Kimble. 2014. Discovery of two GLP-1/Notch target genes that account for the role of GLP-1/Notch signaling in stem cell maintenance. *Proc Natl Acad Sci U S A*. 111:3739-3744.
- Kimble, J., and S.L. Crittenden. 2005. Germline proliferation and its control. *WormBook*:1-14.
- Kimble, J., and H. Seidel. 2008. *C. elegans* germline stem cells and their niche. In *StemBook*, Cambridge (MA).
- Knierim, A.B., J. Röthe, M.V. Cakir, V. Lede, C. Wilde, I. Liebscher, D. Thor, and T. Schöneberg. 2019. Genetic basis of functional variability in adhesion G protein-coupled receptors. *Scientific reports*. 9:11036.
- Kocsisova, Z., K. Kornfeld, and T. Schedl. 2019. Rapid population-wide declines in stem cell number and activity during reproductive aging in *C. elegans*. *Development*. 146.
- Kocsisova, Z., A. Mohammad, K. Kornfeld, and T. Schedl. 2018. Cell Cycle Analysis in the *C. elegans* Germline with the Thymidine Analog EdU. *J Vis Exp*.
- Kodama, Y., M. Shumway, R. Leinonen, and C. International Nucleotide Sequence Database. 2012. The Sequence Read Archive: explosive growth of sequencing data. *Nucleic Acids Res*. 40:D54-56.
- Kodoyianni, V., E.M. Maine, and J. Kimble. 1992. Molecular basis of loss-of-function mutations in the glp-1 gene of *Caenorhabditis elegans*. *Mol Biol Cell*. 3:1199-1213.
- Komatsu, H., M.Y. Chao, J. Larkins-Ford, M.E. Corkins, G.A. Somers, T. Tucey, H.M. Dionne, J.Q. White, K. Wani, M. Boxem, and A.C. Hart. 2008. OSM-11 facilitates LIN-12 Notch signaling during *Caenorhabditis elegans* vulval development. *PLoS biology*. 6:e196.
- Kopan, R., and M.X. Ilagan. 2009. The canonical Notch signaling pathway: unfolding the activation mechanism. *Cell*. 137:216-233.

- L'Hernault, S.W. 2006. Spermatogenesis. *WormBook*:1-14.
- Lambie, E.J., and J. Kimble. 1991. Two homologous regulatory genes, *lin-12* and *glp-1*, have overlapping functions. *Development*. 112:231-240.
- Lamont, L.B., S.L. Crittenden, D. Bernstein, M. Wickens, and J. Kimble. 2004. FBF-1 and FBF-2 regulate the size of the mitotic region in the *C. elegans* germline. *Dev Cell*. 7:697-707.
- Langenhan, T., S. Prömel, L. Mestek, B. Esmaili, H. Waller-Evans, C. Hennig, Y. Kohara, L. Avery, I. Vakonakis, R. Schnabel, and A.P. Russ. 2009. Latrophilin signaling links anterior-posterior tissue polarity and oriented cell divisions in the *C. elegans* embryo. *Dev Cell*. 17:494-504.
- Leinonen, R., H. Sugawara, M. Shumway, and C. International Nucleotide Sequence Database. 2011. The sequence read archive. *Nucleic Acids Res*. 39:D19-21.
- Lin, H.H., G.W. Chang, J.Q. Davies, M. Stacey, J. Harris, and S. Gordon. 2004. Autocatalytic cleavage of the EMR2 receptor occurs at a conserved G protein-coupled receptor proteolytic site motif. *J Biol Chem*. 279:31823-31832.
- Maciejowski, J., N. Ugel, B. Mishra, M. Isopi, and E.J. Hubbard. 2006. Quantitative analysis of germline mitosis in adult *C. elegans*. *Dev Biol*. 292:142-151.
- Michaelson, D., D.Z. Korta, Y. Capua, and E.J. Hubbard. 2010. Insulin signaling promotes germline proliferation in *C. elegans*. *Development*. 137:671-680.
- Miller, D.M., and D.C. Shakes. 1995. Immunofluorescence microscopy. *Methods Cell Biol*. 48:365-394.
- Mohammad, A., K. Vanden Broek, C. Wang, A. Daryabeigi, V. Jantsch, D. Hansen, and T. Schedl. 2018. Initiation of Meiotic Development Is Controlled by Three Post-transcriptional Pathways in *Caenorhabditis elegans*. *Genetics*. 209:1197-1224.
- Müller, A., J. Winkler, F. Fiedler, T. Sastradihardja, C. Binder, R. Schnabel, J. Kungel, S. Rothemund, C. Hennig, T. Schöneberg, and S. Prömel. 2015. Oriented Cell Division in the *C. elegans* Embryo Is Coordinated by G-Protein Signaling Dependent on the Adhesion GPCR LAT-1. *PLoS Genet*. 11:e1005624.
- Okajima, D., G. Kudo, and H. Yokota. 2010. Brain-specific angiogenesis inhibitor 2 (BAI2) may be activated by proteolytic processing. *J Recept Signal Transduct Res*. 30:143-153.
- Pasquale, E.B. 2008. Eph-ephrin bidirectional signaling in physiology and disease. *Cell*. 133:38-52.
- Patat, O., A. Pagin, A. Siegfried, V. Mitchell, N. Chassaing, S. Faguer, L. Monteil, V. Gaston, L. Bujan, M. Courtade-Saidi, F. Marcelli, G. Lalau, J.M. Rigot, R. Mieusset, and E. Bieth. 2016. Truncating Mutations in the Adhesion G Protein-Coupled Receptor G2 Gene ADGRG2 Cause an X-Linked Congenital Bilateral Absence of Vas Deferens. *Am J Hum Genet*. 99:437-442.
- Patra, C., M.J. van Amerongen, S. Ghosh, F. Ricciardi, A. Sajjad, T. Novoyatleva, A. Mogha, K.R. Monk, C. Muhlfeld, and F.B. Engel. 2013. Organ-specific function of adhesion G protein-coupled receptor GPR126 is domain-dependent. *Proc Natl Acad Sci U S A*. 110:16898-16903.
- Pepper, A.S., D.J. Killian, and E.J. Hubbard. 2003. Genetic analysis of *Caenorhabditis elegans glp-1* mutants suggests receptor interaction or competition. *Genetics*. 163:115-132.
- Pertea, M., G.M. Pertea, C.M. Antonescu, T.C. Chang, J.T. Mendell, and S.L. Salzberg. 2015. StringTie enables improved reconstruction of a transcriptome from RNA-seq reads. *Nat Biotechnol*. 33:290-295.
- Pinkston, J.M., D. Garigan, M. Hansen, and C. Kenyon. 2006. Mutations that increase the life span of *C. elegans* inhibit tumor growth. *Science*. 313:971-975.
- Prömel, S., M. Frickenhaus, S. Hughes, L. Mestek, D. Staunton, A. Woollard, I. Vakonakis, T. Schöneberg, R. Schnabel, A.P. Russ, and T. Langenhan. 2012. The GPS motif is a molecular switch for bimodal activities of adhesion class G protein-coupled receptors. *Cell Rep*. 2:321-331.
- Robinson, J.T., H. Thorvaldsdottir, W. Winckler, M. Guttman, E.S. Lander, G. Getz, and J.P. Mesirov. 2011. Integrative genomics viewer. *Nat Biotechnol*. 29:24-26.
- Röthe, J., D. Thor, J. Winkler, A.B. Knierim, C. Binder, S. Huth, R. Kraft, S. Rothemund, T. Schöneberg, and S. Prömel. 2019. Involvement of the Adhesion GPCRs Latrophilins in the Regulation of Insulin Release. *Cell Rep*. 26:1573-1584 e1575.
- Roy, D., D. Michaelson, T. Hochman, A. Santella, Z. Bao, J.D. Goldberg, and E.J.A. Hubbard. 2016. Cell cycle features of *C. elegans* germline stem/progenitor cells vary temporally and spatially. *Dev Biol*. 409:261-271.
- Schindelin, J., I. Arganda-Carreras, E. Frise, V. Kaynig, M. Longair, T. Pietzsch, S. Preibisch, C. Rueden, S. Saalfeld, B. Schmid, J.Y. Tinevez, D.J. White, V. Hartenstein, K. Eliceiri, P. Tomancak, and A. Cardona. 2012. Fiji: an open-source platform for biological-image analysis. *Nat Methods*. 9:676-682.
- Schneider, C.A., W.S. Rasband, and K.W. Eliceiri. 2012. NIH Image to ImageJ: 25 years of image analysis. *Nat Methods*. 9:671-675.
- Schumacher, B., M. Hanazawa, M.H. Lee, S. Nayak, K. Volkmann, E.R. Hofmann, M. Hengartner, T. Schedl, and A. Gartner. 2005. Translational repression of *C. elegans p53* by GLD-1 regulates DNA damage-induced apoptosis. *Cell*. 120:357-368.

- Shin, H., K.A. Haupt, A.M. Kershner, P. Kroll-Conner, M. Wickens, and J. Kimble. 2017. SYGL-1 and LST-1 link niche signaling to PUF RNA repression for stem cell maintenance in *Caenorhabditis elegans*. *PLoS Genet.* 13:e1007121.
- Siebel, C., and U. Lendahl. 2017. Notch Signaling in Development, Tissue Homeostasis, and Disease. *Physiological reviews.* 97:1235-1294.
- Singh, K., M.Y. Chao, G.A. Somers, H. Komatsu, M.E. Corkins, J. Larkins-Ford, T. Tucey, H.M. Dionne, M.B. Walsh, E.K. Beaumont, D.P. Hart, S.R. Lockery, and A.C. Hart. 2011. *C. elegans* Notch signaling regulates adult chemosensory response and larval molting quiescence. *Curr Biol.* 21:825-834.
- Steimel, A., L. Wong, E.H. Najarro, B.D. Ackley, G. Garriga, and H. Hutter. 2010. The Flamingo ortholog FMI-1 controls pioneer-dependent navigation of follower axons in *C. elegans*. *Development.* 137:3663-3673.
- Tourasse, N.J., J.R.M. Millet, and D. Dupuy. 2017. Quantitative RNA-seq meta-analysis of alternative exon usage in *C. elegans*. *Genome Res.* 27:2120-2128.
- Tu, Y.K., J.G. Duman, and K.F. Tolias. 2018. The Adhesion-GPCR BAI1 Promotes Excitatory Synaptogenesis by Coordinating Bidirectional Trans-synaptic Signaling. *J Neurosci.*
- Tursun, B., L. Cochella, I. Carrera, and O. Hobert. 2009. A toolkit and robust pipeline for the generation of fosmid-based reporter genes in *C. elegans*. *PLoS One.* 4:e4625.
- Ward, Y., R. Lake, F. Faraji, J. Sperger, P. Martin, C. Gilliard, K.P. Ku, T. Rodems, D. Niles, H. Tillman, J. Yin, K. Hunter, A.G. Sowalsky, J. Lang, and K. Kelly. 2018. Platelets Promote Metastasis via Binding Tumor CD97 Leading to Bidirectional Signaling that Coordinates Transendothelial Migration. *Cell Rep.* 23:808-822.
- Warming, S., N. Costantino, D.L. Court, N.A. Jenkins, and N.G. Copeland. 2005. Simple and highly efficient BAC recombineering using galK selection. *Nucleic Acids Res.* 33:e36.
- Zetka, M.C., I. Kawasaki, S. Strome, and F. Muller. 1999. Synapsis and chiasma formation in *Caenorhabditis elegans* require HIM-3, a meiotic chromosome core component that functions in chromosome segregation. *Genes & development.* 13:2258-2270.

4.3 G Proteins and GPCRs in *C. elegans* Development: A Story of Mutual Infidelity (Review)

Authors: Daniel Matúš, Simone Prömel

Journal: Journal of Developmental Biology

Impact Factor: not assigned (CiteScore 2018 from Scopus.com: 3.6)

Submitted: 20 Oct 2018

Accepted: 22 Nov 2018

Published: 25 Nov 2018

References: 111

Language: English

Publisher: Multidisciplinary Digital Publishing Institute (MDPI)

PubMed ID: 30477278

DOI: <https://doi.org/10.3390/jdb6040028>

Review

G Proteins and GPCRs in *C. elegans* Development: A Story of Mutual Infidelity

Daniel Matúš and Simone Prömel *

Rudolf Schönheimer Institute of Biochemistry, Medical Faculty, Leipzig University, 04103 Leipzig, Germany; daniel.matus@medizin.uni-leipzig.de

* Correspondence: simone.proemel@medizin.uni-leipzig.de; Tel.: +49-341-9722147

Received: 20 October 2018; Accepted: 22 November 2018; Published: 25 November 2018



Abstract: Many vital processes during *C. elegans* development, especially the establishment and maintenance of cell polarity in embryogenesis, are controlled by complex signaling pathways. G protein-coupled receptors (GPCRs), such as the four Frizzled family Wnt receptors, are linchpins in regulating and orchestrating several of these mechanisms. However, despite being GPCRs, which usually couple to G proteins, these receptors do not seem to activate classical heterotrimeric G protein-mediated signaling cascades. The view on signaling during embryogenesis is further complicated by the fact that heterotrimeric G proteins do play essential roles in cell polarity during embryogenesis, but their activity is modulated in a predominantly GPCR-independent manner via G protein regulators such as GEFs GAPs and GDIs. Further, the triggered downstream effectors are not typical. Only very few GPCR-dependent and G protein-mediated signaling pathways have been unambiguously defined in this context. This unusual and highly intriguing concept of separating GPCR function and G-protein activity, which is not restricted to embryogenesis in *C. elegans* but can also be found in other organisms, allows for essential and multi-faceted ways of regulating cellular communication and response. Although its relevance cannot be debated, its impact is still poorly discussed, and *C. elegans* is an ideal model to understand the underlying principles.

Keywords: GPCRs; G proteins; development; receptor-independent function

1. GPCRs and G Proteins—Together and Apart

G protein-coupled receptors (GPCRs) and heterotrimeric G proteins are molecules, which together form one of the key systems essential to transduce extracellular cues into cells and mediate signals. Thereby, GPCRs are seven transmembrane receptors binding the G proteins with their intracellular parts. These G proteins are trimers composed of α , β , and γ subunits with the α subunit being able to bind the guanine nucleotide GDP when attached to the receptor. Upon receiving a stimulus such as photons, hormones, proteins, or peptides, the GPCR acts as a guanine nucleotide exchange factor (GEF) exchanging the GDP bound to the $G\alpha$ for a GTP. This activates the G protein, which is then able to mediate signals by both the $G\alpha$ subunit and the dissociated $G\beta\gamma$ complex. Subsequently, the GTP is subject to hydrolysis, thereby inactivating the G protein, which re-associates as a trimer with the GPCR and thus completing this so-called G-protein cycle (Figure 1).

In the last few decades, many studies have shown that the classical interaction between G proteins and the corresponding receptor is not the only way these molecules can signal. For GPCRs, an increasing body of data suggests that they are able to signal completely independently of G proteins, for instance via arrestins (reviewed in [1]) or Jak-Kinases [2]. Similarly, heterotrimeric G proteins can function in the absence of GPCRs [3,4]. These findings paved the way for the notion that GPCRs and G proteins can fulfill a plethora of functional roles beyond classical signaling. However, many details of

the mechanisms and the relevance of G protein-independent GPCR signaling and GPCR-independent G-protein signaling remain poorly understood.

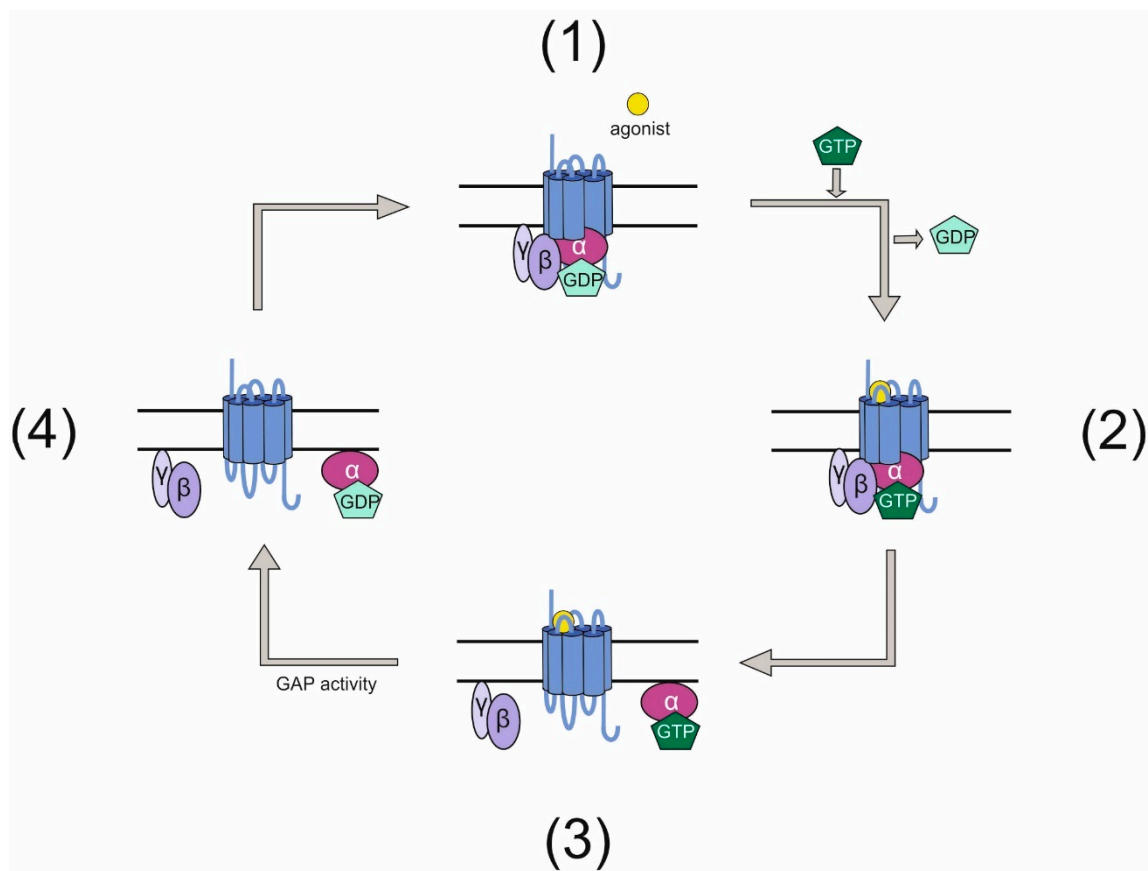


Figure 1. Classical G-protein cycle. (1) An inactive GPCR is associated intracellularly with a heterotrimeric G protein. This G protein has bound GDP on its $G\alpha$ subunit. (2) Upon activation of the GPCR by an agonist, the receptor acts as a GEF for the G protein and exchanges GDP for GTP. (3) The active G protein dissociates into $G\alpha$ and a $G\beta\gamma$ complex, both of which can mediate signals. (4) After signals have been elicited, the GTP bound to $G\alpha$ is hydrolyzed rendering the G protein inactive. The G protein subunits re-associate and bind the GPCR.

2. GPCRs and G Proteins Are Essential for *C. elegans* Development

As GPCRs and G proteins are involved in many physiological processes and are vital in health and disease, it is not surprising that they are also found to be linchpins for orchestrating signaling processes during development in many organisms. The *Caenorhabditis elegans* genome encodes for more than 1000 GPCRs [5] and its heterotrimeric G protein repertoire comprises 21 $G\alpha$ subunits, 2 $G\beta$ and 2 $G\gamma$ proteins [6]. Throughout *C. elegans* development and especially during early embryogenesis, several essential processes are governed by GPCRs and/or G proteins, together or separately. This offers an ideal and well-characterized system to gain insights into the mechanisms underlying the diverse functions of GPCRs and G proteins as well as their fundamental impact in biology. Although certainly not all processes, in which GPCRs/G proteins have a function, are fully uncovered yet, several examples highlight the potential of the system.

2.1. $G\alpha$ Subunits Dictate Asymmetric Spindle Positioning

Already during the first cell division, G proteins are involved in asymmetric positioning of the mitotic spindle in the one-cell-stage embryo to ultimately promote asymmetric cell division. The two maternally required $G\alpha$ subunits GOA-1 and GPA-16 are in part redundantly required for transducing

polarity cues to generate pulling force on the mitotic spindle during cell cleavage [7,8] (Figure 2A). While GOA-1 is a $G\alpha_o$ subunit, homology comparison of the structurally similar GPA-16 with mammalian $G\alpha$ subunits does not allow for its clear identification as a $G\alpha_o$ protein [6]. In wild-type embryos prior to the first cell cleavage, centrosomes align along the anterior–posterior axis by a rotation during prophase [9] and pulling forces are exerted along this axis. These are asymmetric in the way that the posterior spindle pole moves closer to the cortex than the anterior pole [10,11], subsequently leading to the generation of two cells of unequal size. Embryos mutant for *gpa-16* exhibit a reduced and more symmetric pulling force during cell cleavage [12]. Similarly, loss of function of *goa-1* and *gpa-16* causes a loss of nuclear rotation as well as reduced pulling of the spindle toward the posterior [7,8] yielding two symmetric cells. Both G proteins exert a pulling force on astral microtubules in a ternary complex comprising the GoLoco motif-containing GPR-1 or GPR-2 and the coiled-coil protein LIN-5 [7,8,13–15]. Through its myristoylation, the $G\alpha$ protein anchors the complex to the plasma membrane and in parallel binds GPR-1/2, which also associates with LIN-5 [15–18]. How the asymmetric pulling is subsequently realized is not entirely understood, but several studies show the involvement of microtubules and dynein in this process [17,19,20]. Dynein appears to serve as a connecting molecule between the ternary complex and astral microtubules [21]. However, whether it is the core force generator is still debated. Interestingly, the polarity cue triggering the asymmetric spindle pulling is not elicited by a GPCR but rather by cortically localized cytoplasmic PAR proteins (reviewed in [22]) and modulated mostly via regulators of G protein signaling (RGS) such as RGS-7, guanine-nucleotide dissociation inhibitors (GDIs) [8], and GEF proteins such as RIC-8 [23]. The molecular details of G-protein activation involving these modulators and the mechanisms behind its function will be discussed in Section 3.

Not only the $G\alpha$ subunits but also the associated $G\beta$ and $G\gamma$ proteins have been identified to be involved in spindle positioning and pulling force generation. Both β subunits present in *C. elegans* are expressed in embryos [24,25], but only GPB-1 seems to be required for spindle positioning [7,25], functioning with the $G\gamma$ subunit GPC-2 [7]. The distinct roles of $G\beta$ and $G\gamma$ remain elusive to a certain extent. It has been postulated that one function of GPB-1 in this context might be the regulation of $G\alpha$ availability by forming a heterotrimer as the amount of unbound α subunits influences pulling forces. Deficiency of GPB-1 or GPC-2 increases pulling forces toward the anterior and elevates rotational movement [8,23,26], suggesting that the $G\beta\gamma$ complex is negatively regulating force generation. In line with these data, its amount and distribution within the cell is asymmetric and dynamic during cell division [27].

Several lines of evidence show that positioning of mitotic spindles and dictating pulling force during later cell divisions are also likely to be guided by the G proteins GOA-1 and GPA-16. In embryos lacking both $G\alpha$ subunits, the nucleus in the P_1 blastomere does not rotate, and mitotic spindle directionality does not form correctly [7]. Further, embryos contain polyploid nuclei and fewer cells [15]. A second line of evidence using a temperature-sensitive *gpa-16* mutant highlights that spindle orientation is defective in the EMS blastomere when shifting mutant embryos to the restrictive temperature after the second cell division [8]. However, this effect is not fully penetrant, most likely due to the partially redundant signaling of the MES1/SRC-1 pathway [8]. This pathway has also been shown to be involved in controlling spindle polarity via the intracellular modulator LET-99 [28].

As a variation of the aforementioned mechanism of asymmetric spindle positioning can be considered the role of GPA-16 in the establishment of left-right (l-r) asymmetry. In *C. elegans*, l-r asymmetry first becomes apparent at the six-cell stage when the blastomeres ABal/ABpl are located more anteriorly than ABar/ABpr [29,30]. The mechanism underlying cell positioning is based on mitotic spindle orientation. In this context, it has been demonstrated that a temperature-sensitive *gpa-16* mutant displays a randomized ABa/p spindle skew handedness, suggesting that the $G\alpha$ subunit is required for the positioning of ABa and ABp spindles preceding skewing [31]. The role of other G protein signaling components in this context as well as the downstream targets that execute spindle orientation remain to be clarified.

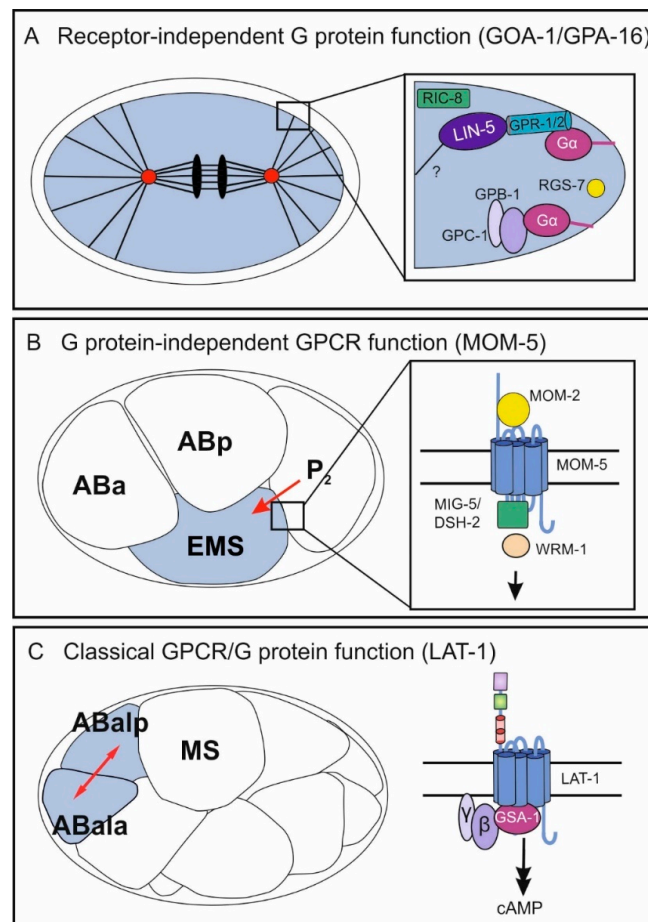


Figure 2. Independent and classical functions of GPCRs/G proteins in different processes during *C. elegans* embryonic development. In the early embryo, all three mechanisms occur in different biological contexts: the receptor-independent G-protein function (GOA-1/GPA-16) (A), the G protein-independent GPCR function (MOM-5) (B), and the classical GPCR/G protein pathway (C). (A) GOA-1 and GPA-1 control pulling force on astral microtubules leading to two asymmetric cells after the first division. The Gα proteins function in a ternary complex with GPR-1/GPR-2 and LIN-5 and are modulated by the GEF RIC-8 and the RGS RGS-7. Further, the Gβ and Gγ subunits GPB-1 and GPC-1 are hypothesized to contribute to regulation of pulling forces. (B) The Frizzled class GPCR MOM-5 mediates a signal from the P₂ blastomere polarizing the neighboring EMS cell. Upon activation by the Wnt ligand MOM-2, MOM-5 activates the disheveled homologs MIG-5/DSH-2 and subsequently involves the β-catenin WRM-1. Note that asymmetric localization of the different components is not depicted. (C) A classical GPCR/G protein pathway in embryonic development is realized by the Adhesion GPCR LAT-1, which controls anterior–posterior cell division of several blastomeres including ABal. LAT-1 activates the Gs pathway via the Gα protein GSA-1 yielding an increase in the second messenger cAMP. For the physiological relevance of each GPCR/G-protein function, see Section 1. Mechanistic details are discussed in Sections 2 and 3.

2.2. The GPCR Frizzled Is Involved in Polarity and Spindle Orientation

The roles of several heterotrimeric G proteins in spindle orientation and cell division in early *C. elegans* embryogenesis has been firmly demonstrated in numerous studies (Section 2.1). However, these G-protein functions are independent of any GPCR and thus are termed “receptor-independent.” GPCRs are also associated with early embryonic cell division and polarity establishment. The most prominent GPCRs in this context are the four Frizzled family Wnt receptors, which control spindle polarity in the fourth round of cell division. In nematodes mutant for components of the Wnt pathway, spindles are tilted compared to those of wild-type embryos leading to severe defects, which in part also

result in embryonic lethality [32–36]. The Wnt signaling pathway is required for anterior–posterior fate decisions. It polarizes the EMS blastomere for asymmetric cell division by conveying a signal from the neighboring P₂ blastomere [34,35,37,38] (Figure 2B). Thereby, the cue produced by P₂ is the Wnt ligand MOM-2 and the Frizzled homolog is MOM-5 [39]. The signals mediated by Wnt/Frizzled in this context involve components of the canonical Wnt signaling pathway, which is realized by several downstream molecules including Disheveled and β -catenin homologs (reviewed in [40,41], for some mechanistic details, see Section 2). However, to date no G proteins have been found to act in this context.

Further, Wnt receptors are involved in other developmental processes, e.g., vulva and larval development, in which they also signal G protein-independently via a canonical pathway (summarized in [42]).

2.3. The GPCR LAT-1 Signals via G Proteins in Oriented Cell Division

As discussed above, GPCRs and G proteins are essential players in controlling spindle positioning and oriented cell division. However, in all these cases both molecules act independently of each other. Despite clear indications, GPCR-dependent and G protein-mediated signaling pathways had not been unambiguously defined for a long time [43,44]. Recently, the Adhesion GPCR Latrophilin-1 (LAT-1) has been identified to mediate spindle orientation in an anterior–posterior direction in distinct blastomeres from the 12-cell stage during symmetric cell division. This GPCR signals via the G α_s protein GSA-1, ultimately increasing intracellular cAMP levels [45–47] (Figure 2C). Mutants null for *lat-1* display skewed division angles of the ABal blastomere (and some daughter cells), in a way that this division plane is almost perpendicular to MS, whereas in wild-type embryos the cell divides in an anterior–posterior direction. Although the details of the underlying mechanism such as whether it is a permissive or an instructive signal, the cell on which the signal is localized and the identification of other pathway components are yet to be clarified. This example shows that classical GPCR/G protein-mediated pathways are present in *C. elegans* development.

2.4. GPCRs and G Proteins in Patterning and Induction of the Vulva

GPCRs and G proteins also play a role in *C. elegans* development beyond early cell cleavages. One process in which both exert functions is the development of the vulva. The vulva of a hermaphrodite connects the uterus to the surrounding environment. It is formed from ventral epidermal precursors during larval development [30]. Besides Wnt/Frizzled signaling, which plays several roles during vulval development, including signaling through the HOX gene *lin-39* to generate six epidermal precursor cells and cell polarity [48,49], the G α_q protein EGL-30 positively affects vulva development [50]. Whether this G protein is activated by a GPCR remains to be clarified. However, there is evidence that it might act in parallel to RAS and involve Wnt signals [50]. Further, the G α protein GPA-5, which shares some homology with mammalian G α_i proteins, negatively affects vulval development upon classical activation of the GPCR SRA-13 and by affecting RAS/MAPK signaling [51]. The site of action in this case is not determined, but the effect might be cell autonomous or stem from sensory neurons [51]. Further, large-scale RNAi screens have also revealed roles for GOA-1 in vulval development [52,53].

2.5. GPCRs and G Proteins in Neuronal Development

Neuronal migration is another process in postembryonic development that has been demonstrated to engage G proteins as well as GPCRs. Several lines of evidence point toward a role for the G proteins GOA-1 and EGL-30, as well as the GPCR Flamingo (FMI-1) in the migration of different neurons. GOA-1 is a serotonin effector in migrating neurons, with the N-type calcium channel homolog UNC-2 being a target for this signal [54]. Further, gain-of-function mutants of *egl-30* display defects in neuronal cell migration [54]. Whether these are GPCR-dependent functions remains to be determined. However, there is a GPCR known to be involved in neuronal cell migration: the Adhesion-GPCR

FMI-1, a Flamingo/CELSR homolog that controls axon guidance. Loss-of-function alleles of *fmi-1* causes axon navigation defects of pioneer and follower axons in the ventral nerve cord [55]. The signal transduction and the molecular details of this receptor remains to be determined, but it has so far not been linked to any G protein activation.

2.6. Further Roles of G Proteins

Besides the relatively well understood processes discussed above, in which GPCRs and G proteins mediate functions in development, several studies point toward additional, yet not well understood, roles of G proteins. Whether these are dependent or independent of GPCRs will be interesting to be determined. For instance, there is some indication that GPB-1 appears to be involved in germline development. A *gpb-1* loss-of-function mutant displays, besides the defects during cell division in early embryonic development, abnormalities at later stages [24]. Some adults rescued by a *gpb-1* transgene in a mosaic manner are sterile and have abnormal germlines [24].

Considering their broad involvement in a plethora of functions, it is likely that many more of the still unknown functions of GPCRs and G proteins will be uncovered in the years to come.

In summary, it can be noted that GPCRs and G proteins in *C. elegans* development do act as both a functional unit and independently of each other, with the latter being a major part of early development, while classical G-protein function is more often found in later developmental stages. One possible reason for this could be the expansion of potential cellular contacts, which ask for increased communication and coordination. Future investigations will need to focus on the details of canonical and atypical G-protein functions, such as additional pathway components and especially their physiological impact.

3. G Protein-Independent Function of GPCRs

The main G protein-independent function of GPCRs in various aspects of *C. elegans* embryonic and larval development is the Wnt/Frizzled signaling pathway. A canonical versus a non-canonical one can be discriminated, which involve partially overlapping effector molecules. These pathways are conserved among species; however, in *C. elegans* cascades involving Wnt homologs and their receptors, which are slightly different from the ones found in mammals or *Drosophila melanogaster*, have been described. The details are summarized and discussed in [40,41]. The Wnt pathway controlling cell division and polarization of the EMS blastomere is mostly referred to as non-canonical despite involving β -catenin (WRM-1). It is somewhat similar to the canonical pathway but also entails asymmetric localization of different components as a general mechanism. Downstream of the GPCR MOM-5, a Frizzled homolog binding the Wnt ligand MOM-2, key molecules such as the Disheveled homologs MIG-5 and DSH-2 and, subsequently, WRM-1 (Figure 2B) are recruited. Further mechanistic details of the different Wnt signaling pathways have been dissected in several studies and are described elsewhere (reviewed in [40,41]). While in other organisms it has been shown that the Wnt receptors Frizzled can act as classical GPCRs coupling to G proteins (reviewed in [56]), this information is lacking for *C. elegans*. However, it will be intriguing to see whether there is an intersection of the Wnt cascade with G proteins.

4. Mechanisms of GPCR-Independent Functions of Heterotrimeric G Proteins

Although it becomes increasingly clear that, during *C. elegans* development, several GPCR-independent functions of G proteins are key modulators in various processes, the control of spindle positioning in asymmetric cell division via GOA-1 and GPA-16 is by far the best understood. It is one key example of how G proteins are regulated by several modulators and what mechanisms are underlying this process.

For a long time, the common belief was that G proteins are activated solely by GPCRs and only convey signals received by an extracellular cue into cells. In the mid-1990s, it became clear that G proteins can be regulated; thus, signaling can be fine-tuned by various accessory proteins such as GDIs

or GTPase-activating proteins (GAPs). Both inhibit the activity of the $G\alpha$ subunit and consequently inactivate the G protein, but through different mechanisms: GDIs prohibit the exchange of GDP for GTP, whereas GAPs, which are also called regulators of G protein signaling (RGS), enhance the GTPase activity of $G\alpha$ subunits. RGS proteins contain a name-coining RGS domain. While first described in yeast (reviewed in [57]), they are present in many species. The *C. elegans* genome encodes more than 20 proteins with one or more RGS domains [58]. Although not for all of them, the $G\alpha$ subunit they regulate has been identified, RGS proteins play extensive roles in the nervous system and influence behaviour, chemosensation, and egg laying.

The only RGS protein which has been beyond doubt identified to be involved in controlling G protein activity during development is RGS-7, which regulates GOA-1 in spindle positioning [13,59]. Loss of *rgs-7* leads to increased $G\alpha$ activity and subsequently to a hyper-asymmetric cell division due to reduced pulling forces on the anterior pole of the dividing cell [59]. RGS-7 function is complemented by two other accessory proteins: the GDIs GPR-1 and GPR-2. Both show homologies to the Pins (partner of inescutable) from *Drosophila melanogaster*. Similar to the Pins, they contain a GoLoco/GPR motif through which they are thought to associate with the G protein and inhibit dissociation of GDP when binding to GOA-1 [13,14,23]. Similarly to depletion of the G protein [7], loss of GPR-1/GPR-2 leads to almost no spindle movement due to a lack of pulling forces [13]. Together with LIN-5 they form the ternary complex.

Interestingly, the G protein cycle regulated by RGS-7 and GPR-1/2 is not activated by a GPCR. In this receptor-independent pathway, GOA-1/GPA-16, bound to the $G\beta$ subunit GPB-1 and the $G\gamma$ subunit GPC-2 [7], are activated by a cytoplasmic GEF. Discovery of these non-receptor GEFs came as a surprise, but they are now established in many different species [60,61]. The receptor-independent GEF controlling activation of the $G\alpha_o$ during early cell division in *C. elegans* is RIC-8 (Synembrin). This widely known GEF, which has also been shown to function in neurons [62] and potentially regulates the $G\alpha_q$ EGL-30 [63,64], functionally couples to $G\alpha_o$ during the first divisions of the *C. elegans* embryo [16,23,62]. RIC-8 can physically interact with both GOA-1 and GPA-16 and has been shown to act as a GEF for GOA-1 [16,23]. Loss of *ric-8* leads to slower nuclear migration, decreased pulling forces, and overall embryonic lethality [23,62]. Even though RIC-8 function has been characterized in great detail, not only in *C. elegans* but also in *Drosophila* and mice [65,66], no binding motif for the G protein interaction has been identified to date.

That a non-receptor GEF rather than a GPCR serves as an activator in the case of G protein-controlled asymmetric cell division at a very early embryonic stage is a conceivable concept. Especially so, as in the two-cell-stage embryo, there is not much communication with the environment due to the egg being in a shell-confined space. Although details of the cues triggering the spindle positioning are not the focus of this review, it is interesting to note that this receptor-independent function of heterotrimeric G proteins to control spindle positioning during cell division is not unique to *C. elegans*. There is evidence from several studies starting to surface suggesting that it is a more general mechanism, which is highly conserved. The ternary complex comprising the G protein, GPR-1/2, and LIN-5, which is required for correct spindle orientation and functions to anchor and localize GPR-1/2 [7,15], has the counterpart $G\alpha_i$ /LGN/NuMA in mammals that is also essential for spindle positioning [67–69]. Further, it was shown in HeLa cells that the GEF RIC-8, the homolog of *C. elegans ric-8*, seems to be involved in this process [69].

As discussed above, the G protein cycle of the receptor-independent function of the $G\alpha_o$ proteins GOA-1 and GPA-16 is completed by RGS-7, which harbors an intrinsic GTPase activity. However, it is puzzling that, while GAPs normally inactivate G proteins, in this case the opposite is true [59]. These data raise the question of the relevance of GTP hydrolysis in the receptor-independent G-protein function. There is some evidence that indeed GTPase activity is required. Firstly, direct anchoring of microtubules to the cortex via dynein is insufficient for cell division [70], indicating that the anchoring apparatus is not just a simple attachment and that pulling force generation is a critical part of its function. This issue was resolved by identifying LIN-5 as the main regulator of force generation

within the anchoring complex, suggesting that no further function is expected of the G protein [70]. Secondly, it is known that, in the ternary complex, GOA-1 and GPA-16, respectively, are interacting with GPR-1/2, which are GDIs and therefore depend on the GDP-bound state to stably interact with the G protein [71]. Furthermore, GPB-1 and GPC-2 act as a competitor of GPR-1/2, as GPB-1 is also a GDI and thus also binds $G\alpha$. This is supported by the observation that loss-of-function mutations of *gpb-1* or *gpc-2* result in increased pulling force-phenotypes in *C. elegans* embryos [8,23,26]. Lastly, it has been shown that cortical enrichment of RGS-7 positively regulates spindle movement [70], which is conceivable in the context of the GDP-bound form of the $G\alpha$ subunit being the point of connection of the ternary complex to the membrane (Figure 2A). Several models have been suggested describing GOA-1 activation and function. However, no model exists that accommodates all the findings on this G protein. The classical G protein cycle certainly does not explain the GOA-1 function. For instance, it has been proposed that the active unit mediating pulling force is the $G\alpha$ -GDP/GPR complex, as GOA-1 and GPR-1/2 positively modulate this process [13,14,23]. However, it cannot be ignored that $G\alpha$ -GTP is the active form, since the GEF RIC-8 also positively influences force generation [15]. Thus, further analyses are required to obtain a more refined model, which also accommodates the role of GPA-16.

Together, while this data suggests that GTPase activity is relevant for G protein function in early *C. elegans* development, one key experiment shows that this does not seem to be entirely true. Fielmich et al. showed that spindle positioning and cortical pull are not significantly compromised when both GPR-1/2 and the $G\alpha$ protein are replaced by an arbitrary membrane anchor [70]. This indicates that, indeed, the basis of G-protein function in the zygote might be GTPase-independent membrane anchoring. Nevertheless, as the G protein can act as a switch between an active and inactive state, it is obvious that throughout evolution this system has evolved to be regulated by various mechanisms (stated above), stressing the need for flexibility and fine tuning during spindle alignment and cell division. It would be interesting to search for regulators of other GTPases with their main role in structure and scaffolding, such as tubulin.

5. The Relationship of GPCRs and G Proteins over Time

The concept of GPCRs and G proteins being able to function together as well as separately renders a versatile system to control cellular processes and a plethora of functional possibilities. While in *C. elegans* all three combinations, GPCR/G-protein function, GPCR-independent G-protein function, and G protein-independent GPCR function, can be extensively found during embryonic development, other species also make use of them. For instance, the Wnt receptor Frizzled in mammals can couple to G proteins but also act independently (for a summary, see [56]). The effectors and modulators such as non-receptor GEFs, GAPs, or RGS are highly conserved (see Section 4) during evolution, suggesting that the independent system has not just developed recently. A closer look at evolutionary aspects of GPCRs and G protein manifests this notion.

5.1. Origin of the GPCR System

G protein and GPCR functions are some of the oldest signaling mechanisms observed to date with strong conservation among a multitude of species and, based on the prevalence of their precursor genes in both prokaryotes and eukaryotes, likely originated from one universal common ancestor (UCA) [72–74]. Still, since there are species containing only GPCRs or G proteins, it is clear that the two do not always have to function together but have also developed independent signaling pathways [60]. Furthermore, in species in which GPCR-dependent G protein signaling is observed, there is considerable variation in the number of pathway components [60]. This observation was previously explained by the system being highly adaptable and modulative, increasing and sometimes decreasing in complexity over time [60,72,75]. Even though unicellular organisms do sense their environment and have mechanisms of signal perception [76–78], there was still a need for more diverse and intricate signaling mechanisms during development of multicellularity [79,80]. This was especially the case as metazoans were faced not just with receiving cues from their environment but

also with the task of coordinating the development, structure, and function of tissues and organs. These circumstances explain the dramatic expansions of different signaling systems, such as the receptor tyrosine kinases [81–83] and the GPCR system, especially in metazoans [60,72,84].

5.2. Origin of G Proteins

G proteins are descendants of the extended clade of Ras-like GTPases, which most likely underwent a split in prokaryotes, giving rise to the ancestors of small G proteins (the Ran-Ras-Rho-Rab-like group) and of G α subunits (the MglA-Arf-G α group), with the latter originally being involved in membrane trafficking. Interestingly, only later in evolution they were recruited to act as downstream signaling molecules of membrane receptors [85–89]. The ancestral G α as well as the classical G protein cycle are likely to have originated in the last eukaryotic common ancestor (LECA) [60,90]. However, all human G α subunits (Gs, Gi/o, Gq, and G12/13, as well as the Gv type—which is constrained to marine animals and some insects), two precursors of G β , and one of G γ can only be dated back to the common ancestor of holozoans [91,92].

In the same way as GPCRs, heterotrimeric G proteins have expanded to a great extent in some eukaryotic species [60,72,91], which was accompanied by strong diversification in genetic sequences (e.g., human and plant G α subunits have approximately 33% similarity). Still, the crystal structures remain nearly identical [90], indicating conserved functions while also enabling different interactions due to sequential differences. On the other hand, there are eukaryotic clades—such as alveolates, kinetoplastids, and diplomonads—in which no evidence for heterotrimeric G proteins can be found to date [72]. A summary of the development of G proteins and their functions over time is shown in Figure 3.

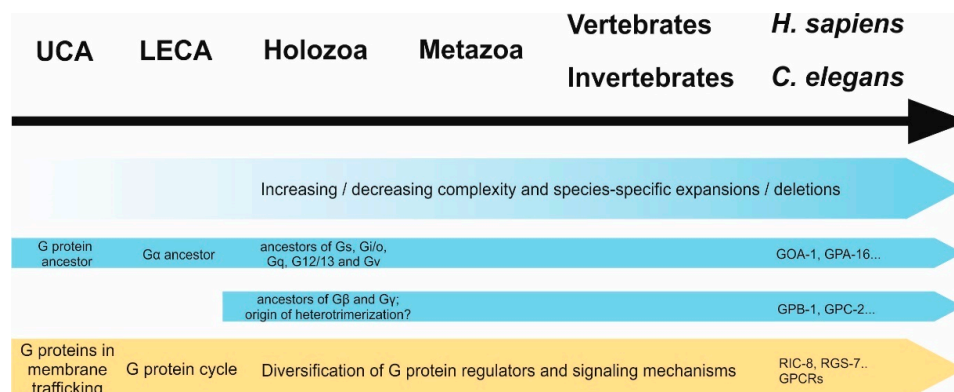


Figure 3. Development of G proteins (blue) and their functions (yellow) over time. First ancestors of G proteins and GPCRs have likely arisen in the universal common ancestor (UCA) of eukaryotes and prokaryotes, whereafter both underwent dramatic expansion and diversification. While the first appearance of a G α protein is thought to be in the last common eukaryotic ancestor (LECA), precursor proteins of human G α families as well as G β and G γ subunits seem to have diverged in holozoans, suggesting that G α could have had β/γ -independent functions pre-dating heterotrimerization. Before G proteins were recruited as downstream signals of membrane-bound receptors, they possibly functioned in membrane trafficking. Over time, not only their regulation through GEFs (such as GPCRs) but also other regulatory proteins (GAPs, GDIs) underwent expansion and gave rise to the multitude of G proteins signaling mechanisms we observe today.

In general, genes for GPCRs have expanded and undergone variation in higher frequency compared to G protein genes, leading to them having a smaller number of orthologs in more distant species [84]. However, many invertebrates including *C. elegans* underwent species-specific expansions of G proteins, even to a greater extent than, for example, humans [91,93], which could be a sign of acquisition of GPCR-independent pathways [90]. *C. elegans* in particular is truly interesting in this manner, since it harbors almost double the number of G proteins and GPCRs compared to humans [61],

both of which have species-specific representatives that do not seem to be related to other species. In the case of GPCRs and many of the G proteins, this could be due to the extreme development of the chemosensory pathways of the nematode [6,94–96].

5.3. Atypical G-Protein Functions across Species

It is not easy to discuss whether GPCR-independent functions of G proteins existed before GPCR-dependent ones, as even though the two protein families appear to have emerged independently, the origins of both lay as far back in evolution as we are able to peek into (see above). However, most signaling pathways are composed of a rigid set of cytoplasmic elements, which can be modulated by various cues, and are transduced by a highly dynamic set of receptors [83,97,98]. This allows us to hypothesize the core signaling system (e.g., heterotrimeric G proteins and their respective downstream effectors) as a receptor-independent machinery that autonomously fulfills essential functions of the cell and ultimately constrains evolution. At the same time, receptors are present to modulate these functions and over the course of time develop different regulatory mechanisms (GEF/GAP), depending on what regulation is needed for the current state of G protein activity [90].

There is some data that supports this hypothesis: First of all, some evolutionary clades—such as embryophytes or unicellular holozoans—have been described to have no detectable or a reduced number of GPCRs or G proteins, respectively [60,91], suggesting that, indeed, they can function independently of each other. In the case of GPCRs, it is most likely that they use different downstream effectors (e.g., arrestins) and in the case of G proteins different regulators such as non-receptor GEFs, GDIs, and GAPs (addressed above). However, it has to be noted that the sole lack of a gene family is not necessarily a sign for an independent evolutionary origin, as loss during evolution can also be a result of irrelevance. For instance, transmembrane receptors are dispensable in the case of intracellular parasitism. In analogy to the lack of GPCRs, there are some species deficient of entire sets of G protein regulatory networks. For instance, in the early-branching eukaryotes such as *Trichomonas* and *Cyanophora paradoxa*, no β or γ subunits could be identified to date [60,72], suggesting that $G\alpha$ acts independently of the other subunits. These data could further implicate that $G\alpha$ subunits functioned on their own at first and only later partnered with $G\beta\gamma$ complexes. This hypothesis is consistent with the fact that $G\alpha$ proteins seem to have emerged earlier in evolution (Figure 3).

However, the incredible variety of possible genetic constitutions of G protein signaling systems in different species does not entirely clarify the question of which of the regulatory elements arose first, but rather underlines the extreme modularity and flexibility of this network. Such flexibility allowed for classical and atypical functions to evolve independently, probably with many pathways diverging and converging throughout evolution. Thus, one challenge of future analyses on the entire spectrum of G-protein functions throughout the tree of life is to explain their evolutionary origin.

6. Tools for Studying GPCRs and G Proteins in *C. elegans*

Future studies need to focus on elucidating the mechanistic details of GPCR and G-protein function separately and together as well as gaining further insights into understanding their impact on development. Several tools have been developed in recent years to facilitate these research endeavors.

6.1. GPCR- and G Protein-Based Methods for Studying *C. elegans* Development

Even though many details of non-canonical functions of heterotrimeric G proteins in *C. elegans* development remain unclear, a solid foundation of knowledge is now established allowing for manipulations of known regulatory elements. The aim is to create new methods and model systems for developmental or general *C. elegans* research. One recent breakthrough was the establishment of a non-mendelian genetics system [99] (Figure 4A). This system is based on overexpression of the pulling force regulator *gpr-1*, which creates two unipolar spindles rather than a bipolar one in the *C. elegans* zygote. This impairs fusion of maternal and parental pronuclei, ultimately leading to genetically different AB and P₁ blastomeres. One of them carries only maternal chromosomes, while the other

inherits the parental counterparts. It remains unclear how the sets of chromosomes achieve diploidy, yet somehow about 30% of embryos survive to form lineage-specific hybrid nematodes and, as germ cells are descendants of the P₁-lineage, the F₂ generation is genetically identical to one of the parents, depending on which pronucleus was pulled to P₁. This model can be used as a toolbox for many different approaches. The authors already described the relevance of parental/maternal hybrid animals as a means to investigate epigenetics, lineage-specific knockouts and mitochondrial or gonosomal gene transmission. It is conceivable that these model strains can also be employed in developmental research. For instance, now it is possible to easily create embryos which lack the ability to produce cues for cell division (in the style of the Wnt signal, that the P₂ cell inflicts onto the EMS) to investigate the necessary communication between neighboring cells during development. In this way, not only necessity but also the directionality of signals between blastomeres can be thoroughly investigated. Furthermore, in tissues which are composed of both AB and P₁ descendants such as the hypodermis, it could be possible to distinguish between genes required in every single cell of the tissue and genes, whose mere diffuse presence in the tissue is relevant.

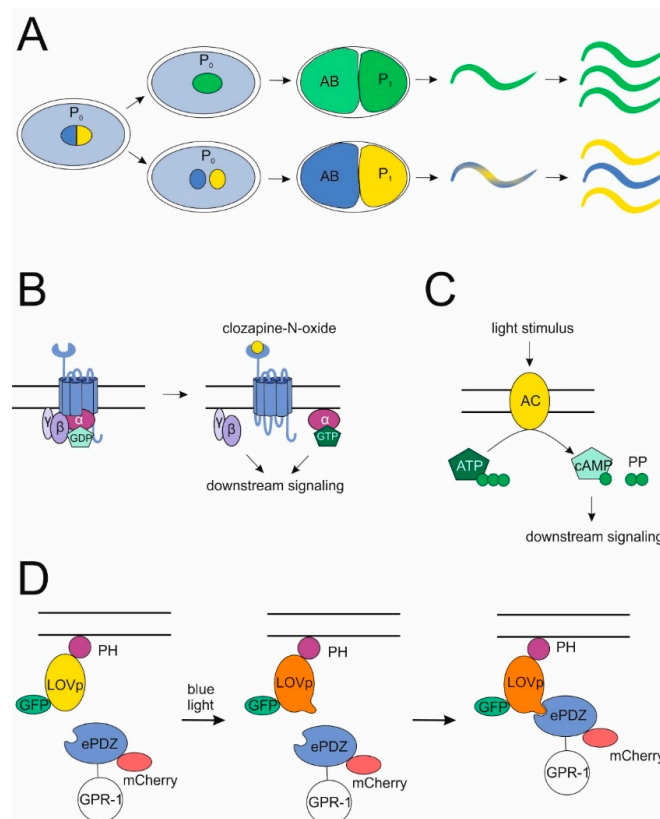


Figure 4. Novel methods for studying G-protein functions. (A) Non-mendelian genetic system. By overexpressing *gpr-1* in the *C. elegans* zygote instead of one bipolar spindle, two unipolar spindles are created, which impeaches pronuclear fusion and leads to chimeric embryos. Progeny of these can be genetic replicates of either the mother or the father, depending on which pronucleus localized to the P₁ cell. (B,C) Specific induction of G-protein signaling. Distinct G protein cascades can be activated either by stimulating a DREADD, which cannot bind its cognate agonist anymore, with the inert drug clozapine-N-oxide (B) or by directly activating downstream effectors of certain G proteins such as an adenylyl-cyclase (downstream of a G_s protein) via photoinduction (C). (D) The PDZ-LOV-system. Exposure to blue light enables PDZ-tagged cytoplasmic proteins (such as GPR-1) to bind to LOV-domains, which are in parallel tethered to the membrane via a PH-anchor. Fluorescent molecules allow for the control of proper localization.

Further, designer receptors and inducible downstream effectors can be used to study the impact of a GPCR or a G protein signaling pathway. Designer receptors exclusively activated by designer drugs (DREADDs) have been developed for the selective control of signaling in vivo in several organisms [100–102]. These modified muscarinic acetylcholine receptors are activated by the inert drug clozapine-N-oxide, but not by their endogenous agonists carbachol or acetylcholine. A DREADD activating the Gq signaling cascade has recently been developed for use in *C. elegans* [103] (Figure 4B). Another way to stimulate GPCR pathways is the use of photoactivatable cyclases producing cyclic AMP [104,105], which is a second messenger downstream of Gs-coupled GPCRs (Figure 4C). Both techniques could be used to selectively activate potential GPCR pathways to gain insights into their role in development.

6.2. Novel Methods Used to Investigate Atypical G-Protein Function

Several techniques potentially useful for G protein research in *C. elegans* have been introduced in the past years. An optogenetic system using a PDZ-tag on cytosolic proteins in combination with a membrane bound PH::LOV fusion protein was developed to selectively upregulate the surface expression of relevant proteins in the early embryo by exposure to blue light [70] (Figure 4D). One intriguing application of this technique was the interchangeability of G proteins in the early blastomeres by the PH::LOV-anchor, which solidifies the working model that GOA-1 and GPA-16 can fulfill their functions independent of their GTPase activity. However, this method harbors even more potential as it enables the selective upregulation of different regulators of cell division and cortical force generation in both wild-type and various mutant backgrounds, to characterize the effects on single cells as well as on the development of the entire embryo. It would also be interesting to express proteins ectopically at the cell surface to investigate their effects on the wild-type machinery.

In contrast to selective upregulation of protein expression, a recently developed method employs cell specific knockdown of mRNA by nonsense-mediated decay (NMD) [106]. In this system, a gene fusion was generated containing a gene of interest and part of the 3'-UTR of *let-858*, which is known to induce NMD on upstream genes [107], as their physiological stop codons are being recognized as premature. Secondly, a NMD-rescuing construct was designed, coding for one of the NMD machinery proteins (*SMG-5*), under the influence of a cell-specific promoter.

Coexpression of these two in nematodes lacking both *smg-5* and the protein of interest leads to the first transgene rescuing gene activity in all cells except the ones defined by the promoter of the second transgene, ultimately leading to cell-specific knockdown. This system was used to show that GOA-1 has a specific function in HSN neurons controlling egg laying behavior, but we further propose the possibility of using blastomere-specific promoters to investigate functions of developmentally relevant proteins such as G proteins or G protein regulators in single blastomeres. Unfortunately, since active transcription only starts at the 8- to 12-cell stage [108], earlier blastomeres cannot be affected in this way. However, as stated above, it is possible to create embryos with genetically different AB and P₁ cells by *gpr-1* overexpression, so that at early stages blastomere-specific knockdown could be achieved by mating mutant and wild-type parents and then generating hybrid offspring. These methods have the potential to increase our knowledge of spatio-temporal requirements of different proteins throughout development.

7. Conclusions and Outlook

The paradigm that GPCRs exclusively activate G proteins and that these heterotrimeric units act solely as signal transducers for the receptors has been disproven in the past decades by the discovery of GPCR effectors such as arrestins as well as different G protein regulators. We are just starting to begin to understand the principles as well as the relevance of this mutual infidelity. *C. elegans* development, especially embryonic development, is a prime example in which the density of GPCRs and G-protein function is high. However, the two do not necessarily act together. We can learn about how the GPCR/G protein system works in different contexts by looking at *C. elegans* development.

For instance, the role of G proteins in left–right asymmetry in *C. elegans* embryos can offer a foundation for the understanding of some basic mechanisms in cardiogenesis. Overexpression of G α during cardiogenesis in mice causes cardiac contractile failure [109] and left–right-handedness might be essential in this pathology. Further, the loss of the GEF Ric8A in mouse B cells causes a severe B cell immunodeficiency, likely due to reduced G α_i protein activity and potential reduction in asymmetric cell division events [110]. Although the underlying mechanisms to establish left–right asymmetry are likely not entirely the same in mammals and *C. elegans*, knowledge of the role of G proteins or regulators such as RIC-8 in *C. elegans* can provide invaluable information to further understand and elucidate some of these processes in mammals. This knowledge transfer from basic principles to pathologies will be one major challenge in the future.

Understanding the GPCR/G protein mechanisms will be tremendously helpful in gaining insights into developmental processes. The question of why GPCR as well as separate G-protein functions mediate similar processes in spindle positioning and polarity during early cell division is highly intriguing, as are the potential GAP-independent G-protein functions. Further, there is evidence for several additional, yet undescribed G-protein functions in *C. elegans*. For instance, the presence of the GEF GBAS-1, which in other organisms preferably activates G α monomers in contrast to GPCRs, which have higher affinity to heterotrimers (reviewed in [111]), has recently been shown [61].

Our understanding of GPCR and G-protein function in *C. elegans* is constantly growing and has yielded the development of a set of valuable tools to further investigate the signaling mechanisms and physiological concepts controlled by them and ultimately to answer the many remaining fundamental questions.

Author Contributions: Both authors performed research and wrote the manuscript.

Funding: This work was funded by the European Social Fonds, the German Research Foundation (DFG: FOR 2149/P02), and the Sächsisches Staatsministerium für Wissenschaft und Kunst (SMWK).

Acknowledgments: We thank Torsten Schöneberg and Samantha Hughes for critical reading of the manuscript. We acknowledge support from the German Research Foundation (DFG) and Universität Leipzig within the program of Open Access Publishing.

Conflicts of Interest: The authors declare no conflict of interest.

References

- Peterson, Y.K.; Luttrell, L.M. The Diverse Roles of Arrestin Scaffolds in G Protein-Coupled Receptor Signaling. *Pharmacol. Rev.* **2017**, *69*, 256–297. [[CrossRef](#)] [[PubMed](#)]
- Ali, M.S.; Sayeski, P.P.; Dirksen, L.B.; Hayzer, D.J.; Marrero, M.B.; Bernstein, K.E. Dependence on the motif YIPP for the physical association of Jak2 kinase with the intracellular carboxyl tail of the angiotensin II AT1 receptor. *J. Biol. Chem.* **1997**, *272*, 23382–23388. [[CrossRef](#)] [[PubMed](#)]
- Cismowski, M.J.; Ma, C.; Ribas, C.; Xie, X.; Spruyt, M.; Lizano, J.S.; Lanier, S.M.; Duzic, E. Activation of heterotrimeric G-protein signaling by a ras-related protein. Implications for signal integration. *J. Biol. Chem.* **2000**, *275*, 23421–23424. [[CrossRef](#)] [[PubMed](#)]
- Tall, G.G.; Krumin, A.M.; Gilman, A.G. Mammalian Ric-8A (synembryn) is a heterotrimeric G α protein guanine nucleotide exchange factor. *J. Biol. Chem.* **2003**, *278*, 8356–8362. [[CrossRef](#)] [[PubMed](#)]
- Bargmann, C.I. Neurobiology of the *Caenorhabditis elegans* genome. *Science* **1998**, *282*, 2028–2033. [[CrossRef](#)] [[PubMed](#)]
- Jansen, G.; Thijssen, K.L.; Werner, P.; van der Horst, M.; Hazendonk, E.; Plasterk, R.H. The complete family of genes encoding G proteins of *Caenorhabditis elegans*. *Nat. Genet.* **1999**, *21*, 414–419. [[CrossRef](#)] [[PubMed](#)]
- Gotta, M.; Ahringer, J. Distinct roles for G α and G $\beta\gamma$ in regulating spindle position and orientation in *Caenorhabditis elegans* embryos. *Nat. Cell Biol.* **2001**, *3*, 297–300. [[CrossRef](#)] [[PubMed](#)]
- Tsou, M.F.; Hayashi, A.; Rose, L.S. LET-99 opposes G α /GPR signaling to generate asymmetry for spindle positioning in response to PAR and MES-1/SRC-1 signaling. *Development* **2003**, *130*, 5717–5730. [[CrossRef](#)] [[PubMed](#)]

9. Hyman, A.A.; White, J.G. Determination of cell division axes in the early embryogenesis of *Caenorhabditis elegans*. *J. Cell Biol.* **1987**, *105*, 2123–2135. [[CrossRef](#)] [[PubMed](#)]
10. Albertson, D.G. Formation of the first cleavage spindle in nematode embryos. *Dev. Biol.* **1984**, *101*, 61–72. [[CrossRef](#)]
11. Grill, S.W.; Gonczy, P.; Stelzer, E.H.; Hyman, A.A. Polarity controls forces governing asymmetric spindle positioning in the *Caenorhabditis elegans* embryo. *Nature* **2001**, *409*, 630–633. [[CrossRef](#)] [[PubMed](#)]
12. Johnston, C.A.; Afshar, K.; Snyder, J.T.; Tall, G.G.; Gonczy, P.; Siderovski, D.P.; Willard, F.S. Structural determinants underlying the temperature-sensitive nature of a Galpha mutant in asymmetric cell division of *Caenorhabditis elegans*. *J. Biol. Chem.* **2008**, *283*, 21550–21558. [[CrossRef](#)] [[PubMed](#)]
13. Colombo, K.; Grill, S.W.; Kimple, R.J.; Willard, F.S.; Siderovski, D.P.; Gonczy, P. Translation of polarity cues into asymmetric spindle positioning in *Caenorhabditis elegans* embryos. *Science* **2003**, *300*, 1957–1961. [[CrossRef](#)] [[PubMed](#)]
14. Gotta, M.; Dong, Y.; Peterson, Y.K.; Lanier, S.M.; Ahringer, J. Asymmetrically distributed *C. elegans* homologs of AGS3/PINS control spindle position in the early embryo. *Curr. Biol.* **2003**, *13*, 1029–1037. [[CrossRef](#)]
15. Srinivasan, D.G.; Fisk, R.M.; Xu, H.; van den Heuvel, S. A complex of LIN-5 and GPR proteins regulates G protein signaling and spindle function in *C. elegans*. *Genes Dev.* **2003**, *17*, 1225–1239. [[CrossRef](#)] [[PubMed](#)]
16. Couwenbergs, C.; Spilker, A.C.; Gotta, M. Control of embryonic spindle positioning and Galpha activity by *C. elegans* RIC-8. *Curr. Biol.* **2004**, *14*, 1871–1876. [[CrossRef](#)] [[PubMed](#)]
17. Nguyen-Ngoc, T.; Afshar, K.; Gonczy, P. Coupling of cortical dynein and G alpha proteins mediates spindle positioning in *Caenorhabditis elegans*. *Nat. Cell Biol.* **2007**, *9*, 1294–1302. [[CrossRef](#)] [[PubMed](#)]
18. Park, D.H.; Rose, L.S. Dynamic localization of LIN-5 and GPR-1/2 to cortical force generation domains during spindle positioning. *Dev. Biol.* **2008**, *315*, 42–54. [[CrossRef](#)] [[PubMed](#)]
19. Couwenbergs, C.; Labbe, J.C.; Goulding, M.; Marty, T.; Bowerman, B.; Gotta, M. Heterotrimeric G protein signaling functions with dynein to promote spindle positioning in *C. elegans*. *J. Cell Biol.* **2007**, *179*, 15–22. [[CrossRef](#)] [[PubMed](#)]
20. Schmidt, D.J.; Rose, D.J.; Saxton, W.M.; Strome, S. Functional analysis of cytoplasmic dynein heavy chain in *Caenorhabditis elegans* with fast-acting temperature-sensitive mutations. *Mol. Biol. Cell* **2005**, *16*, 1200–1212. [[CrossRef](#)] [[PubMed](#)]
21. Kozlowski, C.; Srayko, M.; Nedelec, F. Cortical microtubule contacts position the spindle in *C. elegans* embryos. *Cell* **2007**, *129*, 499–510. [[CrossRef](#)] [[PubMed](#)]
22. Goldstein, B.; Macara, I.G. The PAR proteins: Fundamental players in animal cell polarization. *Dev. Cell* **2007**, *13*, 609–622. [[CrossRef](#)] [[PubMed](#)]
23. Afshar, K.; Willard, F.S.; Colombo, K.; Johnston, C.A.; McCudden, C.R.; Siderovski, D.P.; Gonczy, P. RIC-8 is required for GPR-1/2-dependent Galpha function during asymmetric division of *C. elegans* embryos. *Cell* **2004**, *119*, 219–230. [[CrossRef](#)] [[PubMed](#)]
24. Zwaal, R.R.; Ahringer, J.; van Luenen, H.G.; Rushforth, A.; Anderson, P.; Plasterk, R.H. G proteins are required for spatial orientation of early cell cleavages in *C. elegans* embryos. *Cell* **1996**, *86*, 619–629. [[CrossRef](#)]
25. van der Linden, A.M.; Simmer, F.; Cuppen, E.; Plasterk, R.H. The G-protein beta-subunit GPB-2 in *Caenorhabditis elegans* regulates the G(o)alpha-G(q)alpha signaling network through interactions with the regulator of G-protein signaling proteins EGL-10 and EAT-16. *Genetics* **2001**, *158*, 221–235. [[PubMed](#)]
26. Afshar, K.; Willard, F.S.; Colombo, K.; Siderovski, D.P.; Gonczy, P. Cortical localization of the Galpha protein GPA-16 requires RIC-8 function during *C. elegans* asymmetric cell division. *Development* **2005**, *132*, 4449–4459. [[CrossRef](#)] [[PubMed](#)]
27. Thyagarajan, K.; Afshar, K.; Gonczy, P. Polarity mediates asymmetric trafficking of the Gbeta heterotrimeric G-protein subunit GPB-1 in *C. elegans* embryos. *Development* **2011**, *138*, 2773–2782. [[CrossRef](#)] [[PubMed](#)]
28. Liro, M.J.; Rose, L.S. Mitotic Spindle Positioning in the EMS Cell of *Caenorhabditis elegans* Requires LET-99 and LIN-5/NuMA. *Genetics* **2016**, *204*, 1177–1189. [[CrossRef](#)] [[PubMed](#)]
29. Deppe, U.; Schierenberg, E.; Cole, T.; Krieg, C.; Schmitt, D.; Yoder, B.; von Ehrenstein, G. Cell lineages of the embryo of the nematode *Caenorhabditis elegans*. *Proc. Natl. Acad. Sci. USA* **1978**, *75*, 376–380. [[CrossRef](#)] [[PubMed](#)]
30. Sulston, J.E.; Schierenberg, E.; White, J.G.; Thomson, J.N. The embryonic cell lineage of the nematode *Caenorhabditis elegans*. *Dev. Biol.* **1983**, *100*, 64–119. [[CrossRef](#)]

31. Bergmann, D.C.; Lee, M.; Robertson, B.; Tsou, M.F.; Rose, L.S.; Wood, W.B. Embryonic handedness choice in *C. elegans* involves the Galpha protein GPA-16. *Development* **2003**, *130*, 5731–5740. [[CrossRef](#)] [[PubMed](#)]
32. Kaletta, T.; Schnabel, H.; Schnabel, R. Binary specification of the embryonic lineage in *Caenorhabditis elegans*. *Nature* **1997**, *390*, 294–298. [[CrossRef](#)] [[PubMed](#)]
33. Lin, R.; Hill, R.J.; Priess, J.R. POP-1 and anterior-posterior fate decisions in *C. elegans* embryos. *Cell* **1998**, *92*, 229–239. [[CrossRef](#)]
34. Rocheleau, C.E.; Downs, W.D.; Lin, R.; Wittmann, C.; Bei, Y.; Cha, Y.H.; Ali, M.; Priess, J.R.; Mello, C.C. Wnt signaling and an APC-related gene specify endoderm in early *C. elegans* embryos. *Cell* **1997**, *90*, 707–716. [[CrossRef](#)]
35. Thorpe, C.J.; Schlesinger, A.; Carter, J.C.; Bowerman, B. Wnt signaling polarizes an early *C. elegans* blastomere to distinguish endoderm from mesoderm. *Cell* **1997**, *90*, 695–705. [[CrossRef](#)]
36. Walston, T.; Tuskey, C.; Edgar, L.; Hawkins, N.; Ellis, G.; Bowerman, B.; Wood, W.; Hardin, J. Multiple Wnt signaling pathways converge to orient the mitotic spindle in early *C. elegans* embryos. *Dev. Cell* **2004**, *7*, 831–841. [[CrossRef](#)] [[PubMed](#)]
37. Bei, Y.; Hogan, J.; Berkowitz, L.A.; Soto, M.; Rocheleau, C.E.; Pang, K.M.; Collins, J.; Mello, C.C. SRC-1 and Wnt signaling act together to specify endoderm and to control cleavage orientation in early *C. elegans* embryos. *Dev. Cell* **2002**, *3*, 113–125. [[CrossRef](#)]
38. Goldstein, B. Cell contacts orient some cell division axes in the *Caenorhabditis elegans* embryo. *J. Cell Biol.* **1995**, *129*, 1071–1080. [[CrossRef](#)] [[PubMed](#)]
39. Goldstein, B.; Takeshita, H.; Mizumoto, K.; Sawa, H. Wnt signals can function as positional cues in establishing cell polarity. *Dev. Cell* **2006**, *10*, 391–396. [[CrossRef](#)] [[PubMed](#)]
40. Korswagen, H.C. Canonical and non-canonical Wnt signaling pathways in *Caenorhabditis elegans*: Variations on a common signaling theme. *Bioessays* **2002**, *24*, 801–810. [[CrossRef](#)] [[PubMed](#)]
41. Thorpe, C.J.; Schlesinger, A.; Bowerman, B. Wnt signalling in *Caenorhabditis elegans*: Regulating repressors and polarizing the cytoskeleton. *Trends Cell Biol.* **2000**, *10*, 10–17. [[CrossRef](#)]
42. Hardin, J.; King, R.S. The long and the short of Wnt signaling in *C. elegans*. *Curr. Opin. Genet. Dev.* **2008**, *18*, 362–367. [[CrossRef](#)] [[PubMed](#)]
43. Cabello, J.; Neukomm, L.J.; Gunesdogan, U.; Burkart, K.; Charette, S.J.; Lochnit, G.; Hengartner, M.O.; Schnabel, R. The Wnt pathway controls cell death engulfment, spindle orientation, and migration through CED-10/Rac. *PLoS Biol.* **2010**, *8*, e1000297. [[CrossRef](#)] [[PubMed](#)]
44. Fievet, B.T.; Rodriguez, J.; Naganathan, S.; Lee, C.; Zeiser, E.; Ishidate, T.; Shirayama, M.; Grill, S.; Ahringer, J. Systematic genetic interaction screens uncover cell polarity regulators and functional redundancy. *Nat. Cell Biol.* **2013**, *15*, 103–112. [[CrossRef](#)] [[PubMed](#)]
45. Langenhan, T.; Prömel, S.; Mestek, L.; Esmaili, B.; Waller-Evans, H.; Hennig, C.; Kohara, Y.; Avery, L.; Vakonakis, I.; Schnabel, R.; et al. Latrophilin signaling links anterior-posterior tissue polarity and oriented cell divisions in the *C. elegans* embryo. *Dev. Cell* **2009**, *17*, 494–504. [[CrossRef](#)] [[PubMed](#)]
46. Prömel, S.; Frickenhaus, M.; Hughes, S.; Mestek, L.; Staunton, D.; Woollard, A.; Vakonakis, I.; Schöneberg, T.; Schnabel, R.; Russ, A.P.; et al. The GPS motif is a molecular switch for bimodal activities of adhesion class G protein-coupled receptors. *Cell Rep.* **2012**, *2*, 321–331. [[CrossRef](#)] [[PubMed](#)]
47. Müller, A.; Winkler, J.; Fiedler, F.; Sastradihardja, T.; Binder, C.; Schnabel, R.; Kungel, J.; Rothmund, S.; Hennig, C.; Schöneberg, T.; et al. Oriented Cell Division in the *C. elegans* Embryo Is Coordinated by G-Protein Signaling Dependent on the Adhesion GPCR LAT-1. *PLoS Genet.* **2015**, *11*, e1005624. [[CrossRef](#)] [[PubMed](#)]
48. Eisenmann, D.M.; Maloof, J.N.; Simske, J.S.; Kenyon, C.; Kim, S.K. The beta-catenin homolog BAR-1 and LET-60 Ras coordinately regulate the Hox gene *lin-39* during *Caenorhabditis elegans* vulval development. *Development* **1998**, *125*, 3667–3680. [[PubMed](#)]
49. Gleason, J.E.; Korswagen, H.C.; Eisenmann, D.M. Activation of Wnt signaling bypasses the requirement for RTK/Ras signaling during *C. elegans* vulval induction. *Genes Dev.* **2002**, *16*, 1281–1290. [[CrossRef](#)] [[PubMed](#)]
50. Moghal, N.; Garcia, L.R.; Khan, L.A.; Iwasaki, K.; Sternberg, P.W. Modulation of EGF receptor-mediated vulva development by the heterotrimeric G-protein Galphaq and excitable cells in *C. elegans*. *Development* **2003**, *130*, 4553–4566. [[CrossRef](#)] [[PubMed](#)]
51. Battu, G.; Hoier, E.F.; Hajnal, A. The *C. elegans* G-protein-coupled receptor SRA-13 inhibits RAS/MAPK signalling during olfaction and vulval development. *Development* **2003**, *130*, 2567–2577. [[CrossRef](#)] [[PubMed](#)]

52. Fraser, A.G.; Kamath, R.S.; Zipperlen, P.; Martinez-Campos, M.; Sohrmann, M.; Ahringer, J. Functional genomic analysis of *C. elegans* chromosome I by systematic RNA interference. *Nature* **2000**, *408*, 325–330. [[CrossRef](#)] [[PubMed](#)]
53. Simmer, F.; Moorman, C.; van der Linden, A.M.; Kuijk, E.; van den Berghe, P.V.; Kamath, R.S.; Fraser, A.G.; Ahringer, J.; Plasterk, R.H. Genome-wide RNAi of *C. elegans* using the hypersensitive rrf-3 strain reveals novel gene functions. *PLoS Biol.* **2003**, *1*, e12. [[CrossRef](#)] [[PubMed](#)]
54. Kindt, K.S.; Tam, T.; Whiteman, S.; Schafer, W.R. Serotonin promotes G(o)-dependent neuronal migration in *Caenorhabditis elegans*. *Curr. Biol.* **2002**, *12*, 1738–1747. [[CrossRef](#)]
55. Steimel, A.; Wong, L.; Najarro, E.H.; Ackley, B.D.; Garriga, G.; Hutter, H. The Flamingo ortholog FMI-1 controls pioneer-dependent navigation of follower axons in *C. elegans*. *Development* **2010**, *137*, 3663–3673. [[CrossRef](#)] [[PubMed](#)]
56. Schulte, G.; Wright, S.C. Frizzleds as GPCRs—More Conventional Than We Thought! *Trends Pharmacol. Sci.* **2018**, *39*, 828–842. [[CrossRef](#)] [[PubMed](#)]
57. Dohlman, H.G.; Thorner, J. RGS proteins and signaling by heterotrimeric G proteins. *J. Biol. Chem.* **1997**, *272*, 3871–3874. [[CrossRef](#)] [[PubMed](#)]
58. Porter, M.Y.; Koelle, M.R. Insights into RGS protein function from studies in *Caenorhabditis elegans*. *Prog. Mol. Biol. Transl. Sci.* **2009**, *86*, 15–47. [[CrossRef](#)] [[PubMed](#)]
59. Hess, H.A.; Roper, J.C.; Grill, S.W.; Koelle, M.R. RGS-7 completes a receptor-independent heterotrimeric G protein cycle to asymmetrically regulate mitotic spindle positioning in *C. elegans*. *Cell* **2004**, *119*, 209–218. [[CrossRef](#)] [[PubMed](#)]
60. de Mendoza, A.; Sebe-Pedros, A.; Ruiz-Trillo, I. The evolution of the GPCR signaling system in eukaryotes: Modularity, conservation, and the transition to metazoan multicellularity. *Genome Biol. Evol.* **2014**, *6*, 606–619. [[CrossRef](#)] [[PubMed](#)]
61. Coleman, B.D.; Marivin, A.; Parag-Sharma, K.; DiGiacomo, V.; Kim, S.; Pepper, J.S.; Casler, J.; Nguyen, L.T.; Koelle, M.R.; Garcia-Marcos, M. Evolutionary Conservation of a GPCR-Independent Mechanism of Trimeric G Protein Activation. *Mol. Biol. Evol.* **2016**, *33*, 820–837. [[CrossRef](#)] [[PubMed](#)]
62. Miller, K.G.; Rand, J.B. A role for RIC-8 (Synembryn) and GOA-1 (G(o)alpha) in regulating a subset of centrosome movements during early embryogenesis in *Caenorhabditis elegans*. *Genetics* **2000**, *156*, 1649–1660. [[PubMed](#)]
63. Miller, K.G.; Alfonso, A.; Nguyen, M.; Crowell, J.A.; Johnson, C.D.; Rand, J.B. A genetic selection for *Caenorhabditis elegans* synaptic transmission mutants. *Proc. Natl. Acad. Sci. USA* **1996**, *93*, 12593–12598. [[CrossRef](#)] [[PubMed](#)]
64. Reynolds, N.K.; Schade, M.A.; Miller, K.G. Convergent, RIC-8-dependent Galpha signaling pathways in the *Caenorhabditis elegans* synaptic signaling network. *Genetics* **2005**, *169*, 651–670. [[CrossRef](#)] [[PubMed](#)]
65. Peters, K.A.; Rogers, S.L. Drosophila Ric-8 interacts with the Gα12/13 subunit, Concertina, during activation of the Folded gastrulation pathway. *Mol. Biol. Cell* **2013**, *24*, 3460–3471. [[CrossRef](#)] [[PubMed](#)]
66. Saare, M.; Lulla, S.; Tõnissoo, T.; Meier, R.; Kask, K.; Ruisu, K.; Karis, A.; Salumets, A.; Pooga, M. Expression Pattern and Localization Dynamics of Guanine Nucleotide Exchange Factor RIC8 during Mouse Oogenesis. *PLoS ONE* **2015**, *10*, e0129131. [[CrossRef](#)] [[PubMed](#)]
67. Kiyomitsu, T.; Cheeseman, I.M. Chromosome- and spindle-pole-derived signals generate an intrinsic code for spindle position and orientation. *Nat. Cell Biol.* **2012**, *14*, 311–317. [[CrossRef](#)] [[PubMed](#)]
68. Kotak, S.; Busso, C.; Gonczy, P. Cortical dynein is critical for proper spindle positioning in human cells. *J. Cell Biol.* **2012**, *199*, 97–110. [[CrossRef](#)] [[PubMed](#)]
69. Woodard, G.E.; Huang, N.N.; Cho, H.; Miki, T.; Tall, G.G.; Kehrl, J.H. Ric-8A and Gi alpha recruit LGN, NuMA, and dynein to the cell cortex to help orient the mitotic spindle. *Mol. Cell. Biol.* **2010**, *30*, 3519–3530. [[CrossRef](#)] [[PubMed](#)]
70. Fielmich, L.E.; Schmidt, R.; Dickinson, D.J.; Goldstein, B.; Akhmanova, A.; Van den Heuvel, S. Optogenetic dissection of mitotic spindle positioning in vivo. *eLife* **2018**, *7*, e38198. [[CrossRef](#)] [[PubMed](#)]
71. Blumer, J.B.; Oner, S.S.; Lanier, S.M. Group II activators of G-protein signalling and proteins containing a G-protein regulatory motif. *Acta Physiol.* **2012**, *204*, 202–218. [[CrossRef](#)] [[PubMed](#)]
72. Anantharaman, V.; Abhiman, S.; Souza, R.F.; Aravind, L. Comparative genomics uncovers novel structural and functional features of the heterotrimeric GTPase signaling system. *Gene* **2011**, *475*, 63–78. [[CrossRef](#)] [[PubMed](#)]

73. Jékely, G. Evolution of phototaxis. *Philos. Trans. R. Soc. Lond. Ser. B Biol. Sci.* **2009**, *364*, 2795–2808. [[CrossRef](#)] [[PubMed](#)]
74. Wuichet, K.; Søgaard-Andersen, L. Evolution and diversity of the Ras superfamily of small GTPases in prokaryotes. *Genome Biol. Evol.* **2014**, *7*, 57–70. [[CrossRef](#)] [[PubMed](#)]
75. Wilkie, T.M.; Kinch, L. New roles for Galpha and RGS proteins: Communication continues despite pulling sisters apart. *Curr. Biol.* **2005**, *15*, R843–R854. [[CrossRef](#)] [[PubMed](#)]
76. Crespi, B.J. The evolution of social behavior in microorganisms. *Trends Ecol. Evol.* **2001**, *16*, 178–183. [[CrossRef](#)]
77. King, N. The unicellular ancestry of animal development. *Dev. Cell* **2004**, *7*, 313–325. [[CrossRef](#)] [[PubMed](#)]
78. Rokas, A. The origins of multicellularity and the early history of the genetic toolkit for animal development. *Annu. Rev. Genet.* **2008**, *42*, 235–251. [[CrossRef](#)] [[PubMed](#)]
79. Gerhart, J. 1998 Warkany lecture: Signaling pathways in development. *Teratology* **1999**, *60*, 226–239. [[CrossRef](#)]
80. Pires-daSilva, A.; Sommer, R.J. The evolution of signalling pathways in animal development. *Nat. Rev. Genet.* **2003**, *4*, 39–49. [[CrossRef](#)] [[PubMed](#)]
81. King, N.; Westbrook, M.J.; Young, S.L.; Kuo, A.; Abedin, M.; Chapman, J.; Fairclough, S.; Hellsten, U.; Isogai, Y.; Letunic, I.; et al. The genome of the choanoflagellate *Monosiga brevicollis* and the origin of metazoans. *Nature* **2008**, *451*, 783–788. [[CrossRef](#)] [[PubMed](#)]
82. Manning, G.; Young, S.L.; Miller, W.T.; Zhai, Y. The protist, *Monosiga brevicollis*, has a tyrosine kinase signaling network more elaborate and diverse than found in any known metazoan. *Proc. Natl. Acad. Sci. USA* **2008**, *105*, 9674–9679. [[CrossRef](#)] [[PubMed](#)]
83. Suga, H.; Dacre, M.; Mendoza, A.; Shalchian-Tabrizi, K.; Manning, G.; Ruiz-Trillo, I. Genomic survey of premetazoans shows deep conservation of cytoplasmic tyrosine kinases and multiple radiations of receptor tyrosine kinases. *Sci. Signal.* **2012**, *5*, ra35. [[CrossRef](#)] [[PubMed](#)]
84. Flock, T.; Hauser, A.S.; Lund, N.; Gloriam, D.E.; Balaji, S.; Babu, M.M. Selectivity determinants of GPCR-G-protein binding. *Nature* **2017**, *545*, 317–322. [[CrossRef](#)] [[PubMed](#)]
85. Dong, J.-H.; Wen, J.-F.; Tian, H.-F. Homologs of eukaryotic Ras superfamily proteins in prokaryotes and their novel phylogenetic correlation with their eukaryotic analogs. *Gene* **2007**, *396*, 116–124. [[CrossRef](#)] [[PubMed](#)]
86. Kahn, R.A. Toward a model for Arf GTPases as regulators of traffic at the Golgi. *FEBS Lett.* **2009**, *583*, 3872–3879. [[CrossRef](#)] [[PubMed](#)]
87. Kahn, R.A.; Cherfils, J.; Elias, M.; Lovering, R.C.; Munro, S.; Schurmann, A. Nomenclature for the human Arf family of GTP-binding proteins: ARF, ARL, and SAR proteins. *J. Cell Biol.* **2006**, *172*, 645–650. [[CrossRef](#)] [[PubMed](#)]
88. Lee, C.; Goldberg, J. Structure of coatamer cage proteins and the relationship among COPI, COPII, and clathrin vesicle coats. *Cell* **2010**, *142*, 123–132. [[CrossRef](#)] [[PubMed](#)]
89. Leipe, D.D.; Wolf, Y.I.; Koonin, E.V.; Aravind, L. Classification and evolution of P-loop GTPases and related ATPases. *J. Mol. Biol.* **2002**, *317*, 41–72. [[CrossRef](#)] [[PubMed](#)]
90. Bradford, W.; Buckholz, A.; Morton, J.; Price, C.; Jones, A.M.; Urano, D. Eukaryotic G protein signaling evolved to require G protein-coupled receptors for activation. *Sci. Signal.* **2013**, *6*, ra37. [[CrossRef](#)] [[PubMed](#)]
91. Krishnan, A.; Mustafa, A.; Almén, M.S.; Fredriksson, R.; Williams, M.J.; Schiöth, H.B. Evolutionary hierarchy of vertebrate-like heterotrimeric G protein families. *Mol. Phylogenet. Evol.* **2015**, *91*, 27–40. [[CrossRef](#)] [[PubMed](#)]
92. Oka, Y.; Saraiva, L.R.; Kwan, Y.Y.; Korsching, S.I. The fifth class of Galpha proteins. *Proc. Natl. Acad. Sci. USA* **2009**, *106*, 1484–1489. [[CrossRef](#)] [[PubMed](#)]
93. Nordström, K.J.V.; Sällman Almén, M.; Edstam, M.M.; Fredriksson, R.; Schiöth, H.B. Independent HHsearch, Needleman–Wunsch-based, and motif analyses reveal the overall hierarchy for most of the G protein-coupled receptor families. *Mol. Biol. Evol.* **2011**, *28*, 2471–2480. [[CrossRef](#)] [[PubMed](#)]
94. Bastiani, C.; Mendel, J. Heterotrimeric G proteins in *C. elegans*. *WormBook* **2006**, 1–25. [[CrossRef](#)] [[PubMed](#)]
95. Lans, H.; Rademakers, S.; Jansen, G. A network of stimulatory and inhibitory Galpha-subunits regulates olfaction in *Caenorhabditis elegans*. *Genetics* **2004**, *167*, 1677–1687. [[CrossRef](#)] [[PubMed](#)]
96. O'Halloran, D.M.; Fitzpatrick, D.A.; McCormack, G.P.; McNerney, J.O.; Burnell, A.M. The molecular phylogeny of a nematode-specific clade of heterotrimeric G-protein alpha-subunit genes. *J. Mol. Evol.* **2006**, *63*, 87–94. [[CrossRef](#)] [[PubMed](#)]

97. Gazave, E.; Lapébie, P.; Richards, G.S.; Brunet, F.; Ereskovsky, A.V.; Degnan, B.M.; Borchiellini, C.; Vervoort, M.; Renard, E. Origin and evolution of the Notch signalling pathway: An overview from eukaryotic genomes. *BMC Evol. Biol.* **2009**, *9*, 249. [[CrossRef](#)] [[PubMed](#)]
98. Sebé-Pedrós, A.; Zheng, Y.; Ruiz-Trillo, I.; Pan, D. Premetazoan origin of the hippo signaling pathway. *Cell Rep.* **2012**, *1*, 13–20. [[CrossRef](#)] [[PubMed](#)]
99. Besseling, J.; Bringmann, H. Engineered non-Mendelian inheritance of entire parental genomes in *C. elegans*. *Nat. Biotechnol.* **2016**, *34*, 982–986. [[CrossRef](#)] [[PubMed](#)]
100. Armbruster, B.N.; Li, X.; Pausch, M.H.; Herlitze, S.; Roth, B.L. Evolving the lock to fit the key to create a family of G protein-coupled receptors potentially activated by an inert ligand. *Proc. Natl. Acad. Sci. USA* **2007**, *104*, 5163–5168. [[CrossRef](#)] [[PubMed](#)]
101. Guettier, J.M.; Gautam, D.; Scarselli, M.; Ruiz de Azua, I.; Li, J.H.; Rosemond, E.; Ma, X.; Gonzalez, F.J.; Armbruster, B.N.; Lu, H.; et al. A chemical-genetic approach to study G protein regulation of beta cell function in vivo. *Proc. Natl. Acad. Sci. USA* **2009**, *106*, 19197–19202. [[CrossRef](#)] [[PubMed](#)]
102. Becnel, J.; Johnson, O.; Majeed, Z.R.; Tran, V.; Yu, B.; Roth, B.L.; Cooper, R.L.; Kerut, E.K.; Nichols, C.D. DREADDs in *Drosophila*: A pharmacogenetic approach for controlling behavior, neuronal signaling, and physiology in the fly. *Cell Rep.* **2013**, *4*, 1049–1059. [[CrossRef](#)] [[PubMed](#)]
103. Prömel, S.; Fiedler, F.; Binder, C.; Winkler, J.; Schöneberg, T.; Thor, D. Deciphering and modulating G protein signalling in *C. elegans* using the DREADD technology. *Sci. Rep.* **2016**, *6*, 28901. [[CrossRef](#)] [[PubMed](#)]
104. Gao, S.; Nagpal, J.; Schneider, M.W.; Kozjak-Pavlovic, V.; Nagel, G.; Gottschalk, A. Optogenetic manipulation of cGMP in cells and animals by the tightly light-regulated guanylyl-cyclase opsin CyclOp. *Nat. Commun.* **2015**, *6*, 8046. [[CrossRef](#)] [[PubMed](#)]
105. Steuer Costa, W.; Yu, S.C.; Liewald, J.F.; Gottschalk, A. Fast cAMP Modulation of Neurotransmission via Neuropeptide Signals and Vesicle Loading. *Curr. Biol.* **2017**, *27*, 495–507. [[CrossRef](#)] [[PubMed](#)]
106. Maher, K.N.; Swaminathan, A.; Patel, P.; Chase, D.L. A novel strategy for cell-autonomous gene knockdown in *Caenorhabditis elegans* defines a cell-specific function for the G-protein subunit GOA-1. *Genetics* **2013**, *194*, 363–373. [[CrossRef](#)] [[PubMed](#)]
107. Link, C.D.; Taft, A.; Kapulkin, V.; Duke, K.; Kim, S.; Fei, Q.; Wood, D.E.; Sahagan, B.G. Gene expression analysis in a transgenic *Caenorhabditis elegans* Alzheimer’s disease model. *Neurobiol. Aging* **2003**, *24*, 397–413. [[CrossRef](#)]
108. Edgar, L.G.; Wolf, N.; Wood, W.B. Early transcription in *Caenorhabditis elegans* embryos. *Development* **1994**, *120*, 443–451. [[PubMed](#)]
109. D’Angelo, D.D.; Sakata, Y.; Lorenz, J.N.; Boivin, G.P.; Walsh, R.A.; Liggett, S.B.; Dorn, G.W., 2nd. Transgenic Galphaq overexpression induces cardiac contractile failure in mice. *Proc. Natl. Acad. Sci. USA* **1997**, *94*, 8121–8126.
110. Boularan, C.; Hwang, I.Y.; Kamenyeva, O.; Park, C.; Harrison, K.; Huang, Z.; Kehrl, J.H. B Lymphocyte-Specific Loss of Ric-8A Results in a Galpha Protein Deficit and Severe Humoral Immunodeficiency. *J. Immunol.* **2015**, *195*, 2090–2102. [[CrossRef](#)] [[PubMed](#)]
111. Bos, J.L.; Rehmann, H.; Wittinghofer, A. GEFs and GAPs: Critical elements in the control of small G proteins. *Cell* **2007**, *129*, 865–877. [[CrossRef](#)] [[PubMed](#)]



© 2018 by the authors. Licensee MDPI, Basel, Switzerland. This article is an open access article distributed under the terms and conditions of the Creative Commons Attribution (CC BY) license (<http://creativecommons.org/licenses/by/4.0/>).

5 Summary

Thesis submitted for the degree of:

Dr. med.

Title:

The 7TM-independent (*trans*) function of the Adhesion GPCR Latrophilin-1 in *C. elegans* neuron morphogenesis and germ cell proliferation

Submitted by:

Daniel Matúš

Carried out at:

Rudolf Schönheimer Institute of Biochemistry
Medical Faculty, Leipzig University

Supervisors:

Prof. Dr. med. Torsten Schöneberg
Prof. Simone Prömel, D.Phil (Oxon)

Submitted:

December 2021 in Leipzig

Adhesion G protein-coupled receptors (aGPCRs) are fascinating molecules that have been found to be relevant in a multitude of physiological and pathological contexts. As members of the GPCR superfamily they are able to mediate canonical G protein- and therefore seven transmembrane helices domain (7TM)-dependent (*cis*) functions. However, there is also evidence for receptor functions that can be exerted by the sole extracellular N terminus, independently of the 7TM (*trans* functions). The huge N terminus can be composed of a plethora of different domains, allowing for a multitude of possible interactions with other molecules. This versatility in interaction partners and signaling modes makes aGPCRs putatively capable of multifaceted signaling mechanisms. However, very little is known about how *trans* functions are implemented *in vivo*, whether they indeed trigger signaling pathways, and how they are mediated on a molecular level.

Latrophilins are prototypical aGPCRs with essential functions in mammalian neurodevelopment and mechanosensory neurons of *Drosophila melanogaster* (*D. melanogaster*), both of which have been shown to entail canonical *cis* signaling. Interestingly, the Latrophilin homolog LAT-1 in *Caenorhabditis elegans* (*C. elegans*) has a known *cis* function in embryonic development as well as a *trans* function in

hermaphrodite fertility, making it the perfect model to study Latrophilin and, by extension, aGPCR signaling capabilities.

There is preliminary evidence hinting towards an involvement of LAT-1 in the *C. elegans* male nervous system. The first part of this study was therefore focused on elucidating whether LAT-1 exerts a neuronal *cis* function as has been shown in other organisms or employs the intriguing *trans* mode. The following main results were obtained:

1. *lat-1* expression could be shown in a multitude of neurons and distinct neuronal support cells (cephalic socket cell) of the *C. elegans* male via a transcriptional reporter (*lat-1p::GFP*), suggesting the receptor to be essential in the nervous system.
2. Individual neuron types were defined by using the multicolor neuronal marker NeuroPAL. Interestingly, many of the identified *lat-1* expressing neurons have known functions in male mating behavior, integrating chemo- and mechanosensory cues to coordinate hermaphrodite recognition, vulva localization and sperm transfer.
3. As an unbiased screening for neuronal LAT-1 functions, RNA-Seq data of wild-type worms and *lat-1(ok1465)* null mutants were compared to identify significantly regulated gene products. Subsequent enrichment analyses of these genes pointed – among others – towards a role in copulation, locomotion, cytoskeleton and extracellular matrix organization, and neurodevelopment.
4. Since LAT-1 has a known *cis* function in embryonic development, following up on a possible role of LAT-1 in neurodevelopment was of special interest. Adult *lat-1* mutants were therefore screened for morphological defects in the nervous system. Intriguingly, multiple neuronal defects were identified: Head sensory neurons displayed dysmorphic and crude dendrites, processes of cephalic socket cells failed to establish their characteristic triangular shape and rays of the tail were often shortened, dysmorphic or missing entirely.
5. Interestingly, these defects were ameliorated in a *lat-1* mutant strain expressing the sole LAT-1 N terminus tethered to the membrane by a single transmembrane helix, indicating a *trans* function of the receptor in neuron morphogenesis.
6. *lat-1* mutants also showed a displaced nerve ring, which is a complex network localized in the head composed of axons and dendrites of various neurons. Surprisingly, this defect was not affected by the expression of the sole LAT-1 N terminus, suggesting that certain aspects of LAT-1 function in the *C. elegans* nervous system could still be dependent on *cis* signaling.
7. Finally, the question arose, if the observed neuronal LAT-1 *trans* function could also influence male behavior. Since both *lat-1* expression and RNA-Seq data pointed towards a possible role in copulation and the latter is an established model to study neuronal functions, *lat-1* mutants have been screened for defects in mating. Indeed, *lat-1* mutant males displayed defects in multiple steps of copulation. In particular, they were impaired in finding and

recognizing the hermaphrodite as well as its vulva, all of which lead to a decrease in successful copulations. The observed defects were ameliorated by expression of the sole LAT-1 N terminus, confirming the suspected *trans* function to influence copulation behavior.

In summary, the data presented in the first part of this study strongly suggest a neuronal *trans* function of LAT-1, mediating neurodevelopment of sensory neurons and neuronal support cells. The *trans* function is furthermore essential for male physiology by influencing multiple aspects of mating behavior. It would be intriguing to see, whether neuronal *trans* functions also play roles in vertebrates, possibly complementing the previously described *cis* functions in synaptogenesis.

The goal of the second part of this work was to create a detailed image of the mechanisms underlying *trans* functions and their implementation in an *in vivo* setting. The starting point for this was the known *trans* function of LAT-1 in *C. elegans* hermaphrodite fertility. Interestingly, unpublished data from the Prömel lab showed *lat-1* mutants to have an increased amount of M phase cells within the proliferative zone of the gonad, pointing towards a role of LAT-1 in germ cell proliferation. Pursuing these findings, the main results obtained in this study were the following:

1. An increase of cells in M phase can result from a change in the total amount of germ cells undergoing mitosis within the proliferative zone of the *C. elegans* gonad, which leads to a concomitant increase in M phases. Alternatively, this finding can point towards a deregulated cell cycle, which would not necessarily lead to a change in proliferative zone size. Antibody stainings directed specifically at germ cells within the proliferative zone showed its size in *lat-1* null mutant and wild-type gonads not to be significantly different, making a LAT-1 function in cell cycle regulation more likely.
2. In a next step, cell cycle phases of germ cells in the proliferative zone were analyzed, revealing relatively longer M and S phases on one hand and decreased duration of G1 and G2 phases on the other.
3. Such a shift in cell cycle phase distribution could either result from slower progression through M and S phases or an increased cell cycle speed, leading to a relatively shorter time in the G phases. To differentiate between these two scenarios, pulse chase analyses of germ cell progression were performed, which revealed an increase in germ cell production in *lat-1* mutants, suggesting a faster cell cycle.
4. All of the defects mentioned above were ameliorated in a *lat-1* mutant strain expressing the sole LAT-1 N terminus, supporting a *trans* mode of function in this context.
5. *Trans* functions can putatively affect adjacent cells, but also the same cell the receptor is expressed on. To determine the origin and direction of the LAT-1 *trans* function, *lat-1* expression in the reproductive system was analyzed in single-cell resolution. A single-copy integrated transcriptional *lat-1p::mCherry*

reporter revealed strong expression in the cells of the somatic gonad (distal tip cell (DTC) and gonadal sheath cells), but none in the germ cells themselves, which was in line with previously obtained data from the Prömel lab using a transgenic *lat-1p::GFP* reporter. Since LAT-1 clearly alters germ cell proliferation, these data suggest a non-cell autonomous function of the receptor N terminus originating from somatic cells of the gonad.

6. To verify this hypothesis, the LAT-1 N terminus was selectively expressed in somatic cells of the gonad of *lat-1* mutants using tissue-specific promoter constructs. Thereby, defective proliferation could be ameliorated by expression in the DTC or the gonadal sheath cells, respectively. This confirms the LAT-1 N terminus to influence germ cell proliferation non-cell autonomously from cells of the somatic gonad.
7. Another question to be answered was whether isolated N termini could carry out *trans* functions independently of full-length receptors. Such molecules could be generated for example via receptor autoproteolysis or alternative splicing. While previous data showed receptor autoproteolysis to be dispensable for LAT-1 function in fertility, analyses of RNA-Seq data predicted the presence of *lat-1* variants comprised only of the N terminus. In order to discover the full splice variant repertoire of *lat-1*, *in silico* analyses of publicly available high-coverage RNA-Seq data were performed. These suggested the existence of multiple N-terminal splice variants of *lat-1*.
8. Intriguingly, unpublished data from the Prömel lab confirmed the presence of such variants *in vivo* via 3' rapid amplification of cDNA-ends with PCR (RACE-PCR). Therefore, LAT-1 *trans* functions could be realized independently of the full-length receptor via N-terminal splice variants.
9. Lastly, it remained to be answered whether LAT-1 *trans* function can trigger signaling cascades in affected cells. Interestingly, protein levels of the Notch downstream effector and inhibitor of proliferation GLD-1 were found to be downregulated in the germline of *lat-1* mutants, suggesting cross-talk of the receptor with the Notch pathway.
10. Furthermore, *gld-1* loss-of-function mutants exhibited an increase in M phase cells, similar to *lat-1* mutants. To elucidate whether *lat-1* and *gld-1* lie in the same genetic pathway, epistasis analyses were performed. Thereby, defects of *gld-1; lat-1* double mutants were compared to those of the respective single mutants. An additive effect in the double mutant would suggest the two genes to lie in parallel pathways, while a defect similar to one of the single mutants (= epistasis) suggests them to lie upstream/downstream of each other. Indeed, analyses of a worm strain containing both mutated *lat-1* and *gld-1* alleles and comparison to the single mutants revealed the effects on germline proliferation to be epistatic. Therefore GLD-1 likely is a downstream effector of LAT-1 function.
11. To understand the effect of LAT-1 on the Notch pathway, similar epistasis analyses were performed using loss-of-function mutants of the Notch receptor *glp-1*, the Notch ligand *lag-2* and the direct downstream effectors of

Notch *lst-1* and *sygl-1*. While *lat-1* double mutants containing *lag-2*, *lst-1* and *sygl-1* mutations, respectively, showed an additive effect on the mitotic index, no proliferation phenotype was detected in *lat-1; glp-1* double mutants. Furthermore, a double mutant containing the *lat-1* null allele and a *glp-1* gain-of-function allele showed epistasis when compared to the single mutants. This suggests LAT-1 to regulate GLD-1 independently of most of the canonical Notch-signaling components, but dependent on the presence of the Notch receptor GLP-1.

Taken together, the data obtained in the second part of this study give evidence for the ability of the LAT-1 *trans* function to non-cell autonomously trigger signaling cascades on germ cells within the proliferative zone of the *C. elegans* hermaphrodite gonad, thereby regulating proliferation. Furthermore, this effect could be realized independently of full-length receptors via the generation of N-terminal splice variants.

This study presents a comprehensive view of LAT-1 *trans* functions in the model organism *C. elegans*, revealing them to be essential in multiple physiological contexts and giving first insights into the underlying molecular mechanisms. In particular, it is shown that *trans* functions can coexist with *cis* functions as it is likely the case in the *C. elegans* nervous system, but can also be found independently of canonical receptor function, as is shown for the role of LAT-1 in germ cell proliferation. For the latter, evidence is presented that suggests the separation of *cis*- and *trans* functions on a molecular level via the generation of N-terminal splice variants. Additionally, it is shown, that *trans* functions can trigger signaling cascades on adjacent cells and are therefore not limited to adhesion. These data lay the groundwork for understanding the complex signaling capabilities of Adhesion GPCRs and can be used as a starting point for analyses of *trans* functions in other organisms, possibly even leading to pharmacological applications in the future.

6 References

1. Fredriksson, R., Lagerström, M. C., Lundin, L.-G. & Schiöth, H. B. The G-protein-coupled receptors in the human genome form five main families. Phylogenetic analysis, paralogon groups, and fingerprints. *Molecular pharmacology* **63**, 1256–1272; 10.1124/mol.63.6.1256 (2003).
2. Bjarnadóttir, T. K. *et al.* The human and mouse repertoire of the adhesion family of G-protein-coupled receptors. *Genomics* **84**, 23–33; 10.1016/j.ygeno.2003.12.004 (2004).
3. Hamann, J. *et al.* International Union of Basic and Clinical Pharmacology. XCIV. Adhesion G protein-coupled receptors. *Pharmacological reviews* **67**, 338–367; 10.1124/pr.114.009647 (2015).
4. Brzóška, H. Ł. *et al.* Planar cell polarity genes *Celsr1* and *Vangl2* are necessary for kidney growth, differentiation, and rostrocaudal patterning. *Kidney international* **90**, 1274–1284; 10.1016/j.kint.2016.07.011 (2016).
5. Yates, L. L. *et al.* The PCP genes *Celsr1* and *Vangl2* are required for normal lung branching morphogenesis. *Human molecular genetics* **19**, 2251–2267; 10.1093/hmg/ddq104 (2010).
6. Waller-Evans, H. *et al.* The orphan adhesion-GPCR GPR126 is required for embryonic development in the mouse. *PloS one* **5**, e14047; 10.1371/journal.pone.0014047 (2010).
7. Röthe, J. *et al.* Involvement of the Adhesion GPCRs Latrophilins in the Regulation of Insulin Release. *Cell reports* **26**, 1573–1584.e5; 10.1016/j.celrep.2019.01.040 (2019).
8. Dunér, P. *et al.* Adhesion G Protein-Coupled Receptor G1 (ADGRG1/GPR56) and Pancreatic β -Cell Function. *The Journal of clinical endocrinology and metabolism* **101**, 4637–4645; 10.1210/jc.2016-1884 (2016).
9. Chang, G.-W. *et al.* The Adhesion G Protein-Coupled Receptor GPR56/ADGRG1 Is an Inhibitory Receptor on Human NK Cells. *Cell reports* **15**, 1757–1770; 10.1016/j.celrep.2016.04.053 (2016).
10. Yona, S. *et al.* Ligation of the adhesion-GPCR EMR2 regulates human neutrophil function. *FASEB journal : official publication of the Federation of American Societies for Experimental Biology* **22**, 741–751; 10.1096/fj.07-9435com (2008).
11. Lindenmaier, L. B., Parmentier, N., Guo, C., Tissir, F. & Wright, K. M. Dystroglycan is a scaffold for extracellular axon guidance decisions. *eLife* **8**; 10.7554/eLife.42143 (2019).
12. Duman, J. G. *et al.* The adhesion-GPCR BAI1 regulates synaptogenesis by controlling the recruitment of the Par3/Tiam1 polarity complex to synaptic sites. *The Journal of neuroscience : the official journal of the Society for Neuroscience* **33**, 6964–6978; 10.1523/JNEUROSCI.3978-12.2013 (2013).
13. Anderson, G. R. *et al.* Postsynaptic adhesion GPCR latrophilin-2 mediates target recognition in entorhinal-hippocampal synapse assembly. *The Journal of cell biology* **216**, 3831–3846; 10.1083/jcb.201703042 (2017).
14. Monk, K. R. *et al.* A G protein-coupled receptor is essential for Schwann cells to initiate myelination. *Science (New York, N.Y.)* **325**, 1402–1405; 10.1126/science.1173474 (2009).
15. Giera, S. *et al.* The adhesion G protein-coupled receptor GPR56 is a cell-autonomous regulator of oligodendrocyte development. *Nature communications* **6**, 6121; 10.1038/ncomms7121 (2015).

16. Piao, X. *et al.* G protein-coupled receptor-dependent development of human frontal cortex. *Science (New York, N. Y.)* **303**, 2033–2036; 10.1126/science.1092780 (2004).
17. Vezain, M. *et al.* A de novo variant in ADGRL2 suggests a novel mechanism underlying the previously undescribed association of extreme microcephaly with severely reduced sulcation and rhombencephalosynapsis. *Acta neuropathologica communications* **6**, 109; 10.1186/s40478-018-0610-5 (2018).
18. Weston, M. D., Luijendijk, M. W. J., Humphrey, K. D., Möller, C. & Kimberling, W. J. Mutations in the VLGR1 gene implicate G-protein signaling in the pathogenesis of Usher syndrome type II. *American journal of human genetics* **74**, 357–366; 10.1086/381685 (2004).
19. Arcos-Burgos, M. & Muenke, M. Toward a better understanding of ADHD: LPHN3 gene variants and the susceptibility to develop ADHD. *Attention deficit and hyperactivity disorders* **2**, 139–147; 10.1007/s12402-010-0030-2 (2010).
20. Arcos-Burgos, M. *et al.* A common variant of the latrophilin 3 gene, LPHN3, confers susceptibility to ADHD and predicts effectiveness of stimulant medication. *Molecular psychiatry* **15**, 1053–1066; 10.1038/mp.2010.6 (2010).
21. Michaelson, J. J. *et al.* Whole-genome sequencing in autism identifies hot spots for de novo germline mutation. *Cell* **151**, 1431–1442; 10.1016/j.cell.2012.11.019 (2012).
22. Oozeer, F., Yates, L. L., Dean, C. & Formstone, C. J. A role for core planar polarity proteins in cell contact-mediated orientation of planar cell division across the mammalian embryonic skin. *Scientific reports* **7**, 1880; 10.1038/s41598-017-01971-2 (2017).
23. Panousopoulou, E., Hobbs, C., Mason, I., Green, J. B. A. & Formstone, C. J. Epiboly generates the epidermal basal monolayer and spreads the nascent mammalian skin to enclose the embryonic body. *Journal of cell science* **129**, 1915–1927; 10.1242/jcs.180703 (2016).
24. Patra, C. *et al.* Organ-specific function of adhesion G protein-coupled receptor GPR126 is domain-dependent. *Proceedings of the National Academy of Sciences of the United States of America* **110**, 16898–16903; 10.1073/pnas.1304837110 (2013).
25. Kou, I. *et al.* Genetic variants in GPR126 are associated with adolescent idiopathic scoliosis. *Nature genetics* **45**, 676–679; 10.1038/ng.2639 (2013).
26. Langenhan, T. *et al.* Latrophilin signaling links anterior-posterior tissue polarity and oriented cell divisions in the *C. elegans* embryo. *Developmental cell* **17**, 494–504; 10.1016/j.devcel.2009.08.008 (2009).
27. Usui, T. *et al.* Flamingo, a seven-pass transmembrane cadherin, regulates planar cell polarity under the control of Frizzled. *Cell* **98**, 585–595; 10.1016/s0092-8674(00)80046-x (1999).
28. Scholz, N. *et al.* The adhesion GPCR latrophilin/CIRL shapes mechanosensation. *Cell reports* **11**, 866–874; 10.1016/j.celrep.2015.04.008 (2015).
29. Petersen, S. C. *et al.* The adhesion GPCR GPR126 has distinct, domain-dependent functions in Schwann cell development mediated by interaction with laminin-211. *Neuron* **85**, 755–769; 10.1016/j.neuron.2014.12.057 (2015).
30. White, J. P. *et al.* G protein-coupled receptor 56 regulates mechanical overload-induced muscle hypertrophy. *Proceedings of the National Academy of Sciences of the United States of America* **111**, 15756–15761; 10.1073/pnas.1417898111 (2014).

31. Boyden, S. E. *et al.* Vibratory Urticaria Associated with a Missense Variant in ADGRE2. *The New England journal of medicine* **374**, 656–663; 10.1056/NEJMoa1500611 (2016).
32. Wilde, C. *et al.* The constitutive activity of the adhesion GPCR GPR114/ADGRG5 is mediated by its tethered agonist. *FASEB journal : official publication of the Federation of American Societies for Experimental Biology* **30**, 666–673; 10.1096/fj.15-276220 (2016).
33. Hamann, J., Hsiao, C.-C., Lee, C. S., Ravichandran, K. S. & Lin, H.-H. Adhesion GPCRs as Modulators of Immune Cell Function. *Handbook of experimental pharmacology* **234**, 329–350; 10.1007/978-3-319-41523-9_15 (2016).
34. Aust, G., Zhu, D., van Meir, E. G. & Xu, L. Adhesion GPCRs in Tumorigenesis. *Handbook of experimental pharmacology* **234**, 369–396; 10.1007/978-3-319-41523-9_17 (2016).
35. Kan, Z. *et al.* Diverse somatic mutation patterns and pathway alterations in human cancers. *Nature* **466**, 869–873; 10.1038/nature09208 (2010).
36. Pleasance, E. D. *et al.* A comprehensive catalogue of somatic mutations from a human cancer genome. *Nature* **463**, 191–196; 10.1038/nature08658 (2010).
37. Zhu, D., Hunter, S. B., Vertino, P. M. & van Meir, E. G. Overexpression of MBD2 in glioblastoma maintains epigenetic silencing and inhibits the antiangiogenic function of the tumor suppressor gene BAI1. *Cancer research* **71**, 5859–5870; 10.1158/0008-5472.CAN-11-1157 (2011).
38. Kaur, B., Brat, D. J., Calkins, C. C. & van Meir, E. G. Brain angiogenesis inhibitor 1 is differentially expressed in normal brain and glioblastoma independently of p53 expression. *The American journal of pathology* **162**, 19–27; 10.1016/S0002-9440(10)63794-7 (2003).
39. Hatanaka, H. *et al.* Vascularization is decreased in pulmonary adenocarcinoma expressing brain-specific angiogenesis inhibitor 1 (BAI1). *International journal of molecular medicine* **5**, 181–183; 10.3892/ijmm.5.2.181 (2000).
40. Fukushima, Y. *et al.* Brain-specific angiogenesis inhibitor 1 expression is inversely correlated with vascularity and distant metastasis of colorectal cancer. *International journal of oncology* **13**, 967–970; 10.3892/ijo.13.5.967 (1998).
41. Huang, K.-Y. & Lin, H.-H. The Activation and Signaling Mechanisms of GPR56/ADGRG1 in Melanoma Cell. *Frontiers in oncology* **8**, 304; 10.3389/fonc.2018.00304 (2018).
42. Balenga, N. *et al.* Orphan Adhesion GPCR GPR64/ADGRG2 Is Overexpressed in Parathyroid Tumors and Attenuates Calcium-Sensing Receptor-Mediated Signaling. *Journal of bone and mineral research : the official journal of the American Society for Bone and Mineral Research* **32**, 654–666; 10.1002/jbmr.3023 (2017).
43. Kaucká, M. *et al.* The planar cell polarity pathway drives pathogenesis of chronic lymphocytic leukemia by the regulation of B-lymphocyte migration. *Cancer research* **73**, 1491–1501; 10.1158/0008-5472.CAN-12-1752 (2013).
44. Del Giudice, I. *et al.* Behind the scenes of non-nodal MCL: downmodulation of genes involved in actin cytoskeleton organization, cell projection, cell adhesion, tumour invasion, TP53 pathway and mutated status of immunoglobulin heavy chain genes. *British journal of haematology* **156**, 601–611; 10.1111/j.1365-2141.2011.08962.x (2012).
45. McMillan, D. R., Kayes-Wandover, K. M., Richardson, J. A. & White, P. C. Very large G protein-coupled receptor-1, the largest known cell surface protein, is

- highly expressed in the developing central nervous system. *The Journal of biological chemistry* **277**, 785–792; 10.1074/jbc.M108929200 (2002).
46. Baud, V. *et al.* EMR1, an unusual member in the family of hormone receptors with seven transmembrane segments. *Genomics* **26**, 334–344; 10.1016/0888-7543(95)80218-b (1995).
 47. Hamann, J. *et al.* Expression cloning and chromosomal mapping of the leukocyte activation antigen CD97, a new seven-span transmembrane molecule of the secretion receptor superfamily with an unusual extracellular domain. *Journal of immunology (Baltimore, Md. : 1950)* **155**, 1942–1950 (1995).
 48. Stacey, M. *et al.* The epidermal growth factor-like domains of the human EMR2 receptor mediate cell attachment through chondroitin sulfate glycosaminoglycans. *Blood* **102**, 2916–2924; 10.1182/blood-2002-11-3540 (2003).
 49. Wang, T. *et al.* CD97, an adhesion receptor on inflammatory cells, stimulates angiogenesis through binding integrin counterreceptors on endothelial cells. *Blood* **105**, 2836–2844; 10.1182/blood-2004-07-2878 (2005).
 50. Luo, R. *et al.* G protein-coupled receptor 56 and collagen III, a receptor-ligand pair, regulates cortical development and lamination. *Proceedings of the National Academy of Sciences of the United States of America* **108**, 12925–12930; 10.1073/pnas.1104821108 (2011).
 51. Paavola, K. J., Sidik, H., Zuchero, J. B., Eckart, M. & Talbot, W. S. Type IV collagen is an activating ligand for the adhesion G protein-coupled receptor GPR126. *Science signaling* **7**, ra76; 10.1126/scisignal.2005347 (2014).
 52. Koh, J. T. *et al.* Extracellular fragment of brain-specific angiogenesis inhibitor 1 suppresses endothelial cell proliferation by blocking α v β 5 integrin. *Experimental cell research* **294**, 172–184; 10.1016/j.yexcr.2003.11.008 (2004).
 53. Boucard, A. A., Ko, J. & Südhof, T. C. High affinity neurexin binding to cell adhesion G-protein-coupled receptor C1RL1/latrophilin-1 produces an intercellular adhesion complex. *The Journal of biological chemistry* **287**, 9399–9413; 10.1074/jbc.M111.318659 (2012).
 54. Silva, J.-P. *et al.* Latrophilin 1 and its endogenous ligand Lasso/teneurin-2 form a high-affinity transsynaptic receptor pair with signaling capabilities. *Proceedings of the National Academy of Sciences of the United States of America* **108**, 12113–12118; 10.1073/pnas.1019434108 (2011).
 55. O'Sullivan, M. L. *et al.* FLRT proteins are endogenous latrophilin ligands and regulate excitatory synapse development. *Neuron* **73**, 903–910; 10.1016/j.neuron.2012.01.018 (2012).
 56. Lin, H. H., Stacey, M., Hamann, J., Gordon, S. & McKnight, A. J. Human EMR2, a novel EGF-TM7 molecule on chromosome 19p13.1, is closely related to CD97. *Genomics* **67**, 188–200; 10.1006/geno.2000.6238 (2000).
 57. Krasnoperov, V. *et al.* Post-translational proteolytic processing of the calcium-independent receptor of alpha-latrotoxin (C1RL), a natural chimera of the cell adhesion protein and the G protein-coupled receptor. Role of the G protein-coupled receptor proteolysis site (GPS) motif. *The Journal of biological chemistry* **277**, 46518–46526; 10.1074/jbc.M206415200 (2002).
 58. Araç, D. *et al.* A novel evolutionarily conserved domain of cell-adhesion GPCRs mediates autoproteolysis. *The EMBO journal* **31**, 1364–1378; 10.1038/emboj.2012.26 (2012).

59. Lin, H.-H. *et al.* Autocatalytic cleavage of the EMR2 receptor occurs at a conserved G protein-coupled receptor proteolytic site motif. *The Journal of biological chemistry* **279**, 31823–31832; 10.1074/jbc.M402974200 (2004).
60. Nieberler, M., Kittel, R. J., Petrenko, A. G., Lin, H.-H. & Langenhan, T. Control of Adhesion GPCR Function Through Proteolytic Processing. *Handbook of experimental pharmacology* **234**, 83–109; 10.1007/978-3-319-41523-9_5 (2016).
61. Kishore, A. & Hall, R. A. Versatile Signaling Activity of Adhesion GPCRs. *Handbook of experimental pharmacology* **234**, 127–146; 10.1007/978-3-319-41523-9_7 (2016).
62. Stephenson, J. R. *et al.* Brain-specific angiogenesis inhibitor-1 signaling, regulation, and enrichment in the postsynaptic density. *The Journal of biological chemistry* **288**, 22248–22256; 10.1074/jbc.M113.489757 (2013).
63. Liebscher, I. *et al.* A tethered agonist within the ectodomain activates the adhesion G protein-coupled receptors GPR126 and GPR133. *Cell reports* **9**, 2018–2026; 10.1016/j.celrep.2014.11.036 (2014).
64. Stoveken, H. M., Hajduczuk, A. G., Xu, L. & Tall, G. G. Adhesion G protein-coupled receptors are activated by exposure of a cryptic tethered agonist. *Proceedings of the National Academy of Sciences of the United States of America* **112**, 6194–6199; 10.1073/pnas.1421785112 (2015).
65. Müller, A. *et al.* Oriented Cell Division in the *C. elegans* Embryo Is Coordinated by G-Protein Signaling Dependent on the Adhesion GPCR LAT-1. *PLoS genetics* **11**, e1005624; 10.1371/journal.pgen.1005624 (2015).
66. Demberg, L. M., Rothmund, S., Schöneberg, T. & Liebscher, I. Identification of the tethered peptide agonist of the adhesion G protein-coupled receptor GPR64/ADGRG2. *Biochemical and biophysical research communications* **464**, 743–747; 10.1016/j.bbrc.2015.07.020 (2015).
67. Beliu, G. *et al.* Tethered agonist exposure in intact adhesion/class B2 GPCRs through intrinsic structural flexibility of the GAIN domain. *Molecular cell* **81**, 905–921.e5; 10.1016/j.molcel.2020.12.042 (2021).
68. Prömel, S. *et al.* The GPS motif is a molecular switch for bimodal activities of adhesion class G protein-coupled receptors. *Cell reports* **2**, 321–331; 10.1016/j.celrep.2012.06.015 (2012).
69. Tu, Y.-K., Duman, J. G. & Tolia, K. F. The Adhesion-GPCR BAI1 Promotes Excitatory Synaptogenesis by Coordinating Bidirectional Trans-synaptic Signaling. *The Journal of neuroscience : the official journal of the Society for Neuroscience* **38**, 8388–8406; 10.1523/JNEUROSCI.3461-17.2018 (2018).
70. Ward, Y. *et al.* Platelets Promote Metastasis via Binding Tumor CD97 Leading to Bidirectional Signaling that Coordinates Transendothelial Migration. *Cell reports* **23**, 808–822; 10.1016/j.celrep.2018.03.092 (2018).
71. Okajima, D., Kudo, G. & Yokota, H. Brain-specific angiogenesis inhibitor 2 (BAI2) may be activated by proteolytic processing. *Journal of receptor and signal transduction research* **30**, 143–153; 10.3109/10799891003671139 (2010).
72. Patat, O. *et al.* Truncating Mutations in the Adhesion G Protein-Coupled Receptor G2 Gene ADGRG2 Cause an X-Linked Congenital Bilateral Absence of Vas Deferens. *American journal of human genetics* **99**, 437–442; 10.1016/j.ajhg.2016.06.012 (2016).
73. Knierim, A. B. *et al.* Genetic basis of functional variability in adhesion G protein-coupled receptors. *Scientific reports* **9**, 11036; 10.1038/s41598-019-46265-x (2019).

74. Tourasse, N. J., Millet, J. R. M. & Dupuy, D. Quantitative RNA-seq meta-analysis of alternative exon usage in *C. elegans*. *Genome research* **27**, 2120–2128; 10.1101/gr.224626.117 (2017).
75. Lelianova, V. G. *et al.* Alpha-latrotoxin receptor, latrophilin, is a novel member of the secretin family of G protein-coupled receptors. *The Journal of biological chemistry* **272**, 21504–21508; 10.1074/jbc.272.34.21504 (1997).
76. Sugita, S., Ichtchenko, K., Khvotchev, M. & Südhof, T. C. alpha-Latrotoxin receptor CIRL/latrophilin 1 (CL1) defines an unusual family of ubiquitous G-protein-linked receptors. G-protein coupling not required for triggering exocytosis. *The Journal of biological chemistry* **273**, 32715–32724; 10.1074/jbc.273.49.32715 (1998).
77. Krasnoperov, V. G. *et al.* alpha-Latrotoxin stimulates exocytosis by the interaction with a neuronal G-protein-coupled receptor. *Neuron* **18**, 925–937; 10.1016/s0896-6273(00)80332-3 (1997).
78. Hlubek, M. D., Stuenkel, E. L., Krasnoperov, V. G., Petrenko, A. G. & Holz, R. W. Calcium-independent receptor for alpha-latrotoxin and neurexin 1alpha corrected facilitate toxin-induced channel formation: evidence that channel formation results from tethering of toxin to membrane. *Molecular pharmacology* **57**, 519–528; 10.1124/mol.57.3.519 (2000).
79. van Renterghem, C. *et al.* alpha-latrotoxin forms calcium-permeable membrane pores via interactions with latrophilin or neurexin. *The European journal of neuroscience* **12**, 3953–3962; 10.1046/j.1460-9568.2000.00282.x (2000).
80. Volynski, K. E. *et al.* Latrophilin, neurexin, and their signaling-deficient mutants facilitate alpha -latrotoxin insertion into membranes but are not involved in pore formation. *The Journal of biological chemistry* **275**, 41175–41183; 10.1074/jbc.M005857200 (2000).
81. Volynski, K. E. *et al.* Latrophilin fragments behave as independent proteins that associate and signal on binding of LTX(N4C). *The EMBO journal* **23**, 4423–4433; 10.1038/sj.emboj.7600443 (2004).
82. Nordström, K. J. V., Lagerström, M. C., Wallér, L. M. J., Fredriksson, R. & Schiöth, H. B. The Secretin GPCRs descended from the family of Adhesion GPCRs. *Molecular biology and evolution* **26**, 71–84; 10.1093/molbev/msn228 (2009).
83. Mee, C. J. *et al.* Latrophilin is required for toxicity of black widow spider venom in *Caenorhabditis elegans*. *The Biochemical journal* **378**, 185–191; 10.1042/BJ20031213 (2004).
84. Willson, J. *et al.* Latrotoxin receptor signaling engages the UNC-13-dependent vesicle-priming pathway in *C. elegans*. *Current biology : CB* **14**, 1374–1379; 10.1016/j.cub.2004.07.056 (2004).
85. Lloyd, T. E. *et al.* A genome-wide search for synaptic vesicle cycle proteins in *Drosophila*. *Neuron* **26**, 45–50; 10.1016/s0896-6273(00)81136-8 (2000).
86. King, N., Hittinger, C. T. & Carroll, S. B. Evolution of key cell signaling and adhesion protein families predates animal origins. *Science (New York, N.Y.)* **301**, 361–363; 10.1126/science.1083853 (2003).
87. Liu, M., Zhang, J. & Liu, C. Clinical efficacy of recombinant human latrophilin 3 antibody in the treatment of pediatric asthma. *Experimental and therapeutic medicine* **15**, 539–547; 10.3892/etm.2017.5376 (2018).
88. Brenner, S. The Genetics of Behaviour. *British Medical Bulletin* **29**, 269–271; 10.1093/oxfordjournals.bmb.a071019 (1973).

89. C. elegans Sequencing Consortium. Genome sequence of the nematode *C. elegans*: a platform for investigating biology. *Science (New York, N.Y.)* **282**, 2012–2018; 10.1126/science.282.5396.2012 (1998).
90. Sulston, J. E. & Horvitz, H. R. Post-embryonic cell lineages of the nematode, *Caenorhabditis elegans*. *Developmental biology* **56**, 110–156; 10.1016/0012-1606(77)90158-0 (1977).
91. Horvitz, H. R. & Sulston, J. E. Isolation and genetic characterization of cell-lineage mutants of the nematode *Caenorhabditis elegans*. *Genetics* **96**, 435–454 (1980).
92. White, J. G., Southgate, E., Thomson, J. N. & Brenner, S. The structure of the nervous system of the nematode *Caenorhabditis elegans*. *Philosophical transactions of the Royal Society of London. Series B, Biological sciences* **314**, 1–340; 10.1098/rstb.1986.0056 (1986).
93. Horvitz, H. R. Genetic control of programmed cell death in the nematode *Caenorhabditis elegans*. *Cancer research* **59**, 1701s-1706s (1999).
94. Fire, A. *et al.* Potent and specific genetic interference by double-stranded RNA in *Caenorhabditis elegans*. *Nature* **391**, 806–811; 10.1038/35888 (1998).
95. Struhl, G., Fitzgerald, K. & Greenwald, I. Intrinsic activity of the Lin-12 and Notch intracellular domains in vivo. *Cell* **74**, 331–345; 10.1016/0092-8674(93)90424-o (1993).
96. Byerly, L., Cassada, R. C. & Russell, R. L. The life cycle of the nematode *Caenorhabditis elegans*. I. Wild-type growth and reproduction. *Developmental biology* **51**, 23–33; 10.1016/0012-1606(76)90119-6 (1976).
97. Brenner, S. The genetics of *Caenorhabditis elegans*. *Genetics* **77**, 71–94 (1974).
98. Najarro, E. H. *et al.* *Caenorhabditis elegans* flamingo cadherin *fmi-1* regulates GABAergic neuronal development. *The Journal of neuroscience : the official journal of the Society for Neuroscience* **32**, 4196–4211; 10.1523/JNEUROSCI.3094-11.2012 (2012).
99. Sando, R., Jiang, X. & Südhof, T. C. Latrophilin GPCRs direct synapse specificity by coincident binding of FLRTs and teneurins. *Science (New York, N.Y.)* **363**; 10.1126/science.aav7969 (2019).
100. Zhang, R. S., Liakath-Ali, K. & Südhof, T. C. Latrophilin-2 and latrophilin-3 are redundantly essential for parallel-fiber synapse function in cerebellum. *eLife* **9**; 10.7554/eLife.54443 (2020).
101. Scholz, N. *et al.* Mechano-dependent signaling by Latrophilin/CIRL quenches cAMP in proprioceptive neurons. *eLife* **6**; 10.7554/eLife.28360 (2017).
102. Dannhäuser, S. *et al.* Antinociceptive modulation by the adhesion GPCR CIRL promotes mechanosensory signal discrimination. *eLife* **9**; 10.7554/eLife.56738 (2020).
103. Hammarlund, M., Hobert, O., Miller, D. M. & Sestan, N. The CeNGEN Project: The Complete Gene Expression Map of an Entire Nervous System. *Neuron* **99**, 430–433; 10.1016/j.neuron.2018.07.042 (2018).
104. Hunt-Newbury, R. *et al.* High-throughput in vivo analysis of gene expression in *Caenorhabditis elegans*. *PLoS biology* **5**, e237; 10.1371/journal.pbio.0050237 (2007).
105. Sando, R. & Südhof, T. C. Latrophilin GPCR signaling mediates synapse formation. *eLife* **10**; 10.7554/eLife.65717 (2021).
106. Hobert, O. Neurogenesis in the nematode *Caenorhabditis elegans*. *WormBook : the online review of C. elegans biology*, 1–24; 10.1895/wormbook.1.12.2 (2010).

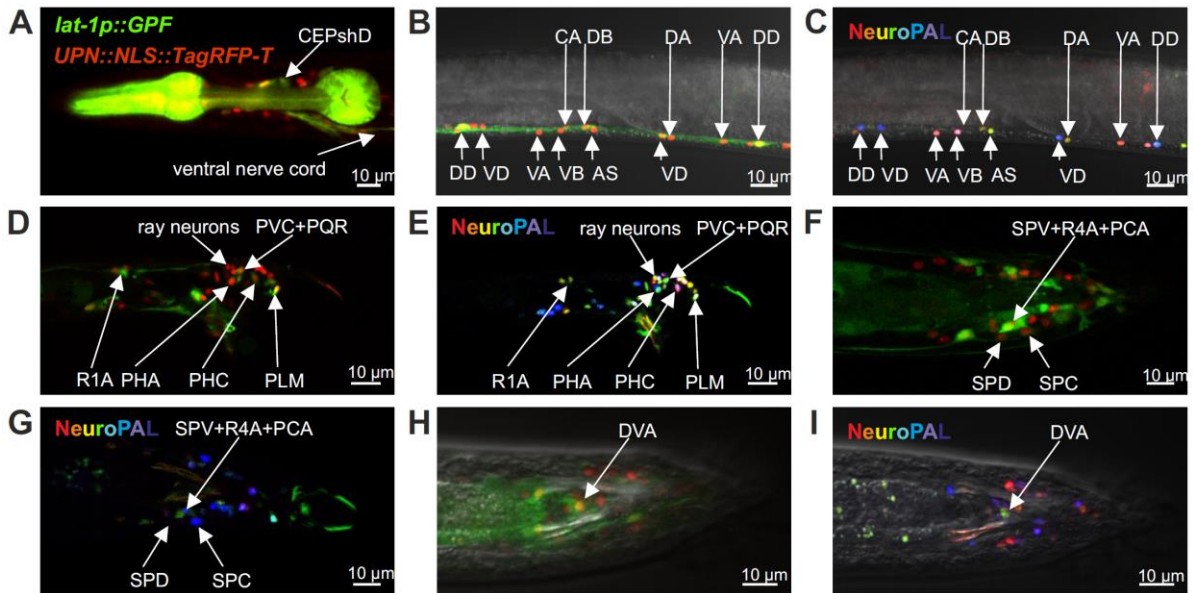
107. Jin, Y. Synaptogenesis. *WormBook : the online review of C. elegans biology*, 1–11; 10.1895/wormbook.1.44.1 (2005).
108. Richmond, J. Synaptic function. *WormBook : the online review of C. elegans biology*, 1–14; 10.1895/wormbook.1.69.1 (2005).
109. Simon, J. M. & Sternberg, P. W. Evidence of a mate-finding cue in the hermaphrodite nematode *Caenorhabditis elegans*. *Proceedings of the National Academy of Sciences of the United States of America* **99**, 1598–1603; 10.1073/pnas.032225799 (2002).
110. Liu, K. S. & Sternberg, P. W. Sensory regulation of male mating behavior in *Caenorhabditis elegans*. *Neuron* **14**, 79–89; 10.1016/0896-6273(95)90242-2 (1995).
111. Garcia, L. R., Mehta, P. & Sternberg, P. W. Regulation of distinct muscle behaviors controls the *C. elegans* male's copulatory spicules during mating. *Cell* **107**, 777–788; 10.1016/s0092-8674(01)00600-6 (2001).
112. LeBoeuf, B., Correa, P., Jee, C. & García, L. R. *Caenorhabditis elegans* male sensory-motor neurons and dopaminergic support cells couple ejaculation and post-ejaculatory behaviors. *eLife* **3**; 10.7554/eLife.02938 (2014).
113. Sulston, J. E., Albertson, D. G. & Thomson, J. N. The *Caenorhabditis elegans* male: postembryonic development of nongonadal structures. *Developmental biology* **78**, 542–576; 10.1016/0012-1606(80)90352-8 (1980).
114. Hubbard, E. J. A. & Greenstein, D. Introduction to the germ line. *WormBook : the online review of C. elegans biology*, 1–4; 10.1895/wormbook.1.18.1 (2005).
115. Kimble, J. & Crittenden, S. L. Germline proliferation and its control. *WormBook : the online review of C. elegans biology*, 1–14; 10.1895/wormbook.1.13.1 (2005).
116. Greenstein, D. Control of oocyte meiotic maturation and fertilization. *WormBook : the online review of C. elegans biology*, 1–12; 10.1895/wormbook.1.53.1 (2005).
117. Gartner, A., Boag, P. R. & Blackwell, T. K. Germline survival and apoptosis. *WormBook : the online review of C. elegans biology*, 1–20; 10.1895/wormbook.1.145.1 (2008).
118. Bukhari, S. I. A. *et al.* The microRNA pathway controls germ cell proliferation and differentiation in *C. elegans*. *Cell research* **22**, 1034–1045; 10.1038/cr.2012.31 (2012).
119. Mohammad, A. *et al.* Initiation of Meiotic Development Is Controlled by Three Post-transcriptional Pathways in *Caenorhabditis elegans*. *Genetics* **209**, 1197–1224; 10.1534/genetics.118.300985 (2018).
120. Austin, J. & Kimble, J. *glp-1* is required in the germ line for regulation of the decision between mitosis and meiosis in *C. elegans*. *Cell* **51**, 589–599; 10.1016/0092-8674(87)90128-0 (1987).
121. Henderson, S. T., Gao, D., Lambie, E. J. & Kimble, J. *lag-2* may encode a signaling ligand for the GLP-1 and LIN-12 receptors of *C. elegans*. *Development (Cambridge, England)* **120**, 2913–2924 (1994).
122. Kershner, A. M., Shin, H., Hansen, T. J. & Kimble, J. Discovery of two GLP-1/Notch target genes that account for the role of GLP-1/Notch signaling in stem cell maintenance. *Proceedings of the National Academy of Sciences of the United States of America* **111**, 3739–3744; 10.1073/pnas.1401861111 (2014).
123. Zhang, B. *et al.* A conserved RNA-binding protein that regulates sexual fates in the *C. elegans* hermaphrodite germ line. *Nature* **390**, 477–484; 10.1038/37297 (1997).

124. Crittenden, S. L. *et al.* A conserved RNA-binding protein controls germline stem cells in *Caenorhabditis elegans*. *Nature* **417**, 660–663; 10.1038/nature754 (2002).
125. Lamont, L. B., Crittenden, S. L., Bernstein, D., Wickens, M. & Kimble, J. FBF-1 and FBF-2 regulate the size of the mitotic region in the *C. elegans* germline. *Developmental cell* **7**, 697–707; 10.1016/j.devcel.2004.09.013 (2004).
126. Francis, R., Barton, M. K., Kimble, J. & Schedl, T. *gld-1*, a tumor suppressor gene required for oocyte development in *Caenorhabditis elegans*. *Genetics* **139**, 579–606 (1995).
127. Francis, R., Maine, E. & Schedl, T. Analysis of the multiple roles of *gld-1* in germline development: interactions with the sex determination cascade and the *glp-1* signaling pathway. *Genetics* **139**, 607–630 (1995).
128. Kadyk, L. C. & Kimble, J. Genetic regulation of entry into meiosis in *Caenorhabditis elegans*. *Development (Cambridge, England)* **125**, 1803–1813 (1998).
129. Eckmann, C. R., Kraemer, B., Wickens, M. & Kimble, J. GLD-3, a bicaudal-C homolog that inhibits FBF to control germline sex determination in *C. elegans*. *Developmental cell* **3**, 697–710; 10.1016/s1534-5807(02)00322-2 (2002).
130. Liu, J., Sato, C., Cerletti, M. & Wagers, A. Notch signaling in the regulation of stem cell self-renewal and differentiation. *Current topics in developmental biology* **92**, 367–409; 10.1016/S0070-2153(10)92012-7 (2010).
131. Koch, U., Lehal, R. & Radtke, F. Stem cells living with a Notch. *Development (Cambridge, England)* **140**, 689–704; 10.1242/dev.080614 (2013).
132. Nowell, C. S. & Radtke, F. Notch as a tumour suppressor. *Nature reviews. Cancer* **17**, 145–159; 10.1038/nrc.2016.145 (2017).
133. D'Amato, G. *et al.* Sequential Notch activation regulates ventricular chamber development. *Nature cell biology* **18**, 7–20; 10.1038/ncb3280 (2016).

7 Appendix

7.1 Supplemental material for “Latrophilin-1 drives neuron morphogenesis and shapes chemo- and mechanosensation-dependent behavior in *C. elegans* via a *trans* function”

Supplementary Figure 1



Supplementary Figure 1: Additional representative images of the *lat-1* expression map using NeuroPAL [1, 2]. *lat-1* expression has been observed in the cephalic sheath cells (A) as well as neurons of the ventral nerve cord (B, C), the lumbar ganglion (D, E), the cloacal ganglion (F, G) and the dorsal ganglion (H, I).

Supplementary Table 1

	neurons also present in hermaphrodites	
	Neuron	Function
anterior pharyngeal bulb	I1	Interneuron, putative sensory neuron
	I3	Interneuron, putative sensory neuron
	M3	Motorneuron, putative proprioceptive neuron
	MI	Motorneuron and interneuron
anterior ganglion	BAG	Chemosensory neuron
	IL1	Polymodal sensory neuron
	IL2D/V	Chemosensory neuron, putative mechanosensory neuron
	OLL	Mechanosensory neuron
	OLQ	Mechanosensory neuron, interneuron
	RIP	Interneuron
	RME	Motorneuron
	URA	Motorneuron, putative sensory neuron
	URB	Interneuron
URY	Sensory neuron	
dorsal ganglion	URX	Chemosensory neuron, interneuron
lateral ganglion	ADF	Chemosensory neuron
	ADL	Chemosensory neuron, nociceptive neuron
	AFD	Chemosensory neuron, thermosensory neuron
	AIB	Interneuron
	AIN	Interneuron
	AIZ	Interneuron
	ASE	Chemosensory neuron
	ASG	Chemosensory neuron
	ASH	Polymodal sensory neuron
	ASI	Chemosensory neuron, thermosensory neuron
	ASJ	Light sensory neuron, electrosensory neuron
	ASK	Polymodal sensory neuron
	AUA	Interneuron
	AVA	Interneuron
	AVB	Interneuron
	AVD	Interneuron
	AVH	Interneuron
	AVJ	Interneuron
	AWA	Chemosensory neuron
	AWB	Polymodal sensory neuron
	AWC	Polymodal sensory neuron
	RIA	Interneuron
	RIC	Interneuron
	RIV	Motorneuron, interneuron
	RMD	Motorneuron
	SAA	Motorneuron, interneuron
	SMDV	Motorneuron
	ventral ganglion	RIR
RMD		Motorneuron
RMF		Motorneuron
SMB		Motorneuron

	SMDD	Motorneuron
midbody	ALM	Mechanosensory neuron
	AS	Motorneuron
	AVM	Mechanosensory neuron
	DA	Motorneuron
	DB	Motorneuron, proprioceptive neuron
	DD	Motorneuron
	PDE	Mechanosensory neuron
	PVD	Polymodal sensory neuron
	VD	Motorneuron
preanal ganglion	PVS (PVPR)	Interneuron
	PVT	Interneuron
	PVU (PVPL)	Interneuron
dorsorectal ganglion	DVA	Mechanosensory neuron, interneuron
	DVC	Interneuron, putative mechanosensory neuron
lumbar ganglion	PHA	Chemosensory neuron
	PHB	Chemosensory neuron
	PHC	Thermosensory neuron, nociceptive neuron, putative mechanosensory neuron
	PLM	Mechanosensory neuron
	PLN	Chemosensory neuron, interneuron
	PQR	Chemosensory neuron
	PVC	Interneuron

	male-specific neurons	
	Neuron	Function
midbody	CA	Motorneuron, interneuron
	CP	Motorneuron, interneuron
preanal ganglion	DX	Interneuron
	EF	Interneuron
	HOB	Sensory neuron
	PDC	Motorneuron, interneuron
	PGA	Interneuron
	PVY	Motorneuron, interneuron
	PVZ	Motorneuron, interneuron
dorsorectal ganglion	DVF	Interneuron
	EF	Interneuron
cloacal ganglion	PCA	Motorneuron, sensory neuron
	PCB	Motorneuron, sensory neuron
	SPC	Motorneuron, proprioceptive neuron
	SPD	Motorneuron, Chemosensory neuron
	SPV	Chemosensory neuron
lumbar ganglion	PHD	Sensory neuron, putative proprioceptive neuron
	ray neurons	Sensory neuron

Supplementary Table 1: Identified *lat-1* expressing neurons of the *C. elegans* male. Depicted is a list of all neurons, which expressed the *lat-1p::GFP* reporter, sorted by localization within the male ganglia. Neurons were mapped by assessing their respective location, morphology and NeuroPAL color [1, 2]. Male-specific neurons and neurons shared by the two *C. elegans* sexes were listed separately. Neurons that play a role in copulation behavior according to the WormBase database (<http://www.wormbase.org>) are colored in grey.

Supplementary Table 2

downregulated genes				
gene	FPKM wild-type	FPKM <i>lat-1</i>	fold-reduction	p-value
<i>abts-2</i>	0.16	0.05	2.98	0.032
<i>acc-3</i>	0.18	0.04	4.58	0.019
<i>acp-5</i>	0.51	0.36	1.41	0.016
<i>acp-6</i>	19.31	12.93	1.49	0.032
<i>act-1</i>	173.44	91.65	1.89	0.032
<i>act-2</i>	218.31	118.43	1.84	0.032
<i>adt-3</i>	0.24	0.12	2.11	0.032
<i>akt-2</i>	0.49	0.27	1.79	0.016
<i>aldo-1</i>	16.41	13.29	1.23	0.016
<i>aldo-2</i>	35.76	29.38	1.22	0.032
<i>alh-13</i>	2.20	0.96	2.28	0.032
<i>alh-2</i>	0.03	0.00	-	0.042
<i>alh-8</i>	26.15	21.11	1.24	0.032
<i>aqp-3</i>	0.54	0.28	1.94	0.016
<i>aqp-7</i>	10.88	5.24	2.08	0.016
<i>argk-1</i>	1.47	0.25	5.88	0.016
<i>arrd-15</i>	0.25	0.16	1.52	0.016
<i>asp-4</i>	14.46	9.23	1.57	0.032
<i>atg-2</i>	1.40	1.11	1.26	0.016
<i>atic-1</i>	1.33	1.09	1.22	0.016
<i>attf-4</i>	1.15	0.78	1.48	0.032
<i>best-23</i>	0.17	0.07	2.34	0.016
<i>best-3</i>	0.63	0.39	1.59	0.016
<i>bgal-2</i>	0.65	0.43	1.49	0.032
<i>bus-2</i>	0.04	0.00	-	0.030
<i>cal-5</i>	3.22	2.19	1.47	0.032
<i>camt-1</i>	1.33	0.71	1.88	0.016
<i>cas-1</i>	2.07	1.64	1.26	0.032
<i>catp-3</i>	1.42	0.58	2.46	0.016
<i>ccep-290</i>	0.07	0.05	1.49	0.016
<i>cdd-1</i>	1.02	0.59	1.72	0.032
<i>cdf-1</i>	1.14	0.84	1.36	0.016
<i>cdr-1</i>	0.13	0.03	4.50	0.016
<i>ceh-23</i>	0.05	0.02	2.62	0.019
<i>ceh-75</i>	0.03	0.00	-	0.042
<i>chil-6</i>	0.05	0.02	2.67	0.032
<i>ckk-1</i>	0.46	0.35	1.31	0.016
<i>clcc-103</i>	1.78	0.92	1.93	0.019
<i>clcc-108</i>	1.28	0.53	2.39	0.019
<i>clcc-116</i>	0.12	0.02	6.28	0.037
<i>clcc-13</i>	0.05	0.01	9.47	0.019
<i>clcc-130</i>	1.17	0.40	2.91	0.019
<i>clcc-15</i>	0.06	0.00	-	0.018
<i>clcc-150</i>	4.69	3.15	1.49	0.016
<i>clcc-158</i>	11.04	4.72	2.34	0.037
<i>clcc-206</i>	0.19	0.06	3.34	0.032

<i>clcc-245</i>	0.18	0.08	2.08	0.032
<i>clcc-258</i>	0.11	0.00	-	0.034
<i>clcc-261</i>	1.18	0.42	2.80	0.019
<i>clcc-49</i>	0.77	0.38	2.01	0.032
<i>clcc-52</i>	0.35	0.14	2.50	0.016
<i>clcc-72</i>	0.13	0.06	2.02	0.032
<i>clcc-76</i>	0.06	0.01	6.43	0.037
<i>clcc-8</i>	0.44	0.27	1.63	0.032
<i>clcc-80</i>	0.23	0.13	1.78	0.016
<i>clcc-86</i>	1.31	0.33	3.98	0.016
<i>clcc-93</i>	0.17	0.06	2.87	0.037
<i>clcc-98</i>	0.14	0.00	-	0.034
<i>clh-4</i>	0.16	0.09	1.73	0.016
<i>clik-1</i>	62.95	41.45	1.52	0.016
<i>cnnm-2</i>	0.42	0.23	1.85	0.016
<i>col-109</i>	0.05	0.00	-	0.018
<i>col-119</i>	365.45	235.44	1.55	0.032
<i>col-124</i>	248.75	141.63	1.76	0.016
<i>col-125</i>	0.40	0.07	5.79	0.032
<i>col-127</i>	0.21	0.02	12.16	0.032
<i>col-129</i>	22.64	5.40	4.19	0.032
<i>col-13</i>	0.70	0.29	2.38	0.016
<i>col-138</i>	0.15	0.05	2.88	0.016
<i>col-139</i>	28.49	7.51	3.79	0.016
<i>col-14</i>	0.11	0.03	4.15	0.032
<i>col-140</i>	314.40	185.60	1.69	0.032
<i>col-145</i>	0.04	0.00	-	0.030
<i>col-149</i>	1.81	0.39	4.68	0.032
<i>col-179</i>	304.38	170.32	1.79	0.032
<i>col-20</i>	160.82	99.95	1.61	0.032
<i>col-46</i>	0.05	0.00	-	0.018
<i>col-52</i>	0.01	0.00	-	0.042
<i>col-8</i>	142.74	93.57	1.53	0.016
<i>col-80</i>	159.68	106.29	1.50	0.032
<i>col-98</i>	30.55	18.30	1.67	0.016
<i>cor-1</i>	1.42	1.06	1.34	0.016
<i>cpg-7</i>	1.85	1.07	1.72	0.016
<i>cpr-6</i>	22.27	18.67	1.19	0.016
<i>csq-1</i>	29.74	21.34	1.39	0.032
<i>ctbp-1</i>	0.24	0.13	1.78	0.032
<i>cth-1</i>	0.83	0.59	1.40	0.016
<i>ctsa-3-2</i>	0.16	0.07	2.34	0.016
<i>cutl-3</i>	0.14	0.04	3.02	0.016
<i>cyp-34A6</i>	0.17	0.06	2.96	0.032
<i>cyp-34A8</i>	0.69	0.43	1.60	0.032
<i>cyp-35B1</i>	0.53	0.27	1.92	0.016
<i>cyp-43A1</i>	0.76	0.46	1.66	0.032
<i>daf-14</i>	0.58	0.27	2.10	0.016
<i>dcar-1</i>	1.20	0.65	1.85	0.032
<i>dct-12</i>	0.01	0.00	-	0.042

<i>deg-1</i>	0.26	0.16	1.65	0.016
<i>del-6</i>	6.80	5.44	1.25	0.016
<i>dgat-2</i>	5.55	2.37	2.34	0.016
<i>dhhc-14</i>	0.40	0.25	1.60	0.032
<i>dhs-2</i>	0.99	0.49	2.03	0.032
<i>dhs-7</i>	1.86	1.33	1.40	0.016
<i>djr-1.2</i>	0.04	0.00	-	0.042
<i>dlhd-1</i>	0.18	0.05	3.96	0.019
<i>dmsr-2</i>	0.76	0.47	1.62	0.016
<i>dnj-24</i>	0.87	0.53	1.63	0.016
<i>dod-19</i>	2.19	1.36	1.62	0.032
<i>dop-5</i>	0.31	0.18	1.70	0.032
<i>dpf-1</i>	0.68	0.50	1.36	0.016
<i>dpf-2</i>	0.94	0.70	1.35	0.032
<i>dpf-4</i>	5.62	3.89	1.44	0.016
<i>droe-4</i>	1.11	0.37	2.97	0.016
<i>egl-4</i>	8.96	7.27	1.23	0.032
<i>elo-6</i>	12.41	6.46	1.92	0.032
<i>ent-7</i>	0.44	0.26	1.73	0.016
<i>eps-8</i>	1.91	1.30	1.47	0.016
<i>exc-7</i>	0.58	0.31	1.87	0.016
<i>exp-1</i>	0.35	0.13	2.77	0.016
<i>far-5</i>	0.74	0.31	2.39	0.032
<i>far-8</i>	12.93	4.70	2.75	0.016
<i>fat-6</i>	13.23	6.41	2.06	0.032
<i>fbxa-19</i>	0.16	0.06	2.54	0.032
<i>fbxa-214</i>	0.03	0.00	-	0.042
<i>fbxa-38</i>	0.09	0.03	2.74	0.019
<i>fbxa-41</i>	0.02	0.00	-	0.011
<i>fbxa-67</i>	0.20	0.15	1.33	0.032
<i>fbxa-77</i>	0.13	0.05	2.44	0.016
<i>fbxb-39</i>	0.03	0.00	-	0.042
<i>fbxb-45</i>	0.02	0.00	-	0.042
<i>fbxc-5</i>	1.03	0.64	1.60	0.032
<i>feh-1</i>	0.26	0.12	2.16	0.032
<i>fgt-1</i>	4.41	3.64	1.21	0.032
<i>fipr-22</i>	0.60	0.09	6.68	0.016
<i>fipr-26</i>	0.04	0.00	-	0.011
<i>fkf-4</i>	0.25	0.07	3.66	0.016
<i>flp-19</i>	0.62	0.40	1.58	0.032
<i>folt-1</i>	0.41	0.18	2.29	0.016
<i>gad-3</i>	1.09	0.74	1.49	0.016
<i>gar-2</i>	0.39	0.20	1.96	0.032
<i>gar-3</i>	0.46	0.26	1.79	0.016
<i>gas-1</i>	6.75	4.53	1.49	0.016
<i>gcy-29</i>	0.03	0.00	-	0.018
<i>gei-3</i>	1.98	1.47	1.35	0.032
<i>glb-15</i>	0.12	0.02	5.76	0.019
<i>gln-1</i>	0.70	0.52	1.37	0.032
<i>gon-1</i>	0.81	0.65	1.25	0.016

<i>gpa-6</i>	0.08	0.00	-	0.011
<i>gpdh-1</i>	1.58	0.41	3.84	0.016
<i>gpx-5</i>	2.34	1.72	1.36	0.032
<i>grd-10</i>	0.62	0.22	2.81	0.016
<i>grd-3</i>	11.52	5.99	1.92	0.016
<i>grd-5</i>	17.18	9.12	1.88	0.016
<i>grl-18</i>	0.01	0.00	-	0.042
<i>gst-18</i>	0.02	0.00	-	0.042
<i>gst-21</i>	0.49	0.24	1.98	0.032
<i>gst-26</i>	1.32	0.94	1.41	0.016
<i>gst-27</i>	2.12	1.50	1.42	0.016
<i>gst-28</i>	0.78	0.37	2.09	0.016
<i>gst-42</i>	1.21	0.90	1.35	0.016
<i>gsto-2</i>	0.04	0.00	-	0.011
<i>haao-1</i>	1.73	0.92	1.87	0.016
<i>hacd-1</i>	0.96	0.51	1.87	0.032
<i>haf-6</i>	1.10	0.15	7.38	0.016
<i>haly-1</i>	1.66	0.81	2.06	0.016
<i>hda-5</i>	1.38	0.92	1.50	0.032
<i>hlh-34</i>	0.01	0.00	-	0.042
<i>hlh-6</i>	0.11	0.02	4.98	0.019
<i>hmit-1.1</i>	0.52	0.11	4.70	0.016
<i>hphd-1</i>	7.65	4.56	1.68	0.016
<i>hsd-2</i>	2.35	1.83	1.29	0.032
<i>hsp-25</i>	9.69	5.28	1.83	0.032
<i>hsp-43</i>	3.59	2.82	1.27	0.032
<i>ifb-1</i>	7.12	4.47	1.59	0.016
<i>ift-139</i>	0.12	0.07	1.76	0.032
<i>ikb-1</i>	0.30	0.11	2.63	0.032
<i>insc-1</i>	0.30	0.17	1.78	0.016
<i>inx-20</i>	0.05	0.01	3.26	0.019
<i>ipla-7</i>	3.34	2.62	1.28	0.032
<i>ketn-1</i>	6.07	4.14	1.47	0.032
<i>kin-32</i>	0.37	0.23	1.60	0.016
<i>klf-1</i>	0.90	0.41	2.19	0.016
<i>klp-3</i>	0.91	0.54	1.69	0.032
<i>kpc-1</i>	1.05	0.65	1.61	0.016
<i>kri-1</i>	0.20	0.07	2.95	0.032
<i>kynu-1</i>	4.72	2.99	1.58	0.016
<i>lat-1</i>	1.73	0.77	2.23	0.016
<i>ldh-1</i>	5.65	4.23	1.34	0.032
<i>lec-2</i>	14.99	6.43	2.33	0.032
<i>lec-9</i>	5.27	3.20	1.65	0.016
<i>let-522</i>	0.34	0.11	2.98	0.032
<i>lev-11</i>	83.23	43.01	1.94	0.032
<i>lgc-22</i>	2.10	1.33	1.58	0.032
<i>lgc-30</i>	0.15	0.07	2.22	0.016
<i>lgc-34</i>	1.27	0.91	1.40	0.016
<i>lgc-40</i>	0.11	0.03	3.53	0.032
<i>lgc-45</i>	0.58	0.37	1.54	0.016

<i>lgc-46</i>	0.09	0.02	4.04	0.032
<i>lin-31</i>	0.13	0.03	4.43	0.032
<i>lipl-4</i>	0.18	0.06	2.93	0.016
<i>lmp-2</i>	0.30	0.21	1.47	0.032
<i>lpr-2</i>	0.27	0.20	1.33	0.032
<i>lron-5</i>	0.16	0.10	1.54	0.016
<i>lrp-2</i>	2.01	1.36	1.48	0.016
<i>maa-1</i>	0.96	0.53	1.81	0.016
<i>magu-4</i>	0.84	0.63	1.34	0.032
<i>mam-2</i>	0.04	0.01	3.91	0.037
<i>marc-5</i>	0.54	0.41	1.32	0.016
<i>math-18</i>	0.34	0.22	1.56	0.016
<i>mboa-2</i>	0.58	0.31	1.90	0.016
<i>mca-1</i>	3.44	2.80	1.23	0.016
<i>mce-1</i>	1.42	1.06	1.34	0.032
<i>mec-17</i>	0.31	0.12	2.65	0.016
<i>mec-5</i>	1.05	0.86	1.22	0.032
<i>mlc-1</i>	48.55	28.82	1.68	0.016
<i>mlc-2</i>	65.70	41.79	1.57	0.016
<i>mlc-3</i>	40.08	25.22	1.59	0.016
<i>mlck-1</i>	0.66	0.54	1.23	0.016
<i>mlt-7</i>	0.52	0.26	2.01	0.016
<i>mlt-9</i>	0.12	0.02	7.03	0.016
<i>mnr-1</i>	1.38	0.89	1.55	0.016
<i>mrpl-9</i>	5.69	3.45	1.65	0.032
<i>mtl-1</i>	0.23	0.00	-	0.034
<i>mup-2</i>	39.03	21.91	1.78	0.032
<i>mup-4</i>	4.69	3.28	1.43	0.032
<i>myo-3</i>	5.30	2.85	1.86	0.016
<i>nas-33</i>	0.12	0.04	2.91	0.032
<i>nas-9</i>	1.01	0.69	1.45	0.032
<i>ncx-8</i>	0.20	0.12	1.66	0.016
<i>ndnf-1</i>	0.26	0.13	2.06	0.016
<i>nep-21</i>	0.52	0.35	1.46	0.032
<i>nhr-101</i>	0.40	0.20	2.06	0.016
<i>nhr-116</i>	0.18	0.08	2.22	0.016
<i>nhr-130</i>	0.58	0.31	1.87	0.016
<i>nhr-131</i>	0.26	0.18	1.39	0.032
<i>nhr-161</i>	0.22	0.10	2.14	0.032
<i>nhr-216</i>	0.03	0.00	-	0.011
<i>nhr-227</i>	0.05	0.00	-	0.034
<i>nhr-56</i>	0.21	0.06	3.86	0.016
<i>nhr-63</i>	0.23	0.06	3.92	0.032
<i>nhr-95</i>	0.31	0.16	1.93	0.032
<i>nlp-15</i>	1.35	0.88	1.53	0.016
<i>nlp-21</i>	4.41	2.63	1.67	0.032
<i>nlp-59</i>	0.65	0.32	2.04	0.037
<i>nlp-71</i>	2.06	0.62	3.30	0.016
<i>npa-1</i>	71.04	48.70	1.46	0.032
<i>npr-10</i>	0.23	0.09	2.64	0.032

<i>npr-18</i>	0.06	0.01	7.04	0.016
<i>npr-25</i>	0.24	0.15	1.65	0.016
<i>oac-39</i>	0.01	0.00	-	0.042
<i>oac-46</i>	1.03	0.67	1.55	0.016
<i>oatr-1</i>	8.15	6.01	1.36	0.016
<i>odc-1</i>	0.71	0.50	1.43	0.016
<i>odd-2</i>	0.19	0.10	1.87	0.032
<i>oig-4</i>	0.21	0.08	2.67	0.016
<i>old-1</i>	0.11	0.07	1.49	0.016
<i>osg-1</i>	0.38	0.20	1.87	0.016
<i>pals-14</i>	0.10	0.02	4.68	0.016
<i>pals-21</i>	0.03	0.00	-	0.042
<i>pat-10</i>	75.53	51.07	1.48	0.032
<i>pat-2</i>	3.18	2.30	1.38	0.032
<i>pcbd-1</i>	0.99	0.56	1.75	0.032
<i>pde-1</i>	0.59	0.28	2.10	0.032
<i>pdf-2</i>	0.37	0.03	12.97	0.019
<i>pes-9</i>	5.34	4.60	1.16	0.016
<i>pfas-1</i>	0.52	0.36	1.45	0.032
<i>pfk-1.1</i>	3.93	2.70	1.45	0.032
<i>pfn-2</i>	3.24	2.01	1.61	0.016
<i>pgp-11</i>	0.47	0.20	2.29	0.016
<i>pgp-13</i>	0.20	0.09	2.19	0.016
<i>pgph-1</i>	6.78	3.77	1.80	0.032
<i>phat-3</i>	0.48	0.20	2.39	0.032
<i>phy-2</i>	0.89	0.68	1.32	0.032
<i>pifk-1</i>	0.24	0.17	1.42	0.016
<i>pitp-1</i>	0.59	0.43	1.37	0.032
<i>plc-4</i>	2.06	1.46	1.41	0.016
<i>plx-2</i>	0.18	0.13	1.38	0.032
<i>pmp-4</i>	0.88	0.62	1.41	0.016
<i>poml-2</i>	0.94	0.34	2.72	0.016
<i>poml-3</i>	1.74	0.78	2.23	0.032
<i>ppat-1</i>	0.91	0.46	1.97	0.016
<i>pph-1</i>	0.58	0.30	1.91	0.016
<i>ppt-1</i>	1.49	0.53	2.83	0.016
<i>pqn-72</i>	0.31	0.13	2.37	0.016
<i>pqn-83</i>	4.21	2.66	1.58	0.032
<i>prk-2</i>	0.40	0.25	1.62	0.032
<i>prx-6</i>	0.61	0.44	1.38	0.016
<i>ptr-16</i>	0.07	0.05	1.50	0.016
<i>ptr-22</i>	0.22	0.06	3.56	0.032
<i>ptr-23</i>	0.63	0.44	1.44	0.016
<i>pxl-1</i>	1.62	0.97	1.66	0.016
<i>ras-1</i>	1.80	1.31	1.37	0.016
<i>rbf-1</i>	0.81	0.57	1.42	0.032
<i>rcan-1</i>	0.72	0.50	1.44	0.032
<i>rga-6</i>	0.18	0.07	2.45	0.016
<i>rhr-1</i>	2.04	1.49	1.37	0.016
<i>rhy-1</i>	0.43	0.25	1.73	0.016

<i>rig-6</i>	1.47	0.93	1.59	0.032
<i>rnf-145</i>	1.19	0.81	1.48	0.032
<i>saeg-1</i>	2.59	1.85	1.40	0.032
<i>sbp-1</i>	0.82	0.62	1.34	0.016
<i>scav-4</i>	0.24	0.11	2.10	0.016
<i>scav-6</i>	0.44	0.30	1.51	0.032
<i>scl-10</i>	0.07	0.00	-	0.042
<i>scl-12</i>	0.34	0.05	7.21	0.032
<i>scrm-5</i>	2.55	1.71	1.49	0.016
<i>sek-1</i>	1.05	0.74	1.42	0.016
<i>set-18</i>	0.75	0.44	1.71	0.032
<i>set-30</i>	0.74	0.48	1.53	0.016
<i>shc-2</i>	0.46	0.37	1.24	0.016
<i>shw-3</i>	0.09	0.03	2.48	0.016
<i>sid-2</i>	0.66	0.47	1.39	0.016
<i>sipa-1</i>	0.80	0.57	1.40	0.016
<i>sir-2-2</i>	0.82	0.51	1.63	0.016
<i>skr-4</i>	1.49	0.69	2.16	0.016
<i>slc-17.7</i>	0.59	0.34	1.73	0.032
<i>slc-25A18.1</i>	0.94	0.73	1.28	0.016
<i>sma-4</i>	0.69	0.47	1.46	0.032
<i>snt-3</i>	0.35	0.16	2.18	0.032
<i>snt-5</i>	0.36	0.19	1.84	0.032
<i>soc-1</i>	0.67	0.40	1.66	0.032
<i>sod-3</i>	0.74	0.22	3.30	0.016
<i>soem-1</i>	0.31	0.22	1.42	0.032
<i>spin-3</i>	0.29	0.19	1.50	0.016
<i>spp-17</i>	34.80	25.92	1.34	0.032
<i>spp-23</i>	4.72	2.15	2.20	0.016
<i>srap-1</i>	1.50	1.12	1.34	0.019
<i>srbc-34</i>	0.01	0.00	-	0.042
<i>srd-36</i>	0.01	0.00	-	0.042
<i>srd-50</i>	0.03	0.00	-	0.042
<i>srg-9</i>	0.07	0.03	2.38	0.037
<i>srh-119</i>	0.06	0.00	-	0.042
<i>srh-129</i>	0.03	0.00	-	0.042
<i>srh-138</i>	0.01	0.00	-	0.042
<i>srh-247</i>	0.01	0.00	-	0.042
<i>srh-258</i>	0.03	0.00	-	0.042
<i>srh-30</i>	0.01	0.00	-	0.042
<i>srp-3</i>	0.40	0.26	1.51	0.016
<i>srsx-1</i>	0.03	0.00	-	0.042
<i>srt-28</i>	0.02	0.00	-	0.015
<i>srt-49</i>	0.02	0.00	-	0.018
<i>srt-55</i>	0.01	0.00	-	0.042
<i>sru-21</i>	0.01	0.00	-	0.042
<i>srx-22</i>	0.02	0.00	-	0.042
<i>srz-1</i>	0.02	0.00	-	0.042
<i>sucl-1</i>	5.08	3.54	1.43	0.016
<i>sulp-1</i>	0.09	0.04	2.40	0.016

<i>sulp-8</i>	0.16	0.09	1.75	0.032
<i>suox-1</i>	0.83	0.62	1.33	0.032
<i>sup-9</i>	0.19	0.06	3.15	0.016
<i>swt-3</i>	3.26	1.99	1.64	0.016
<i>tag-18</i>	10.72	8.29	1.29	0.032
<i>tag-180</i>	0.46	0.27	1.70	0.016
<i>tbc-16</i>	0.26	0.16	1.64	0.016
<i>tbcc-1</i>	16.44	10.94	1.50	0.016
<i>tkr-1</i>	0.07	0.02	4.00	0.016
<i>tln-1</i>	3.48	2.73	1.27	0.032
<i>tmed-4</i>	4.63	3.93	1.18	0.032
<i>tmem-107</i>	0.00	0.00	-	0.042
<i>tni-1</i>	2.89	1.87	1.55	0.016
<i>tni-3</i>	42.81	27.11	1.58	0.016
<i>tnt-2</i>	71.86	43.64	1.65	0.016
<i>tnt-3</i>	3.84	2.44	1.57	0.016
<i>tre-5</i>	0.19	0.12	1.65	0.032
<i>trf-1</i>	0.58	0.36	1.59	0.037
<i>trhr-1</i>	0.19	0.12	1.63	0.032
<i>trx-1</i>	0.04	0.00	-	0.011
<i>tsp-3</i>	0.09	0.02	3.96	0.032
<i>tsp-9</i>	0.22	0.12	1.77	0.016
<i>ttr-18</i>	2.07	1.05	1.98	0.032
<i>ttr-46</i>	20.20	15.14	1.33	0.032
<i>ttr-48</i>	5.45	2.92	1.87	0.032
<i>ttr-49</i>	1.38	0.86	1.61	0.032
<i>tub-1</i>	0.14	0.05	2.63	0.019
<i>tub-2</i>	1.46	1.16	1.25	0.016
<i>twk-31</i>	0.30	0.17	1.74	0.016
<i>twk-34</i>	0.62	0.40	1.54	0.032
<i>twk-43</i>	0.26	0.14	1.83	0.016
<i>twk-44</i>	0.05	0.00	9.35	0.016
<i>tyr-2</i>	0.57	0.29	1.94	0.016
<i>ugt-24</i>	0.09	0.05	1.78	0.032
<i>ugt-30</i>	0.21	0.11	1.95	0.032
<i>ugt-32</i>	0.49	0.18	2.78	0.016
<i>ugt-39</i>	0.66	0.37	1.81	0.016
<i>ugt-46</i>	2.28	1.05	2.16	0.016
<i>unc-15</i>	70.13	49.98	1.40	0.016
<i>unc-23</i>	2.89	2.02	1.43	0.016
<i>unc-27</i>	81.32	49.79	1.63	0.016
<i>unc-55</i>	0.15	0.08	1.90	0.032
<i>unc-6</i>	0.19	0.15	1.28	0.032
<i>unc-68</i>	3.57	2.62	1.36	0.016
<i>unc-7</i>	0.28	0.16	1.73	0.032
<i>unc-87</i>	35.67	22.82	1.56	0.016
<i>unc-93</i>	0.20	0.10	2.06	0.016
<i>unc-95</i>	2.17	1.35	1.60	0.016
<i>unc-97</i>	1.85	1.16	1.60	0.032
<i>vab-8</i>	1.05	0.85	1.23	0.016

<i>vap-2</i>	0.69	0.45	1.53	0.016
<i>vglu-2</i>	1.75	1.37	1.28	0.032
<i>vnut-1</i>	0.86	0.34	2.53	0.016
<i>zig-12</i>	8.75	5.91	1.48	0.016
<i>zig-9</i>	0.47	0.21	2.20	0.016
<i>zip-10</i>	0.04	0.00	20.65	0.037
<i>zipt-13</i>	1.62	1.00	1.62	0.032
<i>zipt-16</i>	0.25	0.14	1.74	0.016
<i>zmp-3</i>	0.80	0.34	2.38	0.016

upregulated genes				
gene	FPKM wild-type	FPKM <i>lat-1</i>	fold-increase	p-value
<i>arx-5</i>	0.79	1.13	1.43	0.016
<i>atz-1</i>	0.00	0.09	-	0.018
<i>cdc-73</i>	1.07	1.48	1.39	0.032
<i>cfz-2</i>	0.10	0.17	1.81	0.032
<i>chtl-1</i>	0.06	0.11	1.73	0.032
<i>cnp-3</i>	0.16	0.21	1.35	0.016
<i>dhhc-10</i>	0.19	0.36	1.90	0.016
<i>dnj-14</i>	0.48	1.00	2.09	0.016
<i>egg-3</i>	0.68	1.15	1.70	0.016
<i>endu-2</i>	0.29	0.96	3.37	0.016
<i>fic-1</i>	2.32	3.87	1.67	0.016
<i>his-44</i>	0.53	1.18	2.21	0.032
<i>igcm-1</i>	0.02	0.07	2.93	0.032
<i>igcm-4</i>	0.10	0.26	2.67	0.016
<i>irld-35</i>	0.05	0.18	3.51	0.016
<i>laat-1</i>	1.87	2.53	1.36	0.016
<i>lam-1</i>	2.50	2.66	1.06	0.016
<i>lbp-2</i>	3.27	5.53	1.69	0.016
<i>lido-6</i>	0.04	0.09	2.40	0.016
<i>maph-1.2</i>	1.47	2.10	1.43	0.032
<i>math-10</i>	0.00	0.04	14.44	0.019
<i>math-14</i>	0.12	0.21	1.72	0.032
<i>mesp-1</i>	0.63	1.12	1.76	0.032
<i>nmy-1</i>	2.11	2.99	1.42	0.032
<i>npl-4.1</i>	2.06	2.44	1.18	0.032
<i>pelo-1</i>	0.48	0.63	1.30	0.032
<i>perm-4</i>	2.04	3.80	1.86	0.032
<i>pho-14</i>	0.70	1.04	1.48	0.032
<i>plrg-1</i>	2.53	3.25	1.29	0.016
<i>pola-1</i>	1.83	2.49	1.36	0.032
<i>rad-51</i>	1.46	2.49	1.70	0.016
<i>rbg-2</i>	1.14	1.41	1.23	0.032
<i>rme-1</i>	6.72	7.56	1.12	0.032
<i>sav-1</i>	0.18	0.29	1.56	0.016

<i>sid-1</i>	0.32	0.46	1.46	0.032
<i>spd-3</i>	1.85	2.37	1.28	0.032
<i>tbx-33</i>	0.09	0.16	1.77	0.016
<i>thoc-7</i>	4.70	7.27	1.55	0.032
<i>tin-10</i>	0.82	1.01	1.23	0.032
<i>ttr-42</i>	0.00	0.03	-	0.044
<i>unc-39</i>	0.01	0.12	16.85	0.037
<i>vps-50</i>	0.15	0.27	1.77	0.032
<i>wrk-1</i>	0.34	0.57	1.71	0.032
<i>ztf-16</i>	0.06	0.10	1.74	0.032

Supplementary Table 2: Significantly down- and upregulated genes of *lat-1* mutant males identified by RNA-Seq analysis. FPKM values of all gene products which were significantly lower or higher in *lat-1* mutant males than in wild-type controls in a RNA-Seq analysis using 250 nematodes of each genotype are given. A two-sided Wilcoxon rank test was performed to determine significance ($p < 0.05$). Genes colored in grey are known to be enriched in males or expressed in male cells and were identified by determining the intersection of all significantly regulated genes found in our analysis and all genes that were listed under the GO term “male” (WBbt:0007850, 2656 genes) in the WormBase database (WS280, <http://www.wormbase.org>).

Supplementary Table 3

all downregulated genes							
tissue enrichment							
Category	Term	WormBase ID	Expected	Observed	Fold Change	p value	q value
neuronal	AVB	WBbt:0005841	0.89	4	4.5	0.0018	0.049
	dorsal nerve cord	WBbt:0006750	16	29	1.8	0.0013	0.042
	IL1L	WBbt:0004553	1	4	4	0.003	0.064
	IL1R	WBbt:0004551	0.97	4	4.1	0.0027	0.061
	IL1VR	WBbt:0004547	0.89	4	4.5	0.0018	0.049
	nerve ring	WBbt:0006749	24	41	1.7	0.00055	0.023
	SIA	WBbt:0005361	1	5	5	0.00043	0.022
	SMD	WBbt:0005353	1.4	6	4.2	0.00053	0.023
muscular	anal depressor muscle	WBbt:0004292	13	28	2.2	0.000057	0.0057
	anal sphincter muscle	WBbt:0005798	3.6	12	3.4	0.000063	0.0057
other	hermaphrodite	WBbt:0007849	62	95	1.5	0.000019	0.0029
	rectal valve cell	WBbt:0005797	1.2	5	4.1	0.0013	0.042
	sex organ	WBbt:0008422	46	79	1.7	2.2E-06	0.00065
	tail	WBbt:0005741	54	82	1.5	0.000079	0.0057

phenotype enrichment							
Category	Term	WormBase ID	Expected	Observed	Fold Change	p value	q value
body morphology	body morphology variant	WBPhenotype:0000072	30.00	46.00	1.50	0.0018	0.026
	body wall muscle thick filament variant	WBPhenotype:0000782	3.30	10.00	3.00	0.00057	0.015
	fat content increased	WBPhenotype:0001184	5.80	15.00	2.60	0.00027	0.0094
	intestinal vacuole	WBPhenotype:0001428	1.40	6.00	4.30	0.0005	0.015
	large	WBPhenotype:0000319	4.60	12.00	2.60	0.0008	0.015
	mitochondria morphology variant	WBPhenotype:0001401	5.10	12.00	2.30	0.0022	0.029
	muscle cell morphology variant	WBPhenotype:0000904	6.20	19.00	3.10	5.70E-06	0.00068
	muscle system morphology variant	WBPhenotype:0000603	6.10	18.00	3.00	1.60E-05	0.00093
	pale	WBPhenotype:0001261	1.10	6.00	5.70	8.70E-05	0.0041
	sluggish	WBPhenotype:0000646	4.90	13.00	2.60	0.0005	0.015
locomotion	frequency body bend reduced	WBPhenotype:0001482	1.10	4.00	3.70	0.00	0.06
	movement variant	WBPhenotype:0001206	43.00	72.00	1.70	9.60E-06	0.00076
	paralyzed	WBPhenotype:0000644	3.90	16.00	4.10	5.00E-07	0.00012
copulation	copulation variant	WBPhenotype:0000647	4.60	12.00	2.60	0.00077	0.015
	sexually dimorphic behavior variant	WBPhenotype:0000821	4.60	12.00	2.60	0.0008	0.015

others	behavior phenotype	WBPhenotype:0000517	68	98	1.4	0.00017	0.0069
	body region phenotype	WBPhenotype:0002557	33	52	1.6	0.00077	0.015
	eating variant	WBPhenotype:0002056	3.6	10	2.8	0.001	0.015
	protein degradation variant	WBPhenotype:0001645	3.9	11	2.8	0.00059	0.015

GO term enrichment							
Category	Term	WormBase ID	Expected	Observed	Fold Change	p value	q value
ion homeostasis	anion channel activity	GO:0005253	2.6	8	3.1	0.001	0.016
	calcium ion transport	GO:0006816	1.9	5	2.7	0.011	0.087
	chloride transport	GO:0006821	3	10	3.4	0.0002	0.0044
	divalent inorganic cation homeostasis	GO:0072507	1.9	8	4.2	0.0001	0.0025
	divalent inorganic cation transport	GO:0072511	3.1	8	2.6	0.0037	0.041
	ion homeostasis	GO:0050801	4.5	10	2.2	0.0055	0.055
	iron ion binding	GO:0005506	3.7	8	2.2	0.011	0.087
	ligand-gated channel activity	GO:0022834	5	12	2.4	0.0015	0.021
	narrow pore channel activity	GO:0022842	1.5	5	3.4	0.0032	0.041
	passive transmembrane transporter activity	GO:0022803	12	27	2.2	0.000065	0.0017
	stabilization of membrane potential	GO:0030322	1.5	5	3.4	0.0032	0.041
	transmembrane transport	GO:0055085	30	54	1.8	0.000013	0.00044
	adhesion / cytoskeleton	A band	GO:0031672	1.2	10	8.6	1.1E-08
actin filament binding		GO:0051015	2.3	7	3.1	0.0018	0.025
actin filament-based process		GO:0030029	6	18	3	0.00001	0.00044
collagen trimer		GO:0005581	1.7	7	4.2	0.00025	0.0051
extracellular structure organization		GO:0043062	1.7	5	3	0.0064	0.061
myofibril		GO:0030016	3	25	8.2	2.5E-17	7.8E-15
regulation of cell junction assembly		GO:1901888	1	5	4.8	0.00051	0.009
striated muscle dense body		GO:0055120	2.9	13	4.5	1.3E-06	0.00008
structural constituent of cuticle		GO:0042302	5.2	18	3.5	1.4E-06	0.00008
supramolecular polymer		GO:0099081	9.3	35	3.8	6.3E-12	9.7E-10

metabolism	cellular amino acid catabolic process	GO:0009063	1.9	7	3.7	0.00057	0.0092
	glutathione transferase activity	GO:0004364	1.7	7	4.1	0.00028	0.0054
	organic acid metabolic process	GO:0006082	15	25	1.7	0.0039	0.041
	oxidoreductase activity acting on CH OH group of donors	GO:0016614	2.2	6	2.7	0.0068	0.061
neuro-development	cell projection	GO:0042995	20	30	1.5	0.011	0.087
	cellular component assembly involved in morphogenesis	GO:0010927	1.1	7	6.4	0.00001	0.00044
	positive regulation of neuron differentiation	GO:0045666	1.7	5	2.9	0.0076	0.067
	regulation of synapse structure or activity	GO:0050803	1.6	6	3.7	0.0011	0.016
neuro-transmission	exocytic vesicle	GO:0070382	1.7	5	2.9	0.0076	0.067
	response to monoamine	GO:0071867	1	4	3.9	0.0035	0.041
others	apical part of cell	GO:0045177	2.8	9	3.2	0.0005	0.009
	basolateral plasma membrane	GO:0016323	1.5	5	3.4	0.0036	0.041
	cell periphery	GO:0071944	51	80	1.6	0.000035	0.00097
	establishment of localization	GO:0051234	60	79	1.3	0.0066	0.061
	mating	GO:0007618	1	4	3.9	0.0035	0.041
	muscle cell development	GO:0055001	1.2	7	5.8	0.000023	0.00072
	muscle system process	GO:0003012	2.1	15	7	2.7E-10	2.7E-08
	response to organic cyclic compound	GO:0014070	1.3	4	3	0.011	0.087

male-associated downregulated genes							
tissue enrichment							
Category	Term	WormBase ID	Expected	Observed	Fold Change	p value	q value
neuronal	AIM	WBbt:0006814	0.17	1	5.8	0.013	0.092
	anterior ganglion	WBbt:0005375	3.2	7	2.2	0.016	0.095
	AUA	WBbt:0006817	0.15	1	6.6	0.01	0.092
	AVB	WBbt:0005841	0.14	3	22	0.000012	0.00069
	AVG	WBbt:0003850	1.3	4	3.1	0.011	0.092
	BDU	WBbt:0006826	0.19	1	5.2	0.016	0.095
	CEM	WBbt:0005246	1.4	9	6.2	2.6E-06	0.00019
	DVA	WBbt:0004823	0.22	2	9.1	0.0014	0.02
	DVC	WBbt:0004821	0.15	2	14	0.00044	0.011
	hook sensillum	WBbt:0006930	1.5	10	6.8	3.8E-07	0.000038
	IL1L	WBbt:0004553	0.16	1	6.4	0.011	0.092
	IL1R	WBbt:0004551	0.15	1	6.6	0.01	0.092
	IL1VR	WBbt:0004547	0.14	1	7.2	0.0086	0.092
	inner labial sensillum	WBbt:0005116	2	9	4.6	0.000035	0.0013
	P1	WBbt:0006770	0.14	1	7.2	0.0086	0.092
	P2	WBbt:0006771	0.14	1	7	0.0091	0.092
	P4	WBbt:0006773	0.15	1	6.8	0.0096	0.092
	P5	WBbt:0006774	0.14	1	7.2	0.0086	0.092
	P6	WBbt:0006775	0.14	1	7	0.0091	0.092
	P7	WBbt:0006776	0.15	1	6.8	0.0096	0.092
	P8	WBbt:0006777	0.14	1	7.2	0.0086	0.092
	P9	WBbt:0006778	0.15	2	14	0.00044	0.011
	P10	WBbt:0006779	0.17	2	12	0.00065	0.011
	P11	WBbt:0004410	0.24	2	8.2	0.0019	0.025
	P12	WBbt:0004409	0.2	2	9.9	0.0011	0.017
	PVQ	WBbt:0006976	0.27	2	7.4	0.0026	0.031
	preanal ganglion	WBbt:0005448	0.96	4	4.1	0.003	0.034
	PVT	WBbt:0004070	0.52	3	5.8	0.0019	0.025
	ray	WBbt:0006941	1.8	12	6.5	6.2E-08	0.000019
	RIC	WBbt:0006834	0.15	2	14	0.00044	0.011
	RMDL	WBbt:0005037	0.15	2	14	0.00044	0.011
	RMDR	WBbt:0005033	0.15	2	14	0.00044	0.011
	RMDVL	WBbt:0005031	0.15	2	14	0.00044	0.011
RMDVR	WBbt:0005029	0.14	2	14	0.0004	0.011	
RMED	WBbt:0005027	0.14	1	7	0.0091	0.092	
SDQL	WBbt:0004993	0.16	1	6.1	0.012	0.092	
SDQR	WBbt:0004991	0.18	1	5.7	0.014	0.092	
SIA	WBbt:0005361	0.16	2	13	0.00052	0.011	
SMD	WBbt:0005353	0.22	2	9	0.0015	0.02	
URX	WBbt:0006846	0.27	3	11	0.00016	0.0054	
muscular	anal depressor muscle	WBbt:0004292	2	8	4	0.00023	0.007
	anal sphincter muscle	WBbt:0005798	0.56	5	9	0.000023	0.0011
	head muscle	WBbt:0006761	0.83	3	3.6	0.01	0.092

	pm3	WBbt:0003740	0.17	1	5.9	0.012	0.092
	pm5	WBbt:0003737	0.17	1	5.9	0.012	0.092
	pm6	WBbt:0003724	0.19	1	5.2	0.016	0.095
	pm7	WBbt:0003721	0.17	1	5.9	0.012	0.092
	uterine muscle	WBbt:0005342	0.57	3	5.3	0.0027	0.031
others	linker cell	WBbt:0005062	0.17	3	18	0.000025	0.0011
	male	WBbt:0007850	11	31	2.8	1.4E-07	0.000021
	rectal valve cell	WBbt:0005797	0.19	1	5.3	0.016	0.093
	sex organ	WBbt:0008422	7.2	13	1.8	0.015	0.093
	uterine seam cell	WBbt:0006789	0.19	1	5.4	0.015	0.093

phenotype enrichment							
Category	Term	WormBase ID	Expected	Observed	Fold Change	p value	q value
locomotion	backward point velocity decreased	WBPhenotype:0002324	0.28	2	7.2	0.0028	0.048
	body posture amplitude decreased	WBPhenotype:0002292	0.42	3	7.1	0.0009	0.027
	coiling frequency increased	WBPhenotype:0002300	0.38	2	5.3	0.0066	0.082
	foraging reduced	WBPhenotype:0000238	0.27	3	11	0.00017	0.021
	forward locomotion decreased	WBPhenotype:0002347	0.35	3	8.5	0.00046	0.026
	forward point velocity decreased	WBPhenotype:0002321	0.28	2	7.1	0.0029	0.048
	path curvature increased	WBPhenotype:0002336	0.32	2	6.3	0.0041	0.054
	reversal variant	WBPhenotype:0002320	1	6	5.9	0.000086	0.021
	sinusoidal movement variant	WBPhenotype:0004018	1.2	4	3.4	0.0067	0.082
	velocity of movement variant	WBPhenotype:0004025	0.97	4	4.1	0.0031	0.048
neuro-development	axon guidance variant	WBPhenotype:0000384	0.58	3	5.2	0.0028	0.048
	neurite morphology variant	WBPhenotype:0001398	0.73	3	4.1	0.0065	8.20E-02
	neuronal outgrowth variant	WBPhenotype:0000572	0.86	4	4.7	0.0018	0.04
	neuropil development variant	WBPhenotype:0000945	0.33	3	9	0.00037	2.60E-02
	ventral cord patterning variant	WBPhenotype:0000976	0.27	2	7.4	0.0026	0.047
copulation	copulation variant	WBPhenotype:0000647	0.68	4	5.9	0.00066	0.026
	male mating efficiency reduced	WBPhenotype:0000843	0.23	2	8.6	0.0017	4.00E-02
	sexually dimorphic behavior variant	WBPhenotype:0000821	0.69	4	5.8	0.00068	0.026
	turning variant	WBPhenotype:0002311	0.9	4	4.5	0.0022	4.40E-02
body morphology	cell membrane morphology variant	WBPhenotype:0001399	0.32	3	9.3	0.00033	0.026

	sluggish	WBPhenotype:0000646	0.74	4	5.4	0.00093	2.70E-02
	thin	WBPhenotype:0000164	1.2	4	3.4	0.0068	0.082

GO term enrichment							
Category	Term	WormBase ID	Expected	Observed	Fold Change	p value	q value
adhesion / cytoskeleton	actin filament polymerization	GO:0030041	0.17	1	5.7	0.013	0.094
	actin filament-based process	GO:0030029	0.74	3	4	0.0069	0.072
	biological adhesion	GO:0022610	0.42	2	4.8	0.0087	0.077
	extracellular structure organization	GO:0043062	0.21	2	9.6	0.0012	0.029
	metalloendo-peptidase activity	GO:0004222	0.41	2	4.9	0.0083	0.077
	myofibril	GO:0030016	0.38	4	11	0.000043	0.0025
	regulation of actin filament length	GO:0030832	0.17	1	5.8	0.013	0.094
	regulation of actin filament organization	GO:0110053	0.17	1	5.7	0.013	0.094
	regulation of cell junction assembly	GO:1901888	0.13	2	15	0.0003	0.0093
	supramolecular polymer	GO:0099081	1.2	4	3.4	0.0066	0.072
neuro-development	cell part morphogenesis	GO:0032990	0.76	3	3.9	0.0074	0.072
	cell projection	GO:0042995	2.5	6	2.4	0.013	0.094
	cell projection organization	GO:0030030	1.3	4	3.1	0.01	0.084
	cellular component assembly involved in morphogenesis	GO:0010927	0.14	1	7.3	0.0083	0.077
	dendritic tree	GO:0097447	0.53	3	5.7	0.002	0.034
	motor neuron axon guidance	GO:0008045	0.14	3	21	0.000012	0.0013
	neuron development	GO:0048666	0.74	3	4	0.0068	0.072
	neuron projection guidance	GO:0097485	0.53	3	5.7	0.002	0.034
	positive regulation of neuron differentiation	GO:0045666	0.22	3	14	0.000069	0.003
intracellular signaling cascades	G protein-coupled receptor signaling pathway coupled to cyclic nucleotide second messenger	GO:0007187	0.24	2	8.5	0.0017	0.034
	intracellular receptor signaling pathway	GO:0030522	0.25	2	8.1	0.002	0.034

	response to endogenous stimulus	GO:0009719	0.51	3	5.9	0.0017	0.034
	response to nitrogen compound	GO:1901698	0.47	3	6.4	0.0013	0.029
	response to organic cyclic compound	GO:0014070	0.17	3	18	0.000025	0.0019
	signal transduction by protein phosphorylation	GO:0023014	0.34	2	5.8	0.005	0.061
	stress-activated protein kinase signaling cascade	GO:0031098	0.13	2	16	0.00027	0.0093
other development	development of primary sexual characteristics	GO:0045137	0.42	2	4.8	0.0087	0.077
	gonad morphogenesis	GO:0035262	0.16	1	6.4	0.011	0.084
	male anatomical structure morphogenesis	GO:0090598	0.53	3	5.6	0.0021	0.034
	muscle cell development	GO:0055001	0.15	1	6.6	0.01	0.084
	reproductive system development	GO:0061458	0.5	2	4	0.014	0.094
ion homeostasis	calcium ion transport	GO:0006816	0.23	2	8.6	0.0017	0.034
	divalent inorganic cation transport	GO:0072511	0.38	2	5.2	0.0069	0.072
	transmembrane transporter complex	GO:1902495	0.35	2	5.8	0.0052	0.061
neuro-transmission	regulation of synapse structure or activity	GO:0050803	0.2	2	9.9	0.0011	0.028
	response to monoamine	GO:0071867	0.13	3	23	8.7E-06	0.0013
others	defense response to Gram-positive bacterium	GO:0050830	0.27	2	7.5	0.0025	0.034
	excretion	GO:0007588	0.19	1	5.3	0.016	0.1
	localization of cell	GO:0051674	0.48	2	4.2	0.013	0.094
	locomotion involved in locomotory behavior	GO:0031987	0.13	2	15	0.0003	0.0093
	mating	GO:0007618	0.13	4	31	1.9E-07	0.00006
	muscle system process	GO:0003012	0.27	3	11	0.00015	0.0059
	oviposition	GO:0018991	0.61	3	4.9	0.0034	0.043

	pharyngeal pumping	GO:0043050	0.23	2	8.6	0.0017	3.40E-02
	positive regulation of programmed cell death	GO:0043068	0.17	1	5.7	0.013	0.094
	regulation of cell motility	GO:2000145	0.38	4	11	0.000041	0.0025
	regulation of extent of cell growth	GO:0061387	0.17	1	6	0.012	0.094
	reproduction	GO:0000003	3.2	8	2.5	0.005	0.061

Supplementary Table 3: Enrichment analysis of significantly regulated genes in *lat-1* mutant males identified by RNA-Seq analysis. Overrepresented cells/tissues, phenotypes and GO terms that were obtained by analyzing up- and downregulated genes in *lat-1* mutants found in our RNA-Seq analysis (Supplementary Table 2) with the Wormbase Enrichment Analysis Tool [3, 4] are listed. We considered overrepresented terms with a q value < 0.1 as significant. We performed the analysis once using all significantly up- or downregulated genes, respectively, and once with a subset of genes, that has been previously associated with the male sex (Supplementary Table 2). Terms are displayed in substantively matching groups. Expected gene numbers (according to the WormBase Enrichment Tool) and observed gene numbers (from our RNA-Seq analysis) are given. Enrichment analyses of upregulated genes gave no significant results.

Supplementary Table 4

	expressed in both tissues																
	sum	both tissues	muscle-specific	neuron-specific	<i>lrp-2</i>	<i>unc-68</i>	<i>tni-3</i>	<i>gon-1</i>	<i>gar-3</i>	<i>lev-11</i>	<i>unc-6</i>	<i>rcan-1</i>	<i>rig-6</i>	<i>unc-55</i>	<i>hsp-43</i>	<i>fbxa-67</i>	<i>unc-7</i>
neurodevelopment	11	6	1	4		1		1			1		1	1			1
adhesion / cytoskeleton	10	6	1	3			1	1		1	1		1				1
body morphology	10	7	1	2		1	1			1	1		1	1			1
fertility	10	6	1	3		1	1	1		1	1		1				
locomotion	10	8	1	1		1	1	1		1	1		1	1			1
lethality	7	4	1	2			1	1		1	1						
non-neuronal development	7	5	0	2	1			1		1	1		1				
copulation	6	4	1	1						1		1		1			1
neurotransmission	6	2	0	4					1					1			
food intake	5	3	1	1			1		1								1
ion homeostasis	5	4	0	1		1			1			1					1
life span	5	3	0	2				1	1							1	
immunity	4	1	0	3										1			
male development	3	2	0	1							1	1					
neurosensation	3	2	0	1								1					1
metabolism	2	0	0	2													
others	4	0	0	4													

Supplementary Table 5

	sum	percentage	AIM	AVB	AVG	AUA	BDU	CEM	DVA	DVC	IL1	PVQ	PVT	RIC	RMD	RME	SDQ	SIA	SMD	URX
neurodevelopment	6	33%			1		1					1	1			1		1		
locomotion	5	28%	1	1							1				1				1	
mechanosensation	3	17%						1	1	1	1									
other sensory functions	3	17%					1										1			1
copulation	2	11%	1				1													
neuromodulation	2	11%	1											1						
feeding behavior	1	6%																		
lifespan	1	6%																		1
immunity	1	6%																		1

Supplementary Table 5: Functions of overrepresented neurons from our enrichment analysis. A summary of known functions of the neurons that we identified in our tissue enrichment analyses of significantly regulated genes in *lat-1* mutant males, based on data from the WormBase database (WS280) is shown.

Supplementary Table 6

strain	genotype	origin of the alleles
OH15262	<i>otIs669</i> V. ^a	Caenorhabditis Genetics Center (CGC)
APR469	<i>lat-1(ok1465) II</i> .	Caenorhabditis Genetics Center (CGC)
CB246	<i>unc-64(e246) III</i> .	Caenorhabditis Genetics Center (CGC)
XA7553	<i>qals7524[lat-1p::GFP::lat-1+rol 6(su1006)]</i> .	previously generated (Langenhan et al. 2009, Dev Cell)
-	<i>pha-1(e2123); him-5 (e1490); gar-3(gk305)</i> .	kind gift of René García (Department of Biology, Texas A&M University)
APR475	<i>lat-1(ok1465) II</i> ; <i>aprEx192[pTL20; mCherry; pBSK]</i> .	this study (microinjection)
APR684	<i>otIs669</i> ; <i>qals7524[lat-1p::GFP::lat-1+rol 6(su1006)]</i> .	this study (genetic cross)
APR728	<i>lat-1(ok1465) II</i> ; <i>qals7524[lat-1p::GFP::lat-1+rol 6(su1006)]</i> .	this study (genetic cross)

Supplementary Table 6: Genotypes of *C. elegans* strains used in this study. ^afull genotype see [2].

Supplementary Table 7

Sample	Organism	Genotype	Collection date	Tissue	Reads	% mapped	% properly paired
N2--1	<i>C. elegans</i>	N2 (var. Bristol), male	2019-12	whole animal	341422139	89	55
N2--2	<i>C. elegans</i>	N2 (var. Bristol), male	2019-12	whole animal	341767664	89	57
N2--3	<i>C. elegans</i>	N2 (var. Bristol), male	2019-12	whole animal	264048315	83	53
N2--4	<i>C. elegans</i>	N2 (var. Bristol), male	2019-12	whole animal	244712889	48	33
N2--5	<i>C. elegans</i>	N2 (var. Bristol), male	2019-12	whole animal	183702909	8	6
APR469--1	<i>C. elegans</i>	lat-1(ok1465), male	2019-12	whole animal	325033153	86	54
APR469--2	<i>C. elegans</i>	lat-1(ok1465), male	2019-12	whole animal	224313740	79	53
APR469--3	<i>C. elegans</i>	lat-1(ok1465), male	2019-12	whole animal	235054065	78	49
APR469--4	<i>C. elegans</i>	lat-1(ok1465), male	2019-12	whole animal	250296767	87	54
APR469--5	<i>C. elegans</i>	lat-1(ok1465), male	2019-12	whole animal	168057274	54	34

Supplementary Table 7: Read mapping results. % mapped: percentage of reads mapped to the reference genome. % properly paired: percentage of reads with both sequenced ends mapping into the same genomic region (e.g. not to different chromosomes).

Supplementary Files

Supplementary videos and shell scripts related to this article can be accessed at <https://doi.org/10.1016/j.bbrc.2021.12.006>.

Supplementary References

- [1] T. Tekieli, E. Yemini, A. Nejatbakhsh, C. Wang, E. Varol, R.W. Fernandez, N. Masoudi, L. Paninski, O. Hobert, Visualizing the organization and differentiation of the male-specific nervous system of *C. elegans*, *Development*, 148 (2021).
- [2] E. Yemini, A. Lin, A. Nejatbakhsh, E. Varol, R. Sun, G.E. Mena, A.D.T. Samuel, L. Paninski, V. Venkatachalam, O. Hobert, NeuroPAL: A Multicolor Atlas for Whole-Brain Neuronal Identification in *C. elegans*, *Cell*, 184 (2021) 272-288 e211.
- [3] D. Angeles-Albores, N.L. RY, J. Chan, P.W. Sternberg, Tissue enrichment analysis for *C. elegans* genomics, *BMC Bioinformatics*, 17 (2016) 366.
- [4] D. Angeles-Albores, R. Lee, J. Chan, P. Sternberg, Two new functions in the WormBase Enrichment Suite, *MicroPubl Biol*, 2018 (2018).

7.2 Supplemental material for “The N terminus-only (*trans*) function of the Adhesion GPCR Latrophilin-1 cross-talks with the Notch pathway to control cell proliferation in the stem cell niche”

Supplementary Figure 1

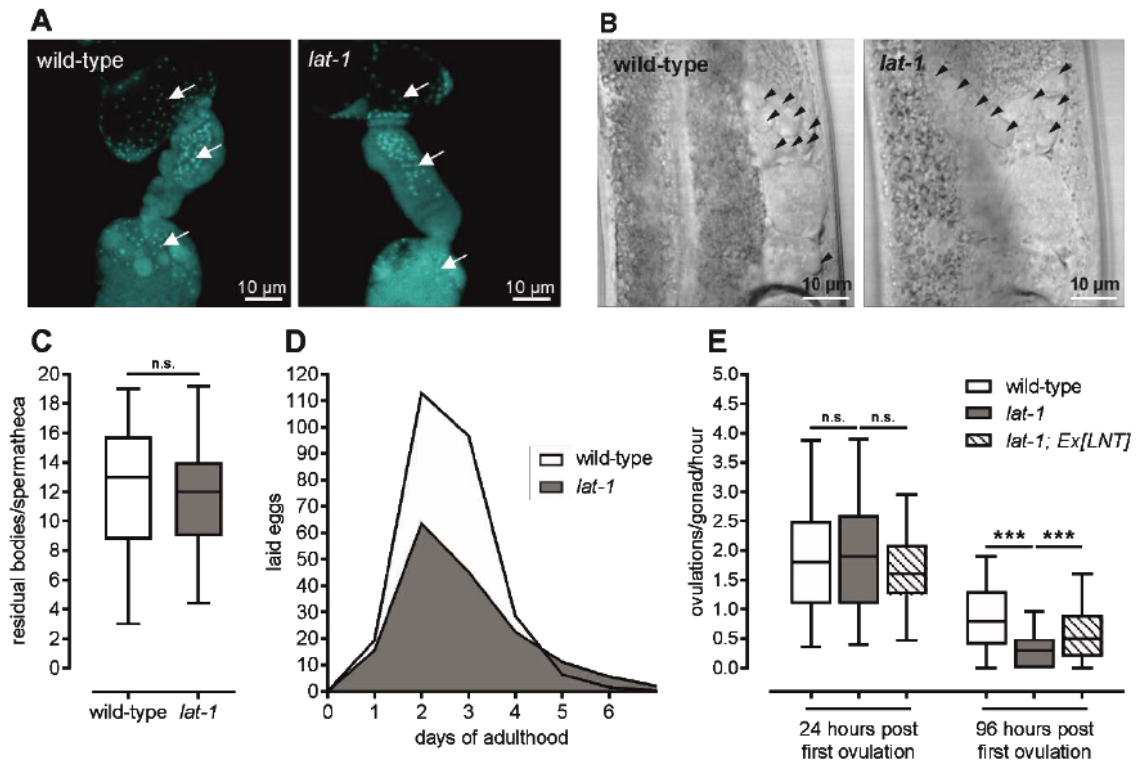


Fig. S1. Nematodes lacking *lat-1* display impaired sperm movement. (A) Spermathecae of young adult *lat-1* mutant hermaphrodites contain the same amount of sperm (white arrows) as wild-type specimen. Gonads of adult hermaphrodites were dissected and subsequently stained with DAPI. (B) Residual bodies (black arrow heads) located close to the spermatheca in *lat-1* mutant and wild-type gonads. Shown are DIC images of unstained living young adult hermaphrodites. (C) Quantification of anucleate residual bodies in young adult hermaphrodites based on DIC images as displayed in (B) revealed no significant difference in number between wild-type nematodes and *lat-1* mutants. Data are shown as box plots with 90% confidence interval of four independent experiments ($n \geq 24$). n.s. = not significant. (D) Hermaphrodites lacking *lat-1* exhibit a continuously smaller brood size over their entire reproductive period with the maximal reduction being visible on the second and third day of egg laying. $n \geq 75$ in nine independent replicates. (E) The ovulation rate in *lat-1* mutants decreases faster than in wild-type individuals or in *lat-1* mutants expressing the LNT. The ovulation rate per gonad per hour was calculated as follows: ((eggs in and out of uterus after 4 hours) - (initial eggs inside uterus)) / (2 * 4 hours). Data are shown as box plots with 90% confidence interval of four independent experiments, $n \geq 51$. n.s. = not significant; *** $p < 0.001$.

Supplementary Figure 2

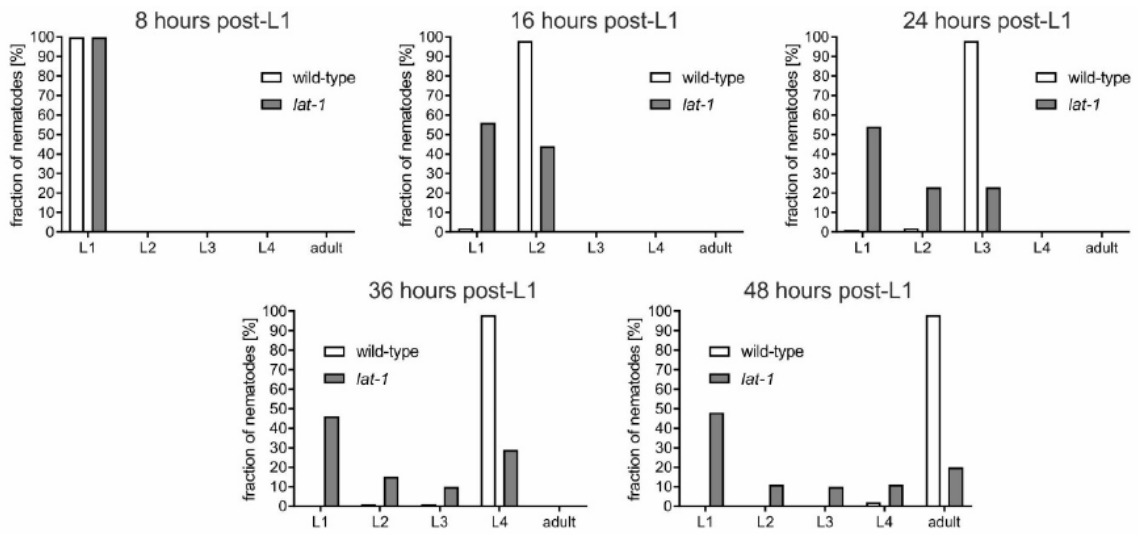


Fig. S2. *lat-1* nematodes display an impaired larval development. A synchronized L1 population of nematodes was evaluated for progression through the larval stages up to adulthood at 8, 16, 24, 36, and 48 hours post-L1. While wild-type worms show a fast and synchronized progression, some *lat-1* nematodes arrest in early larval stages. However, a small percentage of *lat-1* mutants reach L4/adulthood at the same time as wild-type animals.

Supplementary Figure 3

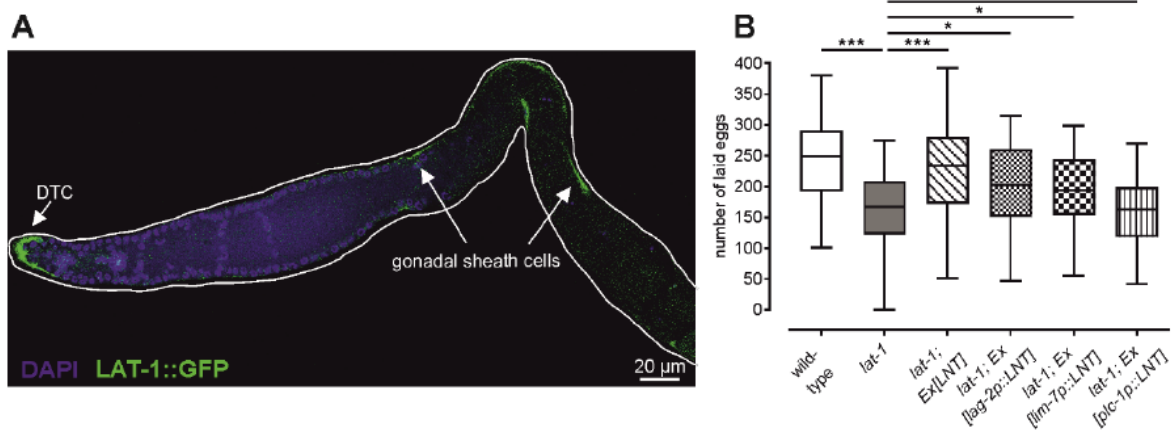


Fig. S3. *Lat-1::GFP* expression and tissue-specific rescue of *lat-1* mutant brood size. (A) Extruded and DAPI-stained gonad of a strain containing an integrated construct encoding a LAT-1::GFP fusion protein (green) driven by its physiological promoter. As has been shown in Fig. 4A-E, *lat-1* expression is restricted to the cells of the somatic gonad (e. g. DTC) and gonadal sheath cells), but is absent from the germ cells visualized by DAPI (blue). (B) Tissue-specific rescue of *lat-1* mutant brood size by transgenic expression of the LAT-1 N terminus (LNT) driven by promoters with activity restricted to distinct cell types. While expression of LNT in the distal tip cell (*lag-2p::LNT*) and the gonadal sheath cells (*lim-7p::LNT*) results in an amelioration of the brood size defect, sole expression in the spermatheca (*plc-1p::LNT*) does not. Boxplots with 90% confidence interval, $n \geq 34$. n.s. = not significant; * $p < 0.05$; *** $p < 0.001$.

Supplementary Figure 4

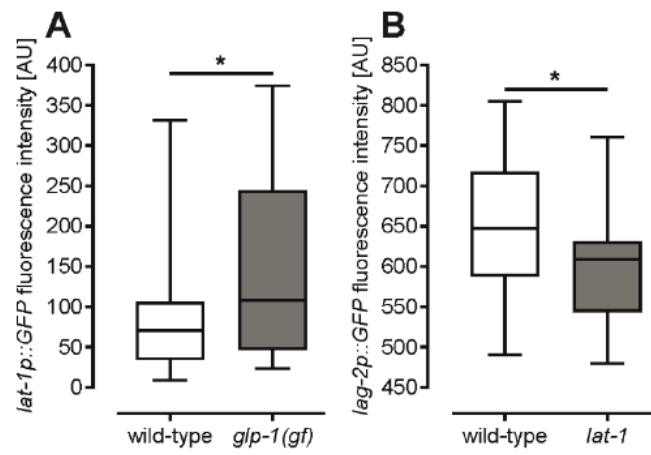


Fig. S4. Quantification of fluorescence levels of images given in Fig. 7A (A) and Fig. 4E (B). Boxplots with 90% confidence interval, $n \geq 34$. * $p < 0.05$.

Supplementary Table 1

PH3-antibody staining		PH3-positive cells (mean ± SEM)	all proliferative zone nuclei (mean ± SEM)	M index (mean ± SEM)	n (biological replicates)
Figure 2g	wild-type	3.2 ± 0.3	237 ± 4	1.9% ± 0.1%	38
	<i>lat-1</i>	6.1 ± 0.4	228 ± 6	2.8% ± 0.2%	35
	<i>lat-1; Ex[LNT]</i>	3.2 ± 0.7	238 ± 7	1.4% ± 0.3%	20
Figure 4h	wild-type	4.4 ± 0.5	203 ± 5	1.5% ± 0.2%	24
	<i>lat-1</i>	6.3 ± 0.4	198 ± 6	3.3% ± 0.3%	35
	<i>lat-1; Ex[lag-2p::LNT]</i>	3.8 ± 0.8	220 ± 6	1.7% ± 0.3%	17
	<i>lat-1; Ex[lim-7p::LNT]</i>	4.3 ± 0.5	181 ± 7	2.3% ± 0.3%	26
Figure 6g	wild-type	3.7 ± 0.4	231 ± 4	1.6% ± 0.2%	44
	<i>lat-1</i>	5.7 ± 0.5	244 ± 5	2.4% ± 0.2%	40
	<i>fbf-1</i>	2.3 ± 0.3	207 ± 5	1.1% ± 0.1%	29
	<i>gld-1</i>	6.5 ± 0.6	180 ± 9	3.6% ± 0.3%	20
	<i>gld-1; lat-1</i>	6.8 ± 0.9	201 ± 12	3.3% ± 0.3%	19
	<i>lst-1; sygl-1</i>	3.3 ± 0.3	157 ± 5	2.1% ± 0.2%	36
	<i>lst-1; sygl-1; lat-1</i>	5.2 ± 0.5	110 ± 5	4.8% ± 0.4%	31
Figure 7d	wild-type	1.6 ± 0.4	239 ± 4	0.7% ± 0.2%	21
	<i>lat-1</i>	3.4 ± 0.4	245 ± 5	1.4% ± 0.2%	24
	<i>glp-1(lf)</i>	0.8 ± 0.2	113 ± 3	0.7% ± 0.2%	36
	<i>lat-1; glp-1(lf)</i>	1.2 ± 0.2	123 ± 7	0.9% ± 0.1%	39
	<i>glp-1(gf)</i>	4.2 ± 0.7	266 ± 10	1.6% ± 0.2%	18
	<i>lat-1; glp-1(gf)</i>	5.5 ± 0.7	280 ± 12	1.9% ± 0.2%	49
	<i>lag-2(lf)</i>	2.0 ± 0.2	147 ± 3	1.4% ± 0.2%	57
	<i>lat-1; lag-2(lf)</i>	3.0 ± 0.3	134 ± 4	2.3% ± 0.2%	46
EdU staining		EdU-positive cells (mean ± SEM)	all proliferative zone nuclei (mean ± SEM)	S index (mean ± SEM)	n (biological replicates)
Figure 3c	wild-type	139 ± 6.6	228 ± 7.8	60.9% ± 1.3%	21
	<i>lat-1</i>	167 ± 7.3	239 ± 6.6	69.5% ± 1.7%	20
	<i>lat-1; Ex[LNT]</i>	150 ± 6.7	241 ± 9.7	62.5% ± 1.5%	23

Table S1. PH3- and EdU-positive cell counts and denominators for index calculation.

Supplementary Table 2

Exon	Chromosome	Start	End
1	II	8805410	8805979
2	II	8805628	8805979
3	II	8846108	8846118
4	II	8890831	8890855
5	II	8896750	8896987
6	II	8896839	8896987
7	II	8896841	8896987
8	II	8899797	8899984
9	II	8899798	8899984
10	II	8903278	8903494
11	II	8903388	8903494
12	II	8903300	8903521
13	II	8903607	8903719
14	II	8903832	8903929
15	II	8903844	8903929
16	II	8903844	8903930
17	II	8903913	8903929
18	II	8903916	8903929
19	II	8904012	8904492
20	II	8904012	8905264
21	II	8905967	8906846
22	II	8906060	8906846
23	II	8906575	8906846
24	II	8906914	8906981
25	II	8906915	8907289
26	II	8907152	8907287
27	II	8907152	8907288
28	II	8907152	8907289
29	II	8907725	8908630
30	II	8907725	8908636
31	II	8964794	8964892

Table S2. Exon positions of *lat-1* variants analyzed in this study. Given are the identified exons for the *lat-1* gene (numbering refers to the reference *C. elegans* genome (WBcel235)).

Supplementary Table 3

Primer	Sequence 5'-3'
lat1_1080F	TTGTTTGTGAGTTTTTCGGTTTTCGCTTTATCTTGTATTGAATCCGAATCCCTATAGTGAATCGTATACATGGTCAFA
lat1_1081R	ATTGCTGCAGGATCTTTTCTACGGGTCTCAGCTCAGTG
lat1_1082F	GATCCTGCAGCAATGCTTCCGAAAACCTCCGAGTTTTTCG
lat1_1083R	GCTACCAGAAATCGTTTGGAGCAACAATAAGTCTGTTTGTACGTCGCATGCCGTTGAACAGATATAGAAGTTGTGATT
lat1_1084F	CTTAACTGTCAGATTTCAAAAAAAGGA
lat1_1085R	CTGTAATTTCTCATATTTGATTTAAAA
lat1_1086F	GATCCTGCAGCTTAACTGT CAGATTTCAAAAA
lat1_1087R	GCTACCAGAAATCGTTTGGAGCAACAATAAGTCTGTTTGTTA CGTCGCATCTGTAATGTCTCATA TTTTGATTTAAAAAGATAAACAC
lat1_1088F	TTTGAATCCGAAAAAGTCTCAAAAAGCAAA
lat1_1089R	AAAAGGCCAAATTTGAAAAGTGTGTGGCT
lat1_1090F	GATCCTGCAGTTTGAATCCGAAAAAGTCTCAAAAAGCAAA
lat1_1091R	GCTACCAGAAATCGTTTGGAGCAACAATAAGTCTGTTTGTTA CGTCGCATAAAAAGGCAAA TTTGAAAAGTGTGTGGC
lat1_1365F	CGGATGAAAAGTGGAAACCATCTC
lat1_1394F	GCTCCAAACGAAATCTGGTAGCTTGTGTC
Oligo d(T)-Anchor Primer	GACCACGGTATCGATGTCGACTTTTTTTTTTTTTTTTTV (V=A, C or G)
PCR Anchor Primer	GACCACGGTATCGATGTCGAC

Table S3. Sequences of primers used in the study.

Supplementary Table 4

GEO Accession	SRA run	raw reads	uniquely aligned raw reads [%]
GSM1862268	SRR2185654	2 x 57999404	94.52
GSM1862269	SRR2185655	2 x 40607164	94.76
GSM1862270	SRR2185656	2 x 49090847	94.62

Table S4. Accession numbers and mapping statistics for transcript analysis of *lat-1* variants.

7.3 Depiction of contribution

For the publication “Latrophilin-1 drives neuron morphogenesis and shapes chemo- and mechanosensation-dependent behavior in *C. elegans* via a *trans* function”, Daniel Matúš performed all experiments and data analyses with the following exceptions: Willem Berend Post performed and analyzed the spicule protraction assays. Dr Susanne Horn and Prof. Dr Torsten Schöneberg analyzed the RNA-Seq raw data. Enrichment analyses were done by Daniel Matúš. Daniel Matúš and Prof. Dr Simone Prömel wrote the manuscript.

Date: 16.12.2021



Daniel Matúš



Prof. Dr Simone Prömel



Prof. Dr Torsten Schöneberg



Willem Berend Post

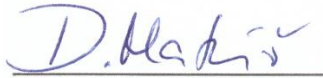


Dr Susanne Horn

For the manuscript “The N terminus-only (*trans*) function of the Adhesion GPCR Latrophilin-1 cross-talks with the Notch pathway to control cell proliferation in the stem cell niche” Daniel Matúš performed the physiological characterization of *lat-1* mutants concerning brood size, sperm loss and larval development, while PH3 antibody, SYTO12-stainings, ovulation and residual body analyses of *lat-1* mutants were done by Dr Franziska Fiedler. Analysis of germline zones via DAPI morphology were done by Dr Franziska Fiedler, while REC-8 and HIM-3 antibody stainings were performed by Daniel Matúš. Daniel Matúš further carried out the EdU labeling / pulse chase experiments and DNA content quantification and received help from Victoria Elisabeth Groß and Prof. Dr Simone Prömel with the analyses of the latter. *lat-1* expression analyses using GFP reporters were performed by Daniel Matúš and Franziska Fiedler. Daniel Matúš additionally analyzed expression and co-localization of the integrated *lat-1p::mCherry* reporter and performed rescue analyses using tissue-specific expression constructs. The latter have been generated by Julia Luterán and Daniel Matúš. Daniel Matúš performed morphological and *lag-2* expression analyses of the distal tip cell based on data sets generated by Dr Franziska Fiedler. Dr Alexander Bernd Knierim and Prof. Dr Torsten Schöneberg performed the splice variant analyses and Victoria Elisabeth Groß carried out the RACE-PCRs. Quantification of GLD-1 protein expression and epistasis analyses of *lat-1* and Notch downstream effectors were done by Daniel Matúš. Epistasis analyses of *lat-1* and *glp-1* / *lag-2* were done by Daniel Matúš with help from Dr Franziska

Fiedler and Johanna Lena Schön. Daniel Matúš, Dr Franziska Fiedler and Prof. Dr Simone Prömel wrote the manuscript.

Date: 16.12.2021



Daniel Matúš



Prof. Dr Simone Prömel



Prof. Dr Torsten Schöneberg



Dr Franziska Fiedler



Victoria Elisabeth Groß



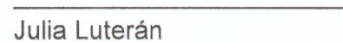
Dr Alexander Bernd Knierim
Dr. vst. erst 03/22



Johanna Lena Schön



Claudia Binder



Julia Luterán

For the Review "G Proteins and GPCRs in *C. elegans* Development: A Story of Mutual Infidelity", Daniel Matúš and Prof. Dr Simone Prömel contributed equally in screening for literature and writing the manuscript.

Date: 16.12.2021



Daniel Matúš



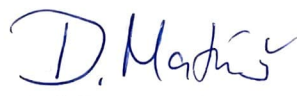
Prof. Dr Simone Prömel

7.4 Statement of authorship

I confirm that, to the best of my knowledge, the doctoral dissertation represents my own work and was prepared independently without any impermissible help or sources. I assure that third parties have not received indirect or direct monetary incentives for work in connection to the contents of the present dissertation, and that the doctoral dissertation contains no material which has been presented for the award of any other degree or diploma in any other university, tertiary education institution, and national or foreign examination board. I certify that, to the best of my knowledge and belief, this doctoral dissertation contains no material previously published or written by another person, except where due reference has been made in the text. All persons directly involved in the present work have been indicated by name. Current legal standards in regard to clinical studies, animal welfare, genetic engineering as well as data protection regulations have not been violated. I assure to know and to adhere to the regulations of good scientific practice of Leipzig University.

22.12.2021

date



signature

7.5 Curriculum vitae

PERSONAL INFORMATION

Date of Birth: 13.06.1996
Place of Birth: Levoča, Slovakia
Citizenship: German, Slovakian
Address: Härtelstraße 9A, 04107 Leipzig, Saxony, Germany
Cell Phone: +4915155974318
Emails: daniel.matus@medizin.uni-leipzig.de, dmatus1306@gmail.com

EDUCATION

2006 – 2014 School Education (Geschwister-Scholl-Gymnasium Freiberg)

- Abitur (GCE A-level) mark: 1.0

2014 – 2021 Medical School (Leipzig University)

- First State Examination mark: 1.0
- Second State Examination mark: 2.0
- Third State Examination mark: 2.0

since Oct. 2016 Doctoral Studies incl. one year full-time lab work (Rudolf Schönheimer Institute of Biochemistry, Leipzig University)

HONORS AND AWARDS

2020 and 2021 Participant of the Lindau Nobel Laureate Meeting
2017-2021 German Academic Scholarship Foundation Scholarship
2017 Scholarship from the Medical Faculty of Leipzig University
2014-2016 Deutschlandstipendium Scholarship
2014 GDCH-Award for best A-levels in chemistry
2014 Karl-von-Frisch-Award for best A-levels in biology
2014 Honors from the Saxon Ministry of State for Education for top grade A levels

LANGUAGE SKILLS

German / Slovak native speaker
English Cambridge Certificate in Advanced English: C1 level
French High School Education: B2 level
Spanish C2-Barcelona Language School: A1 level

TUTORING EXPERIENCE

2016 and 2017 Anatomy Tutor (Institute for Anatomy, Leipzig University)

EXTRACURRICULAR ACTIVITIES

2015-2020 Head of organization for the annual "Medizinerkonzert"

7.6 Publications and presentations

ARTICLES

Matúš D, Fiedler F, Groß VE, Binder C, Schön JL, Luterán J, Knierim AB, Schöneberg T, Prömel S: The N terminus-only (*trans*) function of the Adhesion GPCR Latrophilin-1 cross-talks with the Notch pathway to control cell proliferation in the stem cell niche, *submitted*

Matúš D, Post WB, Horn S, Schöneberg T, Prömel S: Latrophilin-1 drives neuron morphogenesis and shapes chemo- and mechanosensation-dependent behavior in *C. elegans* via a *trans* function, *Biochem Biophys Res Commun.* 2021 Dec 5;589:152-158.

Matúš D, Prömel S: G Proteins and GPCRs in *C. elegans* Development: A Story of Mutual Infidelity, *J Dev Biol.* 2018 Nov 25;6(4):28.

TALKS

“The 7TM-independent (*trans*) function of Latrophilin-1 - a non-cell autonomous role in fertility”, FOR2149-Retreat (03/2018), Bamberg, Germany

POSTERS

Matúš D, Fiedler F, Schön JL, Groß VE, Knierim AB, Luterán J, Binder C, Schöneberg S, Prömel S, “The Adhesion-GPCR LAT-1 mediates germ cell proliferation control via the Notch pathway”, Gordon Research Conference: How Form, Function, Content and Context Shape GPCR Signaling (02/2019), Ventura, California, USA

Matúš D, Fiedler F, Groß VE, Luterán J, Binder C, Schöneberg T, Prömel S: “The enigmatic *trans* function of the Adhesion-GPCR Latrophilin-1 acts non-cell autonomously in fertility”, Adhesion GPCR Workshop (09/2018), Portland, Oregon, USA

Matúš D, Fiedler F, Luterán J, Binder C, Schöneberg T, Prömel S: “The Adhesion-GPCR LAT-1 controls oocyte maturation and sperm guidance in *C. elegans*”, EMBO Workshop – *C. elegans* development, cell biology and gene expression (06/2018), Barcelona, Spain

7.7 Acknowledgments

I want to thank Prof. Dr Torsten Schöneberg for giving me the opportunity to carry out my doctoral thesis in his working group, for his constant support and constructive criticism. Equally, I want to thank Prof. Dr Simone Prömel, who gave me an excellent training at her lab, fostered my curiosity and determination and enabled me to tap into my full potential.

I want to thank Dr Franziska Münzner (maiden name: Fiedler), whose experiments laid the groundwork for my own project and who generously shared her expertise with *C. elegans*.

I want to thank all current and past members of the Prömel lab that I had the privilege to work with: I thank Victoria Elisabeth Groß, Johanna Lena Schön, Willem Berend (Wilbert) Post, Claudia Binder and Vivien Teßmar for supporting me both inside and outside the lab in stressful times, I thank André Dietzsch, Maximilian Korzeniowski and Dr Sandra Huth for the great work environment, I thank Julia Luterán and Dr Jana Winkler for sharing their expertise and warmly welcoming me into the work group and I thank all of the above for their incredible friendship.

I further want to thank all current members and alumni of the Schöneberg and Liebscher labs for their unconditional help and friendship.

I thank all the collaborators of this project: Dr Alexander Bernd Knierim and Dr Susanne Horn for the RNA-Seq analyses, Dr Sonja Kallendrusch and the Langenhan lab for their help with confocal microscopy, PD Dr Martin Krüger and Prof. Dr Ingo Bechmann for sharing staining protocols, Prof. Dr Ralph Schnabel, Prof. Dr Diana S. Chu, Prof. Dr René García and Prof. Dr Oliver Hobert for generously sharing plasmids and *C. elegans* strains, Prof. Dr Monique Zetka for gifting anti-HIM-3 antibody.

I thank the Medical Faculty of Leipzig University for the financial support of my doctoral studies.

I want to thank Robert Heedt for the detailed proofreading of this work.

And last but definitely not least I thank my family, especially my parents and my sister as well as my friends for their endless support and encouragement throughout this challenging time.